

***Carbon and energy use efficiency of soil microorganisms unfolding
over time***

Inaugural-Dissertation

zur

Erlangung des Doktorgrades

der Mathematisch-Naturwissenschaftlichen Fakultät

der Universität zu Köln

vorgelegt von

Martin-Georg Alexander Endress

aus Dresden

Köln

2025

Berichterstatter:

Prof. Dr. Michael Bonkowski, Terrestrische Ökologie, Institut für Zoologie, Universität zu Köln

Prof. Dr. Patrick Fink, Allgemeine Ökologie, Institut für Zoologie, Universität zu Köln

Vorsitz der Prüfung:

Prof. Dr. Christina Bogner, Ökosystemforschung, Geographisches Institut, Universität zu Köln

Beisitzer:

Dr. Sergey Blagodatsky, Karlsruher Institut für Technologie

Tag der mündlichen Prüfung: 11.03.2025

Table of Contents

Acknowledgments	4
Abstract	5
Zusammenfassung	6
List of important abbreviations and symbols	8
Introduction	9
Soil microorganisms play a central role in the terrestrial carbon cycle	9
Microbial carbon use efficiency as an emergent property of the soil system	10
Microbial growth and its efficiency from a thermodynamic perspective	11
Studying carbon and energy fluxes in soils via calorimetry	12
Process-based modeling of microbial activity in soil	14
Objectives and outline of this thesis	15
General approach and methodology	17
Results	19
Chapter 1: The coupling of carbon and energy fluxes reveals anaerobiosis in an aerobic soil incubation with a <i>Bacillota</i> -dominated community	19
Chapter 2: Spatial substrate heterogeneity limits microbial growth as revealed by the joint experimental quantification and modeling of carbon and heat fluxes	29
Chapter 3: Coupling energy balance and carbon flux during cellulose degradation in arable soils	41
Chapter 4: Bioenergetics of microbial maintenance metabolism in soil	55
Discussion	90
Temporal variations in microbial carbon and energy use efficiency	90
Information content and limitations of the calorimetric ratio	94
Unraveling the complexity of microbial life in soil using bioenergetics	98
Utility of process-based models with coupled microbial carbon and energy turnover	100
Conclusion	103
List of resources	105
References	106
Appendix	118
Supplementary material of Endress et al. (2024a)	118
Supplementary material of Endress et al. (2024b)	145
Supplementary material of Wirsching et al. (2024)	169
Erklärung zur Dissertation	187
Curriculum Vitae	188

Acknowledgments

This thesis would not have been possible without the guidance and support of many people, and I would like to thank all of you for the expertise, the help, and the affirmations you contributed over the past years. In many ways, this work is as much your achievement as it is mine.

First and foremost, I will be forever grateful to Dr. Sergey Blagodatsky, who conceived this research project and supervised my attempt at bringing it to fruition. Thank you for your kind and helpful answers to my countless questions on basic soil science, for revising so many pages of my writing, and for generously saving me lots of hours that would have been spent on trains. It could not have been easy to let your student work from far away Aachen all the time, and I hope you will find this work worthy of your trust and patience. I look forward to continuing our research and learning more authentic buckwheat recipes.

I would also like to express my gratitude to Prof. Dr. Michael Bonkowski for being an inexhaustible source of not only academic expertise but also encouragement and inspiration. I felt your genuine interest and fascination for our research in every conversation, and it was impossible to walk away from such a conversation without having a colorful catalog of new ideas in mind. I am sure that the next years will be just as exciting. Furthermore, I want to say thanks to all members of the terrestrial ecology working group at the University of Cologne. While it would be a stretch to claim that our areas of research overlapped much, our joint conversations and trips to the Mensa were the prime reason for my arduous travels to Cologne!

I also want to thank Prof. Dr. Patrick Fink for reviewing this thesis, and I want to thank Prof. Dr. Thilo Streck, Prof. Dr. Tim Mansfeldt, and Prof. Dr. Christina Bogner for being members of my thesis advisory and examination committees. It is my hope that you will find this research insightful.

Moreover, I am grateful to all my colleagues who provided the data required to calibrate my models. In particular, I want to thank Prof. Dr. Ruirui Chen, Fatemeh Dehghani, and Dr. Johannes Wirsching for performing all of the experiments. If it were not for your hard work, this thesis would be quite literally without substance. In addition, I owe thanks to all of the other members of the SoilSystems SPP. Thank you for many fruitful collaborations and discussions. Let's continue our successful work in the next phase.

Lastly, I am deeply thankful to my family and friends. Thank you to my mother, my father, my stepfather, and all those who raised the scientist and the man I am today. Thank you also to my siblings and my friends, for your understanding whenever my time got stretched too thin to give you the attention you all deserve. Finally, thank you to my partner for your unwavering support of my every endeavor and your unconditional love. I love you.

Abstract

We live in a time of unprecedented global change. Understanding its causes and predicting its consequences are challenges of utmost urgency. In a clash of scales, the future of the global climate system depends in no small part on the activity of the microscopic organisms that inhabit the soils beneath us. They mediate the future of the world's soil organic matter stocks, the single largest terrestrial pool of organic carbon on the planet. Consequently, enormous scientific effort has been invested to unravel the details of soil microbial carbon cycling and carbon use efficiency. Yet, the spatial and temporal heterogeneity of the soil environment and the interactions of many physical, chemical, and biological processes across scales continue to limit our mechanistic understanding of the system.

This thesis contributed to the recent endeavor of establishing a bioenergetic framework for the description of microbial carbon cycling in soil based on thermodynamic principles. Specifically, microbial-explicit process-based models were employed to investigate the coupling between carbon and energy fluxes during soil microbial growth. This involved the theoretical analysis of dynamic model behavior as well as model calibration using specific datasets to facilitate the interpretation of experimental observations.

The results revealed a close correspondence between microbial carbon and energy use efficiency in accordance with thermodynamic predictions. In particular, the models accurately captured the complex temporal patterns in microbial efficiency after the addition of labile substrates. Based on these simulations, the effects of oxygen and nutrient limitation, soil organic matter utilization, and microbial maintenance on the dynamics of microbial growth in several experiments could be disentangled and quantified. The calorespirometric ratio of heat to CO₂ release proved to be a particularly valuable tool for such analyses of experimental data and for the generation of falsifiable hypotheses. In terms of process-based modeling, the explicit incorporation of heat dynamics presented the most important novelty. It was instrumental to both the model calibration and the analytical utility of the models. The strengths, weaknesses, and possible extensions of the approaches presented in this thesis are discussed to highlight promising options for future research.

Overall, the thesis demonstrated the feasibility and utility of microbial-explicit process-based modeling for the analysis of coupled carbon and energy flows in the soil system.

Zusammenfassung

Wir leben in einer Zeit nie dagewesenen globalen Wandels. Das Verständnis seiner Ursachen und die Vorhersage seiner Folgen sind Herausforderungen von höchster Dringlichkeit. Die Zukunft des globalen Klimasystems hängt zu einem nicht geringen Teil von der Aktivität mikroskopisch kleiner Organismen ab, die die Böden unter uns bewohnen. Sie entscheiden über die Zukunft des weltweiten Bestands an organischer Substanz im Boden, dem größten terrestrischen Reservoir an organischem Kohlenstoff auf unserem Planeten. Daher wurden enorme wissenschaftliche Anstrengungen unternommen, um die Einzelheiten des mikrobiellen Kohlenstoffkreislaufs und der Effizienz mikrobieller Kohlenstoffnutzung im Boden zu entschlüsseln. Die räumliche und zeitliche Heterogenität natürlicher Böden und die Wechselwirkungen zahlreicher physikalischer, chemischer und biologischer Prozesse über verschiedene Skalen hinweg begrenzen jedoch weiterhin unser mechanistisches Verständnis dieses Systems.

Diese Arbeit leistete einen Beitrag zu aktuellen Bemühungen, eine bioenergetische Beschreibung des mikrobiellen Kohlenstoffkreislaufs im Boden auf der Grundlage thermodynamischer Prinzipien zu schaffen. Insbesondere wurden prozessbasierte Modelle mikrobieller Aktivität eingesetzt, um die Kopplung zwischen Kohlenstoff- und Energieflüssen während des mikrobiellen Wachstums im Boden zu untersuchen. Dazu gehörte die theoretische Analyse des dynamischen Modellverhaltens sowie die Modellkalibrierung anhand spezifischer Datensätze, um die Interpretation experimenteller Beobachtungen zu ermöglichen.

Die Ergebnisse zeigten eine enge Verbindung zwischen der Effizienz mikrobieller Kohlenstoff- und Energienutzung in Übereinstimmung mit den thermodynamischen Vorhersagen. Insbesondere konnten die Modelle die komplexen zeitlichen Muster der mikrobiellen Effizienz nach der Zugabe von labilen Substraten genau erfassen. Auf Basis dieser Simulationen konnten die Auswirkungen der Sauerstoff- und Nährstofflimitierung, der Nutzung organischer Bodensubstanz und des mikrobiellen Basalstoffwechsels auf die Dynamik des mikrobiellen Wachstums in mehreren Experimenten aufgeschlüsselt und quantifiziert werden. Das kalorespirometrische Verhältnis von Wärme- zu CO₂-Freisetzung erwies sich als besonders wertvolles Instrument für derartige Analysen und für die Formulierung falsifizierbarer Hypothesen. Im Hinblick auf die prozessbasierte Modellierung

stellte die explizite Einbeziehung der Wärmedynamik die zentrale Neuerung dar. Diese war sowohl für die Modellkalibrierung als auch für den analytischen Nutzen der Modelle von entscheidender Bedeutung. Die Stärken, Schwächen und möglichen Erweiterungen der in dieser Arbeit vorgestellten Ansätze wurden diskutiert, um vielversprechende Optionen für die zukünftige Forschung aufzuzeigen.

Insgesamt demonstrierte diese Arbeit die Machbarkeit und den Nutzen einer prozessbasierten mikrobiellen Modellierung für die Analyse gekoppelter Kohlenstoff- und Energieflüsse im Bodensystem.

List of important abbreviations and symbols

C, N	Carbon, Nitrogen
CR	Calorespirometric ratio
CUE	Carbon use efficiency
EUE	Energy use efficiency
ODE	Ordinary differential equation
SOM, SOC	Soil organic matter, Soil organic carbon
γ_X	Relative degree of reduction of compound X
$\Delta_c H_X, \Delta_f H_X$	Combustion and formation enthalpies of compound X
$\Delta_r H_i$	Reaction enthalpy of reaction i

Introduction

Soil microorganisms play a central role in the terrestrial carbon cycle

Soil organic matter (SOM) is the largest reservoir of organic carbon (C) in the terrestrial realm, storing approximately 1700 Pg of soil organic C (SOC). This quantity far exceeds the combined C stocks of vegetation (450 Pg C) and the atmosphere (600 Pg C, Batjes, 2016; Jackson et al., 2017; Canadell et al., 2021). Due to its size, even small shifts in the balance between the C inputs and outputs to this pool can significantly influence atmospheric CO₂ levels and the future of global climate change (Jenkinson et al., 1991; Davidson and Janssens, 2006).

Starting with the seminal work of Jenkinson (Jenkinson, 1966), soil microbial biomass has come to be recognized as the central regulator of this delicate balance (Powlson et al., 2017). It has famously been described as “the eye of the needle through which all organic matter entering the soil must pass” (Jenkinson, 1977), which reflects the fact that the biomass of living microorganisms constitutes only a small percentage of the total SOM pool (Xu et al., 2013). Plants provide the bulk of organic inputs through litter and rhizodeposition, but most of these compounds are subsequently transformed by microorganisms before ultimately contributing to the soil C stock and SOM in the form of microbial necromass and products of microbial metabolism (Lehmann and Kleber, 2015; Kästner et al., 2021; Camenzind et al., 2023). This formation and partial stabilization of anabolic products in soil has also been termed the “microbial carbon pump” and represents a key mechanism of soil C sequestration (Liang et al., 2017).

Yet, microorganisms also drive the opposing C flux via the catabolic decomposition of organic matter and the subsequent release of C into the atmosphere, predominantly in the form of CO₂ (e.g., Crowther et al., 2016). This dual role in SOM formation and decomposition makes soil microbial biomass a critical focus of recent research on global change (Liang et al., 2017; Tao et al., 2023). Despite substantial progress, the future balance of these two contrasting C fluxes - and consequently the future of global SOC stocks - remains uncertain (Bradford et al., 2016; Sulman et al., 2018). Much of this uncertainty arises from the incomplete representation of soil microbial processes in Earth system models (Todd-Brown et al., 2013; Luo et al., 2015; Wieder et al., 2015).

Soil microorganisms and their activity mediate many other critical soil functions beyond SOC turnover. These include the cycling of nitrogen (N) and phosphorus (P), the biodegradation of harmful contaminants, the control of plant diseases, and the formation of soil structure (Vogel et al., 2024). In this sense, soils can be regarded as largely biologically driven systems (Bardgett and Van Der Putten, 2014). Therefore, to achieve a mechanistic understanding of these systems and the functions they provide, it is paramount to understand the microbial life within them.

Microbial carbon use efficiency as an emergent property of the soil system

Soil microorganisms must allocate the C they acquire from their surroundings to numerous processes that are essential for their survival. These processes include the growth of new biomass, maintenance and turnover of internal macromolecules, osmoregulation and other forms of physiological maintenance, formation of storage compounds, synthesis of extracellular enzymes and extracellular polymeric substances (EPS), production of stress response compounds, and many more (van Bodegom, 2007; Schimel and Schaeffer, 2012; Kempes et al., 2017).

Over the past decades, the concept of microbial carbon use efficiency (CUE) has become one of the most important tools for studying this allocation (Manzoni et al., 2018) as well as a central parameter regulating soil C gain or loss in models (Schimel, 2023). Broadly, CUE describes the partitioning of microbial C use between biomass growth on one hand and any number of non-growth processes on the other hand. More specifically, it can be defined as the fraction of organic C consumed by microbes that is directed to anabolic reactions for the formation of new biomass compounds (Hagerty et al., 2018). Given this definition, a high CUE reflects efficient C transformation, e.g., converting litter or rhizodeposits into biomass and, ultimately, microbial necromass or stable SOM compounds. In contrast, a low CUE indicates substantial C losses, typically as CO₂ (Geyer et al., 2020).

The actual value of microbial CUE in soil varies widely and depends on a complex interplay of abiotic and biotic factors. Abiotic conditions such as temperature and soil moisture (Manzoni et al., 2012; Frey et al., 2013), the amount and the quality of organic substrates added to or present in the soil (Sinsabaugh et al., 2013; Blagodatskaya et al., 2014a) as well as nutrient availability (Sinsabaugh et al., 2016) are critical determinants of CUE.

Simultaneously, biotic factors like microbial community composition shape CUE through species-specific metabolic constraints and species interactions (Schimel and Schaeffer, 2012; Geyer et al., 2016; Maynard et al., 2017). Furthermore, the use of C depends on the activity state of the microbial community. Under typical conditions, much of the soil microbial biomass is inactive or dormant, and this inactivity is only interrupted during spatially and temporally limited pulses of substrate supply (Blagodatsky et al., 2000; Blagodatskaya and Kuzyakov, 2013; Kuzyakov and Blagodatskaya, 2015). Given this ubiquity of inactive microbes, their maintenance requirements and the costs of emerging from and returning to dormancy are expected to have significant implications for the overall C utilization in soils (Joergensen and Wichern, 2018; Bölscher et al., 2024; but see Dijkstra et al., 2022).

Given this complex interplay of factors, CUE is an emergent property of the soil system and varies significantly through space and time as well as across scales (Geyer et al., 2016; He et al., 2024). However, it is often represented as a fixed constant in models (Hagerty et al., 2018), creating a disconnect between real-world variability and model assumptions. This mismatch is compounded by ambiguities in CUE definitions, experimental measures, and mechanistic interpretations, which have been the subject of ongoing debate (e.g., Geyer et al., 2019; Bölscher et al., 2024). Consequently, developing a process-based, nuanced description of microbial CUE that accounts for the complexity of microbial life in the soil system is critical to reducing the uncertainty of future SOC dynamics and other soil functions.

Microbial growth and its efficiency from a thermodynamic perspective

Heterotrophic microorganisms, whether in soil or any other environment, rely on the decomposition of organic substrates obtained from their surroundings to survive and proliferate. While the carbon-centered concept of CUE emphasizes this microbial need for C to fuel biosynthesis, the anabolic formation of new biomass compounds is generally endergonic, i.e., characterized by a positive change in Gibbs free energy (ΔG , von Stockar and Liu, 1999) due to the low entropy content of the products. Thus, the decomposition of organic compounds supplies not only the C building blocks for anabolism but also the energy necessary to drive these anabolic processes by coupling them to highly exergonic catabolic reactions. Together, anabolism and catabolism constitute the metabolic processes of an organism, which, to be thermodynamically viable, must collectively yield a net negative ΔG (von Stockar et al., 2006; Heijnen and Kleerebezem, 2010). For this reason, the fluxes and

balances of matter and energy during microbial metabolism are inextricably linked based on the laws of thermodynamics. They ensure that cells remain far from thermodynamic equilibrium and maintain the degree of organization essential for life.

It has long been suspected that this coupling of matter and energy fluxes poses fundamental constraints to microbial life, its origin, and evolution (Lotka, 1922; Schrödinger, 1944; Martin et al., 2008) as well as to the efficiency of microbial metabolism (Jin and Bethke, 2007; Liu et al., 2007). This bioenergetic perspective has been successfully applied to study the growth of microbial cultures under controlled conditions in biotechnology (Roels, 1980; von Stockar and Marison, 1993; Battley, 1996; Braissant et al., 2010). More recently, advances in this field have elucidated how bioenergetics shape the trade-off between growth rate, efficiency, and metabolic versatility more generally (Desmond-Le Quémener and Bouchez, 2014; Calabrese et al., 2021; Chakrawal et al., 2022; Cossetto et al., 2024).

The application of bioenergetic frameworks that consider coupled C and energy fluxes in soil systems has become an active area of research but is still at an early stage (Kästner et al., 2024). Initial studies have begun to evaluate microbial energy use efficiency (EUE) as an additional measure complementing CUE (Harris et al., 2012; Gunina and Kuzyakov, 2022; Wang and Kuzyakov, 2023). Additionally, recent theoretical advances have revealed the thermodynamic control of substrate properties and electron acceptor availability on the decomposition of organic matter (Song et al., 2020; Chakrawal et al., 2022; Zheng et al., 2024). Isothermal microcalorimetry has also been established as a valuable experimental tool for investigating soil microbial activity (e.g., Barros et al., 2010; Herrmann et al., 2014; Boye et al., 2018). Nonetheless, a comprehensive bioenergetic description of soil microbial life based on a combination of experimental, modeling, and theoretical results is only beginning to emerge.

Studying carbon and energy fluxes in soils via calorespirometry

The metabolic reactions performed by soil microorganisms typically produce heat and CO₂ as byproducts, which play a major role in achieving the net negative ΔG required for thermodynamically viable microbial metabolism (Cossetto et al., 2024). Because both heat and CO₂ quickly diffuse out of the soil matrix, they are experimentally accessible through calorimetry and respirometry, respectively. Their combined evaluation via calorespirometry

has become an increasingly popular method for studying the coupling of C and energy fluxes in soil science (Barros et al., 2010, 2011; Herrmann and Bölscher, 2015; Chakrawal et al., 2020b; Yang et al., 2024) and also in biotechnology (Brueckner et al., 2017).

One key metric in this approach is the calorespirometric ratio (CR), defined as the ratio of heat release to CO₂ release. It has long been recognized as a potential indicator of microbial growth efficiency and thus of CUE and EUE (Dejean et al., 2001; Hansen et al., 2004). For instance, in a simple aerobic growth reaction where a single, well-characterized substrate is converted into new biomass and CO₂ (along with heat), the resulting CR depends solely on the biomass yield coefficient and the energy contents of the substrate and biomass (Hansen et al., 2004). This theoretical relationship has been applied to estimate microbial traits such as rate and yield coefficients in soil (Chakrawal et al., 2021) and has also been extended from aerobic respiration to anaerobic fermentations involving well-defined compounds (Chakrawal et al., 2020b).

However, the direct one-to-one correspondence between CR and CUE breaks down under more complex conditions typical of real soil systems (Hansen et al., 2004). In measurements obtained from soil incubations, the CR reflects the combined heat and CO₂ contributions of all physical, chemical, and biological processes occurring in the sample. For example, the reaction of CO₂ with carbonates in alkaline soils, CO₂ dissolution in the soil solution, the presence of multiple active metabolic pathways, or the simultaneous utilization of several substrates, including SOM, can significantly influence the observed CR (Barros et al., 2016; Chakrawal et al., 2020b). SOM utilization is particularly relevant in soil incubation experiments where a defined substrate, such as glucose, is added to the soil. While much of the subsequent CO₂ and heat production is typically fueled by the microbial consumption of the added substrate, soil microbes often also decompose additional native SOM in an effect known as positive priming, e.g., to obtain limiting nutrients (Kuzyakov et al., 2000; Blagodatskaya and Kuzyakov, 2008; Blagodatsky et al., 2010). If the composition and energy content of the decomposed SOM differ markedly from those of the added substrate, the priming effect has the potential to skew experimental CR values.

As a result, the CR also represents a dynamic and emergent property of the soil system, analogous to microbial CUE and EUE. Proper interpretation of observed CR values necessitates a quantitative model of the underlying biogeochemistry (Chakrawal et al.,

2020b). However, such dynamic, process-based frameworks are largely absent from current research. Most studies rely on static CR values or CUE-CR relationships (e.g., Herrmann and Bölscher, 2015; Chakrawal et al., 2020b; Yang et al., 2024) or focus only on the exponential growth phase following substrate addition (Chakrawal et al., 2021).

Process-based modeling of microbial activity in soil

The patterns of microbial activity in soils are remarkably diverse and complex, owing to the spatial and temporal heterogeneity of the soil system and the interplay of physical, chemical, and biological processes across scales (Nunan, 2017; Nunan et al., 2020; Vogel et al., 2024). While many biological processes and interactions occur at the microscopic scale, experimental observations, such as CO₂ and heat fluxes or SOM dynamics, are often accessible only at macroscopic scales, such as laboratory soil samples, profiles, landscapes, or entire ecosystems (Smercina et al., 2021). This disparity in scale underscores the need for mechanistic modeling frameworks that can identify, connect, and quantify the processes underpinning microbial activity to provide meaningful insights into soil system behavior.

Foundational biogeochemical models of soil C dynamics, such as CENTURY (Parton et al., 1987) and Roth-C (Jenkinson, 1990), date back to the 1980s and laid the groundwork for understanding SOM dynamics by partitioning SOM into distinct pools with defined turnover times. These models, however, originally did not explicitly represent microbial activity. Since then, considerable effort has been put into developing more complex models that incorporate the active role of microorganisms. Notable examples include the MEND model, which simulates explicit enzymatic depolymerization of SOM as well as active and dormant fractions of microbial biomass (Wang et al., 2015), or the MIMICS model, which divides microbial biomass into two functional groups corresponding to microbes with copiotrophic and oligotrophic life history strategies (Wieder et al., 2014).

Despite these developments, several observers have pointed out persistent challenges and limited progress when it comes to scaling microbial processes in models, including the representation of microbial CUE and priming effects (Sulman et al., 2018; Bernard et al., 2022; Baveye, 2023; Schimel, 2023). They suggest that a deeper understanding of the processes and boundary conditions at the microscopic scale is required to tackle these shortcomings. This is in line with recent calls for a shift towards models based on established

physical rules instead of empirical correlations (Tang et al., 2024). This shift may also help to address the issue of calibration equifinality, the phenomenon that different sets of parameters can yield equally good model agreement with observed data (Beven and Freer, 2001). Equifinality and parameter non-identifiability are widespread even in simple biogeochemical models (Sierra et al., 2015; Marschmann et al., 2019) and continue to represent a major hurdle (Wieder et al., 2015).

The incorporation of thermodynamic principles and bioenergetic constraints into biogeochemical models offers a promising avenue to address these limitations and research needs. Thermodynamics may be leveraged to directly constrain the rates and yield coefficients of specific microbial reactions (Brock et al., 2017; Song et al., 2020; Ugalde-Salas et al., 2020; Zheng et al., 2024). For example, dynamic energy budget (DEB, Kooijman, 1993) models that couple bioenergetics with genome-informed microbial traits represent one of the latest and most ambitious developments in the microbial-explicit modeling of soil biological processes (Marschmann et al., 2024). Beyond such theoretical improvements to model development and parameterization, rates of heat release measured via microcalorimetry also provide additional data at high temporal resolution for the calibration and validation of dynamic models. While this approach has been applied in biotechnological contexts to some extent (Maskow and Babel, 2003; Braissant et al., 2013), its application to soil samples has barely been explored (Chakrawal et al., 2021).

Objectives and outline of this thesis

In this thesis, I apply process-based bioenergetic models to study the coupling between C and energy fluxes during microbial activity in soil. In particular, I focus on the analysis of temporal patterns in microbial CUE and EUE as well as the CR after the addition of labile substrates. This investigation aims to address the research questions and limitations outlined above, which can be summarized as follows:

1. Advance the mechanistic understanding of microbial CUE to reflect its emergent properties and characterize its relationship with microbial EUE
2. Identify the utility and the limitations of the CR for the analysis of microbial activity in soil using a dynamic framework

3. Incorporate heat flow in dynamic models of microbial C cycling and demonstrate its utility for model calibration and data interpretation

The thesis is structured into four major chapters, each of which provides specific contributions to achieve these objectives.

In the first chapter (Endress et al., 2024a), I examine the effect of limited terminal electron acceptor (TEA) availability on microbial CUE, EUE, and CR. Specifically, I analyze and model the dynamics of these quantities during a gradual transition from aerobic respiration to anaerobic fermentations as the dominant metabolic pathways after glucose addition. This research represents the extension and dynamic application of recent theoretical advances on this issue (in particular, Chakrawal et al., 2020b). It also demonstrates a close link between shifts in microbial metabolism as seen in the CR and microbial community composition.

In the second chapter (Endress et al., 2024b), I explore the consequences of spatial substrate heterogeneity and the resulting local nutrient limitation on the kinetics as well as the CUE, EUE, and CR of microbial growth after glucose addition. The study shows strong correlations between C and energy release from soil independent of incubation conditions, and it demonstrates that differences in growth kinetics do not necessarily translate to differences in growth efficiency. It also highlights the sensitivity of dynamic CR measurements to details of the incubation setup and outlines both experimental and modeling approaches to address this limitation.

In the third chapter (Wirsching et al., 2024), I investigate the CUE, EUE, and CR of microbial growth on cellulose as a more complex substrate in a diverse set of arable soils. The results illustrate the utility and the limitations of several estimates of microbial CUE and EUE over the course of longer incubations. In addition, they reveal a substantial positive priming effect in all studied soils and demonstrate how heat flow measurements can be leveraged to estimate the energy content of primed SOM.

In the fourth and final chapter (Endress and Blagodatsky, *in prep.*), I present a theoretical investigation of the consequences of microbial maintenance metabolism for the dynamics of, and connections between, CUE, EUE, and the CR. The analysis predicts distinct temporal patterns of these quantities, particularly during the lag and retardation phases of microbial growth after substrate addition. To connect the theory with empirical evidence on the

energetics of microbial non-growth metabolism, I compile data on the CR and the energy content of SOM in unamended soils from the literature. The compilation reveals a close positive relationship between these two quantities in arable soils and an inverse relationship in forest soils.

General approach and methodology

This dissertation employs dynamic, process-based modeling of microbial growth based on systems of ordinary differential equations (ODEs). In the first three chapters, such systems are constructed to investigate specific aspects of microbial growth, such as anaerobic metabolic pathways (Endress et al., 2024a), nutrient limitation (Endress et al., 2024b), and cellulose decomposition and SOM priming (Wirsching et al., 2024). The parameters governing the behavior of these systems are calibrated using experimental datasets provided by collaboration partners to analyze and interpret the results of their experiments. In the fourth chapter, ODE systems are analyzed theoretically without calibration relative to specific datasets to explore the theoretical relationships between quantities of interest. The mathematical and conceptual details of the dynamic models as well as the numerical integration and calibration procedures are described in the individual publications and their respective supplementary materials. Below, I provide a general overview of this methodology and the underlying rationale.

Each model featured in this dissertation simulates the dynamics of at least 5 key variables per gram dry weight of a soil sample. These include the concentrations of added substrate (glucose or cellulose) and microbial biomass, the active fraction of microbial biomass, the cumulative CO₂ release, and the cumulative heat release. All concentrations of carbon compounds (substrate, biomass, CO₂) are expressed in units of mol C (per gram soil).

A major novelty of these models is the incorporation of the heat variable, which is integral to achieving all of the thesis objectives outlined above. Specifically, it allows for the analysis of microbial EUE and the CR, and together with CO₂ release, it represents the primary variable used for model calibration. If sufficient experimental estimates are available, microbial biomass is also used for model calibration.

To simulate the dynamics of heat release and to couple the carbon and energy balances, it is necessary to ascribe specific heat production rates to all relevant biochemical reactions. In

general, this rate is given by the reaction enthalpy, which can be calculated from the enthalpies of combustion or formation of all of the involved reactants and products via the law of Hess (Chakrawal et al., 2020b; Kästner et al., 2024). If these enthalpies are not known or if the involved compounds are poorly characterized, their energy contents are estimated via Thornton's rule (Thornton, 1917) based on their relative degrees of reduction γ . The degree of reduction, in turn, can be calculated from the number of atoms of major elements in the compounds. Alternatively, they may also be treated as free parameters during model calibration.

The active fraction of microbial biomass is a critical model component that is required to adequately describe the observed kinetics over the full course of the incubation. In particular, this includes the initial lag phase after substrate addition, the exponential growth phase, and the eventual retardation phase after substrate depletion. In this dissertation, I use the index of physiological state, $r \in [0, 1]$, to model the dynamic transition of microbes between active (fraction r) and inactive (fraction $1-r$) states. This framework was established by Panikov (Panikov, 1995) and has frequently been used to describe the activity of soil microbial biomass (e.g., Blagodatsky and Richter, 1998; Blagodatsky et al., 2000; Wutzler et al., 2012; Chakrawal et al., 2021). In addition, I also incorporate dynamic switching from exogenous maintenance fueled by the consumption of external substrate to endogenous maintenance fueled by the consumption of biomass after substrate completion (Wang and Post, 2012).

The numerical integration, calibration, and analysis of the ODE systems were implemented in the Python programming language. Since the incorporation of the activity variable r tends to introduce considerable stiffness into these systems, they were numerically integrated using the *radau* method as implemented in the *solve_ivp* function of the *scipy.optimize* package (Virtanen et al., 2020). Several approaches were employed for the calibration and uncertainty quantification of parameter values in these models, including classical nonlinear least-squares optimization via the Levenberg-Marquardt algorithm (Levenberg, 1944; Marquardt, 1963) combined with the Akaike Information Criterion (AIC, Banks and Joyner, 2017) as well as Bayesian approaches using Markov chain Monte Carlo (MCMC) methods (Foreman-Mackey et al., 2013; Valderrama-Bahamóndez and Fröhlich, 2019).

Results

For high-resolution versions of all figures, please refer to the online versions of the published articles.

Chapter 1: The coupling of carbon and energy fluxes reveals anaerobiosis in an aerobic soil incubation with a *Bacillota*-dominated community

Publication:

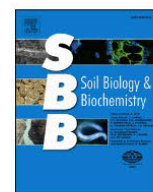
Endress, M.-G., Chen, R., Blagodatskaya, E., Blagodatsky, S., 2024a. The coupling of carbon and energy fluxes reveals anaerobiosis in an aerobic soil incubation with a *Bacillota*-dominated community. *Soil Biology and Biochemistry* 195, 109478. doi:[10.1016/j.soilbio.2024.109478](https://doi.org/10.1016/j.soilbio.2024.109478)

Declaration of personal contributions:

I am one of the first authors and the corresponding author of this publication. The first authorship is shared with R. Chen, who performed all experimental work presented in the study and prepared a first draft of the manuscript based on experimental results. I performed all modeling work and all quantitative analyses. Specifically, I designed the dynamic model and performed all numerical simulations, model calibration, and statistics, and wrote the code required for these tasks. I revised and extended the first draft of the manuscript to reflect the new scope and content of the study. I prepared the final version of the manuscript except for experimental methods with input from all co-authors. I prepared all figures and all supplementary material other than Figure S3 and SI OTU Table with input from all co-authors. I handled revisions with input from all co-authors.

Data availability statement:

All data analyzed during this study are included in this published article and its supplementary files. All code is available from the corresponding author upon reasonable request.



The coupling of carbon and energy fluxes reveals anaerobiosis in an aerobic soil incubation with a *Bacillota*-dominated community

Martin-Georg Endress^{a,*}, Ruirui Chen^{b,1}, Evgenia Blagodatskaya^c, Sergey Blagodatsky^a

^a Institute of Zoology, University of Cologne, 50923, Cologne, Germany

^b College of Chemical Engineering, Nanjing Forestry University, Nanjing, 210037, China

^c Department of Soil Ecology, Helmholtz Centre for Environmental Research – UFZ, 06120, Halle/Saale, Germany

ARTICLE INFO

Keywords:

Carbon use efficiency
Heat release
Bioenergetics
Fermentation
Microbial growth
Anaerobic

ABSTRACT

Soil microorganisms rely on coupled fluxes of carbon and energy to fuel their maintenance, to switch from dormancy to activity and to grow under dynamically changing conditions in microhabitats. To identify the principles underlying this coupling, we measured heat and CO₂ release from soil after glucose addition along with estimates of microbial biomass and community composition. The results revealed bi-directional deviations of the ratio of heat to CO₂ release (Calorespirometric Ratio, CR) that are inconsistent with theoretical predictions for aerobic respiration, which is commonly assumed to be the major metabolic pathway in incubation experiments. Moreover, the microbial community was dominated by members of the *Bacillota*, whose relative abundance increased from 4 percent to 65 percent in 18 h. To interpret these findings, we developed a dynamic model of carbon and energy fluxes during the microbial growth on glucose. The model simulates aerobic respiration as well as anaerobic fermentation pathways to lactate, acetate and propionate depending on the time-varying availability of O₂. Simulations captured the observed temporal CR pattern and suggested a gradual depletion of O₂ and a shift to anaerobic pathways as the main driver. This interpretation is consistent with the dominance of *Bacillota*, many members of which are well adapted to anaerobic conditions. Our results highlight the potential of the joint analysis of matter and energy fluxes in combined experimental and modeling approaches and indicate the presence of facultative anaerobiosis under common experimental conditions, which could confer a competitive advantage to certain microbial taxa during growth on labile substrate.

1. Introduction

Microorganisms mediate the carbon (C) fluxes in soils and are of critical importance for the global C cycle (Bardgett et al., 2008; Liang et al., 2017; Crowther et al., 2019). They release CO₂ to the atmosphere through the decomposition of organic matter on the one hand while contributing to soil organic matter (SOM) formation via the so-called microbial carbon pump on the other hand (Liang et al., 2017; Kästner et al., 2021; Camenzind et al., 2023). Yet, substantial uncertainty about the future balance of these two opposing C fluxes remains (Luo et al., 2015; Bradford et al., 2016, 2019; Sulman et al., 2018).

The fraction of C consumed by microbes that is channeled through anabolism to form new biomass, broadly termed the microbial carbon use efficiency (CUE), has been the subject of a large number of studies (Manzoni et al., 2018). CUE as an emergent property of the soil system

depends on many factors, including temperature and nutrient availability (Manzoni et al., 2012; Frey et al., 2013; Sinsabaugh et al., 2016), substrate quality and quantity (Sinsabaugh et al., 2013; Blagodatskaya et al., 2014), species-specific metabolic constraints and interspecific interactions (Geyer et al., 2016; Maynard et al., 2017). Consequently, CUE exhibits significant spatial and temporal variability. Despite the importance of the concept, its definition, determination, and interpretation remain ambiguous (Manzoni et al., 2012; Hagerty et al., 2018; Geyer et al., 2019), leaving us with an insufficient understanding of CUE patterns in time and space.

The integration of a bioenergetic perspective has the potential to identify principles underlying the CUE and soil C dynamics (Barros et al., 2010; Herrmann et al., 2014; Barros, 2021). All organisms rely on coupled mass and energy fluxes from the decomposition of substrates, and calorimetric measurements of heat release have been employed in

* Corresponding author.

E-mail address: m.endress@uni-koeln.de (M.-G. Endress).

¹ These authors contributed equally to this work.

<https://doi.org/10.1016/j.soilbio.2024.109478>

Received 7 November 2023; Received in revised form 22 April 2024; Accepted 16 May 2024

Available online 17 May 2024

0038-0717/© 2024 Published by Elsevier Ltd.

fields such as biotechnology to characterize microbial growth and metabolism (Roels, 1980; von Stockar and Marison, 1993; Braissant et al., 2010). When combined with measurements of CO_2 , the joint evaluation of energy and C balances can yield insights into metabolic processes and constraints (Calabrese et al., 2021; Chakrawal et al., 2022). In particular, the so-called Calorespirometric Ratio (CR) of heat to CO_2 release provides a useful tool for the analysis of microbial metabolic activity and energetics (Dejean et al., 2001; Hansen et al., 2004) (Fig. 1). For example, CR values have been linked theoretically to the CUE of microbial growth in simple cases like aerobic respiration of a single substrate (Hansen et al., 2004).

Such a bioenergetics perspective has been leveraged to investigate soil processes, but the research is still in an early stage (Barros et al., 2010, 2011, 2016; Herrmann and Bölscher, 2015; Boye et al., 2018; Chakrawal et al., 2020). Similar to CUE, the observed CR represents an emergent property reflecting the sum of all heat and CO_2 contributions from biological, chemical and physical processes in the soil (Barros et al., 2016). Its interpretation thus requires assumptions about the dominant sources of heat and CO_2 , including a biochemical model of the active microbial metabolic pathways (Hansen et al., 2004; Chakrawal et al., 2020). Many of the studies focusing on CUE and CR rely on the addition of a single C source and frequently also assume the aerobic decomposition of these substrates. Under such assumptions, theoretical predictions for the CR can be readily obtained, and any deviations indicate the presence of additional processes contributing to heat or CO_2 production (Hansen et al., 2004; Maskow and Paufler, 2015; Wadsö and Hansen, 2015), e.g., substrate use via anaerobic pathways common in heterogeneous soil micro-habitats (Boye et al., 2018; Chakrawal et al., 2020). Additionally, measured CR values often vary significantly over the course of experiments, but this temporal variability and its causes have received little attention and need to be further studied in a dynamic setting (Barros et al., 2010; Boye et al., 2018; Chakrawal et al., 2021).

Shifts in the microbial community introduce another source of complexity and are frequently found in soil after input of labile substrates (Eilers et al., 2010; Mau et al., 2015; Morrissey et al., 2016, 2017; Papp et al., 2020). Such shifts may alter the metabolic capability and efficiency of the community, which would in turn be reflected in CR. Addition of glucose in particular has been observed to induce the dominant growth of one or few phyla (Mau et al., 2015; Morrissey et al.,

2017; Papp et al., 2020), although these dynamics have not been monitored at high resolution.

The obscure nature of the soil system as compared to, for example, pure cultures, renders quantitative modeling efforts a necessary tool to disclose the complex interplay of the various processes. Specifically, there is a need for mechanistic modeling frameworks linking the heat production, thermodynamic constraints and carbon balance, a challenging task that has only recently been tackled in the context of soils (Chakrawal et al., 2021; Bajracharya et al., 2022).

In this study, we obtain both calorespirometric and community composition data during microbial growth in soil after the single-pulse addition of glucose. Based on the experimental setup, we expected the aerobic decomposition of glucose to be the major metabolic pathway, with a corresponding CR roughly in the range between 380 kJ/mol C (efficient aerobic growth) and 469 kJ/mol C (aerobic catabolism of glucose). Any deviations of the CR from this range would indicate the presence of additional processes such as shifts in the soil microbial community or metabolic pathways. Generally, copiotrophic taxa are expected to dominate after a pulse of labile substrate (Fierer et al., 2007), with phyla such as the *Pseudomonadota* (previously *Proteobacteria*) and *Actinomycetota* (previously *Actinobacteria*) growing disproportionately in previous studies (Eilers et al., 2010; Mau et al., 2015; Morrissey et al., 2017). Finally, we develop a microbial-explicit dynamic model of carbon and energy flows during microbial growth, including aerobic and anaerobic metabolic pathways as well as microbial dormancy, to analyze and interpret our experimental observations.

2. Materials and methods

2.1. Soil

The soil was collected in September 2014, after the harvest of maize from the upper 15 cm of a long-term field fertilization experiment located at the Fengqiu Agroecological Experimental Station (35°00' N, 114°24' E), Henan province, China. The soil is classified as Aquic Inceptisol, derived from alluvial sediments of the Yellow River. The soil, with a sandy loam texture, contained 6.4 g kg⁻¹ organic C, 18.0 g kg⁻¹ total C, 0.55 g kg⁻¹ total N, 0.71 g kg⁻¹ total phosphorus, and 21.3 g kg⁻¹ total potassium (K). The soil had a pH (H_2O , 1:4) of 8.45 and water holding capacity (WHC) of 29% (w/w). Before use, roots and other plant residues were carefully removed, and then the soil was sieved <2 mm and stored at 4 °C.

2.2. Experimental design

Two subsets of soil samples were incubated with glucose addition in parallel for time-course sampling. The first subset with 5 g soil in 20-ml glass containers tightly sealed with butyl rubber stoppers (Nichiden-Rika Glass Co. Ltd, Japan) was used for analysis of gas emissions and microbial growth. Before incubation, glucose was added at a rate of 2 mg g⁻¹ soil. A mixture solution containing 1.9 mg g⁻¹ $(\text{NH}_4)_2\text{SO}_4$, 2.25 mg g⁻¹ K_2HPO_4 and 3.8 mg g⁻¹ $\text{MgSO}_4 \cdot 7\text{H}_2\text{O}$ was added and then distilled water was supplemented to reach the final soil moisture of 60% WHC. Containers were incubated in a dark chamber at 28 °C and remained tightly closed during the incubation. The gas emissions were monitored at 0, 20 min, 1, 2, 4, 6, 8, 10, 12, 14, 16 and 18 h (see section 2.3 below). When sampling, three replicated containers were taken, firstly to collect gas samples and then opened to collect soil samples. In total, 36 containers were prepared for the first subset.

The second subset, with three replicates of 1 g soil in glass ampoules, was used for isothermal calorimetric measurement (keeping the depth of the soil layer and the gaseous-to-solid phase ratio equal to those in subset 1). Before calorimetric measurements, the soil was pre-equilibrated at the calorimeter temperature (28 °C) for 4 h. The calorimeter is a TAM III (TA Instruments, Utah, USA) with 6 measuring channels in the same chamber. The rates of glucose and mineral salt

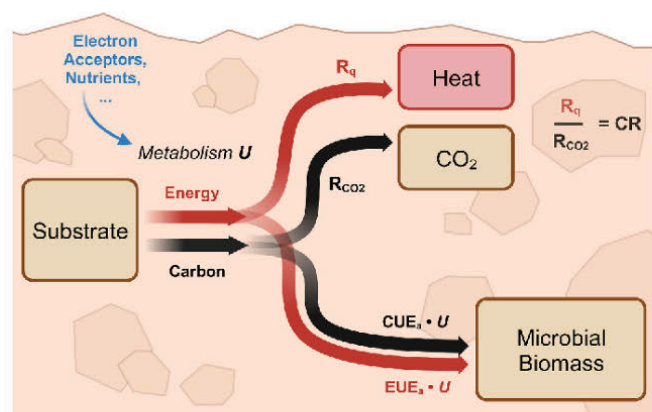


Fig. 1. Schematic of coupled carbon and energy fluxes during microbial substrate uptake in soil. Microbes metabolize available substrates at a rate U to grow and to fuel their maintenance requirements. Only a fraction of the carbon and energy contained in the consumed substrate can be converted to new biomass, depending on the apparent carbon and energy use efficiencies (CUE_a , EUE_a) of the metabolism under the prevailing environmental conditions. The remainder is released as heat and CO_2 with rates R_q and R_{CO_2} , respectively, and can be measured experimentally. Studying the temporal dynamics of the so-called Calorespirometric Ratio (CR) of heat to CO_2 release, R_q/R_{CO_2} , has the potential to elucidate the underlying metabolic processes.

addition were identical to the first subset. Immediately after glucose addition, the ampoules with the treated soils were put into the calorimeter system controlled at 28 °C. The heat flow was continuously monitored and recorded on a computer.

2.3. Analysis of the gaseous phase

Gas probes were sampled from the closed container using a gas-tight syringe. CO₂, N₂O and CH₄ concentrations were analyzed by gas chromatography (Agilent 7890 A, Agilent Technologies) using a flame ionization detector. Gas samples were firstly introduced by a refitted injector, then separated with a 2-m stainless steel column (2 mm in the inner diameter), filled with 13 XMS (60/80 mesh, Sigma-Aldrich Co., St. Louis, MS). The operating column temperature was set at 55 °C and the detector temperature at 250 °C. Cumulative CO₂ emission was expressed as µg C g⁻¹ soil, based on the CO₂ concentration in the closed container. Rates of CO₂ release were estimated as differences in the cumulative values between subsequent time steps.

The soil used in this study is characterized by a high pH of 8.45 owing to high levels of Calcium at the site (~33 g kg⁻¹) (Xin et al., 2019). Such alkaline conditions have the potential to strongly bias CO₂ estimates due to a significant fraction of C remaining in solution as (bi-) carbonates (Martens, 1987; Sparling and West, 1990; Oren and Steinberger, 2008). Therefore, we corrected our measured CO₂ emissions by accounting for additional soil C in carbonate form in the presence of CaCO₃, following calculations in (Mook, 2000). Details are shown in SI methods (section A).

2.4. Quantitative polymerase chain reaction and high-throughput sequencing of 16S rRNA genes

DNA extraction from 0.5 g soil samples was performed using the FastDNA SPIN Kit for soil (MP Biomedicals, Santa Ana, CA). The extracted genomic DNA was dissolved in 50 µL of TE buffer and stored at -20 °C for subsequent use.

The abundances of 16S rRNA gene were estimated via real-time qPCR, using a C1000Tm Thermal Cycler (Bio-Rad, CA, USA). Bacteria were quantified with primer set 519F/907 R. Each qPCR reaction was performed in a 20-µL mixture containing 10 µL of SYBR Premix Ex Taq (Takara, TaKaRa Biotechnology), primer sets (0.2 µM each), 1 µL template DNA diluted 10-fold. A 10-fold series of dilution of the plasmid DNA was then carried out to generate a standard curve covering 10³ to 10¹¹ copies of the template per assay. Blanks were always run with water instead of DNA extract. The final 16S rRNA gene quantities were obtained by calibrating against total DNA concentrations extracted from the soil. As the soil used in our experiment was free of fresh plant residues, we assumed that the content of plant-originated DNA was negligible and did not exceed 3% (Gangneux et al., 2011).

High-throughput sequencing was performed with Illumina Miseq sequencing platform (Illumina Inc.). PCR amplification was conducted for bacteria with primer set 519F/907 R. For detailed sequencing procedures, please refer to (Jing et al., 2017). After completing the sequencing process, the 16S data were analyzed using the Quantitative Insights Into Microbial Ecology (QIIME) pipeline, following the guidelines provided by Caporaso et al. (2010). Sequences were binned into OTUs using a 97% identity threshold, and the most abundant sequence from each OTU was selected as a representative sequence for it. Taxonomy was assigned to OTUs with reference to a subset of the SILVA 119 database (<http://www.arb-silva.de/download/archive/qiime/>).

2.5. Calculations

Soil bacterial biomass C (BBC) and microbial biomass C (MBC). BBC during the incubation process was evaluated by bacterial 16S rRNA gene copy number with Eqn (1) on the level of phylum:

$$BBC = AC \cdot \sum_i \frac{N_{gene} \cdot RA_{P_i}}{AG_{P_i}} \quad (\text{Eq. 1})$$

in which BBC was bacterial biomass C; N_{gene} was total bacterial 16S rRNA gene copy number obtained by qPCR; RA_{P_i} was the relative abundance of certain bacterial phylum obtained by high-throughput sequencing (Supplementary Data S1), AG_{P_i} was the average gene copy number per cell of a certain bacterial phylum (Sun et al., 2013)(Supplementary Table S1); and AC was an average of 20 fg C per bacterial cell (Baath, 1994). We further evaluated soil microbial biomass C (MBC) by the initial rate of substrate-induced respiration (SIR) (Anderson and Joergensen, 1997) as an independent estimate in addition to BBC. The rate of CO₂ production was converted to microbial biomass as proposed by Anderson and Domsch (1978) using the conversion factor for arable soils suggested by Kaiser et al., (1992) with further correction for incubation temperature as detailed in (Beck et al., 1997). We also estimated the lag time and the initial active fraction of biomass from the rate of CO₂ emission during the exponential growth phase as described in (Blagodatsky et al., 2000; Wutzler et al., 2012) (details in SI methods, section B).

Calorespirometric Ratio. CR over the course of the incubation was calculated from the experimental rates of heat and CO₂ release:

$$CR = \frac{R_q}{R_{CO_2}}, \quad (\text{Eq. 2})$$

where R_{CO_2} is the rate of CO₂ release estimated from the change in cumulative CO₂ emissions and R_q is the rate of heat release measured by calorimetry and binned according to the time points with available CO₂ estimates. Specifically, heat release rates were averaged over the corresponding time intervals between subsequent measurements of (cumulative) CO₂.

Carbon use efficiency. We calculated two different estimates of apparent CUE, following the definitions of Hagerty et al. (2018). To evaluate temporal patterns, we calculated 'biomass-based CUE' (CUE_B) as the ratio of ΔMBC to the sum of ΔMBC and cumulative CO₂ release for each time period between subsequent cumulative measurements:

$$CUE_{B,i} = \frac{\Delta MBC_i}{\Delta MBC_i + \Delta_i CO_2^{cumu}} \quad (\text{Eq. 3})$$

Here, ΔMBC_i and $\Delta_i CO_2^{cumu}$ denote the change in MBC and cumulative CO₂ during each time period i between subsequent measurements of the two carbon pools, respectively, and CUE_{B,i} provides an estimate of carbon use efficiency during that period.

In addition, we also estimated a 'concentration-based CUE' (CUE_C) as the ratio of total MBC increase (ΔMBC) to total substrate depletion (ΔS):

$$CUE_C = \frac{\Delta MBC}{\Delta S} \quad (\text{Eq. 4})$$

Eq. (4) was evaluated after 18 h at the end of the experiment, assuming that all added substrate was consumed by microbes at this time.

2.6. Modeling

We developed a dynamic model simulating the carbon and energy fluxes during microbial decomposition of glucose in soil to further explore and interpret the experimental results.

The model structure (Fig. 2) includes four carbon pools (biomass, glucose, lactate and the final fermentation products acetate and propionate) and builds on the framework published by Chakrawal et al. (2020). It represents the metabolism of added glucose (U_{glu}) and of subsequently formed lactate (U_{lac}) fueling microbial growth via aerobic respiration as well as fermentation pathways, where the uptake follows Monod kinetics and is partitioned among the metabolic pathways

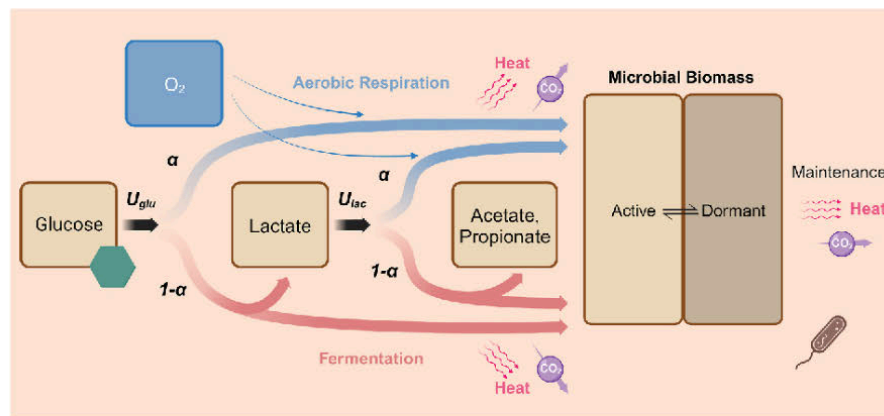


Fig. 2. Schematic of the modeling framework used to investigate the temporal dynamics of the Calorespirometric Ratio during microbial growth on glucose. Microbes take up glucose at a total rate of U_{glu} , a fraction $\alpha \cdot U_{glu}$ of which is metabolized aerobically via respiration according to O_2 availability, while the remaining fraction $(1 - \alpha) \cdot U_{glu}$ is metabolized anaerobically and fermented to lactate. Similarly, lactate is metabolized at a total rate U_{lac} and respired aerobically (at rate $\alpha \cdot U_{lac}$) or fermented further to acetate and propionate (at rate $(1 - \alpha) \cdot U_{lac}$). These four metabolic pathways fuel the growth and maintenance of the active part of the microbial biomass pool as well as the maintenance requirement of its inactive part. The active fraction of microbial biomass changes according to total substrate availability. All processes release heat and CO_2 at specific rates that contribute to the overall CR of the system.

depending on the time-varying availability of oxygen (aerobic fraction, α). We also account for the physiological state of the microbial population by modeling transitions between a growing and a dormant subpopulation according to substrate availability (Panikov, 1996; Blagodatsky et al., 2010).

The system of ordinary differential equations was implemented in Python and numerical integration was carried out using the *solve_ivp* routines in the *Scipy* package (Virtanen et al., 2020). The model was fit to the experimental results for the rate of heat production, the cumulative CO_2 release as well as biomass estimates. Best-fit parameters were obtained using the Levenberg-Marquardt algorithm as implemented in the *minimize* function of the *lmfit* package (Newville et al., 2023). Parameter uncertainty and the corresponding sensitivity of model output was analyzed using a Markov chain Monte Carlo ensemble sampler as implemented in the *emcee* package (Foreman-Mackey et al., 2013), with uniform prior distributions around the best-fit estimates for all parameters.

The detailed model formulation and numerical procedures are described in SI methods (section C) and all modeling code is available from the corresponding author upon reasonable request.

3. Results

Heat release, CO_2 release and bacterial 16S rRNA copy number.

The dynamics of heat and CO_2 release as well as gene copy number displayed the typical pattern of microbial growth after substrate addition (Fig. 3A and B). After an initial lag period of 5.8 h, all variables

increased exponentially and maximum rates of heat and CO_2 release were achieved after 12 h of incubation, with growth slowing down during the following retardation phase. We also observed small but steadily increasing N_2O emissions for the first 9 h, followed by a peak after 15 h when rates of CO_2 and heat release were already in decline (Supplementary Fig. S1). No CH_4 was released during the incubation (Supplementary Fig. S2).

Calorespirometric Ratio. The CR calculated from measured rates of heat and CO_2 release showed a pronounced temporal pattern with a gradual initial increase from 400 kJ/C-mol to a maximum of 525 kJ/C-mol after 11 h, followed by a drop around the time of peak activity to 233 kJ/C-mol after 17 h (Fig. 3C). These values deviate remarkably from the expected CR for simple aerobic growth on glucose, which is predicted to vary in the range of ~380–469 kJ/C-mol, depending on the growth yield of the microbial community (Hansen et al., 2004; Chakrawal et al., 2020).

Microbial community composition and biomass. Initial MBC was estimated as 152 μg C/g via substrate-induced respiration, while initial BBC calculation from gene copy numbers according to equation (1) yielded 146 μg C/g. This result corroborates our assumption that growth during the incubation is well represented by bacterial growth. Based on this observation and the lack of independent biomass measurements, we used the BBC estimates based on copy number for further analysis of biomass dynamics, assuming that other (e.g., fungal) contributions remained small during the experiment. After 18 h of incubation, biomass increased from 146 μg C/g to 517 μg C/g or 3.5 times initial MBC due to microbial growth.

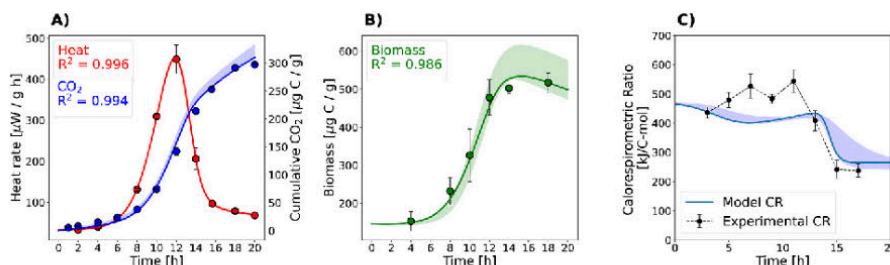


Fig. 3. Experimental observations of heat, CO_2 , biomass and CR (mean \pm SD) along with results of the calibrated dynamic model (best fit \pm range). **A** The dynamics of heat release (red, $n = 3$ replicates) and cumulative CO_2 emissions (blue, $n = 3$ replicates per point) are accurately reproduced by the calibrated model. Symbols may obscure small standard deviations. **B** The model adequately captures the experimental biomass dynamics estimated from gene copy numbers ($n = 3$ replicates per point). **C** CR derived from experimental rates of heat and CO_2 release reveals a pronounced temporal pattern with high values during exponential growth and small values during the onset of growth retardation.

To evaluate bacterial community composition, all soil samples were rarefied to 19798 sequences. A wide diversity of bacteria was observed in the initial soil at 20 min, with representatives categorized into nine dominant phyla (>1% mean relative abundance). These were *Pseudomonadota* (31.19%), *Actinomycetota* (15.67%), *Acidobacteriota* (9.40%, previously *Acidobacteria*), *Bacteroidota* (6.25%, prev. *Bacteroidetes*), *Planctomycetota* (4.66%, prev. *Planctomycetes*), *Bacillota* (4.41%, prev. *Firmicutes*), *Chloroflexota* (2.50%, prev. *Chloroflexi*), *Cyanobacteria* (1.57%) and *Nitrospirota* (1.42%, prev. *Nitrospira*), together accounting for 82.4% of all OTUs.

However, the microbial community changed drastically over the course of the experiment, with members of the *Bacillota* constituting $65\% \pm 3\%$ (Mean \pm SD) of all OTUs after 18 h of growth and decreased relative abundance of all other phyla (Fig. 4). While these bacteria still represented only $6.6\% \pm 0.4\%$ of all OTUs after 4 h of incubation, they already expanded to $33\% \pm 5.7\%$ of OTUs after 8 h during the early exponential growth phase and continued to grow disproportionately for the full duration of the experiment (Fig. 4).

In terms of estimated biomass, the *Bacillota* only accounted for 1.9% of initial MBC, yet their dominant growth corresponded to 62.2% of the estimated MBC increase and resulted in this phylum accounting for 45.2% of total estimated MBC after 18 h. This still rendered them the dominant phylum in terms of MBC, followed by the *Pseudomonadota* with an estimated 12.1% of MBC after 18 h.

This pattern was also consistent across replicates, with a similar share of *Bacillota* for all replicates at each measurement time (Supplementary Fig. S3). The full OTU table that includes the taxonomic assignments and relative abundances for all replicates is provided as a supplementary material (SI OTU Table).

Model results. The full model achieved an excellent fit to the measured rates of heat and CO₂ release as well as the available biomass estimates (Fig. 3A and B) and captured the characteristic growth dynamics typically observed in batch culture. Total biomass increased from the initial 150 $\mu\text{g C/g}$ to just above 500 $\mu\text{g C/g}$ after 18 h, mirroring experimental estimates. The model reproduced key features of the temporal pattern observed in the experimental CR (Fig. 3B). In particular, the timing and magnitude of the drop in CR to around 230 kJ/C-mol during the retardation phase after peak heat and CO₂ release was accurately reflected in simulations. Moreover, the dynamics show the increasing tendency in CR around the time of peak metabolic activity at 12 h of incubation time. However, the model displays an initial drop in CR from around 480 kJ/C-mol to 420 kJ/C-mol during the lag and early exponential phase (first 7 h), in contrast to the continuous increase observed in the experimental values. A full list of parameter estimates is given in Supplementary Table S2 and posterior distributions are shown in Supplementary Fig. S4.

In the model simulations, the dynamics in the C- and energy pools are primarily driven by an activation of dormant microbes during the lag phase and an increase in the anaerobic fraction of metabolism during the exponential and retardation phases (Fig. 5B). At the start of the incubation, the microbial population is dormant, and rates of CO₂ and heat release are determined by maintenance respiration of the inactive fraction with a CR of ~ 480 kJ/C-mol. As microbial activity increases,

aerobic respiration of glucose fueling the growth of the active fraction accelerates, causing an initial drop in CR due to the energy demand of anabolism (Chakrawal et al., 2021). As the exponential phase continues, this rapid aerobic mineralization of glucose gradually consumes the available O₂, such that a larger portion of glucose is metabolized anaerobically and fermented to lactic acid (Supplementary Fig. S5). This pathway is characterized by a very high CR due to the lack of CO₂ production, but its contribution to the overall CR of the population remains small overall. During the retardation phase, when O₂ has been largely depleted, only a small fraction of the formed lactic acid is respired aerobically, while the majority is fermented further to acetate, propionate and CO₂, which yields the pronounced drop in CR. These acids finally accumulate under the prevalent anaerobic conditions (Supplementary Fig. S6), and the microbes begin to return to a dormant state (Fig. 5B). A more detailed analysis of the CR is provided in SI methods (section D).

In contrast, a model variant featuring aerobic respiration as the only metabolic pathway achieves a good fit to heat release and cumulative CO₂ ($R^2 > 0.99$) but fails to appropriately reproduce biomass estimates ($R^2 = 0.72$), substantially overestimating growth during the last third of the incubation with ~ 660 $\mu\text{g C/g}$ at 18 h. It also fails to capture the experimental CR pattern, with the only dynamic changes in CR being caused by microbial emergence from and return to dormancy (Supplementary Fig. S7). While this model features a significantly smaller number of free parameters ($n_{\text{par}} = 7$) compared to the full model ($n_{\text{par}} = 12$), a comparison based on the Akaike Information Criterion (AIC) in the least squares estimation context (Banks and Joyner, 2017) favors the full model including anaerobic pathways (AIC_{full} ≈ 906 , AIC_{aerob} ≈ 899 , details see SI methods, section E).

Dynamics of CUE. Based on the available estimate of 371 $\mu\text{g C/g}$ for biomass growth and assuming that only negligible amounts of the initially added 800 $\mu\text{g C/g}$ glucose remained after 18 h, the average CUE_C (Eq. (3)) over the incubation period was 0.464 g MBC/g C substrate. This average value represents the net result of all metabolic activity during the incubation but does not reflect any temporal dynamics involving dormancy or changing metabolic pathways. For example, in the simplest case of a fully active population growing aerobically, this CUE_C would imply a constant CR of ~ 448 kJ/C-mol (Chakrawal et al., 2020), in strong contrast to our experimental observations.

On the other hand, the average CUE_B (Eq. (4)) over the incubation was 0.573 but showed significant variation over time (Fig. 5A). The efficiency of the population was initially low (<0.4), as the large inactive fraction emits CO₂ from maintenance respiration without achieving any growth, but soon increased dramatically to almost 0.8 during the exponential growth phase, when glucose was decomposed aerobically. CUE_B then gradually decreased to 0.7 up to 12 h, followed by a pronounced drop to 0.2–0.3 during the retardation phase.

This pattern can also be observed when CUE_B is estimated from the dynamic model (Fig. 5A), which offers an interpretation in terms of active metabolic pathways and their yield coefficients (Y). Specifically, the high observed CUE during the exponential growth phase corresponds to the very high estimated yield coefficient of aerobic respiration (est. $Y_{\text{aerobic}} \sim 0.85$), while the subsequent gradual decrease and sharp

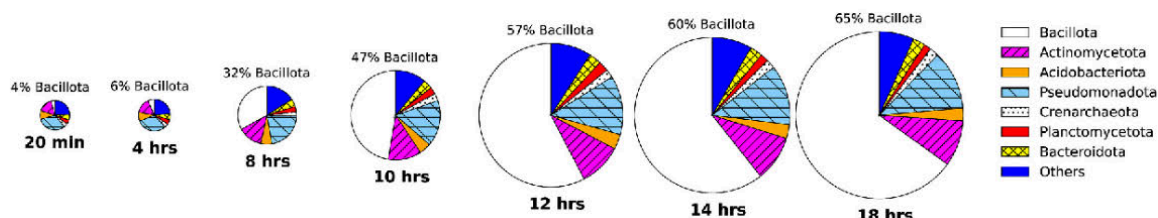


Fig. 4. Changes in microbial community composition during growth on glucose (mean of $n = 3$ replicates each). While the gene copy numbers of all considered phyla increase during the experiment, the relative abundance of members of the *Bacillota* phylum as measured by 16S rRNA increases over the course of the incubation. Pie size is proportional to the total gene copy number at each timepoint.

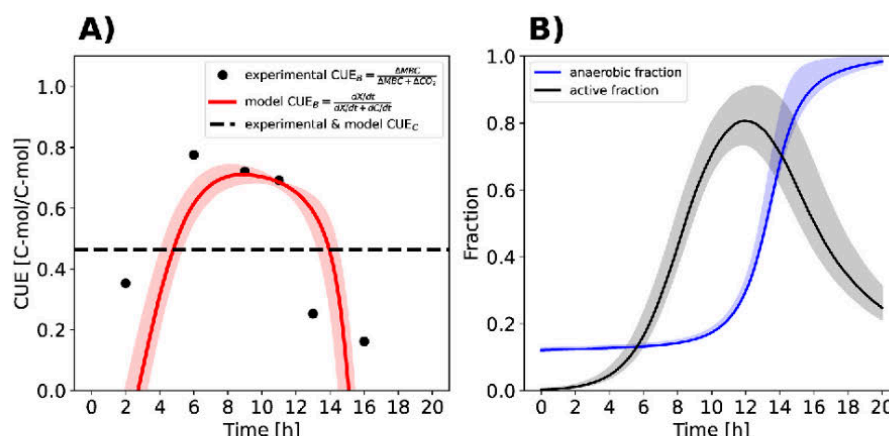


Fig. 5. Temporal dynamics of experimental CUE_B estimates and results of the calibrated model for CUE_B, anaerobic fraction and microbial activity (lines, best fit \pm range). **A** The ratio of the increase in microbial biomass carbon (MBC) to the total increase in MBC and cumulative CO₂ represents a proxy for carbon use efficiency (CUE_B) and shows a temporal pattern with high efficiency during exponential growth and low efficiencies during the lag and retardation phases. Assuming that all added glucose was metabolized after 18 h, the ratio of biomass formed to consumed substrate suggests an intermediate overall efficiency (CUE_C, dashed). **B** The calibrated model features a continuous increase in the fraction of substrate that is metabolized anaerobically due to O₂ limitation (blue) over the course of the incubation, with a sharp rise during the exponential growth phase with high O₂ demand. The model also suggests a gradual activation of initially dormant microbes during the lag phase, followed by a return to dormancy during the retardation phase when the substrate is depleted.

drop in efficiency can be attributed to the shift towards the anaerobic fermentation of glucose (est. $Y_{f,glu} < 0.1$) and lactic acid (est. $Y_{f,lac} \sim 0.28$), respectively.

Notably, the measured experimental C pools after 18 h of incubation remained unbalanced when assuming complete decomposition of glucose, with MBC and CO₂ together accounting for only 687 $\mu\text{g-C/g}$ or around 86% of the 800 $\mu\text{g-C/g}$ added as substrate. This is mirrored in simulations, with the remaining C accounted for by accumulating fermentation products in the dynamic model (Supplementary Fig. S6).

4. Discussion

The joint analysis of carbon and heat fluxes revealed an unexpected pattern of temporal variation in the CR that is inconsistent with the assumption of aerobic growth on glucose (Hansen et al., 2004; Chakrawal et al., 2020). Moreover, we observed a dominance of the *Bacillota* unfolding in the microbial community during the experiment, with this phylum outcompeting others like *Pseudomonadota*, *Actinomycetota* and *Acidobacteriota* that typically dominated the community after glucose addition (Eilers et al., 2010; Mau et al., 2015; Morrissey et al., 2017) and also showed the highest initial abundance in our samples. Modeling indicated that a shift to fermentation pathways presents a plausible and quantitative explanation to connect both experimental findings in a single framework.

First, *Bacillota* are well-known for widespread obligate and facultative fermentative capabilities, including in members that are prevalent in the soil environment such as *Bacillus* (Cruz Ramos et al., 2000) or *Clostridium* (Wiegel et al., 2006). Besides the common lactic acid fermentation of glucose, many groups (e.g., *Clostridium* or *Pelosiinus*) are also able to ferment lactate to acetate and propionate (Seeliger et al., 2002; Mosher et al., 2012; Beller et al., 2013), and *Bacillota* have been shown to expand on lactate under both aerobic and anaerobic conditions, emerging as the dominant phylum after lactate amendment (Mosher et al., 2012; Van Den Berg et al., 2017; Macias-Benitez et al., 2020). There have also been reports of *Bacillota* thriving under alkaline conditions at pH > 8, as observed in the soil used in this study (O'Callaghan et al., 2010; Anderson et al., 2018). More generally, the *Bacillota* have been recognized as a phylum with significant copiotrophic characteristics, which enable their rapid expansion in the presence of labile substrate like glucose. This is also true of some of the other phyla with significant growth in our incubation, such as the *Pseudomonadota*,

although such classifications are more ambiguous (Stone et al., 2023).

Second, this sequence of fermentation of glucose to lactate followed by fermentation of lactate to acetate and propionate predicts a CR pattern as observed in our experimental data (Fig. 3C). More specifically, the gradual shift from aerobic respiration to lactic acid fermentation caused by increasing O₂ limitation during exponential growth yields a slow increase in CR due to a lack of catabolic CO₂ production in this fermentation (Chakrawal et al., 2020). As lactate becomes the dominant substrate after glucose depletion, its further fermentation to acetate and propionate subsequently lowers the observed CR (Seeliger et al., 2002).

Importantly, we did not aim to impose anoxic conditions in our experimental setup. Instead, we suggest that the formation of anoxic microsites in the soil was driven by metabolic demand of the growing microbial population, a mechanism that has recently been shown to be particularly important in sandy loam soils such as the soil used in this study (Lacroix et al., 2022). If oxygen diffusion into structural units such as pedis or aggregates is outpaced by microbial consumptions, oxygen is locally depleted, and anaerobic microsites are established. While this effect was likely enhanced by high nutrient availability and temperature in our experiment, the prevalence of anaerobic microsites and their role in carbon cycling has been recognized more generally, even in well-drained soils (Keiluweit et al., 2016, 2017; Lacroix et al., 2021). Our results further support this finding and highlight the need for careful reconsideration of assuming aerobic respiration as the only (dominant) metabolism under common experimental and field conditions. However, our experiment was conducted in closed containers and using sieved soils, such that a direct comparison to natural soils is not feasible. Although a simple estimation of the initial headspace O₂ in our incubations indicates that there was sufficient O₂ for the observed oxidation of glucose to CO₂, the headspace O₂ saturation may have dropped to approximately 30% of atmospheric levels after 20 h. To explicitly monitor the role of anoxic microsites (as opposed to the depletion of total O₂ in the system) using calorimetry, future studies might consider the use of lower soil-to-headspace ratios and the addition of smaller amounts of substrate to ensure a continuously high O₂ saturation in the headspace, as well as the use of undisturbed soils with intact structural units.

The occurrence of anaerobic conditions in our experiment is also supported by the observed N₂O emissions (Supplementary Fig. S1). Based on these observations, we also investigated heterotrophic

denitrification as another possible anaerobic metabolic pathway. However, its overall contribution was small, with less than 0.5% of the cumulative CO₂ that can be accounted for by denitrification (details in SI methods, section F). Since NH₄ was the only nitrogen source added to the soil, nitrification must also have taken place in our samples. While this cannot be quantified using our data, any chemoautotrophic use of CO₂ as a C source as well as any heat release during nitrification would elevate measured CR. This might also contribute to lower model CR compared to the experimental values during the early (aerobic) stages of the incubation.

The missing 14% of added C in the carbon balance after 18 h along with the temporal pattern of CUE represent another indication of possible fermentative pathways. Specifically, the mismatch between overall CUE_C (0.46) and CUE_B (0.57) could be explained by the accumulation of fermentation products, which are not included in estimates based on CO₂ and biomass alone (i.e., CUE_B) (Hagerty et al., 2018). Moreover, the dynamic model suggests that the drop in CUE even before the time of peak activity might be caused by a gradual shift to less efficient fermentation pathways (Fig. 5A) resulting in reduced microbial growth.

Notably, we were able to obtain realistic biomass estimates from gene copy numbers (Eq. (1)) that were in close agreement with estimates based on SIR. In particular, accounting for different average gene copy numbers per cell in the considered bacterial phyla enables us to more accurately capture the biomass dynamics, whereas the use of a global average for all bacteria would underestimate initial biomass and overestimate growth. This is due to the fact that *Bacillota* feature the highest average gene copy number per cell among bacterial phyla (Sun et al., 2013; Větrovský and Baldrian, 2013) (Supplementary Table S1). This is also reflected in the different estimated contributions of *Bacillota* to the total gene copy numbers and to microbial biomass. While the relative abundances obtained via PCR suggested a 65% share of *Bacillota* after 18 h, our biomass estimates result in a relatively lower contribution of 45% of MBC after 18 h, although this still places the *Bacillota* as the dominant phylum by a wide margin.

Nonetheless, both the relative abundances based on PCR and our corrected biomass estimates are vulnerable to multiple sources of bias. These include DNA extraction, primer mismatches and amplification, but also variation in the average gene copy numbers within phyla and during growth (see for example Eisenstein 2018). Since such biases would be consistent for all samples in our experiment, we conclude that our central finding regarding the community, i.e., the dominance of the *Bacillota* at the high taxonomic level of phylum, is reliable. In particular, we observed a very consistent pattern in all experimental replicates (Supplementary Fig. S3). Yet, a direct comparison with other experimental results, especially at the macro scale, and the interpretation of quantitative details should be treated with great caution. Specifically, these results were derived from an incubation experiment, and thus inevitably depend strongly on the details of the incubation process.

Furthermore, the interpretation of CR values requires a model of the biochemistry of the system, and despite the support for fermentative pathways outlined above, we did not evaluate the specific biochemical processes besides the detection of N₂O and CH₄ as potential products. Since the observed CR is the sum of all heat and CO₂ contributing processes in the soil, any future calorimetric investigation will be strengthened by the experimental validation of its biochemical assumptions, for example by measuring hypothesized metabolic products like those resulting from common fermentations or monitoring the activities of enzymes of interest.

Finally, monitoring O₂ levels explicitly in the soil and in the head-space would be invaluable for model calibration and validation. We were able to achieve a good fit of the dynamic model, and multiple lines of evidence point towards the development of anaerobiosis in our experiment. Nonetheless, the representation of O₂ dynamics in our framework is simplistic with limited flexibility, and even the parameterization of this simple formulation relies on certain assumptions

(details in SI methods, section C2).

More generally, the calibration and development of urgently needed mechanistic dynamic models remains challenging given available data, and issues of parameter non-identifiability are widespread (Sierra et al., 2015; Marschmann et al., 2019; Siade, 2021). In the context of our experiment, measurements of O₂ levels and fermentation products would be most important to infer the dynamics of these variables, which could only be estimated indirectly in this study.

5. Conclusion

Our joint evaluation of carbon and energy fluxes using combined experimental and modeling approaches revealed a time-dependent bidirectional deviation of experimental CR values from theoretical predictions for aerobic respiration of glucose. We suggest fermentative metabolic pathways as a likely explanation of this pattern as well as the rapid expansion of *Bacillota*, which dominated the community. Our study highlights the potential of a mechanistic bioenergetics framework to generate hypotheses and test assumptions that cannot be tackled from either a carbon or energy perspective alone. In particular, the possible development of significant anaerobiosis in aerobic soil incubations needs to be further investigated. Future studies should link the calorimetric evidence with direct monitoring of O₂ levels and products of potential anaerobic pathways. Such data will be instrumental both to advance modeling efforts and to obtain a process-based understanding of the complex soil system.

CRedit authorship contribution statement

Martin-Georg Endress: Writing – review & editing, Writing – original draft, Visualization, Methodology, Investigation, Formal analysis. **Ruirui Chen:** Writing – review & editing, Writing – original draft, Methodology, Investigation, Funding acquisition, Formal analysis, Data curation, Conceptualization. **Evgenia Blagodatskaya:** Writing – review & editing, Writing – original draft, Supervision, Formal analysis, Conceptualization. **Sergey Blagodatsky:** Writing – review & editing, Writing – original draft, Supervision, Funding acquisition, Formal analysis, Conceptualization.

Declaration of competing interest

The authors declare the following financial interests/personal relationships which may be considered as potential competing interests:

Sergey Blagodatsky reports financial support was provided by German Research Foundation. Evgenia Blagodatskaya reports financial support was provided by German Research Foundation. Ruirui Chen reports financial support was provided by National Natural Science Foundation of China. If there are other authors, they declare that they have no known competing financial interests or personal relationships that could have appeared to influence the work reported in this paper.

Data availability

All data analyzed during this study are included in this published article and its supplementary files. All code is available from the corresponding author upon reasonable request.

Acknowledgements

MGE, EB and SB acknowledge funding by the Deutsche Forschungsgemeinschaft (SPP2322 SoilSystems, grant numbers 465124939 and 465122443). RC acknowledges funding by the National Natural Science Foundation of China (grant number 41977045).

Schematics (Figs. 1 and 2) were created with BioRender.

Appendix A. Supplementary data

Supplementary data to this article can be found online at <https://doi.org/10.1016/j.soilbio.2024.109478>.

References

- Anderson, C.R., Peterson, M.E., Frampton, R.A., Bulman, S.R., Keenan, S., Curtin, D., 2018. Rapid increases in soil pH solubilise organic matter, dramatically increase denitrification potential and strongly stimulate microorganisms from the *Firmicutes* phylum. *PeerJ* 6, e6090. <https://doi.org/10.7717/peerj.6090>.
- Anderson, J.P.E., Domsch, K.H., 1978. A physiological method for the quantitative measurement of microbial biomass in soils. *Soil Biology and Biochemistry* 10, 215–221. [https://doi.org/10.1016/0038-0717\(78\)90099-8](https://doi.org/10.1016/0038-0717(78)90099-8).
- Anderson, T.-H., Joergensen, R.G., 1997. Relationship between SIR and FE estimates of microbial biomass C in deciduous forest soils at different pH. *Soil Biology and Biochemistry* 29, 1033–1042. [https://doi.org/10.1016/S0038-0717\(97\)00011-4](https://doi.org/10.1016/S0038-0717(97)00011-4).
- Baath, E., 1994. Thymidine and leucine incorporation in soil bacteria with different cell size. *Microbial Ecology* 27. <https://doi.org/10.1007/BF00182410>.
- Bajracharya, B.M., Smeaton, C.M., Markelov, I., Markelova, E., Lu, C., Cirpka, O.A., Cappellen, P.V., 2022. Organic matter degradation in energy-limited subsurface environments—a bioenergetics-informed modeling approach. *Geomicrobiology Journal* 39, 1–16. <https://doi.org/10.1080/01490451.2021.1998256>.
- Banks, H.T., Joyner, M.L., 2017. AIC under the framework of least squares estimation. *Applied Mathematics Letters* 74, 33–45. <https://doi.org/10.1016/j.aml.2017.05.005>.
- Bardgett, R.D., Freeman, C., Ostle, N.J., 2008. Microbial contributions to climate change through carbon cycle feedbacks. *The ISME Journal* 2, 805–814. <https://doi.org/10.1038/ismej.2008.58>.
- Barros, N., 2021. Thermodynamics of soil microbial metabolism: applications and functions. *Applied Sciences* 11, 4962. <https://doi.org/10.3390/app11114962>.
- Barros, N., Feijóo, S., Hansen, L.D., 2011. Calorimetric determination of metabolic heat, CO₂ rates and the calorimetric ratio of soil basal metabolism. *Geoderma* 160, 542–547. <https://doi.org/10.1016/j.geoderma.2010.11.002>.
- Barros, N., Hansen, L.D., Piñeiro, V., Pérez-Cruzado, C., Villanueva, M., Proupin, J., Rodríguez-Añón, J.A., 2016. Factors influencing the calorimetric ratios of soil microbial metabolism. *Soil Biology and Biochemistry* 92, 221–229. <https://doi.org/10.1016/j.soilbio.2015.10.007>.
- Barros, N., Salgado, J., Rodríguez-Añón, J.A., Proupin, J., Villanueva, M., Hansen, L.D., 2010. Calorimetric approach to metabolic carbon conversion efficiency in soils: comparison of experimental and theoretical models. *Journal of Thermal Analysis and Calorimetry* 99, 771–777. <https://doi.org/10.1007/s10973-010-0673-4>.
- Beck, T., Joergensen, R.G., Kandel, E., Makeschin, F., Nuss, E., Oberholzer, H.R., Scheu, S., 1997. An inter-laboratory comparison of ten different ways of measuring soil microbial biomass C. *Soil Biology and Biochemistry* 29, 1023–1032. [https://doi.org/10.1016/S0038-0717\(97\)00030-8](https://doi.org/10.1016/S0038-0717(97)00030-8).
- Beller, H.R., Han, R., Karaöz, U., Lim, H., Brodie, E.L., 2013. Genomic and physiological characterization of the chromate-reducing, aquifer-derived firmicute *Pelosinus* sp. strain HCF. *Applied and Environmental Microbiology* 79, 11.
- Blagodatskaya, E., Blagodatsky, S., Anderson, T.-H., Kuzyakov, Y., 2014. Microbial growth and carbon use efficiency in the rhizosphere and root-free soil. *PLoS One* 9, e93282. <https://doi.org/10.1371/journal.pone.0093282>.
- Blagodatsky, S., Blagodatskaya, E., Yuyukina, T., Kuzyakov, Y., 2010. Model of apparent and real priming effects: linking microbial activity with soil organic matter decomposition. *Soil Biology and Biochemistry* 42, 1275–1283. <https://doi.org/10.1016/j.soilbio.2010.04.005>.
- Blagodatsky, S.A., Heinemeyer, O., Richter, J., 2000. Estimating the active and total soil microbial biomass by kinetic respiration analysis. *Biology and Fertility of Soils* 32, 73–81. <https://doi.org/10.1007/s003740000219>.
- Boye, K., Herrmann, A.M., Schaefer, M.V., Träily, M.M., Fendorf, S., 2018. Discerning microbially mediated processes during redox transitions in flooded soils using carbon and energy balances. *Frontiers in Environmental Science* 6, 15. <https://doi.org/10.3389/fenvs.2018.00015>.
- Bradford, M.A., Carey, C.J., Atwood, L., Bossio, D., Fenichel, E.P., Gennet, S., Fargione, J., Fisher, J.R.B., Fuller, E., Kane, D.A., Lehmann, J., Oldfield, E.E., Ordway, E.M., Rudek, J., Sanderman, J., Wood, S.A., 2019. Soil carbon science for policy and practice. *Nature Sustainability* 2, 1070–1072. <https://doi.org/10.1038/s41893-019-0431-y>.
- Bradford, M.A., Wieder, W.R., Bonan, G.B., Fierer, N., Raymond, P.A., Crowther, T.W., 2016. Managing uncertainty in soil carbon feedbacks to climate change. *Nature Climate Change* 6, 751–758. <https://doi.org/10.1038/nclimate3071>.
- Braissant, O., Wirz, D., Gäffert, B., Daniels, A.U., 2010. Use of isothermal microcalorimetry to monitor microbial activities. *FEMS Microbiology Letters* 303, 1–8. <https://doi.org/10.1111/j.1574-6968.2009.01819.x>.
- Calabrese, S., Chakrwal, A., Manzoni, S., Van Cappellen, P., 2021. Energetic scaling in microbial growth. *Proceedings of the National Academy of Sciences* 118, e2107668118. <https://doi.org/10.1073/pnas.2107668118>.
- Camenzind, T., Mason-Jones, K., Mansour, I., Rillig, M.C., Lehmann, J., 2023. Formation of necromass-derived soil organic carbon determined by microbial death pathways. *Nature Geoscience*. <https://doi.org/10.1038/s41561-022-01100-3>.
- Caporaso, J.G., Bittinger, K., Bushman, F.D., DeSantis, T.Z., Andersen, G.L., Knight, R., 2010. PyNAST: a flexible tool for aligning sequences to a template alignment. *Bioinformatics* 26, 266–267. <https://doi.org/10.1093/bioinformatics/btp636>.
- Chakrwal, A., Calabrese, S., Herrmann, A.M., Manzoni, S., 2022. Interacting bioenergetic and stoichiometric controls on microbial growth. *Frontiers in Microbiology* 13, 859063. <https://doi.org/10.3389/fmicb.2022.859063>.
- Chakrwal, A., Herrmann, A.M., Manzoni, S., 2021. Leveraging energy flows to quantify microbial traits in soils. *Soil Biology and Biochemistry* 155, 108169. <https://doi.org/10.1016/j.soilbio.2021.108169>.
- Chakrwal, A., Herrmann, A.M., Šantrúčková, H., Manzoni, S., 2020. Quantifying microbial metabolism in soils using calorimetry — a bioenergetics perspective. *Soil Biology and Biochemistry* 148, 107945. <https://doi.org/10.1016/j.soilbio.2020.107945>.
- Crowther, T.W., Van Den Hoogen, J., Wan, J., Mayes, M.A., Keiser, A.D., Mo, L., Averill, C., Maynard, D.S., 2019. The global soil community and its influence on biogeochemistry. *Science* 365, eaav0550. <https://doi.org/10.1126/science.aav0550>.
- Cruz Ramos, H., Hoffmann, T., Marino, M., Nedjari, H., Presecan-Siedel, E., Dreesen, O., Glaser, P., Jahn, D., 2000. Fermentative metabolism of *Bacillus subtilis*: physiology and regulation of gene expression. *Journal of Bacteriology* 182, 3072–3080. <https://doi.org/10.1128/JB.182.11.3072-3080.2000>.
- Dejean, L., Beauvoit, B., Bunoust, O., Fleury, C., Guerin, B., Rigoulet, M., 2001. The calorimetric-respirometric ratio is an on-line marker of enthalpy efficiency of yeast cells growing on a non-fermentable carbon source. *Biochimica et Biophysica Acta* 1503, 329–340.
- Eilers, K.G., Lauber, C.L., Knight, R., Fierer, N., 2010. Shifts in bacterial community structure associated with inputs of low molecular weight carbon compounds to soil. *Soil Biology and Biochemistry* 42, 896–903. <https://doi.org/10.1016/j.soilbio.2010.02.003>.
- Eisenstein, M., 2018. Microbiology: making the best of PCR bias. *Nature Methods* 15, 317–320. <https://doi.org/10.1038/nmeth.4683>.
- Fierer, N., Bradford, M.A., Jackson, R.B., 2007. Toward an ecological classification of soil bacteria. *Ecology* 88, 1354–1364. <https://doi.org/10.1890/05-1839>.
- Foreman-Mackey, D., Hogg, D.W., Lang, D., Goodman, J., 2013. Emcee: the MCMC Hammer. *Publications of the Astronomical Society of the Pacific* 125, 306–312. <https://doi.org/10.1086/670067>.
- Frey, S.D., Lee, J., Melillo, J.M., Six, J., 2013. The temperature response of soil microbial efficiency and its feedback to climate. *Nature Climate Change* 3, 395–398. <https://doi.org/10.1038/nclimate1796>.
- Gangneux, C., Akpa-Vincent, M., Sauvage, H., Desaire, S., Houot, S., Laval, K., 2011. Fungal, bacterial and plant dsDNA contributions to soil total DNA extracted from silty soils under different farming practices: relationships with chloroform-labile carbon. *Soil Biology and Biochemistry* 43, 431–437. <https://doi.org/10.1016/j.soilbio.2010.11.012>.
- Geyer, K.M., Dijkstra, P., Sinsabaugh, R., Frey, S.D., 2019. Clarifying the interpretation of carbon use efficiency in soil through methods comparison. *Soil Biology and Biochemistry* 128, 79–88. <https://doi.org/10.1016/j.soilbio.2018.09.036>.
- Geyer, K.M., Kyker-Snowman, E., Grandy, A.S., Frey, S.D., 2016. Microbial carbon use efficiency: accounting for population, community, and ecosystem-scale controls over the fate of metabolized organic matter. *Biogeochemistry* 127, 173–188. <https://doi.org/10.1007/s10533-016-0191-y>.
- Hagerty, S.B., Allison, S.D., Schimel, J.P., 2018. Evaluating soil microbial carbon use efficiency explicitly as a function of cellular processes: implications for measurements and models. *Biogeochemistry* 140, 269–283. <https://doi.org/10.1007/s10533-018-0489-z>.
- Hansen, L.D., Macfarlane, C., McKinnon, N., Smith, B.N., Criddle, R.S., 2004. Use of calorimetric ratios, heat per CO₂ and heat per O₂, to quantify metabolic paths and energetics of growing cells. *Thermochimica Acta* 422, 55–61. <https://doi.org/10.1016/j.tca.2004.05.033>.
- Herrmann, A.M., Büscher, T., 2015. Simultaneous screening of microbial energetics and CO₂ respiration in soil samples from different ecosystems. *Soil Biology and Biochemistry* 83, 88–92. <https://doi.org/10.1016/j.soilbio.2015.01.020>.
- Herrmann, A.M., Coucheney, E., Nunan, N., 2014. Isothermal microcalorimetry provides new insight into terrestrial carbon cycling. *Environmental Science & Technology* 48, 4344–4352. <https://doi.org/10.1021/es403941h>.
- Jing, Z., Chen, R., Wei, S., Feng, Y., Zhang, J., Lin, X., 2017. Response and feedback of C mineralization to P availability driven by soil microorganisms. *Soil Biology and Biochemistry* 105, 111–120. <https://doi.org/10.1016/j.soilbio.2016.11.014>.
- Kästner, M., Miltner, A., Thiele-Bruhn, S., Liang, C., 2021. Microbial necromass in soils—linking microbes to soil processes and carbon turnover. *Frontiers in Environmental Science* 9, 597. <https://doi.org/10.3389/fenvs.2021.756378>.
- Kaiser, E.A., Mueller, T., Joergensen, R.G., Insam, H., Heinemeyer, O., 1992. Evaluation of methods to estimate the soil microbial biomass and the relationship with soil texture and organic matter. *Soil Biology and Biochemistry* 24, 675–683. [https://doi.org/10.1016/0038-0717\(92\)90046-Z](https://doi.org/10.1016/0038-0717(92)90046-Z).
- Keiluweit, M., Nico, P.S., Kleber, M., Fendorf, S., 2016. Are oxygen limitations under recognized regulators of organic carbon turnover in upland soils? *Biogeochemistry* 127, 157–171. <https://doi.org/10.1007/s10533-015-0180-6>.
- Keiluweit, M., Wanzek, T., Kleber, M., Nico, P., Fendorf, S., 2017. Anaerobic microsites have an unaccounted role in soil carbon stabilization. *Nature Communications* 8, 1771. <https://doi.org/10.1038/s41467-017-01406-6>.
- Lacroix, E.M., Mendillo, J., Gomes, A., Dekas, A., Fendorf, S., 2022. Contributions of anoxic microsites to soil carbon protection across soil textures. *Geoderma* 425, 116050. <https://doi.org/10.1016/j.geoderma.2022.116050>.
- Lacroix, E.M., Rossi, R.J., Bossio, D., Fendorf, S., 2021. Effects of moisture and physical disturbance on pore-scale oxygen content and anaerobic metabolisms in upland soils. *Science of the Total Environment* 780, 146572. <https://doi.org/10.1016/j.scitotenv.2021.146572>.

- Liang, C., Schimel, J.P., Jastrow, J.D., 2017. The importance of anabolism in microbial control over soil carbon storage. *Nature Microbiology* 2, 17105. <https://doi.org/10.1038/nmicrobiol.2017.105>.
- Luo, Y., Ahlström, A., Allison, S.D., Batjes, N.H., Brovkin, V., Carvalhais, N., Chappell, A., Ciais, P., Davidson, E.A., Finzi, A., Georgiou, K., Guenet, B., Hararuk, O., Harden, J. W., He, Y., Hopkins, F., Jiang, L., Koven, C., Jackson, R.B., Jones, C.D., Lara, M.J., Liang, J., McGuire, A.D., Parton, W., Peng, C., Randerson, J.T., Salazar, A., Sierra, C. A., Smith, M.J., Tian, H., Todd-Brown, K.E.O., Torn, M., Groenigen, K.J., Wang, Y.P., West, T.O., Wei, Y., Wieder, W.R., Xia, J., Xu, X., Xia, X., Xiaofeng, Zhou, T., 2015. Toward more realistic projections of soil carbon dynamics by Earth system models. *Global Biogeochemical Cycles* 17.
- Macías-Benitez, S., García-Martínez, A.M., Caballero Jimenez, P., Gonzalez, J.M., Tejada Moral, M., Parrado Rubio, J., 2020. Rhizospheric organic acids as biostimulants: monitoring feedbacks on soil microorganisms and biochemical properties. *Frontiers in Plant Science* 11, 633. <https://doi.org/10.3389/fpls.2020.00633>.
- Manzoni, S., Capek, P., Porada, P., Thurner, M., Winterdahl, M., Beer, C., Brücher, V., Frouz, J., Herrmann, A.M., Lindahl, B.D., Lyon, S.W., Šantrůčková, H., Vico, G., Way, D., 2018. Reviews and syntheses: carbon use efficiency from organisms to ecosystems – definitions, theories, and empirical evidence. *Biogeosciences* 15, 5929–5949. <https://doi.org/10.5194/bg-15-5929-2018>.
- Manzoni, S., Taylor, P., Richter, A., Porporato, A., Ågren, G.I., 2012. Environmental and stoichiometric controls on microbial carbon-use efficiency in soils. *New Phytologist* 196, 79–91.
- Marschmann, G.L., Pagel, H., Kügler, P., Streck, T., 2019. Equifinality, sloppiness, and emergent structures of mechanistic soil biogeochemical models. *Environmental Modelling & Software* 122, 104518. <https://doi.org/10.1016/j.envsoft.2019.104518>.
- Martens, R., 1987. Estimation of microbial biomass in soil by the respiration method: importance of soil pH and flushing methods for the measurement of respired CO₂. *Soil Biology and Biochemistry* 19, 77–81. [https://doi.org/10.1016/0038-0717\(87\)90128-3](https://doi.org/10.1016/0038-0717(87)90128-3).
- Maskow, T., Paufler, S., 2015. What does calorimetry and thermodynamics of living cells tell us? *Methods* 76, 3–10. <https://doi.org/10.1016/j.ymeth.2014.10.035>.
- Mau, R.L., Liu, C.M., Aziz, M., Schwartz, E., Dijkstra, P., Marks, J.C., Price, L.B., Keim, P., Hungate, B.A., 2015. Linking soil bacterial biodiversity and soil carbon stability. *The ISME Journal* 9, 1477–1480. <https://doi.org/10.1038/ismej.2014.205>.
- Maynard, D.S., Crowther, T.W., Bradford, M.A., 2017. Fungal interactions reduce carbon use efficiency. *Ecology Letters* 20, 1034–1042. <https://doi.org/10.1111/ele.12801>.
- Chemistry of carbonic acid in water. In: Mook, W.G. (Ed.), 2000. *Environmental Isotopes in the Hydrological Cycle - Principles and Applications*. UNESCO, Paris, pp. 143–165.
- Morrissey, E.M., Mau, R.L., Schwartz, E., Caporaso, J.G., Dijkstra, P., van Gestel, N., Koch, B.J., Liu, C.M., Hayer, M., McHugh, T.A., Marks, J.C., Price, L.B., Hungate, B. A., 2016. Phylogenetic organization of bacterial activity. *The ISME Journal* 10, 2336–2340. <https://doi.org/10.1038/ismej.2016.28>.
- Morrissey, E.M., Mau, R.L., Schwartz, E., McHugh, T.A., Dijkstra, P., Koch, B.J., Marks, J. C., Hungate, B.A., 2017. Bacterial carbon use plasticity, phylogenetic diversity and the priming of soil organic matter. *The ISME Journal* 11, 1890–1899. <https://doi.org/10.1038/ismej.2017.43>.
- Mosher, J.J., Phelps, T.J., Podar, M., Hurt, R.A., Campbell, J.H., Drake, M.M., Moberly, J. G., Schadt, C.W., Brown, S.D., Hazen, T.C., Arkin, A.P., Palumbo, A.V., Faybishenko, B.A., Elias, D.A., 2012. Microbial community succession during lactate amendment and electron acceptor limitation reveals a predominance of metal-reducing *Pedosinus* spp. *Applied and Environmental Microbiology* 78, 10.
- Newville, M., Otten, R., Nelson, A., Stensitzki, T., Ingargiola, A., Allan, D., Fox, A., Carter, F., Michał, Osborn, R., Pustakhod, D., Ineuhous, Weigand, S., Aristov, A., Glenn, Deil, C., mgunyho, Mark, Hansen, A.L.R., Pasquevich, G., Foks, L., Zobrist, N., Frost, O., Stuermer, azelcer, Polloreno, A., Persaud, A., Nielsen, J.H., Pompili, M., Eendebak, P., 2023. Imfit/Imfit-py: 1.2.2 (1.2.2). doi:10.5281/zenodo.8145703.
- O'Callaghan, M., Gerard, E.M., Carter, P.E., Lardner, R., Sarathchandra, U., Burch, G., Ghani, A., Bell, N., 2010. Effect of the nitrification inhibitor dicyandiamide (DCD) on microbial communities in a pasture soil amended with bovine urine. *Soil Biology and Biochemistry* 42, 1425–1436. <https://doi.org/10.1016/j.soilbio.2010.05.003>.
- Oren, A., Steinberger, Y., 2008. Coping with artifacts induced by CaCO₃-CO₂-H₂O equilibria in substrate utilization profiling of calcareous soils. *Soil Biology and Biochemistry* 40, 2569–2577. <https://doi.org/10.1016/j.soilbio.2008.06.020>.
- Panikov, N.S., 1996. Mechanistic mathematical models of microbial growth in bioreactors and in natural soils: explanation of complex phenomena. *Mathematics and Computers in Simulation* 42, 179–186. [https://doi.org/10.1016/0378-4754\(95\)00127-1](https://doi.org/10.1016/0378-4754(95)00127-1).
- Papp, K., Hungate, B.A., Schwartz, E., 2020. Glucose triggers strong taxon-specific responses in microbial growth and activity: insights from DNA and RNA qSIP. *Ecology* 101. <https://doi.org/10.1002/ecy.2887>.
- Roels, J.A., 1980. Application of macroscopic principles to microbial metabolism. *Biotechnology and Bioengineering* 22, 2457–2514. <https://doi.org/10.1002/bit.260221202>.
- Seeliger, S., Janssen, P.H., Schink, B., 2002. Energetics and kinetics of lactate fermentation to acetate and propionate via methylmalonyl-CoA or acrylyl-CoA. *FEMS Microbiology Letters* 211, 65–70. <https://doi.org/10.1111/j.1574-6968.2002.tb11204.x>.
- Siade, A.J., 2021. Unraveling biogeochemical complexity through better integration of experiments and modeling. *Environmental Sciences* 9.
- Sierra, C.A., Malghani, S., Müller, M., 2015. Model structure and parameter identification of soil organic matter models. *Soil Biology and Biochemistry* 90, 197–203. <https://doi.org/10.1016/j.soilbio.2015.08.012>.
- Sinsabaugh, R.L., Manzoni, S., Moorhead, D.L., Richter, A., 2013. Carbon use efficiency of microbial communities: stoichiometry, methodology and modelling. *Ecology Letters* 16, 930–939. <https://doi.org/10.1111/de.12113>.
- Sinsabaugh, R.L., Turner, B.L., Talbot, J.M., Waring, B.G., Powers, J.S., Kuske, C.R., Moorhead, D.L., Follstad Shah, J.J., 2016. Stoichiometry of microbial carbon use efficiency in soils. *Ecological Monographs* 86, 172–189. <https://doi.org/10.1890/15-2110.1>.
- Sparling, G.W., West, A.W., 1990. A comparison of gas chromatography and differential respirometer methods to measure soil respiration and to estimate the soil microbial biomass. *Pedobiologia* 34, 103–112.
- Stone, B.W.G., Dijkstra, P., Finley, B.K., Fitzpatrick, R., Foley, M.M., Hayer, M., Hofmockel, K.S., Koch, B.J., Li, J., Liu, X.J.A., Martinez, A., Mau, R.L., Marks, J., Monsaint-Queeney, V., Morrissey, E.M., Propster, J., Pett-Ridge, J., Purcell, A.M., Schwartz, E., Hungate, B.A., 2023. Life history strategies among soil bacteria—dichotomy for few, continuum for many. *The ISME Journal*. <https://doi.org/10.1038/s41396-022-01354-0>.
- Sulman, B.N., Moore, J.A.M., Abramoff, R., Averill, C., Kivlin, S., Georgiou, K., Sridhar, B., Hartman, M.D., Wang, G., Wieder, W.R., Bradford, M.A., Luo, Y., Mayes, M.A., Morrison, E., Riley, W.J., Salazar, A., Schimel, J.P., Tang, J., Classen, A. T., 2018. Multiple models and experiments underscore large uncertainty in soil carbon dynamics. *Biogeochemistry* 141, 109–123. <https://doi.org/10.1007/s10533-018-0509-z>.
- Sun, D.-L., Jiang, X., Wu, Q.L., Zhou, N.-Y., 2013. Intragenomic heterogeneity of 16S rRNA genes causes overestimation of prokaryotic diversity. *Applied and Environmental Microbiology* 79, 5962–5969. <https://doi.org/10.1128/AEM.01282-13>.
- Van Den Berg, E.M., Elisário, M.P., Kuenen, J.G., Kleerebezem, R., Van Loosdrecht, M.C. M., 2017. Fermentative bacteria influence the competition between denitrifiers and DNRA bacteria. *Frontiers in Microbiology* 8, 1684. <https://doi.org/10.3389/fmicb.2017.01684>.
- Větrovský, T., Baldrian, P., 2013. The variability of the 16S rRNA gene in bacterial genomes and its consequences for bacterial community analyses. *PLoS One* 8, e57923. <https://doi.org/10.1371/journal.pone.0057923>.
- Virtanen, P., Gommers, R., Oliphant, T.E., Haberland, M., Reddy, T., Cournapeau, D., Burovski, E., Peterson, P., Weckesser, W., Bright, J., van der Walt, S.J., Brett, M., Wilson, J., Millman, K.J., Mayorov, N., Nelson, A.R.J., Jones, E., Kern, R., Larson, E., Carey, C.J., Polat, I., Feng, Y., Moore, E.W., VanderPlas, J., Laxalde, D., Perktold, J., Cimrman, R., Henriksen, I., Quintero, E.A., Harris, C.R., Archibald, A.M., Ribeiro, A. H., Pedregosa, F., van Mulbregt, P., SciPy 1.0 Contributors, 2020. SciPy 1.0: fundamental algorithms for scientific computing in Python. *Nature Methods* 17, 261–272. <https://doi.org/10.1038/s41592-019-0686-2>.
- von Stockar, U., Marison, I.W., 1993. The definition of energetic growth efficiencies for aerobic and anaerobic microbial growth and their determination by calorimetry and by other means. *Thermochimica Acta* 229, 157–172. [https://doi.org/10.1016/0040-6031\(93\)80323-3](https://doi.org/10.1016/0040-6031(93)80323-3).
- Wadsö, L., Hansen, L.D., 2015. Calorespirometry of terrestrial organisms and ecosystems. *Methods* 76, 11–19. <https://doi.org/10.1016/j.ymeth.2014.10.024>.
- Wiedel, J., Tanner, R., Rainey, F.A., 2006. An introduction to the family clostridiaceae. In: Dworkin, M., Falkow, S., Rosenberg, E., Schleifer, K.-H., Stackebrandt, E. (Eds.), *The Prokaryotes: Volume 4: Bacteria: Firmicutes, Cyanobacteria*. Springer US, New York, NY, pp. 654–678. <https://doi.org/10.1007/0-387-30744-3.20>.
- Wutzler, T., Blagodatsky, S.A., Blagodatskaya, E., Kuzyakov, Y., 2012. Soil microbial biomass and its activity estimated by kinetic respiration analysis – statistical guidelines. *Soil Biology and Biochemistry* 45, 102–112. <https://doi.org/10.1016/j.soilbio.2011.10.004>.
- Xin, X., Zhang, X., Chu, W., Mao, J., Yang, W., Zhu, A., Zhang, J., Zhong, X., 2019. Characterization of fluvo-aquic soil phosphorus affected by long-term fertilization using solution 31P NMR spectroscopy. *Science of the Total Environment* 692, 89–97. <https://doi.org/10.1016/j.scitotenv.2019.07.221>.

Chapter 2: Spatial substrate heterogeneity limits microbial growth as revealed by the joint experimental quantification and modeling of carbon and heat fluxes

Publication:

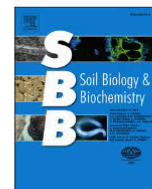
Endress, M.-G., Dehghani, F., Blagodatsky, S., et al., 2024b. Spatial substrate heterogeneity limits microbial growth as revealed by the joint experimental quantification and modeling of carbon and heat fluxes. *Soil Biology and Biochemistry* 197, 109509. doi:[10.1016/j.soilbio.2024.109509](https://doi.org/10.1016/j.soilbio.2024.109509)

Declaration of personal contributions:

I am one of the first authors and the corresponding author of this publication. The first authorship is shared with F. Dehghani, who performed all experimental work presented in the study as well as initial data treatment. I performed all modeling work and all quantitative analyses. Specifically, I designed the dynamic model and performed all numerical simulations, model calibration, and statistics, and wrote the code required for these tasks. I prepared the first draft together with F. Dehghani, took the lead in writing, and prepared the final version of the manuscript with input from all co-authors. Based on the dataset provided, I prepared all figures and all supplementary material other than Table S1 and Figure S1 with input from all co-authors. I handled revisions with input from all co-authors.

Data availability statement:

All data analyzed during this study are included in this published article and its supplementary files. All modeling code is available from the corresponding author upon reasonable request.



Spatial substrate heterogeneity limits microbial growth as revealed by the joint experimental quantification and modeling of carbon and heat fluxes

Martin-Georg Endress^{a,1,*}, Fatemeh Dehghani^{b,1}, Sergey Blagodatsky^{a,c}, Thomas Reitz^b, Steffen Schlüter^d, Evgenia Blagodatskaya^b

^a Institute of Zoology, University of Cologne, 50923, Cologne, Germany

^b Department of Soil Ecology, Helmholtz Centre for Environmental Research – UFZ, 06120, Halle/Saale, Germany

^c Institute of Meteorology and Climate Research, Department of Atmospheric Environmental Research (IMK-IFU), Karlsruhe Institute of Technology (KIT) – Campus Alpin, 82467, Garmisch-Partenkirchen, Germany

^d Department of Soil System Science, Helmholtz Centre for Environmental Research – UFZ, 06120, Halle/Saale, Germany

ARTICLE INFO

Keywords:

Calorespirometry
Nutrient limitation
Oxygen limitation
Carbon use efficiency
Energy use efficiency
Microbial-explicit modeling

ABSTRACT

Spatial heterogeneity is a pervasive feature of soils, affecting the distribution of carbon sources as well as their microbial consumers. Heterogeneous addition of substrates typically results in delayed microbial growth compared to homogeneous addition, and this effect has frequently been attributed to spatial separation of microorganisms from their food. We investigated the importance of two other potential causes of this effect, the availability of nutrients and oxygen, by measuring heat and CO₂ release along with O₂ consumption from soil samples after homogeneous or heterogeneous addition of glucose as well as with or without further addition of a nutrient solution. We then employed a microbial-explicit model to quantitatively interpret our observations. The results revealed that delayed growth after spatially heterogeneous substrate addition was primarily caused by nutrient limitation. While sufficient co-location of all entities – substrate, microorganisms, and nutrients – is required for optimal growth, spatial separation of glucose and microorganisms only played a minor role in our experiment. Model simulations captured the dynamics based on aerobic growth and maintenance, utilizing a simple formulation of nutrient limitation coupled with dynamic transition of microbes between activity and dormancy. The model predicted an overall lower microbial activity over the course of the incubation in treatments with heterogeneous substrate addition. Despite reduced rates, neither the experimental carbon and energy balances nor modeling showed an effect of heterogeneity on the growth efficiency after 50 h of incubation. In all treatments, energy use efficiency exceeded carbon use efficiency by 9–21%. We found no evidence of anaerobiosis. The application of a bioenergetic framework facilitated the interpretation of complex experimental data and quantitatively captured the mechanisms underlying the effects of spatial heterogeneity.

1. Introduction

The fate of organic carbon (C) entering soil or stored as soil organic matter (SOM) is of critical importance to future climate change and to the provisioning of soil ecosystem services, and it is mediated in large part by soil microorganisms (Bardgett et al., 2008; Phillips and Nickerson, 2015; Crowther et al., 2019). The processes and factors controlling the decomposition and cycling of C and especially the fraction of consumed C that is used by microbes to form new biomass, often termed the microbial carbon use efficiency (CUE), have thus played a central

role in soil research for decades (Manzoni et al., 2018). Yet, the complexity and variability of natural soil environments that arises from the simultaneous occurrence of many physico-chemical (e.g., diffusion and sorption) and biological processes (e.g., diverse metabolic activity and microbial interactions) continue to challenge our understanding of microbial carbon cycling and especially CUE (Sinsabaugh et al., 2013; Geyer et al., 2016; Hagerty et al., 2018).

One important source of such challenges is the high degree of spatial and temporal heterogeneity in soils, both regarding the distribution of C substrates (e.g., Peth et al., 2014; Schlüter et al., 2022) as well as their

* Corresponding author.

E-mail address: m.endress@uni-koeln.de (M.-G. Endress).

¹ Equal contributions.

<https://doi.org/10.1016/j.soilbio.2024.109509>

Received 12 April 2024; Received in revised form 15 June 2024; Accepted 28 June 2024

Available online 28 June 2024

0038-0717/© 2024 The Authors. Published by Elsevier Ltd. This is an open access article under the CC BY-NC license (<http://creativecommons.org/licenses/by-nc/4.0/>).

potential microbial consumers (e.g., Raynaud and Nunan, 2014). Availability and input of C as well as suitable habitat in soils are necessarily patchy, e.g., concentrated in the rhizosphere or detritosphere, and the ecological relevance of this heterogeneity for microbial strategies and communities as well as for SOM persistence is well recognized (Kuzakov and Blagodatskaya, 2015; Nunan, 2017; Lehmann et al., 2020). Multiple studies have evaluated the effect of substrate spatial heterogeneity on microbial C use by manipulating the substrate distribution experimentally. C derived from various compounds, ranging from labile C sources (Shi et al., 2021) to pesticides (Pinheiro et al., 2015), plant litter (Gaillard et al., 1999; Kandeler, 1999; Coppens et al., 2006; Magid et al., 2006; Poll et al., 2006; Védère et al., 2020) and plant-derived organic matter (Inagaki et al., 2023) has been used for this purpose. The role of spatial heterogeneity was also investigated by manipulating soil spatial structure (Strong et al., 2004; Juarez et al., 2013; Tian et al., 2015). The results of such experiments revealed pronounced effects of spatial heterogeneity, like a steep decline in activity with increasing distance from substrate hotspots, or a reduced and delayed activity in the case of heterogeneous substrate addition when compared to homogeneous addition (but see Juarez et al., 2013 and the subsoil results in Inagaki et al., 2023).

Mechanistically, several processes could explain these experimental observations. Granted that most soil microbes are expected to follow stationary sit-and-wait strategies (Nunan et al., 2020), the most frequently offered explanation invokes the spatial separation between microbial consumers and C sources. In this situation, the availability of assimilable substrate is mediated by the diffusion of monomers (either added directly or resulting from the decomposition of polymers) and enzymes (to decompose polymers, Or et al., 2007) as well as by physical C source accessibility (Dungait et al., 2012). Conceptually, a reduction and delay in activity in the case of heterogeneous substrate distribution may then result from a considerable portion of soil microbes that cannot access the substrate and remains C- and energy-limited. However, other limitations may also occur, especially under local excess of substrate. For example, low availability of essential nutrients like nitrogen (N) has the potential to limit the rate of anabolism and thus microbial growth even if sufficient C is present. Such imbalanced stoichiometry reduces CUE and alters SOM utilization in natural soils, for example due to N-mining (Manzoni et al., 2012; Chen et al., 2014; Manzoni, 2017; Chakrawal et al., 2022), and might lead to overflow respiration (Russell and Cook, 1995). Likewise, microbial growth can be impeded if the rate of energy acquisition through catabolism is limited by local O₂ availability in the soil. While this is very common under water-saturated conditions, the mechanism is also relevant at intermediate moisture levels, in particular in microsites with high microbial activity, where the demand-driven onset of anaerobiosis may lower the rate and efficiency of microbial carbon use (Loecke and Robertson, 2009; Schlüter et al., 2019; Kim et al., 2021; Lacroix et al., 2023).

These mechanisms, depending on local availability of substrate, nutrients, and oxygen, likely mediate the effect of substrate spatial heterogeneity to varying degrees *in situ*, but untangling their contributions in particular experimental settings is a challenging task.

Theoretical and modelling frameworks frequently used to interpret experiments (e.g., Korsaeht et al., 2001; Kuka et al., 2007; Moyano et al., 2013; Babey et al., 2017; Zech et al., 2022) recently turned towards leveraging the coupling between C and energy fluxes in soil as a new avenue to elucidate the microbial metabolism and specifically CUE and energy use efficiency (EUE) (e.g., Chakrawal et al., 2020; Bajracharya et al., 2022; Gunina and Kuzakov, 2022; Wang and Kuzakov, 2023). For example, several studies evaluated the calorimetric ratio (CR, Hansen et al., 2004; Barros et al., 2016) of heat to CO₂ production during microbial growth in soil, both experimentally (e.g., Barros et al., 2010; Herrmann and Bölscher, 2015) and theoretically (Chakrawal et al., 2020, 2021; Endress et al., 2024). These efforts demonstrated the potential of the framework to, e.g., monitor changes in microbial CUE or to detect a switch to anaerobic metabolism, especially if CR observations

are supported by modelling efforts to disentangle and quantify these effects. However, this integration of experimental data with process-based bioenergetic models that include an explicit representation of microbial biomass and its dynamics is still at an early stage, a challenge that persists with regard to biogeochemical models more generally (Wieder et al., 2015; Marschmann et al., 2019).

In this study, we investigated the impact of substrate spatial heterogeneity on the dynamics and the efficiency of soil microbial growth from the perspective of coupled C and energy fluxes. To that end, we measured CO₂ and heat production after either homogeneous or heterogeneous addition of glucose as a labile C- and energy source. Based on similar studies, we hypothesized (i) that heterogeneous substrate application would result in lower and delayed microbial growth compared to a homogeneous treatment. To distinguish the potential limiting factors underlying such a pattern, we also monitored the consumption of O₂ throughout the incubations and factorially added nutrients along with glucose. Using this design, transitions to anaerobic pathways due to local O₂ deficiency can be detected both in the CR as well as in the direct O₂ measurements, while local nutrient depletion in hotspots with excess glucose would be alleviated in treatments where glucose is supplied in combination with additional nutrients. We further hypothesized (ii) that these mechanisms are more important causes of reduced microbial growth compared to the spatial availability of glucose itself. Finally, we combined our experimental findings with a simple microbial-explicit model including coupled C- and heat fluxes during growth on glucose to analyze and interpret our results in a quantitative framework, and to discern the degree to which growth limitation (e.g., by O₂ or nutrients) can be inferred from the C- and energy balance.

2. Materials and methods

2.1. Incubation setup

The soil used in this experiment is classified as a Haplic Luvisol and was sampled during September 2021 from the experimental site of Dikopshof, University of Bonn, Germany, established in 1904 (Holthausen et al., 2012; Seidel et al., 2021). Relevant characteristics of the soil are given in Table S1. The soil was sieved through a 2 mm mesh, air dried and stored at room temperature. It was then preincubated at a water content of 14% (w/w, 45.5% of water holding capacity, WHC) for 10 days before the start of the experiment. Water loss due to evaporation was compensated by regular water addition, and any seedlings growing during the preincubation were removed by hand.

Four treatments were considered to investigate the effect of substrate heterogeneity in soil. The soil samples were either amended with a solution of glucose in water or glucose in a nutrient solution ((NH₄)₂SO₄ 9.5 g/L, KH₂PO₄ 14.75 g/L, MgSO₄(H₂O)₇ 19 g/L) at a rate of 1 mg glucose per g soil and with a C:N:P ratio of 10:1:1. In addition, application of glucose was either drop by drop on the soil surface without additional mixing, inducing a heterogeneous substrate distribution, or the soil was manually well mixed after substrate amendment. The added solutions brought the final soil water content to 16% (w/w, 52 % WHC).

2.2. Calorimetry and respirometry measurement

CO₂ efflux after substrate addition was monitored using a Respirometer (Respicond V, Sweden) in which 25.8 g (DW) of soil were incubated in 280 ml vessels that were kept in a water bath at a constant temperature of 20 °C. CO₂ release rate (mg CO₂ h⁻¹) was quantified via the decrease in the conductance of a KOH solution (10 ml, 0.6 M) in the vessels (Chapman, 1971; Nordgren, 1988). Heat release was measured from 3.88 g (DW) soil incubated in 20 ml glass ampoules using an isothermal calorimeter (TAM Air, TA Instruments, Germany) at the same constant temperature of 20 °C. A comparable soil height of 0.9 cm as well as a minimum headspace to soil ratio of 4 was used in both the Respirometer vessels and TAM Air ampoules. The vessels used for the

incubations are shown in Fig. S1.

2.3. O₂ measurement

In a parallel setup, we measured O₂ consumption via needle-type O₂ microsensors (NFSG-PST1, PreSens Precision Sensing GmbH, Regensburg, Germany) that were placed in the headspace of 20 ml glass ampoules with the same experimental setup as used for the TAM Air measurements. O₂ saturation (%; 100% = 21.22 kPa) was monitored every 15 min.

2.4. Microbial biomass quantification and determination of residual glucose

Additional incubations were carried out for well-mixed samples with only glucose addition (i.e., without nutrient addition) for the determination of microbial biomass production via an increase in double-stranded DNA (dsDNA) as well as quantification of the residual amount of glucose. Again, these incubations were carried out in 20 ml ampoules ensuring the same experimental setup as used for the TAM Air measurements. 300 mg of fresh soil was sampled destructively at several time points (0, 18, 21, 25, and 47 h after substrate addition). The dsDNA in the soil was extracted using the PowerSoil DNA isolation kit (QIAGEN, Germany) with small modifications in the protocol by performing an additional physical cell lysis using a homogenizer (Precelleys-24, PEQLAB, Germany) in three batches each for 45 s at 5000 rpm. DNA quantification was done by a NanoDrop ND-8000 spectrophotometer (Thermo Fisher Scientific, Dreieich, Germany). An increase in the microbial biomass was related to changes in the DNA by a conversion factor of $f_{DNA} = 16.5$ calculated as (Zheng et al., 2019):

$$f_{DNA} = \frac{MBC_i}{DNA_i} \quad (\text{Eqn. 1})$$

Here, MBC_i is the initial amount of soil microbial biomass carbon (MBC) as determined by chloroform fumigation extraction (155 $\mu\text{g C g}^{-1}$ soil, details in S1 Text), and DNA_i is the initial dsDNA content of the soil (9.4 $\mu\text{g DNA g}^{-1}$). For the quantification of residual glucose, 200 mg of soil (DW), taken at 0, 3, 6, 21, 23, and 24 h after glucose addition to the soil, was dispersed in 30 ml of DI water followed by shaking on a rotary shaker at room temperature for 30 min. Afterwards, the suspension was centrifuged at 4000 rpm for 10 min. Thereafter, 20 ml of supernatant was transferred to determine residual glucose by a glucose colorimetric/fluorometric assay kit MAK263 (Sigma-Aldrich, Germany) in which glucose is oxidized to generate a fluorometric product, proportional to the glucose amount. Glucose quantification was performed based on the manufacturer's protocol.

CO₂ measurements were performed with 4 replicates, all other experiments were performed in triplicate. All process rates (CO₂ and heat production, O₂ consumption) were corrected by subtracting the average rates of unamended (control) incubations, which were also performed in triplicate.

2.5. Calculations and statistics

Analysis of CO₂ and heat production. Maximum rates of CO₂ and heat release as well as their corresponding time points were determined from the time series of all replicates. For heat release, maximum rates and time points could be identified unambiguously from the raw time series. For CO₂ and O₂, we applied a moving average with a window width of 2 h to the time series prior to determination of maximum rates and time points to enable unambiguous identification. The results were tested for the effects of substrate heterogeneity and nutrient addition using a two-way ANOVA with contrasts between treatments at a significance level $\alpha = 0.05$ as implemented in the emmeans package (v. 1.8.9, Lenth, 2023) in R (v. 4.3.2, R Core Team, 2023).

Cumulative and dynamic ratios. The cumulative ratios of heat to CO₂ production (CR), heat production to O₂ consumption (CR_{O₂}) and CO₂ production to O₂ consumption (respiratory quotient, RQ) were calculated using the respective mean cumulative values after 50 h of incubation time. Standard deviations were estimated via error propagation of the standard deviations of the constituting variables (S1 Text). Due to initial disturbance in the Respicond and the calorimeter, the first 2.5 h were discarded for the cumulative analysis (but raw data are provided in S1 Data). The effects of substrate heterogeneity and nutrient addition were tested using an approximate permutation test for pairwise differences (van den Broek, 2012) with 10000 bootstrap iterations (details in S1 Text).

The dynamic ratios were calculated hourly from the corresponding rate data (mean of replicates). To mitigate the fluctuations caused by the high temporal resolution, the rates were smoothed using a moving average with a width of 4 h prior to calculating ratios. Due to the high sensitivity of the dynamic ratio to even small perturbations, it was calculated in the interval between 5 h and 50 h of incubation time to avoid artifacts caused by initial disturbance.

CUE and EUE. Apparent carbon and energy use efficiency was estimated from the cumulative release of CO₂ and heat, respectively, after 50 h of incubation time, i.e.,

$$CUE_s = 1 - \frac{C_{CO_2}}{C_{Glu}}$$

$$EUE_s = 1 - \frac{Q}{\Delta E_{Glu}}$$

Here, C_{CO_2} and Q denote the mean cumulative CO₂ and heat produced per gram of soil after 50 h, respectively, whereas C_{Glu} and ΔE_{Glu} denote the initial amount of carbon and energy added as glucose per gram of soil. We use the subscript s for CUE and EUE to denote the substrate-based nature of these estimates (Hagerty et al., 2018) and emphasize that these rely on the assumption of complete substrate consumption at the time of calculation (Wang and Kuzyakov, 2023). Again, the effects of substrate spatial heterogeneity and nutrient addition were tested using a two-way ANOVA with contrasts.

O₂ consumption. O₂ saturation O_{sat} [%] was converted to mol per gram soil (DW) via the ideal gas law according to

$$O_2 \left[\frac{\text{mol}}{\text{g}} \right] = \frac{O_{sat}}{100} O_{atm} \frac{V}{T \cdot R} \frac{1}{W}$$

where $O_{atm} = 21.22$ [kPa] denotes the atmospheric oxygen partial pressure, $V = 0.019$ [l] is the estimated volume of air in the ampoule, $T = 293.15$ [K] is experimental temperature, $R = 8.314$ [J/(mol·K)] is the gas constant, and $W = 3.88$ [g] is the dry weight of the soil sample (DW).

2.6. Modeling

We use a modified version of the ordinary differential equation (ODE) model presented in (Endress et al., 2024) to quantitatively simulate the coupled carbon and energy fluxes during microbial growth on glucose in soil. In contrast to the original formulation, the model only includes aerobic metabolism, but considers an additional nutrient limitation.

The model structure (Fig. 1) includes three carbon pools: biomass X , glucose S , and CO₂, similar to the complex physiological model used in Chakrawal et al. (2021). It represents the microbial utilization of added glucose following Monod kinetics (at rate U) for aerobic growth, as well as maintenance respiration, fueled first by glucose (exogenous maintenance, M_S) and later by biomass consumption (endogenous maintenance, M_X , see Wang and Post, 2012). In addition, the model also accounts for changes in microbial activity via the index of physiological state r (Panikov, 1996; Blagodatsky and Richter, 1998), which partitions the biomass into an active, growing fraction rX as well as a dormant

fraction $(1-r)X$ that only performs maintenance, depending on substrate availability. Finally, we also model nutrient limitation by including an additional unspecified nutrient pool N , which acts as an additional essential component for the anabolic reaction and also follows Michaelis-Menten kinetics (i.e., the growth kinetics U now depend on two substrates, carbon S and nutrient N , Zinn et al., 2004). In contrast to glucose, which is added in batch at time 0, the model nutrient concentration gradually replenishes at a rate $I(N_0 - N)$ proportional to the degree of nutrient depletion, thus mimicking diffusive (re-)supply from the surrounding soil.

To investigate the potential impact of a delayed CO_2 detection due to diffusion of CO_2 from the soil to the KOH solution, we also implemented a model variant with an additional carbon pool representing the concentration of CO_2 -C accumulating in the KOH solution (C_{Alkali}). This pool is characterized by slightly delayed dynamics due to the additional transport process, and it is utilized for all subsequent analyses of the modified model instead of the (soil) CO_2 pool that is used in the standard model.

All model ODEs were implemented in Python (version 3.9.18) and simulations were obtained via numerical integration using the 'Radau' method of the `solve_ivp` function in the `Scipy` package (Virtanen et al., 2020). Initial biomass and glucose concentrations were set to the experimental values, whereas initial cumulative heat and CO_2 were set to 0. The initial nutrient concentration as well as the initial active fraction of microbes were treated as free parameters. The model was calibrated against the measured rates of heat and CO_2 release of the individual treatments, i.e., we obtained 4 sets of optimized parameter values corresponding to the combinations of substrate spatial heterogeneity (homogeneous, heterogeneous) and nutrient addition (with, without). Parameter optimization was done using the Levenberg-Marquardt algorithm in the `minimize` function of the `lmfit` package (Newville et al., 2023) with upper and lower bounds on individual parameters.

The detailed model formulation and rationale as well as an in-depth description of the numerical procedures are provided in the supplementary materials and methods (S1 Text). A list of all variables and parameters including their units is provided in Table S2.

3. Results

3.1. CO_2 and heat release and O_2 consumption

The rates of CO_2 and heat release as well as O_2 consumption showed a broadly consistent pattern indicating substantial microbial growth

after batch glucose input in all treatments, with a distinct maximum after 20–25 h (Fig. 2). However, both the mode of glucose application and the addition of nutrients had characteristic and interacting effects on the observed dynamics.

In treatments without nutrient addition, heterogeneous application of glucose resulted in significantly lower maximum rates of carbon and heat release (Fig. 2 a, c), which reached only 50–55% of the maximum values observed after homogeneous glucose application (ANOVA results in S1 Data). On the other hand, both CO_2 and heat continued to be released at elevated rates in these incubations over the full 50 h duration, whereas they returned to near-basal levels within that time span in samples with homogeneous glucose addition (Fig. 2a–c). While less pronounced, these characteristics were also present in the measured rates of O_2 consumption (Fig. 2e). Headspace O_2 concentrations remained oxalic throughout the experiment in all treatments (Fig. S2).

In contrast, such effects of heterogeneous substrate application were strongly reduced in treatments with nutrient addition. Maximum rates of CO_2 and heat release as well as O_2 consumption were similar or only slightly lower in heterogeneous treatments when compared to homogeneous ones, and all rates also decreased to similar levels within 50 h (Fig. 2b–d,f). Nonetheless, maximum values in incubations with heterogeneous glucose application were reached slightly later (~2 h) than in those with homogeneous application. While this effect was only significant for heat, it was entirely absent in the treatments without nutrient addition (ANOVA results in S1 Data).

Thus, the effect of heterogeneous substrate application was most pronounced in samples without added nutrients. At the same time, nutrient addition altered the observed dynamics only in the case of heterogeneous substrate application, with barely any discernible impact in samples with homogeneous application.

3.2. Cumulative calorimetric ratios and respiratory quotient

The ratios of cumulative heat release to CO_2 release as well as to O_2 consumption (CR and CR_{O_2} , respectively) showed similar values with no significant differences across treatments. The same was true for the respiratory quotient (RQ) of CO_2 release to O_2 consumption. Hence, from a cumulative perspective, neither the mode of substrate application nor the addition of nutrients had a significant effect (Fig. 3).

Furthermore, no ratio indicated any substantial deviation from values expected for aerobic metabolism in our incubation after 50 h. Specifically, the observed average CR values of 344–403 kJ/mol C agree with predictions for efficient aerobic growth on glucose, which lie in the range of ~250–469 kJ/mol C (Barros et al., 2010). Similarly, average

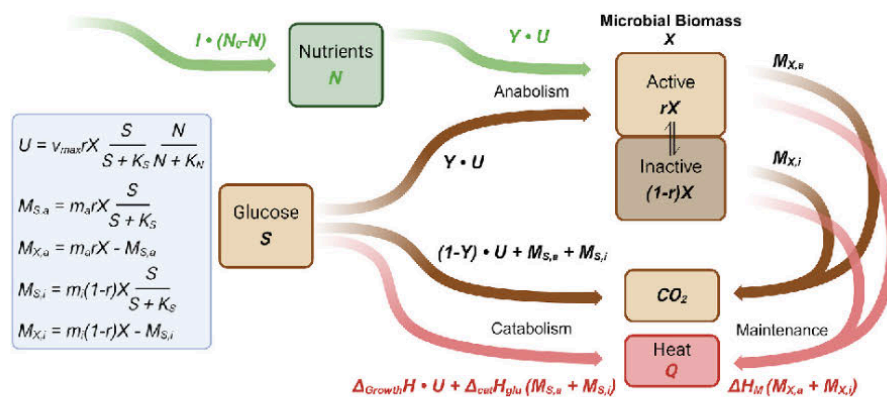


Fig. 1. Dynamic model structure representing aerobic microbial growth after glucose addition to soil. Microbial biomass X is initially in a largely inactive state (fraction $1-r$), but quickly becomes active (fraction r) in the presence of substrate S . This substrate is consumed following Michaelis-Menten kinetics at a rate U and partitioned between anabolic and catabolic pathways according to a growth yield coefficient Y . The uptake rate is further co-limited by the availability of a proxy nutrient pool N required for anabolism. Moreover, both active and inactive biomass produce additional CO_2 and heat via exogenous maintenance ($M_{S,i}$, fueled by glucose consumption) and endogenous maintenance ($M_{X,i}$, fueled by biomass consumption). The total modelled CO_2 and heat production is used to calibrate the model against experimental observations for each treatment. A detailed model description is provided in S1 Text.

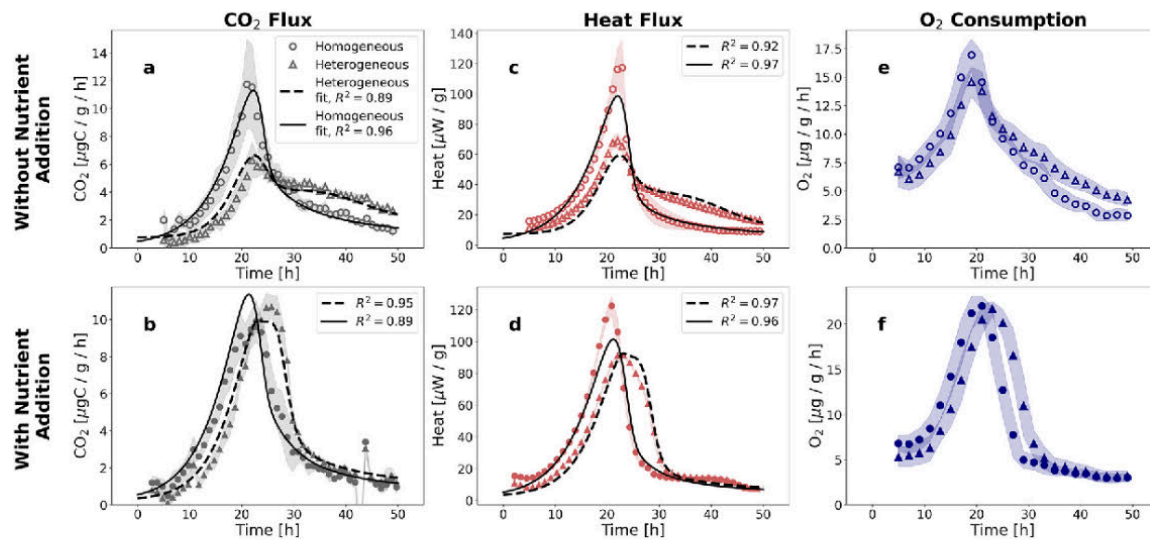


Fig. 2. Experimental observations (mean \pm SD) and model simulations of CO₂ production (a, b, $n = 4$), heat production (c, d, $n = 3$) production and O₂ consumption (e, f, $n = 3$) in soil after glucose amendment. The top row shows results obtained without nutrient addition (open symbols), while the bottom row shows results with addition of NPK solution (filled symbols). In both cases, rates of CO₂ and heat production as well as O₂ consumption differed markedly between homogeneous (circles) and heterogeneous (triangles) addition of glucose to the soil.

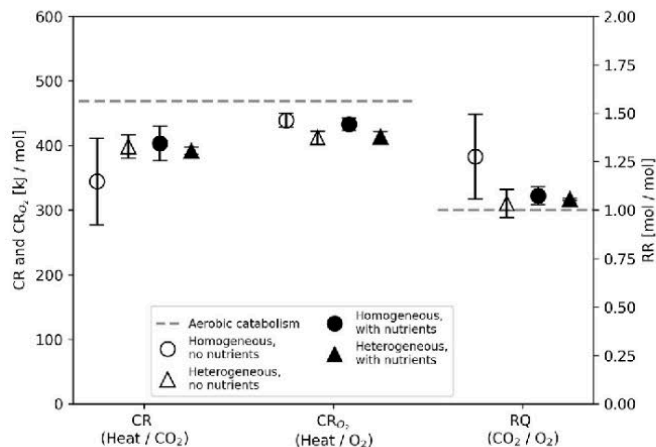


Fig. 3. Experimental ratios (mean \pm SD) calculated from cumulative CO₂ production, heat production and O₂ consumption after 50 h of incubation time. Open symbols indicate incubations without nutrient addition, filled symbols indicate incubations with NPK addition. Circles indicate homogeneous addition of glucose; triangles indicate heterogeneous addition. Dashed lines indicate the theoretical predictions for the corresponding ratios for the case of aerobic glucose catabolism.

CR_{O₂} varied between 411 and 439 kJ/mol O₂, while anaerobic heat contributions would elevate this ratio above the theoretical prediction of 469 kJ/mol O₂ (enthalpy of combustion of glucose, Hansen et al., 2004). Finally, the average RQ in all treatments was not significantly different from 1, which is the expected value for the aerobic decomposition of carbohydrates.

3.3. CUE and EUE

Both CUE_S and EUE_S based on cumulative CO₂ and heat release after 50 h indicated efficient aerobic growth with an average growth yield of 0.56–0.63 (carbon-based) and 0.65–0.68 (energy-based) across treatments (Fig. 4a). Generally, EUE was slightly higher than CUE in all incubations (i.e., observations are above the dotted line in Fig. 4a), and their relationship was in line with the theoretical expectation for aerobic

growth on glucose (dashed and solid lines in Fig. 4a, details in S1 Text). Moreover, the observed relationship between CUE_S and CR also was broadly consistent with theory (Fig. 4b), although the quantitative prediction depends on the assumed composition of microbial biomass as summarized by its degree of reduction, γ_B (which is controlled by the C: N ratio of biomass, see Hansen et al., 2004; Chakrawal et al., 2020; Yang et al., 2024 and S1 Text). However, both CUE_S and CR showed substantial variability, in particular for the treatment with homogeneous glucose application and no nutrient addition, which was characterized by larger deviations in the CO₂ release rate between replicates (Fig. 2a).

Overall, neither the mode of substrate application nor the addition of nutrients significantly affected CUE_S, while nutrient addition slightly reduced EUE_S irrespective of the mode of substrate application (ANOVA results in S1 Data).

3.4. Model behavior and performance

The dynamic model achieved good fits to the experimental observations in all treatments (Fig. 2 a–d, $R^2 = 0.89$ – 0.97) and adequately represented the general dynamics of CO₂ and heat release over the 50 h after addition of glucose. In particular, the model captured the prolonged release of CO₂ and heat in the case of heterogeneous substrate application without nutrient addition (Fig. 2 a, c) via its simple representation of nutrient dynamics.

The model also achieves a very good correspondence with experimental measurements of remaining glucose over time in the one treatment where this data is available (Fig. S3a). There was also a broad agreement between the predicted microbial biomass growth in the model and that inferred from dsDNA, although the relative biomass increase in the model (2.45-fold after 50h) exceeded the relative increase in dsDNA in the same treatment (which increased 1.84-fold, Fig. S3b, details in S1 Text).

The calibration results for all parameters and treatments along with uncertainty estimates are provided in S1 Data. Generally, the optimized values of most parameters were well comparable for all treatments and showed a plausible range and pattern (e.g., high aerobic yield coefficients and higher maintenance costs for the active fraction than the inactive fraction, calibration results in S1 Data). However, the parameters controlling the activity state of the microbial population differed between treatments with homogeneous and heterogeneous glucose

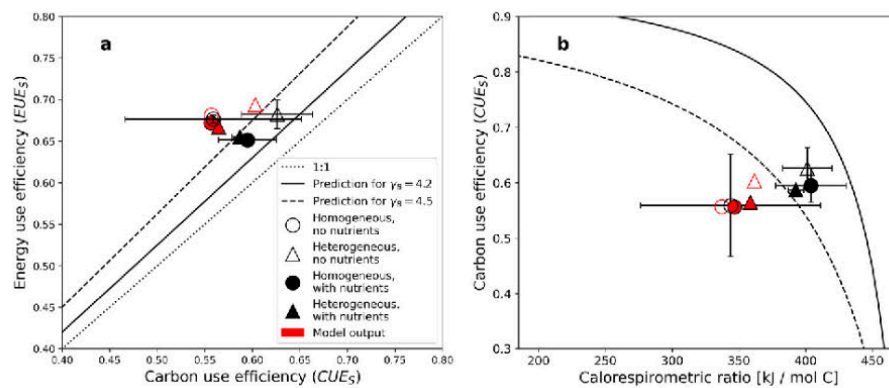


Fig. 4. Estimates of CUE, EUE and CR (mean \pm SD) based on cumulative CO_2 and heat production after 50 h of incubation. Black symbols are based on experimental observations, red symbols were obtained from corresponding model simulations. The solid and dashed lines show the theoretical CUE-CR relationships for aerobic growth on glucose assuming a biomass degree of reduction (γ_B) corresponding to C:N ratios of 5 ($\gamma_B = 4.2$) and 10 ($\gamma_B = 4.5$), respectively (Yang et al., 2024). Symbol styles correspond to Fig. 3. **a** EUE_S and CUE_S were comparable across treatments and are in line with theoretical predictions. **b** Relationship between estimated CUE_S and CR.

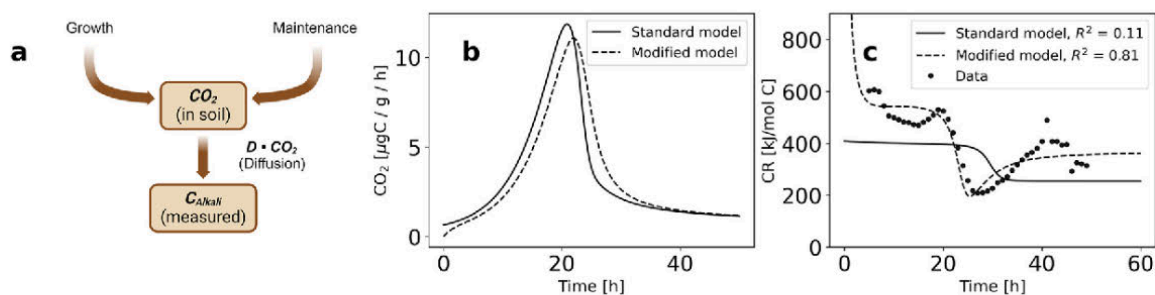


Fig. 5. Potential time delay between the production of CO_2 by microbes in the soil and its experimental detection in the alkali solution complicate the evaluation of dynamic CR. **a** In a modified model variant, CO_2 diffuses to the site of detection (e.g., alkali solution), where it accumulates in an additional pool (C_{Alkali}). **b** In the modified model, the measured rate of CO_2 release (i.e., C_{Alkali}) is systematically delayed compared to the standard model, which assumes instantaneous detection after production by microbes in the soil. **c** If CR is calculated from the ratio of the rates of heat and (measured) CO_2 release, the systematic delay of CO_2 in the modified model induces a temporal pattern that is qualitatively similar to those observed in experimental data (shown are the results for homogeneous glucose application and with nutrient addition, all curves and fits are shown in Fig. S4).

application. Specifically, the model predicted a lower initial active fraction of microbes as well as an overall lower activity over the course of the whole incubation in treatments with heterogeneous substrate application (Fig. S3c), regardless of nutrient addition. In terms of model calibration, this difference is tied to the overall slower dynamics in those treatments (see 3.1), and it can be intuitively thought of as a smaller fraction of the biomass being exposed (and reacting) to the available glucose, as expected in the case of heterogeneous application.

In terms of CR, the (purely aerobic) growth reaction used in the model corresponds to the solid line in Fig. 4b. However, the actual relationship between model CUE_S and CR is altered by the maintenance metabolism (details in S1 Text) and broadly resembled experimental observations after calibration. Nonetheless, model CR tended to be lower than observations in all treatments other than the incubations with homogeneous substrate application and no nutrient addition, indicating that the final calibration slightly overestimated cumulative CO_2 release compared to cumulative heat release in those treatments (Figs. 2 and 4b).

3.5. Dynamic CR and model variant with delayed CO_2 detection

The dynamic CR calculated from the rates of heat and CO_2 production showed strong temporal variation in all treatments, including values well above and below those expected for simple aerobic growth (Fig. S4). Specifically, rate-based CR was high early in the incubation followed by a drop after the time of peak activity during the retardation

phase, and while this general pattern was observed for all treatments, it was more pronounced in the case of heterogeneous substrate addition (Figs. S4c and d).

Although the dynamic model captured such a qualitative shift from high to low CR, it did not reproduce the quantitative details, especially the very high values during the exponential growth phase (Fig. S4). However, the introduction of a moderate delay of the measured CO_2 release rate in the modified model variant improved the CR representation considerably (Fig. 5). In particular, the model delay of 1.2–1.8 h due to diffusion of CO_2 from the site of production in the soil to the site of detection in the KOH solution (Fig. 5a and b) resulted in a pronounced and characteristic pattern in the dynamic model CR similar to observations (Fig. 5c). While the model fit to the rate data improved only slightly across treatments compared to the standard model ($R^2 = 0.93$ – 0.99 instead of 0.89 – 0.97), this difference was much more pronounced in the CR, where small changes in modelled rates induced large changes in modelled CR due to its nature as quotient (with R^2 improving from -0.09 – 0.81 to 0.27 – 0.81 , Fig. S4).

4. Discussion

4.1. Substrate spatial heterogeneity induces nutrient limitation of microbial growth

We observed marked differences in the dynamics of CO_2 and heat release from an arable soil after the heterogeneous drop-by-drop

application of glucose when compared to the well-mixed, homogeneous application of the substrate. This effect of spatial heterogeneity can in large part be attributed to nutrient limitation: in the heterogeneous treatment, the local availability of nutrients in the substrate hotspots was not sufficient to sustain the high microbial growth rate in the presence of a large excess of C. On the other hand, mixing alleviated this limitation by distributing the same amount of glucose more evenly across the sample, such that sufficient soil-derived nutrients were available. This is plausible given that the soil used was sampled from an experimental site with long-term fertilization with farmyard manure (Holthusen et al., 2012; Seidel et al., 2021, Table S1 soil characteristics) and because the addition of a full nutrient solution instead of just glucose did not yield any discernible difference in the dynamics of the homogenized treatments (Fig. 2). This indicates no general nutrient limitation in this soil, although such limitations are commonly found in respiration experiments with many diverse soils (e.g., Sawada et al., 2017).

However, the fact that the dropwise heterogeneous addition of glucose was sufficient to induce local nutrient limitation in this soil highlights the need for careful consideration of both (i) experimental protocols and (ii) microbial dynamics in natural soils, where substrate (and nutrient) availability is highly localized in space and time (Kuznyakov and Blagodatskaya, 2015). Notably, we only used a single rate of glucose addition (1 mg glucose/g soil, corresponding to ~2.5 MBC) across treatments in this experiment. According to our results, we would predict that adding larger amounts of C should begin to induce a similar nutrient limitation even in homogenized samples, as the (equally distributed) glucose concentration approaches the one experienced locally by microbes in our heterogeneous incubations. Conversely, lower rates of C addition should alleviate the nutrient limitation even in heterogeneous treatments. The rate of glucose addition is well known to strongly affect the outcome of respiration experiments (e.g., Schneckengerber et al., 2008; Reischke et al., 2014; Rousk et al., 2014), and varying it would thus be an option to investigate the details of the induced nutrient limitation and its role in determining the effect of substrate spatial heterogeneity (see also Ilstedt et al., 2006; Gnankam-bary et al., 2008). In particular, functional differences in microbial communities may only affect soil C dynamics under conditions that do not constrain microbial activity (Nunan et al., 2017).

A similar pattern of reduced maximum heat release rates and prolonged heat production after glucose addition in soil microcosms with varying degrees of substrate spatial heterogeneity has previously been explained by the possible effects of substrate diffusion and the co-location of substrate and microorganisms (Shi et al., 2021). The importance of such effects has long been studied both empirically and via modelling across scales (e.g., Gaillard et al., 1999; Portell et al., 2018), yet they cannot explain the strongly reduced effect of substrate spatial availability in our experiment in the presence of additional nutrients (critically, no nutrients were added along with glucose in the experiment of Shi et al., 2021). Nonetheless, we do still find a small delay and reduction in the activity of the heterogeneous treatment after nutrient addition (Fig. 2b–d), which we assume to be caused by such a consumer-resource dislocation as discussed in Shi et al. (2021). Specifically, even if nutrients are sufficient, the exponential growth of microbes exposed to substrate in a smaller number of hotspots lagged behind that of samples in which all microbes had immediate access to the evenly distributed substrate (Fig. 2b–d).

The dynamics of CO₂ and heat release of all treatments were adequately captured by the simple model of aerobic microbial growth on glucose and an additional nutrient pool, representing a nutrient proxy comprising all essential nutrients. Specifically, the elevated rates of CO₂ and heat release well beyond the respective peaks in the heterogeneous treatment in Fig. 2a–c can be explained by the continued consumption of glucose by microbes in the model, which are unable to make use of all of the available substrate during the exponential growth phase due to nutrient limitation. Instead, they continue to grow for a longer period

and reach a similar biomass by the time all available glucose has been consumed (Fig. S3b), even though they cannot grow as quickly under the nutrient-limited conditions early in the incubation. This intuition is supported by very similar overall CUE (and EUE) in the model after 50 h across treatments (Fig. 4a).

Importantly, the model did not include any spatially explicit structure, and a minimal representation of nutrient availability via Michaelis-Menten-type kinetics was sufficient to quantitatively capture the patterns in the observed data (Fig. 2). Effectively, the low nutrient concentrations (corresponding to the limited amount available in substrate hotspots) acted to lower the overall microbial growth rate, an effect that was studied in detail by Chakrawal et al. (2022). Intriguingly, the model calibration also accounted for the substrate spatial heterogeneity by reducing overall microbial activity in heterogeneous treatments, regardless of nutrient status (Fig. S3c). While the initial MBC in the model was fixed to the experimentally determined value (155 µg C g⁻¹, details in S1 Text), this behavior can be interpreted as lowering the effective initial model MBC, with a smaller part of the microbial community reacting to the constant amount of added substrate. This mimics the smaller co-location of (or larger distance between) substrate and consumers (e.g., Pinheiro et al., 2015; Babey et al., 2017) without a spatially explicit structure and accounts for the residual effect of substrate spatial heterogeneity in the absence of nutrient limitation.

While the nutrient limitation changed the temporal dynamics of microbial growth in the corresponding treatments, neither the model nor the experimental data indicated a substantial reduction in microbial growth yield after 50 h (Fig. 4a). Instead, all incubations and simulations were characterized by very similar values of CUE_s and EUE_s broadly in the range of 0.55–0.65 (Fig. 4a), which is consistent with theoretical constraints and empirical observations of efficient aerobic growth on glucose (e.g., Heijnen and Van Dijken, 1992; Trapp et al., 2018). Remarkably, Inagaki et al. (2023) observed a very similar pattern in a recent study, but these authors were using plant-derived organic matter as a more complex carbon source and performed longer incubations. After substrate addition either in hotspots or homogeneously to topsoil, they also found a pronounced effect of heterogeneity on the process rates but not on the efficiency based on cumulative CO₂.

Although the estimation of growth based solely on CO₂ or heat release using CUE_s and EUE_s is generally problematic (Hagerty et al., 2018), both estimates were in good agreement in our experiment, and their underlying assumption of complete substrate consumption was justified after 50 h (Fig. S3a). Moreover, we found that EUE_s consistently exceeded CUE_s, in line with theory (S1 Text) and contrary to the recent review by Wang and Kuznyakov (2023). However, both estimates as well as model simulations indicated a larger biomass growth than did dsDNA, although dsDNA was only measured in the homogenized treatment without nutrient addition. In part, these differences may be explained by variability in the initial biomass in our incubations (S1 Text). Yet, this observation might also indicate that not all glucose consumed is immediately used for growth with a corresponding proportional increase in dsDNA, and that the conversion factor between dsDNA and biomass carbon initially increases after substrate addition (Čapek et al., 2023, details in S1 Text). In any case, the direct quantification of MBC and especially the use of isotope-labeled substrates would greatly strengthen any future investigations.

Overall, our first hypothesis regarding microbial growth was therefore only partly confirmed. While we did observe reduced and delayed microbial activity under spatially heterogeneous conditions in the treatment without nutrient addition, this impaired activity was only partly observed when nutrients were added in parallel. Moreover, all available estimates and the dynamic model indicate that net growth was comparable among the treatments after 50 h of incubation. Finally, nutrient limitation (though not O₂, see below) was indeed the more important cause behind this effect of substrate spatial heterogeneity when compared to the spatial separation of glucose and microbes, confirming the nutrient aspect of our second hypothesis.

4.2. Substrate spatial heterogeneity does not induce local O₂ limitation

We also hypothesized that local oxygen availability might be another limiting factor for microbial growth under heterogeneous substrate conditions and could potentially induce anaerobic metabolism. Conceptually, microbial O₂ demand in the presence of high substrate concentrations has the potential to locally outpace physical O₂ supply and contribute to the formation of anoxic microsites that form on microbial hotspots. The importance of this mechanism has been recognized even in well-drained upland soils (e.g., Keiluweit et al., 2017; Lacroix et al., 2022). However, we found no evidence of substantial anaerobiosis in our experiment, with neither the direct O₂ measurements nor any of the cumulative ratios (CR, CR_{O₂}, RQ) indicating such an O₂ limitation in our incubations (Figs. 2 and 3, Fig. S2). Furthermore, substantial contributions of anaerobic metabolism would leave a distinct signature in the CR depending on the specific metabolic pathway (Barros et al., 2016; Boye et al., 2018; Chakrawal et al., 2020), and any CO₂ produced anaerobically would elevate RQ values. In addition, any demand-driven O₂ limitation should arguably be at least as severe in the treatments with nutrient addition, yet we did not find substantial differences in the dynamics or microbial efficiency of those incubations. Lastly, the model was also able to accurately capture the observed dynamics assuming a purely aerobic (growth and maintenance) metabolism.

Importantly, even though the soil in the treatments simulating heterogeneous conditions was not mixed after the dropwise application of glucose, the soil used for all samples had been sieved, dried, rewetted, and mixed beforehand. Consequently, any comparison or inference to natural soils with intact structure that may promote the formation of anoxic conditions is not feasible. Similarly, the soil disturbance will disrupt the local microbial community and alter its use of the labile substrate, e.g., regarding rate and efficiency, when compared to undisturbed soil (Thomson et al., 2010; Ruamps et al., 2011).

Finally, we note that anaerobic pathways such as fermentations may also be carried out by microbes under purely aerobic conditions if substrate concentration is high, a phenomenon sometimes termed overflow metabolism (Basan et al., 2015). While this would affect the assumption of complete conversion of glucose to biomass and CO₂, we suggest that it likely did not occur to a significant extent in our experiment, since the measured cumulative ratios (Fig. 3) did not reveal any pattern characteristic of these fermentations (Chakrawal et al., 2020).

4.3. Leveraging coupled carbon and energy fluxes

Our estimates of the cumulative CR were consistent with efficient aerobic growth of microbes on glucose and indicated no substantial deviations, e.g., caused by anaerobiosis (Barros et al., 2016; Chakrawal et al., 2020). In essence, both the carbon and energy balances suggest a similar, simple interpretation of our experimental findings (Figs. 3 and 4). CR should be understood as the ratio of the corresponding (instantaneous) rates of CO₂ and heat production, and thus as a dynamic quantity (Hansen et al., 2004). In fact, the use of total cumulative values for the CR calculation is equivalent to using the average production rates over the incubation, thereby muting any temporal pattern. While such a simplification has been used before (e.g., Herrmann and Bölscher, 2015), it greatly reduces the amount of available information, and we found pronounced temporal variation of the CR in all treatments (Fig. 5, Fig. S4). Hence, the full potential of the framework could be leveraged by including this dynamic information in the analysis.

For example, the consistent shift from higher CR values during the exponential growth phase to lower values after the onset of the retardation phase when substrate is depleted (Fig. S4) was also recently observed in a similar experiment using the same soil (Yang et al., 2024) and may be interpreted as a shift from growth metabolism to a metabolism dominated by maintenance processes. When using cumulative CR, averaging the rates across the exponential and retardation phases would mask the individual CR values of these processes and alter the

relationship between observed CUE and (cumulative) CR. This may also account for some of the observed deviation from theoretical predictions in Fig. 4B, which are based on pure growth without maintenance (for details, see also S1 Text).

In contrast, the shift in dynamic CR is mechanistically captured by the dynamic model via a decrease in the active fraction of biomass (Fig. S3c) and a transition from exogenous (glucose-consuming) to endogenous (biomass carbon-consuming) maintenance (Wang and Post, 2012) once the substrate is depleted (Fig. S4). Nonetheless, based on heat and CO₂ alone, the model cannot distinguish between different equally plausible (biochemical) processes that could result in the specific lower CR value during the retardation phase, e.g., the use of SOM, necromass formation, or consumption of storage compounds (details S1 Text). This conceptual limitation of the CR, which integrates the contributions of all heat- and CO₂-producing processes, could at least in part be overcome by additional measurements, in particular by monitoring biomass (composition) and by using labeled substrates. Such measurements would also help to improve parameter identifiability, which is often low in soil biogeochemical models like the one employed here (see e.g. Sierra et al., 2015; Marschmann et al., 2019). Specifically, observations of these additional carbon pools can reduce equifinality, the phenomenon that multiple (complex) model formulations and parameterizations yield identical dynamics of the (limited) observed data, which remains a major challenge (Wieder et al., 2015).

The quantitative interpretation of dynamic CR curves also faces substantial challenges from an experimental perspective. One source of error stems from the fact that the (dynamic) CR is highly sensitive to even minor shifts in the relative timing of CO₂ and heat, due to its nature as a quotient. In particular, the measurement of CO₂ and heat in separate incubations, which frequently also takes place in different types of vessels, requires matching experimental conditions (e.g., keeping the same soil-to-head space volume as in our study) to minimize potential effects on CR dynamics. This problem has been recognized, but the development of setups allowing the simultaneous measurement of CO₂ and heat is still ongoing (Barros et al., 2010; Yang et al., 2024).

Our modified model variant (Fig. 5a), in which CO₂ is measured after an additional transport process mimicking the diffusion of the gas from its site of production (microbes in the soil) to the site of detection (alkali solution above the headspace), illustrates this problem. The transport causes a relative delay of CO₂ compared to heat of around 1.2–1.8h, which is consistent with simple estimates of the diffusion time in our experimental system (Fig. 5b, details are presented in S1 Text). Intriguingly, this moderate shift in timing induced an artificial temporal CR pattern in the model which resembles those observed in our treatments (Fig. 5c) as well as in the literature (e.g., Barros et al., 2010). Thus, the quantitative evaluation of the dynamic CR requires a careful disentanglement of features that may be caused by the experimental setup from those corresponding to actual microbial activity, such as a slightly faster (0.5–2 h) heat vs CO₂ release in response to the input of labile substrate. While this is beyond the scope and data availability of this study, future work aiming at simultaneous measurements of carbon and energy fluxes would benefit from the use of labeled substrates to quantify potential biases. This will enable the full utilization of this promising tool to obtain a mechanistic, bioenergetic understanding of the soil system.

4.4. Conclusion

Based on rates of CO₂ and heat production, substrate spatial heterogeneity resulted in reduced but prolonged microbial activity in glucose-amended soil. This effect could be attributed to local nutrient limitation and was mitigated if nutrients were added along with glucose, while we found no evidence of substantial oxygen limitation in any of our incubations. The observed dynamics were well described by a simple model of aerobic microbial growth. Notably, both simulations and experimental evidence revealed no significant effect of spatial

heterogeneity or nutrient addition on the overall CUE and EUE after 50 h. These findings demonstrate that local nutrient availability in soils can be the major factor limiting microbial growth rates, but not necessarily efficiency, if C sources have patchy distributions in space and time. Conversely, microbes in substrate hotspots may be able to compensate for the smaller overall co-location of consumers and substrate in the soil if ample nutrients are available in those hotspots.

Furthermore, the joint application experimental and process-based modeling techniques is a powerful tool for the analysis of microbial dynamics in soil. In this study, data-model integration provided mechanistic insights on the contributions of nutrient limitation and reduced microbial activity to the observed effect of substrate spatial heterogeneity, and quantitatively revealed potential biases arising from the combination of temporal CO₂ and heat measurements. If such artifacts are accounted for, future analyses may harness the full potential of this bioenergetic framework to study the dynamics of coupled C- and energy fluxes in the soil system.

Finally, our observations also illustrate that even relatively minor differences in the application of labile substrate to soils, like (lack of) thorough mixing after glucose amendment, do not affect the overall CUE and EUE values, but they have the potential to significantly alter the dynamics in a laboratory setting. The possibility of such methodological details introducing artificial patterns must be carefully evaluated in the specific context of similar experiments.

CRediT authorship contribution statement

Martin-Georg Endress: Writing – review & editing, Writing – original draft, Visualization, Software, Formal analysis, Data curation. **Fatemeh Dehghani:** Writing – review & editing, Writing – original draft, Visualization, Validation, Investigation, Data curation. **Sergey Blagodatsky:** Writing – review & editing, Supervision, Project administration, Methodology, Funding acquisition, Conceptualization. **Thomas Reitz:** Writing – review & editing, Supervision, Project administration, Methodology, Funding acquisition, Conceptualization. **Steffen Schlüter:** Writing – review & editing, Supervision, Project administration, Methodology, Funding acquisition, Conceptualization. **Evgenia Blagodatskaya:** Writing – review & editing, Supervision, Project administration, Methodology, Funding acquisition, Conceptualization.

Declaration of competing interest

The authors declare the following financial interests/personal relationships which may be considered as potential competing interests:

All authors report that financial support was provided by the German Research Foundation. All authors declare that they have no other known competing financial interests or personal relationships that could have appeared to influence the work reported in this paper.

Data availability

All data analyzed during this study are included in this published article and its supplementary files. All modeling code is available from the corresponding author upon reasonable request.

Acknowledgments

This study was performed within the framework of the German Science Foundation (DFG) Priority Program “SPP 2322 – System ecology of soils – Energy Discharge Modulated by Microbiome and Boundary Conditions (SoilSystems)”. The work was funded by the DFG under the grants 465124939 (MGE, SB) and 465122443 (FD, TR, SS, EB). Schematics (Figs. 1 and 5a) were created with BioRender.

Appendix A. Supplementary data

Supplementary data to this article can be found online at <https://doi.org/10.1016/j.soilbio.2024.109509>.

References

- Babey, T., Vieublé-Gonod, L., Rapaport, A., Pinheiro, M., Garnier, P., De Dreuzy, J.-R., 2017. Spatiotemporal simulations of 2,4-D pesticide degradation by microorganisms in 3D soil-core experiments. *Ecological Modelling* 344, 48–61. <https://doi.org/10.1016/j.ecolmodel.2016.11.006>.
- Bajracharya, B.M., Smeaton, C.M., Markelov, I., Markelova, E., Lu, C., Cirpka, O.A., Cappellen, P.V., 2022. Organic matter degradation in energy-limited subsurface environments—a bioenergetics-informed modeling approach. *Geomicrobiology Journal* 39, 1–16. <https://doi.org/10.1080/01490451.2021.1998256>.
- Bardgett, R.D., Freeman, C., Ostle, N.J., 2008. Microbial contributions to climate change through carbon cycle feedbacks. *The ISME Journal* 2, 805–814. <https://doi.org/10.1038/ismej.2008.58>.
- Barros, N., Hansen, L.D., Piñeiro, V., Pérez-Cruzado, C., Villanueva, M., Proupín, J., Rodríguez-Añón, J.A., 2016. Factors influencing the calorimetric ratios of soil microbial metabolism. *Soil Biology and Biochemistry* 92, 221–229. <https://doi.org/10.1016/j.soilbio.2015.10.007>.
- Barros, N., Salgado, J., Rodríguez-Añón, J.A., Proupín, J., Villanueva, M., Hansen, L.D., 2010. Calorimetric approach to metabolic carbon conversion efficiency in soils: comparison of experimental and theoretical models. *Journal of Thermal Analysis and Calorimetry* 99, 771–777. <https://doi.org/10.1007/s10973-010-0673-4>.
- Basan, M., Hui, S., Okano, H., Zhang, Z., Shen, Y., Williamson, J.R., Hwa, T., 2015. Overflow metabolism in *Escherichia coli* results from efficient proteome allocation. *Nature* 528, 99–104. <https://doi.org/10.1038/nature15765>.
- Blagodatsky, S.A., Richter, O., 1998. Microbial growth in soil and nitrogen turnover: a theoretical model considering the activity state of microorganisms. *Soil Biology and Biochemistry* 30, 1743–1755. [https://doi.org/10.1016/S0038-0717\(98\)00028-5](https://doi.org/10.1016/S0038-0717(98)00028-5).
- Boye, K., Herrmann, A.M., Schaefer, M.V., Tfaily, M.M., Fendorf, S., 2018. Discerning microbially mediated processes during redox transitions in flooded soils using carbon and energy balances. *Frontiers in Environmental Science* 6, 15. <https://doi.org/10.3389/fenvs.2018.00015>.
- Čapek, P., Choma, M., Kaštovská, E., Tahovská, K., Glanville, H.C., Šantrůčková, H., 2023. Revisiting soil microbial biomass: considering changes in composition with growth rate. *Soil Biology and Biochemistry* 184, 109103. <https://doi.org/10.1016/j.soilbio.2023.109103>.
- Chakraborty, A., Calabrese, S., Herrmann, A.M., Manzoni, S., 2022. Interacting bioenergetic and stoichiometric controls on microbial growth. *Frontiers in Microbiology* 13, 859063. <https://doi.org/10.3389/fmicb.2022.859063>.
- Chakraborty, A., Herrmann, A.M., Manzoni, S., 2021. Leveraging energy flows to quantify microbial traits in soils. *Soil Biology and Biochemistry* 155, 108169. <https://doi.org/10.1016/j.soilbio.2021.108169>.
- Chakraborty, A., Herrmann, A.M., Šantrůčková, H., Manzoni, S., 2020. Quantifying microbial metabolism in soils using calorimetry — a bioenergetics perspective. *Soil Biology and Biochemistry* 148, 107945. <https://doi.org/10.1016/j.soilbio.2020.107945>.
- Chapman, S.B., 1971. A simple conductimetric soil respirometer for field use. *Oikos* 22, 348–353. <https://doi.org/10.2307/3543857>.
- Chen, R., Senbayram, M., Blagodatsky, S., Myachina, O., Dittler, K., Lin, X., Blagodatskaya, E., Kuzyakov, Y., 2014. Soil C and N availability determine the priming effect: microbial N mining and stoichiometric decomposition theories. *Global Change Biology* 20, 2356–2367. <https://doi.org/10.1111/gcb.12475>.
- Coppens, F., Merckx, R., Recous, S., 2006. Impact of crop residue location on carbon and nitrogen distribution in soil and in water-stable aggregates. *European Journal of Soil Science* 57, 570–582. <https://doi.org/10.1111/j.1365-2389.2006.00825.x>.
- Crowther, T.W., Van Den Hoogen, J., Wan, J., Mayes, M.A., Keiser, A.D., Mo, L., Averill, C., Maynard, D.S., 2019. The global soil community and its influence on biogeochemistry. *Science* 365, eaav0550. <https://doi.org/10.1126/science.aav0550>.
- Dungait, J.A.J., Hopkins, D.W., Gregory, A.S., Whitmore, A.P., 2012. Soil organic matter turnover is governed by accessibility not recalcitrance. *Global Change Biology* 18, 1781–1796. <https://doi.org/10.1111/j.1365-2486.2012.02665.x>.
- Endress, M.-G., Chen, R., Blagodatskaya, E., Blagodatsky, S., 2024. The coupling of carbon and energy fluxes reveals anaerobiosis in an aerobic soil incubation with a *Bacillota*-dominated community. *Soil Biology and Biochemistry* 195, 109478. <https://doi.org/10.1016/j.soilbio.2024.109478>.
- Gaillard, V., Chenu, C., Recous, S., Richard, G., 1999. Carbon, nitrogen and microbial gradients induced by plant residues decomposing in soil. *European Journal of Soil Science* 50, 567–578. <https://doi.org/10.1046/j.1365-2389.1999.00266.x>.
- Geyer, K.M., Kyker-Snowman, E., Grandy, A.S., Frey, S.D., 2016. Microbial carbon use efficiency: accounting for population, community, and ecosystem-scale controls over the fate of metabolized organic matter. *Biogeochemistry* 127, 173–188. <https://doi.org/10.1007/s10533-016-0191-y>.
- Gnankambary, Z., Ilstedt, U., Nyberg, G., Hien, V., Malmér, A., 2008. Nitrogen and phosphorus limitation of soil microbial respiration in two tropical agroforestry parklands in the south-Sudanese zone of Burkina Faso: the effects of tree canopy and fertilization. *Soil Biology and Biochemistry* 40, 350–359. <https://doi.org/10.1016/j.soilbio.2007.08.015>.
- Gunina, A., Kuzyakov, Y., 2022. From energy to (soil organic) matter. *Global Change Biology* 28, 2169–2182. <https://doi.org/10.1111/gcb.16071>.

- Hagerty, S.B., Allison, S.D., Schimel, J.P., 2018. Evaluating soil microbial carbon use efficiency explicitly as a function of cellular processes: implications for measurements and models. *Biogeochemistry* 140, 269–283. <https://doi.org/10.1007/s10533-018-0489-z>.
- Hansen, L.D., Macfarlane, C., McKinnon, N., Smith, B.N., Criddle, R.S., 2004. Use of calorimetric ratios, heat per CO₂ and heat per O₂, to quantify metabolic paths and energetics of growing cells. *Thermochimica Acta* 422, 55–61. <https://doi.org/10.1016/j.tca.2004.05.033>.
- Heijnen, J.J., Van Dijken, J.P., 1992. In search of a thermodynamic description of biomass yields for the chemotrophic growth of microorganisms. *Biotechnology and Bioengineering* 39, 833–858. <https://doi.org/10.1002/bit.260390806>.
- Herrmann, A.M., Bölscher, T., 2015. Simultaneous screening of microbial energetics and CO₂ respiration in soil samples from different ecosystems. *Soil Biology and Biochemistry* 83, 88–92. <https://doi.org/10.1016/j.soilbio.2015.01.020>.
- Holthuisen, D., Jänicke, M., Peth, S., Horn, R., 2012. Physical properties of a Luvisol for different long-term fertilization treatments: I. Mesoscale capacity and intensity parameters. *Journal of Plant Nutrition and Soil Science* 175, 4–13. <https://doi.org/10.1002/jpln.201100075>.
- Ilstedt, U., Nordgren, A., Malmer, A., 2006. Soil chemical and microbial properties after disturbance by crawler tractors in a Malaysian forest plantation. *Forest Ecology and Management* 225, 313–319. <https://doi.org/10.1016/j.foreco.2006.01.008>.
- Inagaki, T.M., Possinger, A.R., Schweizer, S.A., Mueller, C.W., Hoeschen, C., Zachman, M.J., Kourkouts, L.F., Kögel-Knabner, I., Lehmann, J., 2023. Microscale spatial distribution and soil organic matter persistence in top and subsoil. *Soil Biology and Biochemistry* 178, 108921. <https://doi.org/10.1016/j.soilbio.2022.108921>.
- Juarez, S., Nunan, N., Duday, A.-C., Pouteau, V., Schmidt, S., Hapca, S., Falconer, R., Otten, W., Chenu, C., 2013. Effects of different soil structures on the decomposition of native and added organic carbon. *European Journal of Soil Biology* 58, 81–90. <https://doi.org/10.1016/j.ejsobi.2013.06.005>.
- Kandel, E., 1999. Xylanase, invertase and protease at the soil–litter interface of a loamy sand. *Soil Biology and Biochemistry* 31, 1171–1179. [https://doi.org/10.1016/S0038-0717\(99\)00035-8](https://doi.org/10.1016/S0038-0717(99)00035-8).
- Keilweit, M., Wanzek, T., Kleber, M., Nico, P., Fendorf, S., 2017. Anaerobic microsites have an unaccounted role in soil carbon stabilization. *Nature Communications* 8, 1771. <https://doi.org/10.1038/s41467-017-01406-6>.
- Kim, K., Kutlu, T., Kravchenko, A., Guber, A., 2021. Dynamics of N₂O in vicinity of plant residues: a microsensor approach. *Plant and Soil* 462, 331–347. <https://doi.org/10.1007/s11104-021-04871-7>.
- Korsaeth, A., Molstad, L., Bakken, L.R., 2001. Modelling the competition for nitrogen between plants and micro-ora as a function of soil heterogeneity. *Soil Biology*.
- Kuka, K., Franko, U., Rühlmann, J., 2007. Modelling the impact of pore space distribution on carbon turnover. *Ecological Modelling* 208, 295–306. <https://doi.org/10.1016/j.ecolmodel.2007.06.002>.
- Kuzakov, Y., Blagodatskaya, E., 2015. Microbial hotspots and hot moments in soil: concept & review. *Soil Biology and Biochemistry* 83, 184–199. <https://doi.org/10.1016/j.soilbio.2015.01.025>.
- Lacroix, E.M., Aeppli, M., Boye, K., Brodie, E., Fendorf, S., Keilweit, M., Naughton, H.R., Noël, V., Sihi, D., 2023. Consider the anoxic microsite: acknowledging and appreciating spatiotemporal redox heterogeneity in soils and sediments. *ACS Earth and Space Chemistry* 7, 1592–1609. <https://doi.org/10.1021/acsearthspacechem.3c00032>.
- Lacroix, E.M., Mendillo, J., Gomes, A., Dekas, A., Fendorf, S., 2022. Contributions of anoxic microsites to soil carbon protection across soil textures. *Geoderma* 425, 116050. <https://doi.org/10.1016/j.geoderma.2022.116050>.
- Lehmann, J., Hansel, C.M., Kaiser, C., Kleber, M., Maher, K., Manzoni, S., Nunan, N., Reichstein, M., Schimel, J.P., Torn, M.S., Wieder, W.R., Kögel-Knabner, I., 2020. Persistence of soil organic carbon caused by functional complexity. *Nature Geoscience* 13, 529–534. <https://doi.org/10.1038/s41561-020-0612-3>.
- Lenth, R.V., 2023. Emmeans: Estimated Marginal Means, Aka Least-Squares Means.
- Loecke, T.D., Robertson, G.P., 2009. Soil resource heterogeneity in terms of litter aggregation promotes nitrous oxide fluxes and slows decomposition. *Soil Biology and Biochemistry* 41, 228–235. <https://doi.org/10.1016/j.soilbio.2008.10.017>.
- Magid, J., De Neergaard, A., Brandt, M., 2006. Heterogeneous distribution may substantially decrease initial decomposition, long-term microbial growth and N-immobilization from high C-to-N ratio resources. *European Journal of Soil Science* 57, 517–529. <https://doi.org/10.1111/j.1365-2389.2006.00805.x>.
- Manzoni, S., 2017. Flexible carbon-use efficiency across litter types and during decomposition partly compensates nutrient imbalances—results from analytical stoichiometric models. *Frontiers in Microbiology* 8.
- Manzoni, S., Čapek, P., Porada, P., Thurner, M., Winterdahl, M., Beer, C., Brüchert, V., Frouz, J., Herrmann, A.M., Lindahl, B.D., Lyon, S.W., Šantrůčková, H., Vico, G., Way, D., 2018. Reviews and syntheses: carbon use efficiency from organisms to ecosystems – definitions, theories, and empirical evidence. *Biogeosciences* 15, 5929–5949. <https://doi.org/10.5194/bg-15-5929-2018>.
- Manzoni, S., Taylor, P., Richter, A., Porporato, A., Ågren, G.I., 2012. Environmental and stoichiometric controls on microbial carbon-use efficiency in soils. *New Phytologist* 196, 79–91.
- Marschmann, G.L., Pagel, H., Kügler, P., Streck, T., 2019. Equifinality, sloppiness, and emergent structures of mechanistic soil biogeochemical models. *Environmental Modelling & Software* 122, 104518. <https://doi.org/10.1016/j.envsoft.2019.104518>.
- Moyano, F.E., Manzoni, S., Chenu, C., 2013. Responses of soil heterotrophic respiration to moisture availability: an exploration of processes and models. *Soil Biology and Biochemistry* 59, 72–85. <https://doi.org/10.1016/j.soilbio.2013.01.002>.
- Newville, M., Otten, R., Nelson, A., Stensitzki, T., Ingargiola, A., Allan, D., Fox, A., Carter, F., Michał, Osborn, R., Pustakhod, D., Ineuhous, Weigand, S., Aristov, A., Glenn, Deil, C., ngunyhoo, Mark, Hansen, A.L.R., Pasquevich, G., Foks, L., Zobrist, N., Frost, O., Stuermer, azed, Polloreno, A., Persaud, A., Nielsen, J.H., Pompili, M., Eendebak, P., 2023. Lmfit/Lmfit-Py: 1.2.2. <https://doi.org/10.5281/zenodo.8145703>.
- Nordgren, A., 1988. Apparatus for the continuous, long-term monitoring of soil respiration rate in large numbers of samples. *Soil Biology and Biochemistry* 20, 955–957. [https://doi.org/10.1016/0038-0717\(88\)90110-1](https://doi.org/10.1016/0038-0717(88)90110-1).
- Nunan, N., 2017. The microbial habitat in soil: scale, heterogeneity and functional consequences. *Journal of Plant Nutrition and Soil Science* 180, 425–429. <https://doi.org/10.1002/jpln.201700184>.
- Nunan, N., Ledoup, J., Ruamps, L.S., Pouteau, V., Chenu, C., 2017. Effects of habitat constraints on soil microbial community function. *Scientific Reports* 7, 4280. <https://doi.org/10.1038/s41598-017-04485-z>.
- Nunan, N., Schmidt, H., Raynaud, X., 2020. The ecology of heterogeneity: soil bacterial communities and C dynamics. *Philosophical Transactions of the Royal Society B: Biological Sciences* 375, 20190249. <https://doi.org/10.1098/rstb.2019.0249>.
- Or, D., Smets, B.F., Wraith, J.M., Dechesne, A., Friedman, S.P., 2007. Physical constraints affecting bacterial habitats and activity in unsaturated porous media – a review. *Advances in Water Resources* 30, 1505–1527. <https://doi.org/10.1016/j.advwatres.2006.05.025>.
- Panikov, N.S., 1996. Mechanistic mathematical models of microbial growth in bioreactors and in natural soils: explanation of complex phenomena. *Mathematics and Computers in Simulation* 42, 179–186. [https://doi.org/10.1016/0378-4754\(95\)00127-1](https://doi.org/10.1016/0378-4754(95)00127-1).
- Peth, S., Chenu, C., Leblond, N., Mordhorst, A., Garnier, P., Nunan, N., Pot, V., Ogurek, M., Beckmann, F., 2014. Localization of soil organic matter in soil aggregates using synchrotron-based X-ray microtomography. *Soil Biology and Biochemistry* 78, 189–194. <https://doi.org/10.1016/j.soilbio.2014.07.024>.
- Phillips, C., Nickerson, N., 2015. Soil Respiration.
- Pinheiro, M., Garnier, P., Beguet, J., Martin Laurent, F., Vieublé Gonod, L., 2015. The millimetre-scale distribution of 2,4-D and its degraders drives the fate of 2,4-D at the soil core scale. *Soil Biology and Biochemistry* 88, 90–100. <https://doi.org/10.1016/j.soilbio.2015.05.008>.
- Poll, C., Ingwersen, J., Stemmer, M., Gerzabek, M.H., Kandeler, E., 2006. Mechanisms of solute transport affect small-scale abundance and function of soil microorganisms in the detritusphere. *European Journal of Soil Science* 57, 583–595. <https://doi.org/10.1111/j.1365-2389.2006.00835.x>.
- Portel, X., Pot, V., Garnier, P., Otten, W., Bavey, P.C., 2018. Microscale heterogeneity of the spatial distribution of organic matter can promote bacterial biodiversity in soils: insights from computer simulations. *Frontiers in Microbiology* 9, 1583. <https://doi.org/10.3389/fmicb.2018.01583>.
- R Core Team, 2023. R: A Language and Environment for Statistical Computing. R Foundation for Statistical Computing, Vienna, Austria.
- Raynaud, X., Nunan, N., 2014. Spatial ecology of bacteria at the microscale in soil. *PLoS One* 9, e87217. <https://doi.org/10.1371/journal.pone.0087217>.
- Reischke, S., Rousk, J., Bååth, E., 2014. The effects of glucose loading rates on bacterial and fungal growth in soil. *Soil Biology and Biochemistry* 70, 88–95. <https://doi.org/10.1016/j.soilbio.2013.12.011>.
- Rousk, J., Hill, P.W., Jones, D.L., 2014. Using the concentration-dependence of respiration arising from glucose addition to estimate in situ concentrations of labile carbon in grassland soil. *Soil Biology and Biochemistry* 77, 81–88. <https://doi.org/10.1016/j.soilbio.2014.06.015>.
- Ruamps, L.S., Nunan, N., Chenu, C., 2011. Microbial biogeography at the soil pore scale. *Soil Biology and Biochemistry* 43, 280–286. <https://doi.org/10.1016/j.soilbio.2010.10.010>.
- Russell, J.B., Cook, G.M., 1995. Energetics of bacterial growth: balance of anabolic and catabolic reactions. *Microbiological Reviews* 59.
- Sawada, K., Inagaki, Y., Toyota, K., Kosaki, T., Funakawa, S., 2017. Substrate-induced respiration responses to nitrogen and/or phosphorus additions in soils from different climatic and land use conditions. *European Journal of Soil Biology* 83, 27–33. <https://doi.org/10.1016/j.ejsobi.2017.10.002>.
- Schlüter, S., Leuther, F., Albrecht, L., Hoeschen, C., Kilian, R., Surey, R., Mikutta, R., Kaiser, K., Mueller, C.W., Vogel, H.-J., 2022. Microscale carbon distribution around pores and particulate organic matter varies with soil moisture regime. *Nature Communications* 13, 2098. <https://doi.org/10.1038/s41467-022-29605-w>.
- Schlüter, S., Zawallich, J., Vogel, H.-J., Dörsch, P., 2019. Physical constraints for respiration in microbial hotspots in soil and their importance for denitrification. *Biogeosciences* 16, 3665–3678. <https://doi.org/10.5194/bg-16-3665-2019>.
- Schneckenberger, K., Demin, D., Stahr, K., Kuzakov, Y., 2008. Microbial utilization and mineralization of [14C]glucose added in six orders of concentration to soil. *Soil Biology and Biochemistry* 40, 1981–1988. <https://doi.org/10.1016/j.soilbio.2008.02.020>.
- Seidel, S.J., Gaiser, T., Ahrends, H.E., Hüging, H., Siebert, S., Bauke, S.L., Gocke, M.I., Koch, M., Schweitzer, K., Schaaf, G., Ewert, F., 2021. Crop response to P fertilizer omission under a changing climate - experimental and modeling results over 115 years of a long-term fertilizer experiment. *Field Crops Research* 268, 108174. <https://doi.org/10.1016/j.fcr.2021.108174>.
- Shi, A., Chakrawal, A., Manzoni, S., Fischer, B.M.C., Nunan, N., Herrmann, A.M., 2021. Substrate spatial heterogeneity reduces soil microbial activity. *Soil Biology and Biochemistry* 152, 108068. <https://doi.org/10.1016/j.soilbio.2020.108068>.
- Sierra, C.A., Malghani, S., Müller, M., 2015. Model structure and parameter identification of soil organic matter models. *Soil Biology and Biochemistry* 90, 197–203. <https://doi.org/10.1016/j.soilbio.2015.08.012>.

- Sinsabaugh, R.L., Manzoni, S., Moorhead, D.L., Richter, A., 2013. Carbon use efficiency of microbial communities: stoichiometry, methodology and modelling. *Ecology Letters* 16, 930–939. <https://doi.org/10.1111/ele.12113>.
- Strong, D.T., Wever, H.D., Merckx, R., Recous, S., 2004. Spatial location of carbon decomposition in the soil pore system. *European Journal of Soil Science* 55, 739–750. <https://doi.org/10.1111/j.1365-2389.2004.00639.x>.
- Thomson, B.C., Ostle, N.J., McNamara, N.P., Whiteley, A.S., Griffiths, R.L., 2010. Effects of sieving, drying and rewetting upon soil bacterial community structure and respiration rates. *Journal of Microbiological Methods* 83, 69–73. <https://doi.org/10.1016/j.mimet.2010.07.021>.
- Tian, J., Pausch, J., Yu, G., Blagodatskaya, E., Gao, Y., Kuzyakov, Y., 2015. Aggregate size and their disruption affect ¹⁴C-labelled glucose mineralization and priming effect. *Applied Soil Ecology* 90, 1–10. <https://doi.org/10.1016/j.apsoil.2015.01.014>.
- Trapp, S., Brock, A.L., Nowak, K., Kästner, M., 2018. Prediction of the formation of biogenic nonextractable residues during degradation of environmental chemicals from biomass yields. *Environmental Science & Technology* 52, 663–672. <https://doi.org/10.1021/acs.est.7b04275>.
- van den Broek, E., 2012. In: Good, P.I. (Ed.), *A Practitioner's Guide to Resampling for Data Analysis, Data Mining, and Modeling*. Chapman & Hall/CRC, Boca Raton, FL, 2011. - ISBN 978-1-439855-50-8. Computing Reviews CR139920.
- Védère, C., Vieublé Gonod, L., Pouteau, V., Girardin, C., Chenu, C., 2020. Spatial and temporal evolution of detritusphere hotspots at different soil moistures. *Soil Biology and Biochemistry* 150, 107975. <https://doi.org/10.1016/j.soilbio.2020.107975>.
- Virtanen, P., Gommers, R., Oliphant, T.E., Haberland, M., Reddy, T., Cournapeau, D., Burovski, E., Peterson, P., Weckesser, W., Bright, J., van der Walt, S.J., Brett, M., Wilson, J., Millman, K.J., Mayorov, N., Nelson, A.R.J., Jones, E., Kern, R., Larson, E., Carey, C.J., Polat, I., Feng, Y., Moore, E.W., VanderPlas, J., Laxalde, D., Perktold, J., Cimrman, R., Henriksen, I., Quintero, E.A., Harris, C.R., Archibald, A.M., Ribeiro, A. H., Pedregosa, F., van Mulbregt, P., SciPy 1.0 Contributors, 2020. SciPy 1.0: fundamental algorithms for scientific computing in Python. *Nature Methods* 17, 261–272. <https://doi.org/10.1038/s41592-019-0686-2>.
- Wang, C., Kuzyakov, Y., 2023. Energy use efficiency of soil microorganisms: driven by carbon recycling and reduction. *Global Change Biology* gcb.16925. <https://doi.org/10.1111/gcb.16925>.
- Wang, G., Post, W.M., 2012. A theoretical reassessment of microbial maintenance and implications for microbial ecology modeling. *FEMS Microbiology Ecology* 81, 610–617. <https://doi.org/10.1111/j.1574-6941.2012.01389.x>.
- Wieder, W.R., Allison, S.D., Davidson, E.A., Georgiou, K., Hararuk, O., He, Y., Hopkins, F., Luo, Y., Smith, M.J., Sulman, B., Todd-Brown, K., Wang, Y., Xia, J., Xu, X., 2015. Explicitly representing soil microbial processes in Earth system models. *Global Biogeochemical Cycles* 29, 1782–1800. <https://doi.org/10.1002/2015GB005188>.
- Yang, S., Di Lodovico, E., Rupp, A., Harms, H., Fricke, C., Miltner, A., Kästner, M., Maskow, T., 2024. Enhancing insights: exploring the information content of calorimetric ratio in dynamic soil microbial growth processes through calorimetry. *Frontiers in Microbiology* 15, 1321059. <https://doi.org/10.3389/fmicb.2024.1321059>.
- Zech, S., Schweizer, S.A., Bucka, F.B., Ray, N., Kögel-Knabner, I., Prechtel, A., 2022. Explicit spatial modeling at the pore scale unravels the interplay of soil organic carbon storage and structure dynamics. *Global Change Biology* 28, 4589–4604. <https://doi.org/10.1111/gcb.16230>.
- Zheng, Q., Hu, Y., Zhang, S., Noll, L., Böckle, T., Richter, A., Wanek, W., 2019. Growth explains microbial carbon use efficiency across soils differing in land use and geology. *Soil Biology and Biochemistry* 128, 45–55. <https://doi.org/10.1016/j.soilbio.2018.10.006>.
- Zinn, M., Witholt, B., Egli, T., 2004. Dual nutrient limited growth: models, experimental observations, and applications. *Journal of Biotechnology* 113, 263–279. <https://doi.org/10.1016/j.jbiotec.2004.03.030>.

Chapter 3: Coupling energy balance and carbon flux during cellulose degradation in arable soils

Publication:

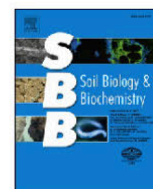
Wirsching, J., **Endress, M.-G.**, Di Lodovico, E., et al., 2024. Coupling energy balance and carbon flux during cellulose degradation in arable soils. *Soil Biology and Biochemistry* 202, 109691. doi:[10.1016/j.soilbio.2024.109691](https://doi.org/10.1016/j.soilbio.2024.109691)

Declaration of personal contributions:

I am one of the first authors of this publication. The first authorship is shared with J. Wirsching, who performed the experimental work presented in this study. I performed all modeling work. Specifically, I designed the dynamic model and performed all numerical simulations and model calibration, and wrote the code required for these tasks. J. Wirsching and I contributed equally to all other formal analyses, statistics, and validation. J. Wirsching and I contributed equally to the first draft of the manuscript with input from all co-authors. C. Poll and I contributed equally to the final version of the manuscript with input from all co-authors. I prepared Figures 1, 2, 3, 4, and 5 and contributed all supplementary material pertaining to modeling. Specifically, I prepared the corresponding methods along with Table S4 and Figures S4, S5, and S6. C. Poll and I contributed equally to revisions with input from all co-authors.

Data availability statement:

Original data produced during this study is available from the corresponding author upon reasonable request. Data required for model calibration and analysis is provided via the figshare repository (doi:10.6084/m9.figshare.28183439). All modeling code is available from me upon reasonable request.



Coupling energy balance and carbon flux during cellulose degradation in arable soils

Johannes Wirsching^{a,1}, Martin-Georg Endress^{b,1}, Eliana Di Lodovico^c,
Sergey Blagodatsky^{b,d}, Christian Fricke^{c,f}, Marcel Lorenz^e, Sven Marhan^a,
Ellen Kandeler^a, Christian Poll^{a,*}

^a Institute of Soil Science and Land Evaluation, Soil Biology Department, University of Hohenheim, Germany

^b Institute of Zoology, Faculty of Mathematics and Natural Sciences, University of Cologne, Germany

^c Faculty of Natural and Environmental Sciences, University of Kaiserslautern-Landau, Germany

^d Campus Alpin, Institute of Meteorology and Climate Research, Department of Atmospheric Environmental Research (IMK-IFU), Karlsruhe Institute of Technology (KIT), Germany

^e Department of Soil Science, University of Trier, Helmholtz Centre for Environmental Research, Leipzig, Germany

^f Berufsakademie Sachsen-Staatliche Studienakademie Riesa, University of Cooperative Education, Germany

ARTICLE INFO

Keywords:

Energy use efficiency (EUE)

Calorimetric ratio (CR)

Carbon use efficiency (CUE)

¹³C-Labeled cellulose

Fertilized and unfertilized arable soils

ABSTRACT

Microbial carbon use efficiency (CUE) is an important metric for understanding the balance between anabolic and catabolic metabolism, while energy use efficiency (EUE) provides insight into microbial energy requirements. They are linked by the ratio between released heat and respiration (calorespirometric ratio, CR), which can be used to describe the efficiency of microbial growth. In this study, microbial C and energy use during the degradation of ¹³C-labeled cellulose in eight different soils was investigated experimentally and simulated using a process-based model. Our results show close agreement between the cumulative C and energy balances during the incubations, with a total C and energy release equal to 30–50% of the amount added as cellulose. Both energy and C fluxes indicated that a positive priming effect of soil organic matter (SOM) increased the release of heat and CO₂ by 10–32% relative to the added substrate. The CR-CUE relationship indicated that growth on cellulose was energy limited during the early but not the later stages of the incubation, especially in soils with high SOM content. We partly observed systematic differences between estimates for CUE based either on the ¹³C label or on the calorespirometric ratio. Both approaches were constrained by technical and methodological limitations and agreed best during the phase of microbial growth in the SOM-rich soils, with CUE values between 0.4 and 0.75 indicating efficient aerobic growth. During early stages or after transition to a maintenance phase, both estimates were less meaningful for cellulose degradation, a substrate with a lower turnover rate than glucose. Still, the coupled heat and mass balances during cellulose degradation in combination with process-based modeling provided additional information on growth yields as well as the contribution of SOM priming to microbial growth compared to considering mass balances alone.

1. Introduction

Microorganisms utilize soil organic matter (SOM) for catabolic and anabolic processes (Chakrawal et al., 2020). This C allocation or the ratio of C used for biosynthesis to C consumed is commonly referred to as carbon use efficiency (CUE; (Geyer et al., 2019)), from which we can

deduce how much C is either emitted from the soil as CO₂ or retained and eventually stabilized in the SOM (Chakrawal et al., 2020). Studies have highlighted the importance of substrate availability, nutrient composition, environmental conditions, and microbial community composition to explain the variability in CUE (Manzoni et al., 2012; Qiao et al., 2019; Domeignoz-Horta et al., 2020). What is missing are

This article is part of a special issue entitled: Soil C and energy fluxes published in Soil Biology and Biochemistry.

* Corresponding author.

E-mail address: christian.poll@uni-hohenheim.de (C. Poll).

¹ Authors contributed equally.

<https://doi.org/10.1016/j.soilbio.2024.109691>

Received 28 June 2024; Received in revised form 20 November 2024; Accepted 9 December 2024

Available online 11 December 2024

0038-0717/© 2024 The Author(s). Published by Elsevier Ltd. This is an open access article under the CC BY license (<http://creativecommons.org/licenses/by/4.0/>).

studies that take into account that biosynthesis is a purely non-equilibrium process that depends not only on carbon alone but also on the energy that can be provided by catabolism (Kästner et al., 2024). This perspective emphasizes the quantification of energy fluxes alongside traditional carbon-centered analyses. Currently, there are a growing number of model-based descriptions, such as those published by Chakrawal et al. (2020), in which the potential application of coupled mass and energy balance models for glucose can be used to create a generalized understanding of metabolic pathways during substrate utilization and implement physiological constraints in C-cycle models (Calabrese et al., 2021; Endress et al., 2024a). However, there is a lack of experimental data to support this theoretical notion, also with regard to more complex molecules that better reflect the natural composition of fresh litter in the soil, e.g. cellulose, while revealing possible technical limitations in determining and combining energy and mass fluxes.

The measurement of heat production via calorimetry opens up a non-destructive, label-free method in soil science that provide useful thermodynamic, kinetic and stoichiometric quantities (Yang et al., 2024). One of these is the calorespirometric ratio (CR), i.e. the quotient of the specific heat (Q_b ; kJ g^{-1}) and the CO_2 release (R_{CO_2} ; $\text{mol CO}_2\text{-C g}^{-1}$). This ratio contains valuable information about the soil microbial metabolism, because it reflects the fact that a certain fraction of energy contained in the substrate is released as heat during catabolic oxidation of substrate-C to CO_2 , while the remainder is used for reducing C during biosynthesis. Hence, it links heat and CO_2 production during substrate consumption to the efficiency with which microorganisms synthesize new biomass from the substrate. Hansen et al. (2004) developed a widely used quantitative model linking the CR to CUE which allows estimating the CUE of microbial growth from the simultaneous measurement of heat and CO_2 production. This model simplifies soil processes by focusing on aerobic metabolic processes and a single substrate and neglecting any interactions involving minerals or SOM (Yang et al., 2024). Building on these findings, Chakrawal et al. (2020) expanded the model to include both SOM utilization as well as anaerobic processes such as ethanol and lactic acid fermentation. This extension enabled a more comprehensive and nuanced understanding of CR-CUE relationships. In particular, the authors showed how the CR-CUE relationship for a simple microbial growth reaction differs depending on the energy content of the substrate: if a substrate that is more oxidized than microbial biomass is consumed, the CR values decrease with increasing CUE and are limited to values below the combustion enthalpy (=energy content) of the biomass, whereas more reduced substrates result in CR values that increase with increasing CUE and fall above this threshold. The former corresponds to energy limited growth with relatively more C than energy being released per unit substrate, while the latter corresponds to C-limited growth, with relatively more energy than C being released (Chakrawal et al., 2020). The CR-CUE relation in the complex soil environment can, however, be influenced by many other factors that may cause deviations from such simple predictions (Barros et al., 2016; Herrmann and Bölscher, 2015). For instance, technical limitations may result in alterations to the CR when attempting to carry out the combined measurement of heat and CO_2 in parallel experiments in separate vessels (Yang et al., 2024; Endress et al., 2024b). Other processes that consume C and energy such as the production of extracellular enzymes or the formation of biofilms (Bölscher et al., 2024), might also affect the CR-CUE relation through the anabolic use of C that is not directly linked to biomass production. Similarly, extracellular enzymes can release heat during hydrolysis and depolymerization of complex substrates, which could elevate measured CR values. The additional use of SOM after substrate addition can contribute to microbial growth and, hence, to heat production that is not directly linked to the added substrate (Arcand et al., 2017). The intensity of priming depends, among other factors, on the competition for energy and nutrients between microbial groups using the fresh added substrate and other groups using SOM (Fontaine et al., 2003). The degree to which SOM priming affects the CR-CUE relation depends, therefore, also on the amount and energy

content of the SOM.

The different substrate preference and growth strategies control not only the decomposition rate but also the course of CUE (De Graaff et al., 2010). According to Geyer et al. (2016), the beginning of substrate utilization is characterized by a population-level CUE, which is determined by species-specific metabolic and thermodynamic constraints and, over time, transforms into an ecosystem-level CUE reflecting the efficiency of microbial net biomass production (growth) per unit of ingested substrate, including recycling of microbial products (Geyer et al., 2016). An often-used method for estimating CUE is the use of ^{13}C -labeled substrates in conjunction with measuring the ^{13}C -flux into CO_2 and the microbial biomass. However, both methods (i.e. the quantitative model of Hansen et al. (2004) and ^{13}C -labeled substrates) have their specific strengths and weaknesses and a simultaneous application of both may provide new insights into the C and energy use of soil microorganisms (Geyer et al., 2019). In addition, the CO_2 and heat release (including priming of SOM) can be related to the amount of C and energy initially added to the soil as substrate. Such a comparison accounts both for CO_2 and heat production from other sources as well as for any incomplete decomposition of the added substrate, and is referred to in this study as net carbon balance (CB_{net}) and net energy use efficiency (EUE_{net} , Fig. 1). Both might be considered as the storage efficiency of the soil system (Manzoni et al., 2018) and CB_{net} might be seen in a continuum following population CUE and ecosystem CUE. In this context, a CB_{net} and $\text{EUE}_{\text{net}} > 0$ indicate a net C and energy gain in the soil system after substrate addition, while negative values indicate net C and energy loss from the system. It is important to note, that EUE_{net} differs from (instantaneous) EUE, which is defined as the fraction of total substrate-derived energy required for anabolism (Klemm et al., 2005; Wang and Kuzyakov, 2023). EUE_{net} can, therefore, only be related to CB_{net} and both are not directly relatable to the CUE estimates derived from ^{13}C mass balance or CR, but instead broaden the concepts of CUE and EUE.

The research aim of this study was to investigate the C and energy use from added cellulose in either organically fertilized or unfertilized arable soils during a 64-days incubation. We used ^{13}C -labeled cellulose and isothermal calorimetry in combination with a process-based model to provide an in-depth analysis of microbial cellulose degradation. This approach was used to address the following objectives: 1) apply and evaluate the concepts of CB_{net} , EUE_{net} , CR and CUE to cellulose degradation and 2) determine if growth on cellulose is energy limited as

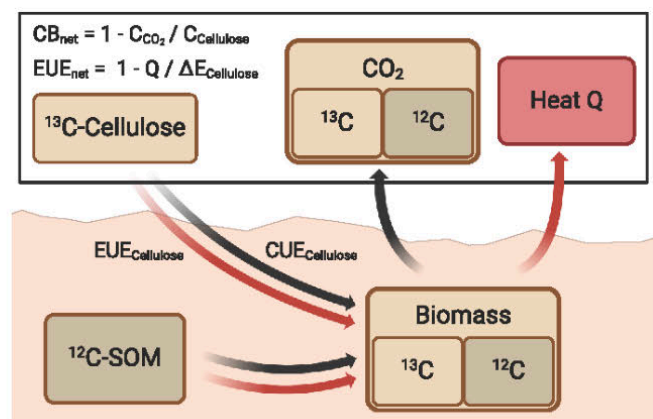


Fig. 1. Schematic of major C and energy flows in soil incubation experiments. Microorganisms consume ^{13}C -labeled substrate added to the soil to form new biomass, CO_2 and heat with a certain carbon and energy use efficiency (CUE- $_{\text{Cellulose}}$ and $\text{EUE}_{\text{Cellulose}}$). Additionally, they also metabolize native (^{12}C)-SOM. The net storage or release of C (CB_{net}) and energy (EUE_{net}) in the soil thus depends on the balance between the total amount of C and energy initially added as substrate ($\text{C}_{\text{Cellulose}}$, $\Delta E_{\text{Cellulose}}$) on the one hand and the total amount of C and energy lost as CO_2 and heat over time (C_{CO_2} , Q) on the other hand.

predicted based on its energy content (Chakrawal et al., 2020). Furthermore, we want to 3) determine how priming of SOM and the fertilizer status affects CUEs, CB_{net} and EUE_{net}, and finally 4) evaluate technical difficulties in measuring and combining heat and CO₂ release in the CR.

2. Materials and methods

2.1. Soil origin and sampling

The soil samples originate from four long-term field experiments, each with an unfertilized (UF) and a fertilized (FYM) variant. The soils included in the study had different textures: a loamy sand called "Thyrow" (TH), a sandy loam called "Dikopshof" (DI), a loamy sand called "Reckenholz" (RE), and a silty loam called "QualiAgro" (QA). The soils cover a wide range of soil properties of arable soils, which allowed us to study the impact of background SOM and energy content on microbial cellulose utilization. Further details on the soil properties can be found in the published database (Lorenz et al., 2024a). Sampling was carried out randomly with a spade from the top 20 cm after harvest. Soil sampling took place in August for DI, in September for QA and RE and in October for TH, each in 2021. Thyrow (TH) is located at 52°16'N, 13°12'E in Brandenburg, Germany. The climate is characterized by an annual mean temperature of 9.2 °C and precipitation of 510 mm. The crop rotation, which has been implemented since 2005, consists of silage maize and winter rye. Since 1938, fertilizer has been applied exclusively with farmyard manure, which is applied at a rate of 20 t ha⁻¹ (Ellmer and Baumecker, 2005; Kroschewski et al., 2023). The Dikopshof (DI) agricultural area is located at 50°81'N, 6°95'E in North Rhine-Westphalia, Germany. The area has an average annual temperature of 10.5 °C and a precipitation of 688 mm. Since 1953, the farm has been cultivated as part of a five-year crop rotation, with sugar beet, winter wheat, winter rye, Persian clover and potatoes being grown. Since 1904, farmyard manure has been applied at a rate of 60 t ha⁻¹ (Ahrends et al., 2018). The Reckenholz (RE) site is an arable field at 47°43' N, 8°52' E near Zurich, Switzerland. Reckenholz has an annual mean temperature of 9.5 °C and a precipitation of 1050 mm. The 8-year crop rotation includes winter wheat, maize, potatoes, winter wheat, maize and spring barley. Since 1949, 5 t ha⁻¹ of farm manure has been applied every second year (Cagnarini et al., 2021). QualiAgro (QA) soil samples were collected from a field situated at 48°87' N, 1°95' E in Île-de-France, with an average annual temperature of 10.8 °C and 644 mm of precipitation. The crop rotation includes barley, oats, barley and maize, with farmyard manure applied at a rate of 4 t ha⁻¹ every two years since 2014 (Nest et al., 2016).

2.2. Experimental design

The soils were stored air-dry and pre-incubated for 10 days at a water content corresponding to 45–50% water holding capacity (Supplementary Table S2, Table S3) to restore and stabilize microbial activity. After pre-incubation, the soils were incubated with 97 at% ¹³C-labeled cellulose derived from maize (*Zea mays*; IsoLife, Wageningen, Netherlands). The amount added corresponded to four times the C content of the microbial biomass in each soil (Table 1).

The cellulose was frozen at –80 °C and ground in a ball mill to a fine powder that allowed homogeneous mixing with the soil. Soils without cellulose addition served as controls. Soil equivalent to 3.78 g dry matter was incubated in 20 ml airtight calorimeter vials, which, together with aeration of the vials at three time points, ensured sufficient oxygen availability during the incubation. The experiment was run for 64 days in three replicates, with the assumption that a significant proportion would be utilized by that time. Additional sets of vials were sampled at 4, 8, 16 and 32 days to cover, together with the frequent respiration measurements, the dynamic phase of cellulose utilization during the early stages of incubation (Table 2).

Table 1

Cellulose addition.

Soil	Fertilization	C _{mic} (μg g ⁻¹ soil)	400% C-cellulose (μg g ⁻¹ soil)	Cellulose addition (mg 3.8 g ⁻¹ soil)
Dikopshof	Fertilized	155	622	5.4
Dikopshof	Unfertilized	70	280	2.4
Reckenholz	Fertilized	213	853	7.4
Reckenholz	Unfertilized	162	650	5.6
Thyrow	Fertilized	106	425	3.7
Thyrow	Unfertilized	31	126	1.1
QualiAgro	Fertilized	227	908	7.8
QualiAgro	Unfertilized	167	668	5.8

Table 2

Sampling schedule.

Analyses	Sampling time
CO ₂ respiration	0, 4, 5, 8, 12, 16, 20, 26, 32, 43, 46, 56, and 64 d
¹³ C respiration	4, 8, 16, 32, and 64 d
¹³ C _{mic}	4, 8, 16, 32, and 64 d

A flowchart illustrating the experimental design as well as a nomenclature of important quantities and their units are provided in the supplementary material (Supplementary Fig. S1, Supplementary Table S1).

2.3. CO₂ measurement

Gas samples were taken from the incubation vials according to the experiment schedule (Table 2) to measure CO₂ accumulation between the sampling dates. In a first step, exetainers were flushed with CO₂-free air at the start of the experiment and after taking the head space samples at each sampling date. At the sampling dates (i.e. before flushing the vials with CO₂-free air), gas samples from the head space were transferred into exetainers (Labco, UK). The CO₂ concentration was quantified using a gas chromatograph (Agilent 7890, USA). To calibrate and calculate the CO₂ concentrations, three standard gases with known CO₂ concentrations were used. ¹³CO₂ was measured with a mass spectrometer (Thermo Finnigan MAT, Bremen, Germany). The at% of the CO₂-C respired between the sampling dates $t = i$ and $t = i + 1$ was calculated as follows:

$$at\% = \left(\frac{C_i \cdot at\%_i - C_{i+1} \cdot at\%_{i+1}}{C_i - C_{i+1}} \right) \quad (1)$$

where C_i and C_{i+1} are the CO₂-C concentrations and $at\%_i$ and $at\%_{i+1}$ the atom% of the CO₂-C at the respective sampling dates. The $at\%$ values of the evolved CO₂-C were taken to calculate the proportion of cellulose-derived C (%cellulose C) in CO₂-C at $t = i + 1$:

$$\%CelluloseC = \left(\frac{at\%_{sample} - at\%_{control}}{at\%_{cellulose} - at\%_{control}} \right) \cdot 100 \quad (2)$$

where $at\%_{sample}$ is the $at\%$ content of the sample, $at\%_{control}$ corresponds to the $at\%$ of the control soil, $at\%_{cellulose}$ refers to the $at\%$ of the added cellulose. As ¹³C and CO₂ were not measured in the same interval, the missing $at\%$ values were estimated by linear interpolation between two time points. The respired CO₂ was partitioned based on the isotopic signature of the substrate and priming effect was calculated (Boos et al., 2023):

$$PE = CO_{2,total} - {}^{13}C - CO_2 - CO_{2,control} \quad (3)$$

where PE is the priming effect, CO_{2,total} is the CO₂ evolved from the substrate enriched soil, CO_{2,control} is the CO₂ evolved without substrate addition and ¹³C – CO₂ is the amount of labeled CO₂ evolved from the amended soil.

2.4. Bomb combustion calorimetry

The background energy content of the different soils was determined by combustion calorimetry and TG-DSC measurements. Following the methodological procedure described by Lorenz et al. (2024b), a subset of the homogenized soil was first dried at 105 °C and stored in a desiccator until combustion calorimetric measurements were performed. The energy content was determined as enthalpy of combustion $\Delta_c H$ according to DIN 51900 using an isoperibol combustion calorimeter (IKA C 200, IKA-Analysentechnik, Heitersheim, Germany; Lorenz et al., 2024b). In brief, 0.5 g of soil was mixed with benzoic acid in a 1:1 (w/w) ratio as an auxiliary combustion source and placed in a quartz crucible inside the bomb. This was done to achieve a complete combustion of SOM (Lorenz et al., 2024b). A volume of 5 ml of distilled water (25 °C) was added to the bomb to collect gases containing N and S from the combustion reaction to correct for energy releases by formation of nitric and sulfuric acid (for details see Lorenz et al., 2024b). The sealed bomb was pressurized with pure oxygen (purity 99.998 mol%, ALPHAGAZ) to 30 bar. After the combustion reaction, the residual material was weighed to account for the ash content of the analyzed sample. In case the combustion failed or was incomplete (recognizable by black soot in the sample residue), the respective measurement was discarded and repeated. Analysis of the C content in the combustion residues using an elemental analyzer (Vario EL cube, Elementar Analysensysteme GmbH, Langenselbold, Germany) confirmed that SOM had been completely burned in all samples. The combustion enthalpy is reported normalized to the organic C content (Lorenz et al., 2024a) of the sample in $\text{kJ g}^{-1} \text{C}$ to better characterize the energetic signature of SOM, which is of particular importance for mineral soil samples.

2.5. Thermogravimetry-differential scanning calorimetry (TG-DSC)

The thermogravimetric and differential scanning calorimetric analyses were performed with STA 449 F3 Jupiter® simultaneous thermal analyzer equipped with type-S thermocouple (Pt-Pt/Rh) DSC/TG Octo sample carrier (Netzsch-Gerätebau GmbH, Selb, Germany) and coupled via a heated transfer line at 300 °C, untreated fused silica capillary, $l = 2.2 \text{ m}$, $d = 75 \text{ }\mu\text{m}$ (SGE Analytical Science, Ringwood, Victoria, Australia) with the QMS 403 Aeolos® Quadro quadrupole mass spectrometer (Netzsch-Gerätebau GmbH, Selb, Germany). Samples were weighted in Al_2O_3 crucibles ($d = 6.8 \text{ mm}$, $V = 85 \text{ }\mu\text{L}$) on the Cubis® II Ultra-Micro lab balance (Sartorius AG, Göttingen, Germany). The sample mass was approx. 30 mg. An empty Al_2O_3 crucible was used as a reference. The samples were heated from 45 °C to 1000 °C at $10 \text{ }^\circ\text{C min}^{-1}$ under an oxidative atmosphere of 50 mL min^{-1} of synthetic air (N_2/O_2 , 80/20 %) and 20 mL min^{-1} of Argon as a protective gas. The temperature and enthalpy calibration of the DSC was carried out at regular intervals. The performance of the TG unit was regularly checked by the thermal decomposition of calcium oxalate monohydrate. For the TG data, a correction measurement (blank value determination) was performed with an empty Al_2O_3 crucible under the same conditions to consider the influence of buoyancy on the thermobalance. Measurements were conducted in triplicates for each soil. Data evaluation was done by the Software NETZSCH Proteus Thermal Analysis (Netzsch-Gerätebau GmbH, Selb, Germany). The mass loss of soil organic matter m_{SOM} (in mg) in the sample was determined for the TG data. The heat of combustion Q_c (in J) was evaluated by combusting each replicate two times and subtracting the corresponding DSC curves (Fernández et al., 2011). A linear baseline was used to determine the Q_c from the DSC data according to (Barros, 2021). The combustion enthalpy of SOM in each soil is expressed as $\Delta_c H_{\text{SOM}}$ (in $\text{kJ g}^{-1} \text{SOM}$) or related to the carbon content (in $\text{kJ g}^{-1} \text{C}$).

2.6. Calorespirometry

Heat production rate was determined using a TAM Air (TA In-

struments, New Castle, USA) isothermal heat conduction microcalorimeter with eight twin channels at an internal temperature of 20 °C. The set of calorimeter vials sampled at 64 days (see chapter 2.2) was used for continuous measurement of the heat production rate. The vials were removed from the calorimeter at the three aeration events. Each time the vials were (re-)placed in the calorimeter, a 45-min thermal equilibration period was applied before the heat signal was considered stable. Vials filled with water of the same heat capacity as the soil samples were used as a reference. The specific heat production rate $P(t)$ per gram soil is derived from Eqn. (4) (Yang et al., 2024):

$$P(t) = \sum_{i=1}^n r_i(t) \cdot \Delta_r H_i \quad (4)$$

where $r_i(t)$ is the rate of all i reactions (per gram soil) and their combined reaction enthalpies $\Delta_r H_i$ (Yang et al., 2024; Assael et al., 2022).

The specific heat ($Q(t)$; kJ g^{-1}) was determined by

$$Q(t) = \int_{t_0}^t P(t) dt \quad (5)$$

as the integrated specific heat production rate $P(t)$ (Yang et al., 2024).

The net energy use efficiency EUE_{net} was determined by dividing the cumulative heat production, including the utilization of cellulose and the priming of SOM, by the energy that was initially added via the cellulose and subtracting the result from 1. The EUE_{net} , therefore, provides a measure of how much energy the system gained or lost during the incubation. The equation for EUE_{net} is as follows:

$$\text{EUE}_{\text{net}} = 1 - \frac{Q(t)}{\Delta E_{\text{cellulose}}} \quad (6)$$

where $Q(t)$ is the specific heat per gram soil (Eqn. (5)), and $\Delta E_{\text{cellulose}}$ is the total combustion enthalpy ($\Delta_c H$) of the added cellulose per gram soil (kJ g^{-1}).

The calorespirometric ratio (CR; $\text{kJ mol}^{-1} \text{CO}_2\text{-C}$) was calculated from the quotient of the cumulative, metabolic heat ($Q(t)$; $\text{kJ g}^{-1} \text{soil}$) and the cumulative CO_2 respiration ($R_{\text{CO}_2}(t)$; $\text{mol CO}_2\text{-C g}^{-1} \text{soil}$ (Yang et al., 2024);):

$$\text{CR} = \frac{Q}{R_{\text{CO}_2}} \quad (7)$$

We also determined the enthalpy change according to Chakrawal et al. (2020) of the growth reaction on cellulose under aerobic conditions as a function of the relative degree of reduction (DR, γ) of cellulose and microbial biomass:

$$\Delta_r H_{\text{cellulose}} = \left(1 - Y_{\text{cellulose}} \frac{\gamma_{\text{MB}}}{\gamma_{\text{cellulose}}} \right) \Delta_c H_{\text{cellulose}} \quad (8)$$

where $\Delta_r H_{\text{cellulose}}$ is the reaction enthalpy of the growth reaction on cellulose and $\Delta_c H_{\text{cellulose}}$ is the combustion enthalpy of cellulose and $Y_{\text{cellulose}}$ is the yield coefficient for biomass formation. The relative degree of reduction of cellulose $\gamma_{\text{cellulose}}$ and microbial biomass γ_{MB} were calculated using

$$\gamma = \frac{4 \cdot n_{\text{C}} + n_{\text{H}} - 2 \cdot n_{\text{O}} - 3 \cdot n_{\text{N}}}{n_{\text{C}}} \quad (9)$$

where n_X is the number of atoms of X in the compound and CO_2 , NH_3 and H_2O are assumed as the reference compounds with zero degree of reduction (Chakrawal et al., 2020). This equation yields $\gamma_{\text{cellulose}} = 4$ as well as $\gamma_{\text{MB}} = 4.284$ for an empirical biomass composition of $\text{CH}_{1.571}\text{O}_{0.429}\text{N}_{0.143}$ as recently suggested by Yang et al. (2024) for soil.

2.7. Microbial biomass (C_{mic})

Microbial biomass was determined using the chloroform fumigation

extraction method, originally introduced by Vance et al. (1987) and further modified by Poll et al. (2010) to allow additional quantification of ^{13}C . To quantify the ^{13}C content, 1.5 g of soil was fumigated (f) with ethanol-free chloroform for 24 h and then extracted with 6 mL of 0.025 M K_2SO_4 . A non-fumigated (nf) 1.5 g control was extracted simultaneously. The difference in DOC concentration between the fumigated and non-fumigated sample corresponds to the microbial biomass C (extraction efficiency = 0.45). Since the quantification efficiency of the infrared detector of the TOC analyzer (Multi-N/C 2100S, Analytik Jena, Jena, Germany) decreases with increasing ^{13}C atom% content, the data were corrected with a calibration curve ranging from 1 to 99 atom% $^{13}\text{C}_{\text{mic}}$ in $\mu\text{g C g}^{-1}$ soil was determined by multiplying the total microbial biomass with the labeled microbial biomass (% $^{13}\text{C}_{\text{mic}}$ (Geyer et al., 2019);):

$$\text{atom}\%C_{\text{mic}} = \left(\frac{\text{atom}\%f \cdot fC_{\text{mic}} - \text{atom}\%nf \cdot nfC_{\text{mic}}}{fC_{\text{mic}} - nfC_{\text{mic}}} \right) \quad (10)$$

$$\text{atom}\%^{13}C_{\text{mic}} = \left(\frac{\text{atom}\%_s - \text{atom}\%_c}{\text{atom}\%_{\text{cellulose}} - \text{atom}\%_c} \right) \cdot 100 \quad (11)$$

$$^{13}C_{\text{mic}} = \frac{C_{\text{mic}} \cdot \text{atom}\%^{13}C_{\text{mic}}}{100} \quad (12)$$

where the organic carbon content of the fumigated and non-fumigated samples ($\mu\text{g C g}^{-1}$ soil) was expressed as fC_{mic} and nfC_{mic} , while the corresponding ^{13}C atom% values were labeled as $\text{atom}\%f$ and $\text{atom}\%nf$. $\text{atom}\%_s$ and $\text{atom}\%_c$ represent the atom percent of sample treatments and the natural abundance in the soil, respectively. $\text{atom}\%_{\text{cellulose}}$ represents the atom percent of the cellulose.

2.8. C use and storage efficiency

The CUE was derived from the ^{13}C mass balance, and from the calorespirometric ratio.

1. CUE_L: experiment-based CUE used for labeled substances (Geyer et al., 2016).

$$\text{CUE}_L = \frac{^{13}C_{\text{mic}}}{^{13}C_{\text{mic}} + ^{13}C_{\text{CO}_2}} \quad (13)$$

where: $^{13}C_{\text{mic}}$ is the C uptake in microbial biomass, and $^{13}C_{\text{CO}_2}$ is the cumulated mineralized cellulose-derived C.

2. CUE_{Rq}: calorespirometric ratio (CR)-based CUE.

$$\text{CUE}_{Rq} = \left(\frac{406 \left(1 - \frac{\text{Ox}_{\text{cell}}}{4} \right) - \frac{Q}{R_{\text{CO}_2}}}{115(\text{Ox}_{\text{cell}} - \text{Ox}_{\text{MB}})} \right) \cdot \left(\frac{406 \left(1 - \frac{\text{Ox}_{\text{cell}}}{4} \right) - \frac{Q}{R_{\text{CO}_2}}}{115(\text{Ox}_{\text{cell}} - \text{Ox}_{\text{MB}})} + 1 \right)^{-1} \quad (14)$$

where 406 (kJ mol⁻¹ O₂) is the combustion enthalpy of cellulose, Ox_{cell} - Ox_{MB} is the difference between the oxidation states of C in the substrate (cellulose = 0; Saito et al. (2007)) and in the microbial biomass (-0.3; Von Stockar and Liu (1999)) and 115 is the average energy loss (kJ) per change in oxidation state of C during the conversion of substrate to microbial biomass (Geyer et al., 2019; Kemp, 2000).

3. CB_{net}: net carbon balance including C released from cellulose and SOM:

$$\text{CB}_{\text{net}} = 1 - \frac{C_{\text{CO}_2}}{C_{\text{cellulose}}} \quad (15)$$

where C_{CO_2} is the total cumulative CO₂ release ($\mu\text{g C g}^{-1}$ soil) and

$C_{\text{cellulose}}$ is the total amount of carbon added to the soil in the form of cellulose ($\mu\text{g C g}^{-1}$). CB_{net} thus measures the net retention ($\text{CB}_{\text{net}} > 0$) or loss ($\text{CB}_{\text{net}} < 0$) of C in the soil after substrate addition. Note that $\text{CB}_{\text{net}}(t = 0) = 1$ and that CB_{net} decreases over time.

2.9. Data analyses

All data analyses were carried out using the statistical software R 4.0.2 (R Core Team, 2020). Significant differences were tested using a linear mixed-effects model with C_{mic}^{13} , CO_2^{13} and heat production rate as dependent variables and time, fertilizer status and experimental sites as explanatory variables. Models were fitted to the data using the "lme4" package (Bates et al., 2008). For the $^{13}\text{CO}_2$ data, we integrated the time factor for repeated measurements by crossing it with the treatment structure, including an interaction effect between site and site-time point and a random effect of the individual microcosms in which the CO₂ measurement took place (Piepho et al., 2004). We carried out a three-way anova to identify significant effects ($p < 0.05$) and then compared the estimated marginal means. Normal distribution and variance homogeneity were tested by means of residual diagnostic plots. If an interaction with time point was significant, we evaluated simple contrasts per time point level.

2.10. Dynamic model

We simulated the coupled fluxes of carbon and energy with an ordinary differential equation (ODE) model of microbial growth after the addition of ^{13}C -labeled cellulose. The model is based on similar formulations by Chakrawal et al. (2020, 2021) and Endress et al. (2024a), which were extended to represent ^{13}C dynamics. In total, the model features 5 major carbon pools including the concentrations of substrate (^{13}C -cellulose) as well as microbial biomass and CO₂, each with separate pools for ^{12}C and ^{13}C . In the model, microorganisms grow aerobically on the added ^{13}C -cellulose following Monod kinetics with a threshold concentration, forming new ^{13}C -biomass as well as ^{13}C -CO₂. To capture potential priming, microbes also utilize native soil ^{12}C -SOM to form new ^{12}C -biomass and ^{12}C -CO₂ via a second aerobic growth reaction. Model SOM is characterized by its average degree of reduction γ_{SOM} , which is incorporated as a free parameter. Counteracting the growth reactions, total biomass ($^{12}\text{C} + ^{13}\text{C}$) is constantly consumed to fuel endogenous maintenance respiration, releasing both ^{12}C - and ^{13}C -CO₂, and finally gets turned over to necromass at a specific rate.

In addition to the distinction between ^{12}C - and ^{13}C -biomass, the model also partitions the total biomass into an active fraction, which performs both growth and maintenance reactions, as well as an inactive fraction, which only performs maintenance. Changes in the activity state are modeled via the index of physiological state framework and depend on the availability of cellulose as the primary substrate (Panikov, 1996; Blagodatsky and Richter, 1998). Note that this partitioning implies that the same proportion of ^{12}C - and ^{13}C -biomass is considered active at any time.

This ODE model was implemented in Python (version 3.9.18) and numerical integration was carried out using the Radau method of the solve_ivp function in the Scipy package (Virtanen et al., 2020). The model was calibrated against the measured pools of total and ^{13}C -biomass, cumulative total and ^{13}C -CO₂, as well as the heat production rate. Parameter optimization was performed for each individual soil, i.e., we obtained eight calibrated parameter sets in total for the fertilized and unfertilized soils of the four field experiments. The optimization was carried out numerically using the Levenberg-Marquardt algorithm as implemented in the minimize function of the lmfit package (Newville et al., 2023). Initial conditions for substrate and biomass concentrations were chosen according to the measured experimental values and lower and upper bounds were provided for individual parameters. The full ODE model as well as a detailed description of the

calibration routine is presented in the supplementary materials and methods (SI Text). A list of all variables and parameters with units is given in the supplementary material (Supplementary Table S4).

3. Results

3.1. $^{13}\text{C}_{\text{mic}}$ content and $^{13}\text{CO}_2$ release

The $^{13}\text{C}_{\text{mic}}$ content began to increase after 3 days and was comparable in its dynamics for all soils and fertilizer status. Averaged over the fertilization status, since we observed no significant difference, the maximum $^{13}\text{C}_{\text{mic}}$ content at day 16 ranged from $20 \mu\text{g g}^{-1}$ soil at TH to $100 \mu\text{g g}^{-1}$ soil at QA (Fig. 2a–d; dashed lines), i.e. there was a significant increase from the baseline value of about $0.0017 \mu\text{g g}^{-1}$ soil on day 0 ($p < 0.05$; Fig. 2a–d).

This increase corresponds to approximately 10% (TH) and 20% (QA) of the initially added cellulose-C. After day 16, growth was counter-balanced to some extent by continued ^{13}C losses from the biomass pool and fell back to baseline by day 64 (Fig. 2a–d). Microbial growth was accompanied by an sigmoidal increase in cumulative $^{13}\text{CO}_2$ release, whereby after a lag phase of about 3 days, an exponential phase occurred until day 16, which then turned into a saturation phase (Fig. 2e–h; dashed line). The statistical comparison of the cumulative $^{13}\text{CO}_2$ release at the end of incubation showed no statistical difference between the fertilized and unfertilized treatment and ranged on average from TH-UF with 22.5 ± 11.7 to $261.2 \pm 131.7 \mu\text{g g}^{-1}$ soil in RE-FYM (Fig. 2e–h). The general increase in biomass (C_{mic}) and respiration (CO_2) evolved at a comparable rate as the ^{13}C content (Fig. 2; solid lines).

3.2. Priming effect

The percentage of labeled cellulose-C in relation to the total CO_2 release, corrected for the CO_2 coming from the control soil, ranged from 37% (TH-UF) to 79% (RE-FYM) on day 64. After cellulose application, we observed a positive priming effect in all soils. PE started to increase immediately after cellulose application and was higher in the fertilized

soils and in the soils with a higher C content (QA, RE). In the fertilized soils, the PE ranged from $74.5 \mu\text{g g}^{-1}$ soil (TH) to $182.9 \mu\text{g g}^{-1}$ soil (QA). At the unfertilized sites, PE ranged from 38.4 to $131.7 \mu\text{g g}^{-1}$ soil in the same order. The priming effect as a percentage of C added as cellulose showed an inverse pattern compared to the total amount of primed C, with values ranging from 10% in the RE-FYM to 32% in the TH-UF (Fig. 3).

3.3. Combustion enthalpy of SOM

The combustion enthalpy determined by combustion calorimetry in the unfertilized variants tended to be higher than in the fertilized soils, ranging from $436 \pm 143 \text{ kJ mol}^{-1} \text{C}$ in QA to $732 \pm 30 \text{ kJ mol}^{-1} \text{C}$ in TH. In the fertilized soils, the energy content ranged from 306 ± 106 in DI to $439 \pm 21 \text{ kJ mol}^{-1} \text{C}$ in TH. TH-UF was therefore the soil with the highest SOM combustion enthalpy according to combustion calorimetry (Supplementary Fig. S3, Table S5). Combustion enthalpy values determined by TG-DSC tended to be higher than those determined by combustion calorimetry, but followed the same pattern across soils. The energy content ranged from $397 \pm 12 \text{ kJ mol}^{-1} \text{C}$ in QA to $820 \pm 181 \text{ kJ mol}^{-1} \text{C}$ in TH for the unfertilized soils and from $407 \pm 177 \text{ kJ mol}^{-1} \text{C}$ in QA to $609 \pm 40 \text{ kJ mol}^{-1} \text{C}$ in TH in the fertilized soils. Thus, TH-UF was also the soil with the highest SOM combustion enthalpy when determined via TG-DSC.

3.4. Heat production rate and specific heat

The heat production rate P_t increased exponentially without any significant lag phase, peaking after about eight days and falling back to the initial value after about 20 days, indicating that growth took place up to day eight (Fig. 4a; the apparent specific growth rate is included in Supplementary Fig. S5). On fertilized sites, the maximum P_t ranged from the lowest value at DI with $7.0 \pm 1.7 \mu\text{W g}^{-1}$ to the highest value of $21.73 \pm 2.2 \mu\text{W g}^{-1}$ (Fig. 4a–d) at RE, which was reached after eight to ten days. In the unfertilized soils, P_t at the maximum was significantly reduced in RE and QA ($p < 0.01$) and peaked at $14.73 \pm 1.56 \mu\text{W g}^{-1}$ (–32.21%) and $12.50 \pm 1.5 \mu\text{W g}^{-1}$ (–23.8%).

In TH and DI there was no statistically significant difference between

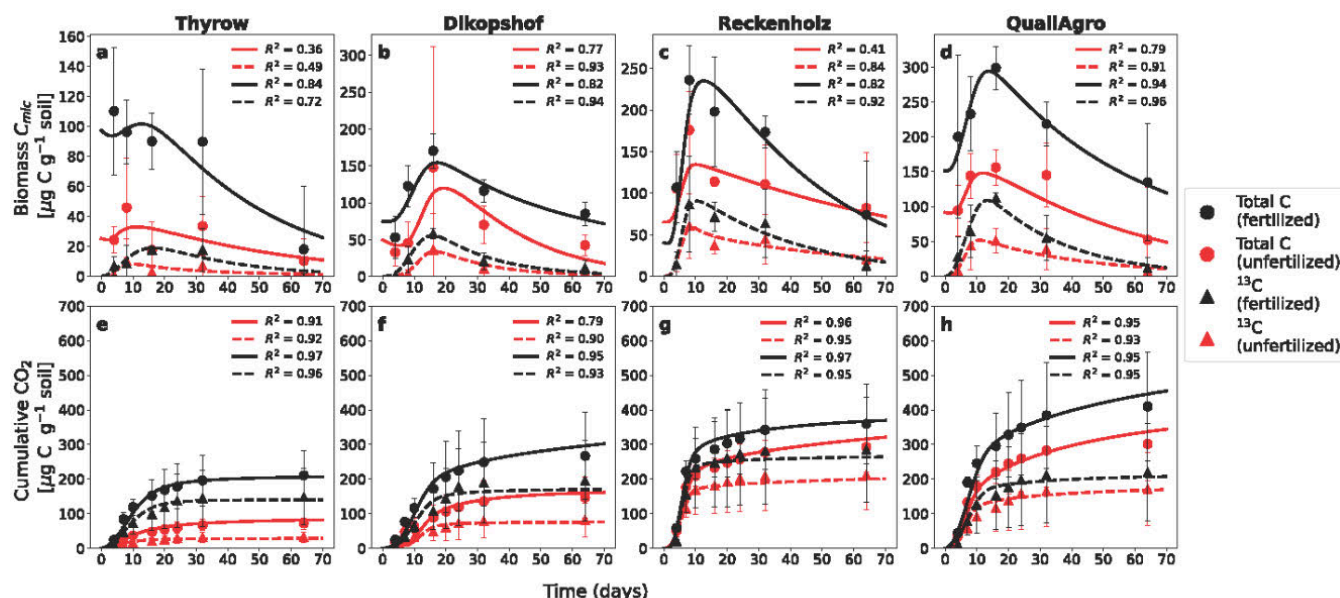


Fig. 2. Microbial biomass content (C_{mic} , a–d) and cumulative CO_2 release (e–h) of all soils. Dots and solid lines correspond to total C measurements and model fits, respectively. Triangles and dashed lines correspond to ^{13}C measurements and model fits. Results for the fertilized soils are shown in black, results for unfertilized soils are shown in red. Data shown represent mean values and standard deviation ($n = 3$). (For interpretation of the references to colour in this figure legend, the reader is referred to the Web version of this article.)

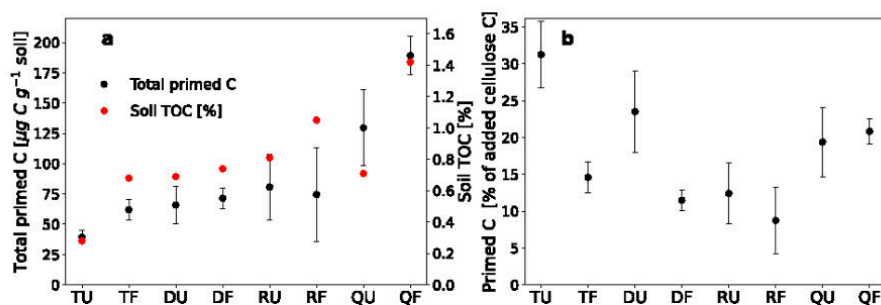


Fig. 3. Observed priming effect after cellulose addition. **a** Total primed C as measured by cumulative ^{12}C - CO_2 release (black). Soil TOC (%) as reported by Lorenz et al. (2024a) is shown in red (note the second y-axis). **b** Priming effect expressed as a percentage of C added as cellulose. Data shown represent mean values and standard deviation ($n = 3$). (For interpretation of the references to colour in this figure legend, the reader is referred to the Web version of this article.)

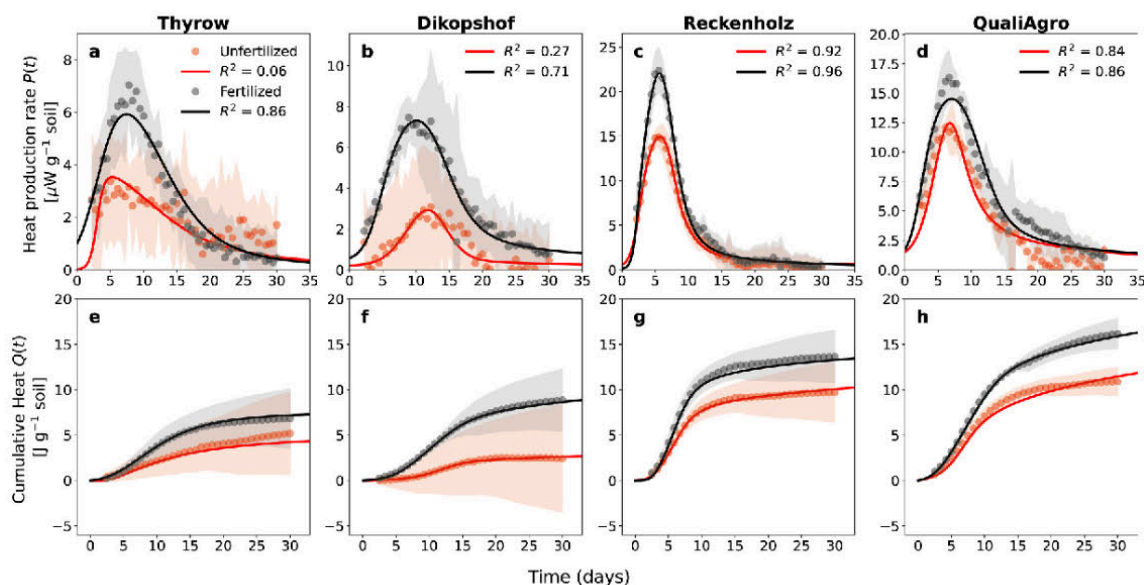


Fig. 4. Heat production rate P_t (a–d) and cumulative heat Q_t (e–h) for all soils (black dots = fertilized, red dots = unfertilized). The corresponding lines represent the mechanistic model fit. Shaded areas represent standard deviation ($n = 3$). (For interpretation of the references to colour in this figure legend, the reader is referred to the Web version of this article.)

fertilized and unfertilized soils. In these less active soils, in which we could not observe this increase up to about $20 \mu\text{W g}^{-1}$, the TAM Air operated at the detection limit ($0\text{--}10 \mu\text{W g}^{-1}$, based on the fluctuations in the measurement of the heat production rate) even in the phase of

exponential increase between three and eight days, which is reflected in the higher standard deviation (Fig. 4a–d). The same dependence on fertilization status as observed for P_t was also observed for the specific heat Q_t (Fig. 4e–h). After 30 days, $16.5 \pm 2.1 \text{ J g}^{-1}$ and $13.8 \pm 3.4 \text{ J g}^{-1}$

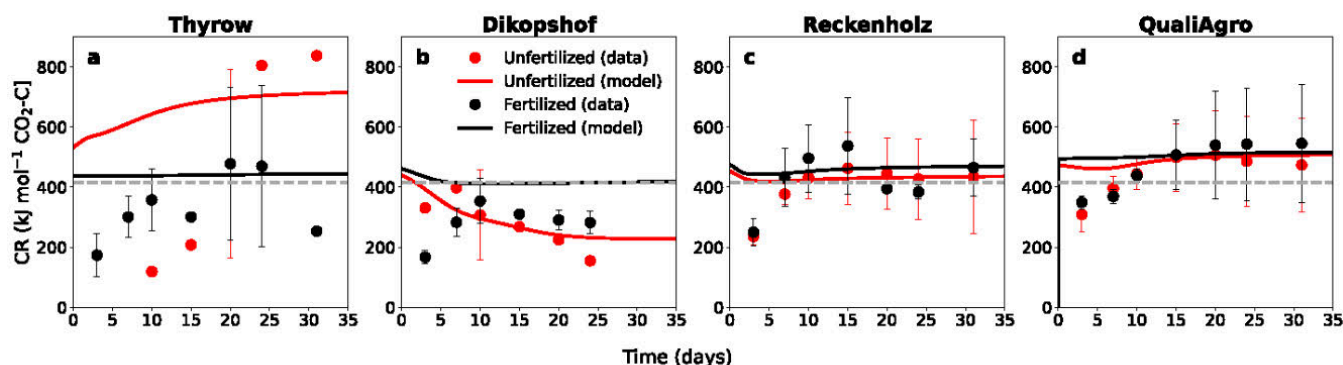


Fig. 5. Calorespirometric ratio over 35 d following cellulose amendment for all soils (black = fertilized, red = unfertilized). The dotted line is the expected calorespirometric ratio upon complete oxidation of cellulose ($406 \text{ kJ mol}^{-1} \text{ CO}_2\text{-C}$). Dots correspond to the measured data and respective lines represent the output of the mechanistic model. Data shown represent mean values and standard deviation ($n = 3$). (For interpretation of the references to colour in this figure legend, the reader is referred to the Web version of this article.)

were attained in QA-FYM and RE-FYM, whereas only 11.2 ± 1.7 (–32%; $p < 0.01$) and $9.8 \pm 5.2 \text{ J g}^{-1}$ (–29%; $p < 0.01$) were reached at the unfertilized sites (Fig. 4e–h). Again, due to the measurement uncertainty of the heat production rate in TH and DI and the resulting high standard deviation (Fig. 4e–h), no significant difference between the fertilized and unfertilized treatments could be determined.

3.5. Calorespirometric ratio

The CR calculated from the ratio of cumulative heat production and respiration started to increase during the exponential growth phase (0–16 days) from about 250 to about 540 kJ mol^{-1} at least for QA and RE, regardless of the fertilization status (Fig. 5).

At DI and TH, this relationship between heat production and respiration was more difficult to establish, due to the low general activity, making it difficult to correctly determine the heat production. Once more, this is reflected in a high standard deviation. Nevertheless, the pattern of increase was still discernible, but the value of 700 kJ mol^{-1} achieved in the unfertilized TH is exceptionally high (Fig. 5).

3.6. C and energy use and storage

The metrics describing C and energy use and storage in the soils were only calculated up to 32 days, because at this point the heat production rate approached very low levels, increasing the uncertainty of the data. When considering the net carbon balance over time, there was a decrease of CB_{net} from its initial value of 1 down to 0.5–0.7 (Fig. 6). The EUE_{net} showed almost identical dynamics, also falling from around 1 on day 0 to around 0.55 on day 32 (Fig. 6).

When the net balance measures CB_{net} and EUE_{net} were compared with CUE_L and CUE_{Rq} , CB_{net} and EUE_{net} were significantly higher ($p < 0.001$) during the first days (day 0–day three). Over time, the CUE_{Rq} derived from the calorespirometric ratio at times exceeded the CB_{net} and EUE_{net} , but the CUE_L was always lower than the net C and energy balance. CUE_{Rq} decreased until days eight and ten down to 0.19 to 0.65 in most of the soils. It should be noted that Eqn. (14) does not permit to estimate the CUE_{Rq} for CR values above 406 kJ mol^{-1} , which substantially reduced the number of CUE_{Rq} estimates. CUE_L was between 0.3 (DI-UF) and 0.71 (QA-FYM) on day four. As expected, the CUE_L

decreased after day 16 when the concentration of labeled biomass had peaked on day 16 while $^{13}\text{CO}_2$ losses continued (Fig. 6).

In addition to analyzing CR as a function of time (Fig. 5), we describe here the relationship between CUE_L and CR (Fig. 7).

We use CUE_L , because CUE_{Rq} is directly derived from the CR and therefore not a CR-independent measure of CUE. The two components of the CR (heat and CO_2 release rates) vary to different degrees and therefore allow conclusions to be drawn about C or energy limitation of microbial growth. Specifically, CR values that decrease with CUE and are limited to below the combustion enthalpy of biomass ($\approx 485 \text{ kJ mol}^{-1}\text{C}$ using our assumptions) are taken to indicate energy limitation, whereas CR values that increase with CUE and are limited to values above this threshold are taken to indicate C limitation of growth (Fig. 7). CUE was found to decrease with increasing CR up to day eight across soils. When CUE is at its maximum, about 0.5–0.75, and not much heat is released, CR is lowest in the range of 200–300 kJ mol^{-1} . On the contrary, when growth stops (i.e. $\text{CUE} \approx 0.18$ to 0.25 after 32 days), CR is maximised. On the other hand, we also observed CR values around or exceeding the combustion enthalpy of cellulose ($406 \text{ kJ mol}^{-1}\text{C}$) and biomass ($485 \text{ kJ mol}^{-1}\text{C}$), in particular during the later stages and in the SOM-rich soils of RE and QA (Fig. 5). This can be explained by the use of an additional energy and C-source such as SOM that is more reduced than cellulose and would correspond to C limited growth in these instances.

3.7. Model behavior and performance

The dynamic model adequately reproduced the time series of CO_2 and heat production as well as biomass growth and turnover over the course of the incubation for all soils. In particular, the simulated combination of growth reactions using either added ^{13}C -cellulose or native ^{12}C -SOM as substrates properly captured the dynamics of both ^{12}C and ^{13}C pools (Fig. 2). Moreover, the sum of their corresponding heat contributions was in good agreement with measured total heat production rate (Fig. 4), although the experimental results showed high variance in the SOM-poor soils (TH and DI).

This close coupling of carbon and energy release was also reflected in the simulated CR, which was generally aligned with experimental estimates, especially in the SOM-rich soils (RE and QA, Fig. 5). Overall, the

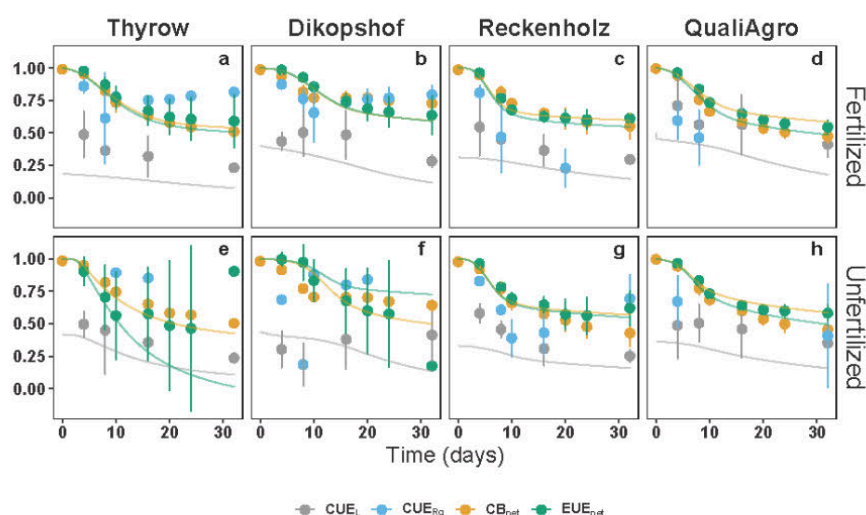


Fig. 6. C use efficiency and net C and energy balances during the incubation for the fertilized (a–d) and unfertilized (e–h) soils. Grey represents the CUE derived from the labeled C (CUE_L), blue the CUE based on the CR (CUE_{Rq}), and orange the net carbon balance (CB_{net}). Green represents the net energy use efficiency (EUE_{net}). The corresponding lines indicate the respective outputs of the mechanistic model. Data shown represent mean values and standard deviation ($n = 3$). For CUE_{Rq} , only values derived from $\text{CR} < 406 \text{ kJ mol}^{-1}$ are shown. (For interpretation of the references to colour in this figure legend, the reader is referred to the Web version of this article.)

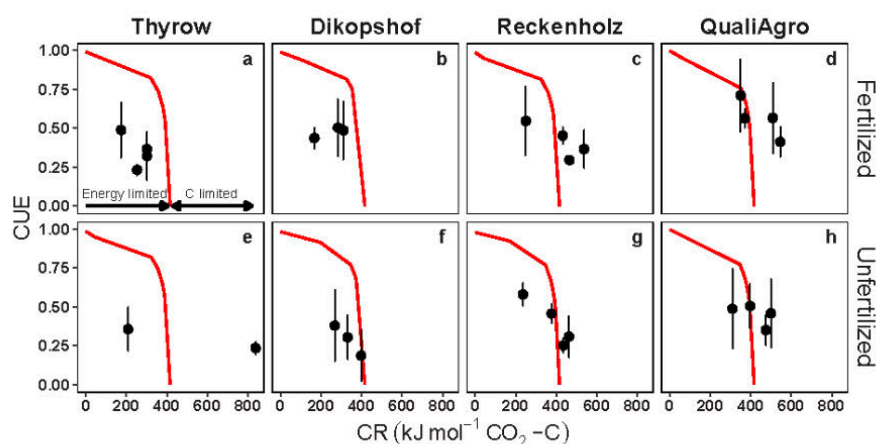


Fig. 7. CUE_L as a function of CR (black dots) for the fertilized (a–d) and unfertilized (e–h) soils. In TH and DI there are lacking data points due to the missing ^{13}C determination. The total enthalpy change of cellulose metabolism ($\Delta_c H_{cellulose}$; red line) can be described as a function of the degree of reduction for both cellulose and the microbial biomass ($\gamma_{cellulose} = 4$, $\gamma_{MB} = 4.284$). Data shown represent mean values and standard deviation ($n = 3$). (For interpretation of the references to colour in this figure legend, the reader is referred to the Web version of this article.)

cumulative model CR showed less temporal variation than the observations and was instead dominated by its value during the growth phase. The two soils with the lowest SOM content, i.e., the unfertilized soils of TH and DI, were an exception to this, with cumulative CR increasing and decreasing from its initial value over time, respectively.

As suggested by the close model fit to the cumulative data, CB_{net} and EUE_{net} as well as ^{13}C - CUE_L estimates obtained from simulations resembled their experimental counterparts (Fig. 6). In addition to these directly obtainable experimental measures, model simulations also allowed the estimation of ^{12}C - CUE_L , i.e., modeled $^{12}C_{mic}$ formation relative to modeled SOM consumption, as well as total CUE_L , i.e., modeled net C_{mic} formation relative to the combined modeled consumption of cellulose and SOM (Supplementary Fig. S4). These modeled measures showed generally lower (TH, QA) or similar (DI, RE-UF) ^{12}C – CUE relative to ^{13}C – CUE , with the exception of RE-FYM, where growth on SOM was modeled as more efficient. The analysis also revealed a temporal pattern of biomass formation being first fueled by cellulose consumption, followed by later contributions due to SOM utilization (Supplementary Fig. S4). In terms of net growth, the experimental cellulose amendment resulted in an increase in total C_{mic} after 32 days in all soils except TH, where biomass levels dropped to (TH-UF) or below (TH-FYM) their initial values within that time span (Fig. 2a–d).

In terms of the calibrated parameter sets, optimized values indicated that specific growth rates μ_{max} fueled by cellulose exceeded those fueled by SOM in all soils (Supplementary Fig. S5), and μ_{max} was higher in the unfertilized soil for all sites except RE, where this trend was reversed. Finally, the modeled degree of reduction γ_{SOM} of the consumed SOM were in good agreement with experimental measurements derived from the average energy content of the bulk SOM determined via bomb calorimetry and TG-DSC in most soils (Supplementary Fig. S3, Fig. S6). QA and DI-UF presented notable exceptions, with higher (QA) and lower (DI-UF) values compared to experimental estimates, respectively.

4. Discussion

It is established that the CUE, CR and microbial growth kinetics can be reliably derived from calorimetric measurements for growth on rapidly metabolized substrates, especially under aerobic conditions (Yang et al., 2024; Von Stockar et al., 2006; Barros et al., 2000; Chakrawal et al., 2020). In the following, we will discuss to what extent CR is related to microbial growth on added cellulose as a slowly degradable substrate compared to glucose, how a possible priming of SOM affects CR and how the measurement accuracy of calorimetry affects CUE and

EUE_{net} estimates as well as CR compared to the determination of microbial CUE by other methods. Finally, we address technical issues that arise when combining the energy and carbon flow in the CR framework.

4.1. The CR reflects the coupling of energy and carbon flux during microbial growth after cellulose amendment

Across the studied soils, our observed CR values in the range of 200–540 $kJ\ mol^{-1}\ CO_2-C$ are broadly consistent with aerobic growth on cellulose. They are comparable to the findings of previous studies that reported CR values during microbial growth on glucose with yields of 0.5–0.75, characteristic of highly efficient aerobic growth (Hansen et al., 2004; Chakrawal et al., 2021). Since glucose units form the primary structure of cellulose, the metabolic processes involved in microbial growth on these substrates are very similar, apart from the hydrolysis required for the extracellular depolymerization of the cellulose (Blagodatskaya et al., 2014; Popovic et al., 2019; Sørensen et al., 2015; Datta et al., 2017). Given this context, the theoretical framework proposed by Chakrawal et al. (2020) for the variation of the CR of different metabolic pathways of glucose (and SOM) utilization can be applied to our data. The principal distinction is that we measured a combustion enthalpy of $\Delta_c H_{cellulose} = 406\ kJ\ mol^{-1}\ C$ for the cellulose used in this study, in contrast to the literature value of $\Delta_c H_{glucose} = 469\ kJ\ mol^{-1}\ C$ for glucose. If the growth reaction fueled by cellulose was the only process contributing to observed CO_2 and heat production, the range of possible CR values would be fully determined by this combustion enthalpy along with the microbial CUE and the degree of reduction γ_{MB} of the newly formed microbial biomass (Eqn. (14)). Assuming a biomass composition of $C_1H_{1.571}O_{0.429}N_{0.143}$ as suggested for soils in this context (Yang et al., 2024), cellulose represents a more oxidized substrate relative to biomass, i.e., $\gamma_{cellulose} < \gamma_{MB}$, and the growth reaction is characterized by a decrease in CR for increasing CUE (Fig. 7), with a maximum of $CR = \Delta_c H_{cellulose} = 406\ kJ\ mol^{-1}\ C$ for pure catabolism (i.e., $CUE = 0$, Kästner et al., 2024). Minor deviations from this predicted CR-CUE relationship may be attributed to variations in the actual biomass composition and thus in γ_{MB} as noted by Chakrawal et al. (2020). However, we observed CR values well above and below this theoretical prediction (Fig. 7). Yang et al. (2024) also reported an average CR of $577.7\ kJ\ mol^{-1}\ C$ obtained from cumulative heat measurements and $567.6\ kJ\ mol^{-1}\ C$ obtained from the corresponding heat production rate after glucose addition to the DI-FYM soil, well above their theoretical predictions, and pointed to additional SOM utilization or partial anoxic conditions as potential explanations of this

observation. Our results using labeled ^{13}C -cellulose confirmed such substantial SOM utilization over the course of the incubation and associated observed deviations from the predicted CR-CUE curve. Critically, this predicted CR-CUE relationship is only applicable to the pure growth reaction on cellulose, and will be altered by additional contributions of heat and CO_2 from the growth reaction fueled by SOM, which is characterized by its own degree of reduction and yield coefficient. Following Chakrawal et al. (2020), the simple relationship predicted for cellulose corresponds to energy limited microbial growth, which releases relatively more C than heat as efficiency increases. In our data, we observe this pattern only during the early stages of the incubation across soils (at least up to day eight after substrate addition). However, this pattern is no longer evident later during the incubation, especially in the SOM-rich soils and in TH-UF (Figs. 5 and 7). For all of these soils, our model predicts the utilization of more reduced SOM (Supplementary Fig. S6) that corresponds to C-limited growth in this framework, and our findings could thus be interpreted as an increasing contribution of SOM utilization after the cellulose addition in these soils.

In addition, we observed no net growth and lower activity for a large fraction of the later stages of our incubations (Figs. 2 and 4). If no further growth occurs during this time, the observed CO_2 and heat production will primarily result from maintenance and turnover processes (Manzoni et al., 2012) and thus again deviate from the CR of the growth reaction. In our dynamic model formulation, this slow conversion of biomass to CO_2 and heat due to maintenance predicts a CR of $\approx 490 \text{ kJ mol}^{-1} \text{ C}$ equal to the combustion enthalpy of microbial biomass (Chakrawal et al., 2020), which is in good agreement with the observed values especially in the SOM-rich soils (RE and QA, Fig. 7). However, future studies will benefit from a more nuanced consideration of the carbon and energy flux due to maintenance and turnover during the retardation and onset of starvation following the growth phase.

In principle, deviations of the CR from predictions for the aerobic growth reaction may also be caused by anaerobic metabolism (Chakrawal et al., 2020; Endress et al., 2024a; Barros et al., 2016). However, total O_2 concentration was not limiting in our vials, as the observed CR deviations occurred in incubations that differed strongly in the amount of added C and cumulative CO_2 release. Similarly, the formation of substantial anoxic microsites seems unlikely given the slow rate of cellulose decomposition in our samples, whereas such sites might be important in the case of more labile substrates and in natural, intact soils (e.g., Lacroix et al. (2022); Keiluweit et al. (2016)).

4.2. ^{13}C -labeling and dynamic modeling reveal a substantial priming effect

We observed a substantial PE after cellulose addition across soils, which cover a wide range of SOM contents (Tables S1 and S2) as well as total rates of C addition (Table 1) and were deliberately chosen for this study. The release of ^{12}C - CO_2 , presumably fueled by the degradation of native SOM, accounted for a large share of total CO_2 emissions in all of these soils (Fig. 3). In absolute terms, the observed PE is consistent with the relationship described in the literature between the input of ^{13}C -labeled plant residues and the primed $\text{CO}_2 - \text{C}$ (Blagodatskaya et al., 2014; Perveen et al., 2019). Blagodatskaya et al. (2014) ascribed the pronounced increase in the amount of active microbial biomass that occurs during the intensive phase of cellulose degradation to the elevated enzyme activity for the hydrolysis of chitin, cellulose and hemicellulose, which are also involved in the decomposition of SOM. While the absolute amount of primed C showed the expected relationship of increasing PE with native SOM content and amount of added cellulose across soils (Fig. 3), the PE relative to the amount of added C showed a more variable pattern (Fig. 3), ranging from 8.7% (RE-FYM) to 31% (TH-UF). In particular, the amount of degraded SOM per added substrate was strongly elevated in the unfertilized variants of the SOM-poor soils at TH and DI when compared to their fertilized variants ($p < 0.05$), whereas no such difference was observed in the SOM-rich

soils. While the C content in the fertilized soils is always slightly higher compared to the unfertilized counterparts for all sites, this is not true for the C/N ratios (Tables S1–S2). Nevertheless, a C/N ratio of 7–9 indicates a good nutrient supply in all soils. It is conceivable that the fertilisation effect of farmyard manure could be partly offset, as Arcand et al. (2017) noted that the long-term application of organic material (e.g. straw) can reduce the N availability. As a result, in addition to the joint decomposition of soil organic matter and cellulose, additional N mining could have been stimulated, with potential further release of CO_2 and heat (Arcand et al., 2017; Chakrawal et al., 2021).

Combining the measured heat production with the carbon-based considerations offers further insights into the nature of the degraded SOM. Specifically, our observed CR values are consistent with substantial priming, given the deviations from predictions for the simple aerobic growth reaction fueled by cellulose. For example, an elevated CR, in particular above $\geq 406 \text{ kJ mol}^{-1} \text{ C}$, would indicate heat and CO_2 contributions from the degradation of relatively reduced, energy-rich SOM, whereas low CR values might indicate the utilization of more oxidized and energy-poor SOM (Chakrawal et al., 2020; Barros, 2021). We observed both comparatively high and low CR values over the course of the incubation experiments, potentially reflecting the varying energy contents of SOM in the studied soils, which ranged from 305 to 732 $\text{kJ mol}^{-1} \text{ C}$ when determined via combustion calorimetry and from 397 to 820 $\text{kJ mol}^{-1} \text{ C}$ when determined via TG-DSC (Supplementary Fig. S3). More specifically, the parameter calibration of the dynamic model suggested a degree of reduction of the SOM consumed by microbes that is consistent with the measured energy contents of the bulk SOM (e.g., in the RE and TH soils as well as in DI-FYM, Supplementary Fig. S6). The TH-UF soil, which is characterized by both the lowest organic carbon content (Supplementary Table S2, Table S3) as well as the highest SOM energy content (Supplementary Fig. S3, Table S5) of all soils, provides a compelling illustration, with the model suggesting an extremely high $\gamma_{\text{SOM}} \approx 7$ that is in line with our experimental results (Supplementary Fig. S6). This soil also showed the most pronounced CR deviation, consistent with microbial utilization of such highly reduced SOM (Fig. 5). In contrast, we found discrepancies between the measured energy content of the bulk SOM and the modeled γ_{SOM} of microbially consumed SOM in some of the other soils. In the QA soils, the microbially degraded SOM was predicted to be more reduced than measurements of bulk energy contents would suggest, whereas the opposite was true in the DI-UF soil (Supplementary Fig. S6). In both cases, these discrepancies are consistent with observed CR deviations (Fig. 5) and may indicate a preferential use of SOM components that differ from the bulk SOM in terms of their average DR, although our data are insufficient to test this interpretation.

4.3. CUEs are indicative of cellulose metabolism, while CB_{net} and EUE_{net} reflect the balance of C and energy after the cellulose application

Our experimental and modeling evaluation of various estimators for the fate of substrate-derived C and energy revealed systematic differences between these approaches as well as their respective limitations. The interpretation of CUE based on ^{13}C -labeled substrates strongly depends on the considered time scale. While the efficiency of the immediate substrate use is reflected by the population CUE, the ecosystem CUE also considers processes such as microbial recycling at a longer time scale and is usually declining with time compared to the population CUE (Geyer et al., 2016). Notably, the ^{13}C -based CUE_L (Eqn. (13)), which we consider to be the most direct estimate, consistently yielded lower efficiencies than the other methods, ranging from 0.18 to roughly 0.7 and the decrease over time and across soils reflects the transition from the population to the ecosystem CUE. Nonetheless, these values indicate efficient aerobic growth in all incubations, and a lower efficiency than obtained for growth on more labile substrates such as glucose can be expected for the more complex cellulose (Manzoni et al., 2018; Öquist et al., 2017).

Efficiency estimates based on CUE_{Rq} (Eqn. (14)) turned out to be problematic. First and foremost, its derivation rests on the assumption that the CR primarily reflects the CO_2 and heat production of the aerobic growth reaction fueled by the added substrate (Hansen et al., 2004; Geyer et al., 2019). Yang et al. (2024) recently questioned whether this condition was met even in the case of glucose amendment, and it was certainly not met in our experiment, where we observed substantial SOM decomposition as well as substantial periods primarily characterized by maintenance and turnover processes. Accordingly, we obtained CR values (namely, $CR > 406 \text{ kJ mol}^{-1} \text{ C}$) that Eqn. (14) maps to nonsensical (< 0 or > 1) CUE estimates for several time points in many of our incubations, as did Yang et al. (2024) in their recent experiments with glucose. Moreover, CUE_{Rq} estimates in the interval between 0 and 1 may still not reflect the actual growth efficiency due to, e.g., the impact of SOM utilization. For example, low CR values in the range of $200 \text{ kJ mol}^{-1} \text{ C}$ (e.g., as seen in the TH and DI soils, Fig. 5) correspond to a CUE_{Rq} exceeding ≈ 0.9 . Such values would indicate that the C is channelled almost exclusively to anabolism (Geyer et al., 2016), which is beyond the physiological limits imposed by the energy demands of these reactions that need to be fueled by corresponding catabolism (Chakrawal et al., 2020). Similarly, biosynthesis is only possible when growth-independent energy requirements are met and a sufficient surplus of C and energy is available (Ingraham et al., 1983). Overall, maximum efficiency is limited to around 0.85 by respiration losses, even for the most reduced and energy-rich compounds (Gommers et al., 1988). Another example of an implausible pattern predicted by CUE_{Rq} can be seen in the DI-UF soil, which is characterized by consistently decreasing CR values that are mapped to increasing CUE estimates over time by Eqn. (14), in contrast to the ^{13}C -based CUE_L and the growth dynamics seen in the biomass time series (Fig. 2a–d). Overall, we conclude that CUE_{Rq} is only an appropriate estimator of growth efficiency if the underlying CR values can be reasonably assumed to primarily reflect the growth reaction on the added substrate. Accordingly, we observed the best agreement of this estimate with CUE_L during the phase of intense, cellulose-fueled growth, at least in the SOM-rich soils (RE and QA, Fig. 6).

The susceptibility of CUE_{Rq} to processes such as priming translates to CB_{net} (Eqn. (15)) and EUE_{net} (Eqn. (6)), which can be considered as storage efficiencies of the whole soil system (Manzoni et al., 2018) and are purely based on the cumulative release of CO_2 and heat, respectively. They continuously decreased from their initial value of 1 over the course of the experiment (Fig. 6), reflecting a continuous loss of C and energy. Notably, the use of ^{13}C -labeled cellulose enabled us to disentangle the contributions of substrate and SOM degradation to the loss and storage of both C and energy over the course of a long incubation using cellulose as a less degradable substrate. This revealed substantial priming and preferential use of SOM (Supplementary Fig. S6), but also retention of undecomposed cellulose across soils, highlighting the potential of combining ^{13}C - and energy based metrics as emphasized by Kästner et al. (2024). Both storage metrics can parallel CUE in the case of rapidly metabolized substrates such as glucose, which are quickly and completely converted to microbial biomass, CO_2 and heat (Hagerty et al., 2018; Wang and Kuzyakov, 2023; Yang et al., 2024; Endress et al., 2024a). For example, glucose may be taken up by microbial cells within few minutes without being immediately metabolized (Geyer et al., 2019). In such a case, both metrics would be close to 1 and start to constantly decrease while the glucose is being metabolized. However, it is important to consider that CUE focuses on the efficiency of the anabolic use of the substrate that was taken up, while CB_{net} focuses on the C retention within the whole soil system. The assumption of a complete rapid utilization of the added substrate is not applicable to our incubations, in which considerable amounts of cellulose remained in the soil by the end of the incubation after 64 days and considerable priming of SOM was observed. Under such circumstances, which may be more reflective of litter inputs in natural soils, CB_{net} and EUE_{net} differ from the estimated CUE (Fig. 6) both conceptually and numerically, as evidenced

by measured biomass increases (Fig. 2) and CUE_L , especially early during the incubation and the exponential growth phase. Thus, CB_{net} and EUE_{net} can be taken to reflect the temporal evolution of the net carbon and energy remaining in the soil after substrate addition. From this perspective, our results indicate a net accumulation of carbon (and energy) in the soil after 32 days, as the combined CO_2 (heat) losses from both added cellulose and native SOM do not exceed the amount of initially added carbon (energy) within the time span of the experiment (i.e., $CB_{net}, EUE_{net} > 0$). While the interpretation of these value is thus more akin to a storage efficiency (Manzoni et al., 2018), they themselves do not reveal the nature of the carbon (energy) remaining in the soil, e.g., as undecomposed cellulose, biomass, or necromass.

A more complex understanding of the connection between CR and CUE beyond the simple correspondence suggested by Eqn. (14) can be leveraged to interpret the experimental patterns. This has been demonstrated theoretically for the case of SOM utilization and anaerobic pathways (Chakrawal et al., 2020) as well as using process-based models calibrated to experimental data, which explicitly considered anaerobic and maintenance processes (Endress et al., 2024a). Likewise, the results of our model calibration offer the most nuanced interpretation of the efficiency and carbon-energy coupling over the course of the experiments. First, CB_{net} , EUE_{net} and CUE_L estimated from model output are in good agreement with those obtained from data, although model CUE_L tended to be slightly lower than experimental values due to the inclusion of necromass in the model carbon balance, which is missing from Eqn. (13) (Fig. 6). The model provides a mechanistic description that shows a plausible and consistent interpretation of the observed dynamics of all carbon pools in combination with the total heat production, despite the failure of a simple estimate like CUE_{Rq} in Eqn. (14). In addition, the model offers dynamic estimates of the actual growth efficiencies, i.e., the ratio of (cumulative) biomass formation to the (cumulative) amount of consumed substrate, both for ^{12}C and the combined $^{12}\text{C} + ^{13}\text{C}$ pools (Supplementary Fig. S4). These include negative values corresponding to net loss of (^{12}C or total) biomass compared to initial measured values, which is also evident from the experimental biomass time series, and reveal periods of highly efficient growth on SOM, e.g., in the RE-FYM soil (Supplementary Fig. S4). Overall, the model nonetheless suggests that growth was predominantly driven by consumption of the added cellulose in most soils, in particular early during the incubation.

While the use of a labeled substrate is essential for this kind of detailed model calibration and greatly enhances model performance, the calibrated model parameters (e.g., γ_{SOM}) and behavior should still be treated with caution. In particular, models of soil C cycling such as the one employed here frequently face substantial equifinality and limited parameter identifiability (Sierra et al., 2015; Marschmann et al., 2019). Moreover, our model formulation relied on a simple threshold parameter to capture the observed levels of undecomposed cellulose remaining in the soil, and we used a simple conversion of biomass to CO_2 and heat to represent the bioenergetic coupling during maintenance, as opposed to a more complex process like continued SOM use to fuel maintenance requirements. The more detailed characterization of such processes as well as a systematic analysis of model parameter identifiability in the presence of labeled substrates will be critical next steps for the proper representation of microbial-explicit C cycling in biogeochemical models, which remains challenging (Wieder et al., 2015).

4.4. Technical constraints in the combination of C and heat fluxes to dissipate the CR

Although Eqn. (14) from Hansen et al. (2004) shows a relationship between CR and CUE, it is limited to the exponential growth phase fueled by cellulose consumption and is therefore not applicable during maintenance processes or in the case of simultaneous utilization of substrates with different degrees of reduction. As stated by Yang et al. (2024), the accuracy requirements of this model for the CR and the actual determination errors of currently available instruments, such as

TAM Air, imply that CUE can only be inferred from the CR in a best-case scenario. If the heat measurement takes place in low-activity soils at levels close to the detection limit, the stability of the baseline for long-term experiments (e.g. over weeks) can no longer be guaranteed, and it may even be in the negative range (Supplementary Fig. S2). For TH and DI, a subsequent baseline correction had to be carried out in order to obtain realistic heat production rates.

5. Conclusion

Measures of microbial CUE and EUE are frequently based on the fate of added substrates, thus neglecting microbial use of native SOC. We extended these concepts to the net balances of C (CB_{net}) and energy (EUE_{net}) of the whole soil system, which also integrate additional C and energy fluxes due to microbial SOC consumption. They thus quantify whether the system loses or gains C and energy after substrate addition and complement traditional measures of growth efficiency. Application of these concepts to eight cellulose-amended fertilized and unfertilized arable soils demonstrated a net C and energy gain in all soils after 32 days of incubation, despite substantial SOC priming in all soils as indicated by ^{13}C -labeling. The calorimetric ratio proved to be a useful metric to link the C and energy fluxes in the presence of priming, showing that the initial energy limitation of microbial growth fueled by cellulose was alleviated by SOC consumption during later stages of incubation. Dynamic modeling further suggested a close connection between microbial SOC utilization and the average energy content of SOC in the studied soils. The applied approaches are well suited for the joint evaluation of C and energy fluxes in soils with high microbial biomass and SOC content, but face some limitations in soils with low microbial activity, highlighting a need for further methodological development. Overall, we demonstrated how a combination of experimental and modeling techniques can disentangle the complex dynamics of microbial substrate and SOC utilization from a bioenergetic perspective.

CRedit authorship contribution statement

Johannes Wirsching: Writing – original draft, Validation, Methodology, Investigation, Formal analysis. **Martin-Georg Endress:** Writing – original draft, Methodology, Formal analysis. **Eliana Di Lodovico:** Writing – review & editing, Investigation. **Sergey Blagodatsky:** Writing – review & editing, Validation. **Christian Fricke:** Writing – review & editing, Validation. **Marcel Lorenz:** Writing – review & editing, Investigation. **Sven Marhan:** Writing – review & editing, Conceptualization. **Ellen Kandeler:** Writing – review & editing, Conceptualization. **Christian Poll:** Writing – review & editing, Supervision, Conceptualization.

Funding

This study was performed within the framework of the German Science Foundation (DFG) Priority Program “SPP 2223 – System ecology of soils – Energy Discharge Modulated by Microbiome and Boundary Conditions (SoilSystems)”. The work was funded by the DFG under the grants 465124939, 465120774 and 465120347.

Declaration of competing interest

The authors declare the following financial interests/personal relationships which may be considered as potential competing interests: Christian Poll reports financial support was provided by German Research Foundation. If there are other authors, they declare that they have no known competing financial interests or personal relationships that could have appeared to influence the work reported in this paper.

Acknowledgements

The authors acknowledge support by the State of Baden-Württemberg through bwHPC. We would like to thank Wolfgang Armbruster from Institute for Food Chemistry in Hohenheim for the IRMS analysis. Fig. 1 was created using BioRender.

Appendix A. Supplementary data

Supplementary data to this article can be found online at <https://doi.org/10.1016/j.soilbio.2024.109691>.

References

- Ahrends, H.E., Eugster, W., Gaiser, T., Rueda-Ayala, V., Hüging, H., Ewert, F., Siebert, S., 2018. Genetic yield gains of winter wheat in Germany over more than 100 years (1895–2007) under contrasting fertilizer applications. *Environmental Research Letters* 13, 104003. <https://doi.org/10.1088/1748-9326/aade12>.
- Arcand, M.M., Levy-Booth, D.J., Helgason, B.L., 2017. Resource legacies of organic and conventional management differentiate soil microbial carbon use. *Frontiers in Microbiology* 8, 309266. <https://doi.org/10.3389/fmicb.2017.02293>.
- Assael, M.J., Maitland, G.C., Maskow, T., von Stockar, U., Wakeham, W.A., Will, S., 2022. Commonly Asked Questions in Thermodynamics. CRC Press.
- Barros, N., 2021. Thermodynamics of soil microbial metabolism: applications and functions. *Applied Sciences* 11, 4962. <https://doi.org/10.3390/app11114962>.
- Barros, N., Feijóo, S., Simoni, A., Critter, S., Airolidi, C., 2000. Interpretation of the metabolic enthalpy change, ΔH_{met} , calculated for microbial growth reactions in soils. *Journal of Thermal Analysis and Calorimetry* 63, 577–588. <https://doi.org/10.1023/A:1010162425574>.
- Barros, N., Hansen, L., Piñeiro, V., Pérez-Cruzado, C., Villanueva, M., Proupín, J., Rodríguez-Añón, J., 2016. Factors influencing the calorimetric ratios of soil microbial metabolism. *Soil Biology and Biochemistry* 92, 221–229. <https://doi.org/10.1016/j.soilbio.2015.10.007>.
- Bates, D., Mächler, M., Bolker, B., Walker, S., 2008. Fitting linear mixed-effects models using the lme4 package in R. In: *Presentation at Potsdam GLIMM Workshop*.
- Blagodatskaya, E., Khomyakov, N., Myachina, O., Bogomolova, I., Blagodatsky, S., Kuzyakov, Y., 2014. Microbial interactions affect sources of priming induced by cellulose. *Soil Biology and Biochemistry* 74, 39–49. <https://doi.org/10.1016/j.soilbio.2014.02.017>.
- Blagodatsky, S., Richter, O., 1998. Microbial growth in soil and nitrogen turnover: a theoretical model considering the activity state of microorganisms. *Soil Biology and Biochemistry* 30, 1743–1755. [https://doi.org/10.1016/S0038-0717\(98\)00028-5](https://doi.org/10.1016/S0038-0717(98)00028-5).
- Boos, E.F., Braun, S., Magid, J., 2023. Priming is frequently overestimated in studies using ^{14}C -labelled substrates due to underestimation of $^{14}CO_2$ activity. *Soil Biology and Biochemistry* 181, 109020. <https://doi.org/10.1016/j.soilbio.2023.109020>.
- Bölscher, T., Vogel, C., Olagoke, F.K., Meurer, K.H., Herrmann, A.M., Colombi, T., Brunn, M., Domeignoz-Horta, L.A., 2024. Beyond growth: the significance of non-growth anabolism for microbial carbon-use efficiency in the light of soil carbon stabilisation. *Soil Biology and Biochemistry* 193, 109400. <https://doi.org/10.1016/j.soilbio.2024.109400>.
- Cagnarini, C., Lofts, S., D'Acqui, L.P., Mayer, J., Grüter, R., Tandy, S., Schulin, R., Costerousse, B., Orlandini, S., Rendla, G., 2021. Modelling of long-term Zn, Cu, Cd and Pb dynamics from soils fertilised with organic amendments. *Soils* 7, 107–123. <https://doi.org/10.5194/soil-7-107-2021>.
- Calabrese, S., Chakrawal, A., Manzoni, S., Van Cappellen, P., 2021. Energetic scaling in microbial growth. *Proceedings of the National Academy of Sciences* 118, e2107668118. <https://doi.org/10.1073/pnas.2107668118>.
- Chakrawal, A., Herrmann, A., Šantrková, H., Manzoni, S., 2020. Quantifying microbial metabolism in soils using calorimetry—a bioenergetics perspective. *Soil Biology and Biochemistry* 148, 107945. <https://doi.org/10.1016/j.soilbio.2020.107945>.
- Chakrawal, A., Herrmann, A.M., Manzoni, S., 2021. Leveraging energy flows to quantify microbial traits in soils. *Soil Biology and Biochemistry* 155, 108169. <https://doi.org/10.1016/j.soilbio.2021.108169>.
- Datta, R., Kelkar, A., Baraniya, D., Molaei, A., Moulick, A., Meena, R.S., Formanek, P., 2017. Enzymatic degradation of lignin in soil: a review. *Sustainability* 9, 1163. <https://doi.org/10.3390/su9071163>.
- De Graaff, M.A., Classen, A.T., Castro, H.F., Schadt, C.W., 2010. Labile soil carbon inputs mediate the soil microbial community composition and plant residue decomposition rates. *New Phytologist* 188, 1055–1064. <https://doi.org/10.1111/j.1469-8137.2010.03427.x>.
- Domeignoz-Horta, L.A., Pold, G., Liu, X.J.A., Frey, S.D., Melillo, J.M., DeAngelis, K.M., 2020. Microbial diversity drives carbon use efficiency in a model soil. *Nature Communications* 11, 3684. <https://doi.org/10.1038/s41467-020-17502-z>.
- Elmer, F., Baumecker, M., 2005. Static nutrient depletion experiment throw results after 65 experimental years. *Archives of Agronomy and Soil Science* 51, 151–161. <https://doi.org/10.1080/03650340400026669>.
- Endress, M.G., Chen, R., Blagodatskaya, E., Blagodatsky, S., 2024a. The coupling of carbon and energy fluxes reveals anaerobiosis in an aerobic soil incubation with a *Bacillota*-dominated community. *Soil Biology and Biochemistry* 195, 109478. <https://doi.org/10.1016/j.soilbio.2024.109478>.

- Endress, M.G., Dehghani, F., Blagodatsky, S., Reitz, T., Schlüter, S., Blagodatskaya, E., 2024b. Spatial substrate heterogeneity limits microbial growth as revealed by the joint experimental quantification and modeling of carbon and heat fluxes. *Soil Biology and Biochemistry* 197. <https://doi.org/10.1016/j.soilbio.2024.109509>.
- Fernández, J.M., Plante, A.F., Leifeld, J., Rasmussen, C., 2011. Methodological considerations for using thermal analysis in the characterization of soil organic matter. *Journal of Thermal Analysis and Calorimetry* 104, 389–398. <https://doi.org/10.1007/s10973-010-1145-6>.
- Fontaine, S., Mariotti, A., Abbadie, L., 2003. The priming effect of organic matter: a question of microbial competition? *Soil Biology and Biochemistry* 35, 837–843. [https://doi.org/10.1016/S0038-0717\(03\)00123-8](https://doi.org/10.1016/S0038-0717(03)00123-8).
- Geyer, K.M., Dijkstra, P., Sinsabaugh, R., Frey, S.D., 2019. Clarifying the interpretation of carbon use efficiency in soil through methods comparison. *Soil Biology and Biochemistry* 128, 79–88. <https://doi.org/10.1016/j.soilbio.2018.09.036>.
- Geyer, K.M., Kyker-Snowman, E., Grandy, A.S., Frey, S.D., 2016. Microbial carbon use efficiency: accounting for population, community, and ecosystem-scale controls over the fate of metabolized organic matter. *Biogeochemistry* 127, 173–188. <https://doi.org/10.1007/s10533-016-0191-y>.
- Gommers, P., Van Schie, B., Van Dijken, J., Kuennen, J., 1988. Biochemical limits to microbial growth yields: an analysis of mixed substrate utilization. *Biotechnology and Bioengineering* 32, 86–94. <https://doi.org/10.1002/bit.260320112>.
- Hagerty, S.B., Allison, S.D., Schimel, J.P., 2018. Evaluating soil microbial carbon use efficiency explicitly as a function of cellular processes: implications for measurements and models. *Biogeochemistry* 140, 269–283. <https://doi.org/10.1007/s10533-018-0489-z>.
- Hansen, L.D., Macfarlane, C., McKinnon, N., Smith, B.N., Criddle, R.S., 2004. Use of calorimetric ratios, heat per CO₂ and heat per O₂, to quantify metabolic paths and energetics of growing cells. *Thermochimica Acta* 422, 55–61. <https://doi.org/10.1016/j.tca.2004.05.033>.
- Herrmann, A.M., Bölscher, T., 2015. Simultaneous screening of microbial energetics and CO₂ respiration in soil samples from different ecosystems. *Soil Biology and Biochemistry* 83, 88–92. <https://doi.org/10.1016/j.soilbio.2015.01.020>.
- Ingraham, J.L., Maalae, O., Neidhardt, F.C., et al., 1983. *Growth of the Bacterial Cell*. Sinauer Associates Sunderland, MA.
- Kästner, M., Maskow, T., Miltner, A., Lorenz, M., Thiele-Bruhn, S., 2024. Assessing energy fluxes and carbon use in soil as controlled by microbial activity—a thermodynamic perspective a perspective paper. *Soil Biology and Biochemistry* 193, 109403. <https://doi.org/10.1016/j.soilbio.2024.109403>.
- Keilweit, M., Nico, P.S., Kleber, M., Fendorf, S., 2016. Are oxygen limitations under recognized regulators of organic carbon turnover in upland soils? *Biogeochemistry* 127, 157–171. <https://doi.org/10.1007/s10533-015-0180-6>.
- Kemp, R., 2000. “fire burn and cauldron bubble” (w. shakespeare): what the calorimetric–respirometric (cr) ratio does for our understanding of cells? *Thermochimica Acta* 355, 115–124. [https://doi.org/10.1016/S0040-6031\(00\)00442-1](https://doi.org/10.1016/S0040-6031(00)00442-1).
- Klemm, D., Heublein, B., Fink, H.P., Bohn, A., 2005. Cellulose: fascinating biopolymer and sustainable raw material. *Angewandte Chemie International Edition* 44, 3358–3393. <https://doi.org/10.1002/anie.200460587>.
- Kroschewski, B., Richter, C., Baumecker, M., Kautz, T., 2023. Effect of crop rotation and straw application in combination with mineral nitrogen fertilization on soil carbon sequestration in the thyrow long-term experiment thy.d5. *Plant and Soil* 488, 121–136. <https://doi.org/10.1007/s11104-022-05459-5>.
- Lacroix, E.M., Mendillo, J., Gomes, A., Dekas, A., Fendorf, S., 2022. Contributions of anoxic microsites to soil carbon protection across soil textures. *Geoderma* 425, 116050. <https://doi.org/10.1016/j.geoderma.2022.116050>.
- Lorenz, M., Blagodatskaya, E., Finn, D., Fricke, C., Hüging, H., Kandeler, E., Kaiser, K., Kästner, M., Lechtenfeld, O., Marhan, S., Maskow, T., Mayer, J., Miltner, A., Normant-Sarembe, M., Poll, C., Resseguier, C., Rupp, A., Schrupp, M., Schweitzer, K., Simon, C., Tebbe, C., Yang, S., Yousaf, U., Thiele-Bruhn, S., 2024a. Database for the Priority Program 2322 SoilSystems – Soils and Substrates Used in the First Phase (2021–2024). <https://doi.org/10.5281/zenodo.11207502>.
- Lorenz, M., Maskow, T., Thiele-Bruhn, S., 2024b. Energy stored in soil organic matter is influenced by litter quality and the degree of transformation—a combustion calorimetry study. *Geoderma* 443, 116846. <https://doi.org/10.1016/j.geoderma.2024.116846>.
- Manzoni, S., Čapek, P., Porada, P., Thurner, M., Winterdahl, M., Beer, C., Brüchert, V., Frouz, J., Herrmann, A.M., Lindahl, B.D., et al., 2018. Reviews and syntheses: carbon use efficiency from organisms to ecosystems—definitions, theories, and empirical evidence. *Biogeosciences* 15, 5929–5949. <https://doi.org/10.5194/bg-15-5929-2018>.
- Manzoni, S., Taylor, P., Richter, A., Porporato, A., Ågren, G.I., 2012. Environmental and stoichiometric controls on microbial carbon-use efficiency in soils. *New Phytologist* 196, 79–91. <https://doi.org/10.1111/j.1469-8137.2012.04225.x>.
- Marschmann, G.L., Pagel, H., Kügler, P., Streck, T., 2019. Equifinality, sloppiness, and emergent structures of mechanistic soil biogeochemical models. *Environmental Modelling & Software* 122, 104518. <https://doi.org/10.1016/j.envsoft.2019.104518>.
- Nest, T.V., Ruysschaert, G., Vandecasteele, B., Houot, S., Baken, S., Smolders, E., Coughon, M., Reheul, D., Merckx, R., 2016. The long term use of farmyard manure and compost: effects on p availability, orthophosphate sorption strength and p leaching. *Agriculture, Ecosystems & Environment* 216, 23–33. <https://doi.org/10.1016/j.agee.2015.09.009>.
- Newville, M., Otten, R., Nelson, A., Stensitzki, T., Ingargiola, A., Allan, D., Fox, A., Carter, F., Michał, Osborn, R., Pustakhod, D., Ineubaus, Weigand, S., Aristov, A., Glenn, Deil, C., ngunyo, Mark, Hansen, A.L.R., Pasquevich, G., Foks, L., Zobrist, N., Frost, O., Stuermer, azed, Pollreno, A., Persaud, A., Nielsen, J.H., Pompili, M., Eendebak, P., 2023. Lmfit/Lmfit-Py: 1.2.2. <https://doi.org/10.5281/zenodo.8145703>.
- Öquist, M.G., Erhagen, B., Haei, M., Sparrman, T., Ilstedt, U., Schleucher, J., Nilsson, M. B., 2017. The effect of temperature and substrate quality on the carbon use efficiency of saprotrophic decomposition. *Plant and Soil* 414, 113–125. <https://doi.org/10.1007/s11104-016-3104-x>.
- Panikov, N., 1996. Mechanistic mathematical models of microbial growth in bioreactors and in natural soils: explanation of complex phenomena. *Mathematics and Computers in Simulation* 42, 179–186. [https://doi.org/10.1016/0378-4754\(95\)00127-1](https://doi.org/10.1016/0378-4754(95)00127-1).
- Perveen, N., Barot, S., Maire, V., Cotrufo, M.F., Shahzad, T., Blagodatskaya, E., Stewart, C.E., Ding, W., Siddiq, M.R., Dimassi, B., et al., 2019. Universality of priming effect: an analysis using thirty five soils with contrasted properties sampled from five continents. *Soil Biology and Biochemistry* 134, 162–171. <https://doi.org/10.1016/j.soilbio.2019.03.027>.
- Piepho, H., Büchse, A., Richter, C., 2004. A mixed modelling approach for randomized experiments with repeated measures. *Journal of Agronomy and Crop Science* 190, 230–247. <https://doi.org/10.1111/j.1439-037X.2004.00097.x>.
- Poll, C., Pagel, H., Devers-Lamrani, M., Martin-Laurent, F., Ingwersen, J., Streck, T., Kandeler, E., 2010. Regulation of bacterial and fungal mcpa degradation at the soil–litter interface. *Soil Biology and Biochemistry* 42, 1879–1887. <https://doi.org/10.1016/j.soilbio.2010.07.013>.
- Popovic, M., Woodfield, B.F., Hansen, L.D., 2019. Thermodynamics of hydrolysis of cellulose to glucose from 0 to 100°C: cellular biofuel applications and climate change implications. *The Journal of Chemical Thermodynamics* 128, 244–250. <https://doi.org/10.1016/j.jct.2018.08.006>.
- Qiao, Y., Wang, J., Liang, G., Du, Z., Zhou, J., Zhu, C., Huang, K., Zhou, X., Luo, Y., Yan, L., et al., 2019. Global variation of soil microbial carbon-use efficiency in relation to growth temperature and substrate supply. *Scientific Reports* 9, 5621. <https://doi.org/10.1038/s41598-019-42145-6>.
- Saito, T., Kimura, S., Nishiyama, Y., Isogai, A., 2007. Cellulose nanofibers prepared by tempo-mediated oxidation of native cellulose. *Biomacromolecules* 8, 2485–2491. <https://doi.org/10.1021/bm0703970>.
- Sierra, C.A., Malghani, S., Müller, M., 2015. Model structure and parameter identification of soil organic matter models. *Soil Biology and Biochemistry* 90, 197–203. <https://doi.org/10.1016/j.soilbio.2015.08.012>.
- Sørensen, T.H., Cruys-Bagger, N., Borch, K., Westh, P., 2015. Free energy diagram for the heterogeneous enzymatic hydrolysis of glycosidic bonds in cellulose. *Journal of Biological Chemistry* 290, 22203–22211. <https://doi.org/10.1074/jbc.M115.659656>.
- Vance, E.D., Brookes, P.C., Jenkinson, D.S., 1987. An extraction method for measuring soil microbial biomass C. *Soil Biology and Biochemistry* 19, 703–707. [https://doi.org/10.1016/0038-0717\(87\)90052-6](https://doi.org/10.1016/0038-0717(87)90052-6).
- Virtanen, P., Gommers, R., Oliphant, T.E., Haberland, M., Reddy, T., Cournapeau, D., Burovski, E., Peterson, P., Weckesser, W., Bright, J., van der Walt, S.J., Brett, M., Wilson, J., Millman, K.J., Mayorov, N., Nelson, A.R.J., Jones, E., Kern, R., Larson, E., Carey, C.J., Polat, I., Feng, Y., Moore, E.W., VanderPlas, J., Laxalde, D., Perktold, J., Cimrman, R., Henriksen, I., Quintero, E.A., Harris, C.R., Archibald, A.M., Ribeiro, A. H., Pedregosa, F., van Mulbregt, P., SciPy 1.0 Contributors, 2020. SciPy 1.0: fundamental algorithms for scientific computing in Python. *Nature Methods* 17, 261–272. <https://doi.org/10.1038/s41592-019-0686-2>.
- Von Stockar, U., Liu, J.S., 1999. Does microbial life always feed on negative entropy? thermodynamic analysis of microbial growth. *Biochimica et Biophysica Acta (BBA) - Bioenergetics* 1412, 191–211. [https://doi.org/10.1016/S0005-2728\(99\)00065-1](https://doi.org/10.1016/S0005-2728(99)00065-1).
- Von Stockar, U., Maskow, T., Liu, J., Marison, I.W., Patino, R., 2006. Thermodynamics of microbial growth and metabolism: an analysis of the current situation. *Journal of Biotechnology* 121, 517–533. <https://doi.org/10.1016/j.biotech.2005.08.012>.
- Wang, C., Kuzyakov, Y., 2023. Energy use efficiency of soil microorganisms: driven by carbon recycling and reduction. *Global Change Biology* 29, 6170–6187. <https://doi.org/10.1111/gcb.16925>.
- Wieder, W.R., Allison, S.D., Davidson, E.A., Georgiou, K., Hararuk, O., He, Y., Hopkins, F., Luo, Y., Smith, M.J., Sulman, B., Todd-Brown, K., Wang, Y., Xia, J., Xu, X., 2015. Explicitly representing soil microbial processes in earth system models. *Global Biogeochemical Cycles* 29, 1782–1800. <https://doi.org/10.1002/2015GB005188>.
- Yang, S., Di Lodovico, E., Rupp, A., Harms, H., Fricke, C., Miltner, A., Kästner, M., Maskow, T., 2024. Enhancing insights: exploring the information content of calorimetric ratio in dynamic soil microbial growth processes through calorimetry. *Frontiers in Microbiology* 15, 1321059. <https://doi.org/10.3389/fmicb.2024.1321059>.

Chapter 4: Bioenergetics of microbial maintenance metabolism in soil

Publication:

Endress, M.-G., and Blagodatsky, S., *in prep.* Bioenergetics of microbial maintenance metabolism in soil.

Declaration of personal contributions:

I am the first author and designated corresponding author of this manuscript. S. Blagodatsky and I jointly conceived this study. I performed all modeling work and all quantitative analyses and took the lead in writing the manuscript. Specifically, I designed the dynamic model and performed all numerical simulations, and wrote the code required for these tasks. I compiled and analyzed experimental data from the literature and carried out all theoretical analyses. I prepared the first draft and the current version of the manuscript with input from S. Blagodatsky. I prepared all of the figures with input from S. Blagodatsky.

Data availability statement:

No original data was produced in this study. Data compiled from the literature is available from the respective cited references. The data compilation will be submitted for publication as supplementary material to the manuscript. All modeling code is available from the corresponding author upon reasonable request and will be made publicly available via deposition in a repository upon the first submission of the manuscript.

Bioenergetics of microbial maintenance metabolism in soil

Martin-Georg Endress¹, Sergey Blagodatsky^{1,2}

Affiliations:

¹ Institute of Zoology, University of Cologne, 50923 Cologne, Germany

² Institute of Meteorology and Climate Research, Department of Atmospheric Environmental Research (IMK-IFU), Karlsruhe Institute of Technology (KIT) – Campus Alpin, 82467, Garmisch-Partenkirchen, Germany

Corresponding Author(s): Martin-Georg Endress

Email: m.endress@uni-koeln.de

Acknowledgments:

This study was performed within the framework of the German Science Foundation (DFG) Priority Program "SPP 2223 – System ecology of soils – Energy Discharge Modulated by Microbiome and Boundary Conditions (SoilSystems)". The work was funded by the DFG under the grant 465124939.

Author contributions:

MGE: Formal analysis, Writing – original draft, Writing – review & editing, designed the modelling framework, SB: Writing – review & editing, conceived the study and designed the modelling framework.

Competing interest statement:

20 The authors declare no competing interests.

21 **Keywords:**

22 Calorespirometry; Carbon use efficiency; Energy use efficiency; Microbial-explicit modeling;
23 Maintenance

24 **Abstract:**

25 Soil microorganisms spend most of their time in an inactive state due to limited substrate
26 availability, yet microbial maintenance metabolism remains poorly characterized quantitatively
27 and inadequately represented in soil carbon cycle models. Calorespirometry, the simultaneous
28 measurement of heat and CO₂ release from soil, provides a powerful tool to investigate the
29 bioenergetics of microbial non-growth activity. In this study, we use dynamic modeling to assess
30 how different maintenance processes influence the relationship between the calorespirometric
31 ratio (CR) of heat to CO₂ release and microbial carbon use efficiency (CUE). We find that
32 maintenance metabolism reduces apparent CUE, while its effects on CR depend on the
33 substrates consumed to meet maintenance requirements. To explore the energetics of
34 maintenance empirically, we compile literature data on CR and soil organic matter (SOM)
35 energy content in unamended soils. In arable soils, this analysis uncovers a close linear
36 relationship between CR and SOM energy content, suggesting the utilization of high-energy
37 compounds when available. In contrast, we observe an inverse relationship in forest soils. Our
38 study demonstrates the value of bioenergetic models for generating testable hypotheses and
39 highlights research needs for the better characterization of microbial maintenance processes in
40 soil.

41

42

43 **Introduction:**

44 Soil organic matter (SOM) represents the largest reservoir of terrestrial organic carbon (C) and
45 plays an important role for the future of the global C cycle and climate change (Jobbágy and
46 Jackson, 2000; Batjes, 2016; Jackson et al., 2017). Although microbial biomass constitutes only
47 a small portion of this vast C pool, microbial activity is critical in determining the fate of SOM and
48 has become a focus of global change studies (Liang et al., 2017; Tao et al., 2023). Soil
49 microorganisms determine the balance between processes that produce and stabilize new
50 SOM, such as the formation of biomass, metabolic byproducts and necromass, and those that
51 decompose existing SOM, resulting in C losses to the atmosphere as CO₂ (Schimel and
52 Schaeffer, 2012; Lehmann and Kleber, 2015; Crowther et al., 2019).

53 In the context of the delicate balance between C gains and losses, microbial carbon use
54 efficiency (CUE) has emerged as a key concept (Geyer et al., 2016; Manzoni et al., 2018). CUE
55 is broadly defined as the fraction of C consumed by microbes that is converted into new
56 biomass during growth. This efficiency varies widely depending on environmental factors
57 (Manzoni et al., 2012; Frey et al., 2013; Sinsabaugh et al., 2016), the quality and availability of
58 substrates (Sinsabaugh et al., 2013; Blagodatskaya et al., 2014), and the composition of the
59 microbial community (Geyer et al., 2016; Maynard et al., 2017). Recent advances have
60 integrated this carbon-centered view in a bioenergetic framework that also considers microbial
61 energy use efficiency (EUE, Gunina and Kuzyakov, 2022; Wang and Kuzyakov, 2023; Kästner
62 et al., 2024). This approach builds on a thermodynamic understanding of microbial growth (von
63 Stockar and Liu, 1999; von Stockar et al., 2006; Heijnen and Kleerebezem, 2010) that
64 recognizes the fundamental links between the flows of matter and energy during metabolism as
65 well as its thermodynamic constraints (Calabrese et al., 2021). While this framework has been
66 successfully applied under highly controlled conditions, e.g., in biotechnology (von Stockar and
67 Marison, 1993), its application to the soil environment is still in an early stage (Herrmann and
68 Bölscher, 2015; Barros, 2021; Chakrawal et al., 2021; Kästner et al., 2024).

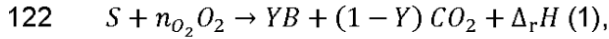
69 The simultaneous measurement of heat and CO₂ release from soil via calorimetry is a
 70 simple yet powerful method for investigating the coupling between C and energy during
 71 microbial growth in the complex soil system (Barros et al., 2011, 2016). A key metric derived
 72 from this approach is the calorimetric ratio (CR), which is defined as the ratio of heat to
 73 CO₂ released from the soil (Box 1, Fig. 1). It is closely linked to the efficiency and stoichiometry
 74 of microbial metabolism and can be used to estimate CUE and EUE in substrate amendment
 75 experiments (Hansen et al., 2004; Chakrawal et al., 2021; Yang et al., 2024) or to distinguish
 76 between aerobic and anaerobic metabolic pathways (Chakrawal et al., 2020; Endress et al.,
 77 2024a). Additionally, when combined with estimates of SOM energy content, the CR can
 78 provide insights into the quality and quantity of SOM mineralization. For example, it can reveal
 79 the activity of non-growing microorganisms in unamended soils (Barros et al., 2020; Lestido-
 80 Cardama et al., 2024) or the increased mineralization of SOM after the addition of labile C
 81 sources to soil, also known as the priming effect (Blagodatskaya and Kuzyakov, 2008;
 82 Chakrawal et al., 2020; Wirsching et al., 2024). Therefore, it offers a promising avenue to
 83 investigate SOM stability and the characteristics of microbial SOM consumption that ultimately
 84 drive soil C stock dynamics (Gunina and Kuzyakov, 2022; Kästner et al., 2024).
 85 Efforts to develop a process-based understanding of the CR have focused on simple growth
 86 reactions fueled by well-defined substrates or on the dynamics during the exponential growth
 87 phase after substrate amendment, when CO₂ and heat contributions from other processes are
 88 negligible (Hansen et al., 2004; Chakrawal et al., 2021; Endress et al., 2024a, 2024b). However,
 89 in most soils and for most of the time, microbial growth is limited by low substrate availability.
 90 Under these conditions, the majority of microbial cells are non-growing or persist in a dormant
 91 state, with periods of activity triggered by spatially and temporally constrained pulses of
 92 substrate supply (Blagodatsky et al., 2000; Blagodatskaya and Kuzyakov, 2013; Kuzyakov and
 93 Blagodatskaya, 2015). Given the extensive times of microbial dormancy and the overall volume
 94 of soils dominated by inactive microbes, maintenance metabolism and energetic costs

associated with transitions into and out of dormancy are likely to have a strong impact on soil C dynamics (Joergensen and Wichern, 2018; Dijkstra et al., 2022; Bölscher et al., 2024). Microbial maintenance processes, however, are defined ambiguously in the literature. They encompass diverse processes such as physiological maintenance (e.g., cell motility, osmoregulation, and internal turnover of macromolecules), the formation and consumption of storage compounds, and the secretion of extracellular polymeric substances (EPS) and extracellular enzymes (van Bodegom, 2007; Kempes et al., 2017). In this study, we differentiate between two types of maintenance metabolism: exogenous maintenance, fueled by the consumption of external substrates without a net change in biomass, and endogenous maintenance, fueled by the net consumption of microbial biomass (Box 1, Fig. 1). The ambiguity in defining microbial maintenance and activity is also reflected in mechanistic model representations (van Bodegom, 2007; Wang and Post, 2012), contributing to the considerable uncertainties associated with microbial C turnover in earth system models (Treseder et al., 2012; Wieder et al., 2013, 2015; Wang et al., 2015). While incorporating bioenergetic principles offers a promising way to alleviate these limitations, a systematic evaluation of non-growth processes within the CR framework is still lacking.

In this study, we employ a process-based modeling approach to examine the information contained in joint observations of heat and CO₂ release as obtained in soil incubation experiments. Our analysis focuses specifically on microbial processes beyond growth that have not been described in detail within the CR framework, such as exogenous and endogenous maintenance. We explore the quantitative implications of these maintenance processes for the theoretical relationship between CUE and CR. Finally, we compile and interpret CR values and SOM energy contents from unamended soils, providing experimental insights into the energetics of microbial non-growth metabolism and SOM mineralization.

Box 1: The calorespirometric ratio and microbial maintenance

120 In biochemical reactions, the flows of matter and energy are tightly coupled. For an aerobic
121 microbial growth reaction fueled by a substrate S ,



123 the CO_2 release per mol C of substrate is determined by the yield Y , which corresponds to the
124 stoichiometric coefficient of biomass B formation. Similarly, the heat produced per mol C of
125 substrate is given by the reaction enthalpy $\Delta_r H$,

126 $\Delta_r H = \left(1 - Y \frac{\gamma_B}{\gamma_S}\right) \Delta_c H_S$ (2)

127 which depends on the relative degrees of reduction of biomass γ_B and substrate γ_S as well as
128 the combustion enthalpy of the substrate $\Delta_c H_S$. Equation (2) results from the application of the
129 law of Hess to the growth reaction (1) (Chakrawal et al., 2020; Kästner et al., 2024). In this
130 simple scenario, the reaction will produce a calorespirometric ratio (CR) of heat to CO_2 given by

131 $CR = \frac{\Delta_r H}{(1 - Y)}$ (3)

132 which can be observed experimentally. However, if processes other than reaction (1) like
133 maintenance metabolism also produce heat and CO_2 , the observed CR will systematically
134 deviate from Eqn. (3). In this article, we consider two types of maintenance (Fig. 1):

- 135 (i) exogenous maintenance, in which an external substrate is catabolized to fuel energy
136 requirements and no biomass is consumed. The substrate may be identical to the
137 one fueling the growth reaction (1), or it may be a different chemical compound, e.g.,
138 SOM.
- 139 (ii) endogenous maintenance, in which internal compounds are consumed to meet
140 maintenance requirements and thus a net biomass decrease occurs. The consumed
141 biomass compounds may be identical to the average biomass, or it may be more
142 specific, such as a storage compound.

143 Note that both types of maintenance may also yield additional products other than CO₂ (e.g.,
144 necromass or metabolic byproducts). In any case, the CR of each individual reaction may be
145 estimated in a manner equivalent to equation (3) (A detailed derivation is presented in the
146 methods section).

147 **Results:**

148 **The joint dynamics of CO₂ and heat release following substrate addition grant insights**
149 **into processes beyond microbial growth.**

150 Plotting the cumulative heat produced by a soil sample over the course of an incubation
151 experiment against the cumulative CO₂ emissions offers a simple connection to the net C and
152 energy balance of the system (Fig. 2a). In such a plot, the observations trace out a trajectory
153 that begins at the origin when substrate is first added, moving upward and to the right as heat
154 and CO₂ are continuously released. When expressed as a percentage of the initial C and
155 energy added as substrate, the endpoint of the trajectory reflects the C and energy retained in
156 the soil system after the incubation. While this measure does not reveal anything about the
157 nature of the retained C (e.g., biomass, necromass, or residual substrate) or the origin of the
158 evolved CO₂ (e.g., substrate or SOM), it indicates the net storage or loss of C and energy due to
159 the substrate amendment. In our model simulations with and without a priming effect, the
160 additional release of C and energy per added substrate due to SOM decomposition is
161 immediately discernible (Fig. 2a, red and black lines).

162 The diagonal in this plot corresponds to the complete aerobic oxidation of the added substrate,
163 i.e., the catabolic reaction that fuels both growth and exogenous maintenance demands.
164 Deviations from this diagonal direction reveal C and energy flows resulting from biochemical
165 reactions other than growth or from physical processes (Fig. 2a). For instance, trajectories
166 curving to the right of the diagonal suggest processes that release less heat per CO₂ compared

to the aerobic catabolism of the substrate. Such processes might include the catabolism of more oxidized compounds (e.g., SOM), or a highly efficient growth reaction if the substrate is more oxidized than microbial biomass ($\gamma_S < \gamma_B$). Conversely, trajectories curving upward indicate processes with a higher relative heat release, such as catabolism or growth fueled by a more reduced compound. For example, the positive priming of highly reduced SOM causes such a deviation from the trajectory without priming in our example simulations (Fig. 2a).

Therefore, the trajectory records shifts in dominant processes and their cumulative contributions over the course of an experiment or a simulation. During exponential growth following the addition of a labile substrate, the trajectory is primarily driven by the microbial growth reaction, which accounts for most of the C and energy flow. However, deviations before and after this phase indicate contributions from other sources of heat and CO₂. These variations can be discerned in more detail through an analysis of the temporal dynamics of the CR (Fig. 2b).

When the CR is calculated from cumulative heat and CO₂ release (CR_{cumu}), its dynamics mirror the trajectories observed in the cumulative state space (compare the solid black and red lines Fig. 2a and 2b). By contrast, the CR calculated from the instantaneous rates of heat and CO₂ release (CR_{rate}) reflects the dominant processes producing heat and CO₂ at each specific time point. As a result, CR_{rate} is far more sensitive to changes in the dominant processes (dashed lines in Fig. 2b). Its value determines the direction of the trajectory at each time point in the cumulative plot, i.e., it corresponds to the tangent to the trajectory at that point.

In our simulations, CR_{rate} clearly reveals distinct phases dominated by other processes than the growth reaction. During the initial lag phase, there is a strong contribution from exogenous maintenance with a CR of 469 kJ mol⁻¹ C. Later, during the retardation phase as substrate becomes depleted, endogenous maintenance fueled by biomass consumption with a CR of ~490 kJ mol⁻¹ C dominates.

The precise quantitative values of the CR depend on the characteristics of the underlying processes, such as the energy contents of the compounds involved and the yield coefficients of the reactions. Notably, any fixed CR value can arise from multiple processes (Fig. 2c). For example, a CR of $300 \text{ kJ mol}^{-1} \text{ C}$ could result from the oxidation of a low-energy substrate with a degree of reduction (γ_S) of approximately 2.64 and no growth, i.e., a yield coefficient of 0. Alternatively, the same value might be produced by a growth reaction fueled by a more energy-rich, more reduced substrate with $\gamma_S = 3.42$ and a yield of 0.5. In fact, numerous such combinations of energy contents and yield coefficients can result in the same CR value (Fig. 2c). Consequently, the specific parameter combination responsible for an observed CR value in an experiment cannot be identified based solely on the CR, especially if the dominant substrate is unknown or its properties poorly characterized. Nonetheless, the observed value provides information about the set of feasible parameter combinations (e.g., lines in Fig. 2c) and can thus be combined with additional measurements, e.g., quantification of yield coefficients or energy contents of consumed substrates, to unravel the quantitative details of the process.

Maintenance metabolism alters the relationship between CUE and CR.

Both exogenous and endogenous maintenance reactions systematically alter the relationship between CUE and CR, depending on the energy content of the external (exogenous) or microbial (endogenous) compounds consumed in these reactions and their relative contributions to overall CO_2 and heat flow (Fig. 3). In a simple growth reaction, the apparent CUE equals the true growth yield (Y) of that reaction, defined as the stoichiometric coefficient of biomass formation. However, the inclusion of maintenance reactions reduces the apparent CUE below this value of Y . For exogenous maintenance, the CUE may decline to zero if all the C and energy are channeled through the maintenance reaction. In the case of endogenous maintenance, the apparent CUE can even become negative if the rate of biomass decomposition exceeds the gains from growth, resulting in a net loss of biomass.

The effect of maintenance on the CR is more complex and depends on the energy content of the maintenance substrate. When the same substrate fuels both growth and exogenous maintenance, the reaction enthalpy of the maintenance reaction equals the reaction enthalpy of substrate catabolism (under aerobic conditions, this is the combustion enthalpy of the substrate, i.e., $\Delta H_{exo} = \Delta_C H_S$, see Fig. 3). In this scenario, exogenous maintenance shifts the CR-CUE relationship along the original curve of the pure growth reaction, toward lower CUE values. However, if different substrates fuel growth and maintenance, the enthalpy of the maintenance reaction will differ from that of growth reaction's catabolic component, shifting the CR-CUE relationship both toward lower CUE values and toward a distinct ΔH_{exo} (not shown). Similarly, endogenous maintenance shifts the relationship toward lower CUE values and toward the enthalpy of the endogenous maintenance reaction consuming microbial biomass (i.e., ΔH_{endo}), which varies depending on the characteristics of biomass being consumed (e.g., bulk biomass or storage compounds).

During an incubation experiment or a simulation, estimates of CUE and CR trace out a trajectory on this plot (Fig. 3). For example, a model simulation incorporating a concentration-dependent transition from exogenous to endogenous maintenance again reveals distinct phases. In the initial lag phase, microbial growth is minimal, and the abundant substrate primarily fuels exogenous maintenance. During exponential growth, the trajectory converges toward the theoretical prediction for the growth reaction, as most C is allocated to biomass formation. Once the substrate is depleted, microbes switch to consuming their own biomass during the retardation phase, resulting in a net biomass loss. Consequently, the relationship between CUE and CR deviates most markedly from that of a pure growth reaction during the early and late stages of incubation, when the relative contributions of maintenance reactions to total C and energy flows are largest.

Unamended soils display a wide range of CR values and SOM energy contents.

We collected a total of 69 experimental CR values derived from heat and CO₂ measurements of unamended soils reported by seven studies (Barros et al., 2011, 2017, 2020; Herrmann and Bölscher, 2015; Barros, 2021; Lestido-Cardama et al., 2024; Wirsching et al., 2024) to investigate the bioenergetics of soil microorganisms in the absence of growth. These values were obtained from forest, grassland, and arable soils, with a strong bias towards Spanish forest soils. The average CR across the three land types was $393 \pm 154 \text{ kJ mol}^{-1} \text{ C}$ and there was no significant effect of land type, but observed values spanned a wide range from below 200 kJ mol⁻¹ C to more than 800 kJ mol⁻¹ C (Fig. 4a). While all measurements from arable and grassland soils were obtained from the top 5 cm of the mineral layer, some forest samples were also collected from organic horizons (LF, H) and the 5-10 cm mineral layer. Across the forest soils, CR values obtained from the organic layers ($445 \pm 86 \text{ kJ mol}^{-1} \text{ C}$) were significantly higher than those obtained from the mineral layer ($336 \pm 140 \text{ kJ mol}^{-1} \text{ C}$).

In addition, three of the studies also provided a measure of SOM energy content ($\Delta_C H_{\text{SOM}}$) in a total of 47 soils via thermal analysis. The average $\Delta_C H_{\text{SOM}}$ across all samples was $466 \pm 49 \text{ kJ mol}^{-1} \text{ C}$, with most values falling between 360 and 700 kJ mol⁻¹ C and no effect of land type. In forest soils, SOM energy content in the LF layer was significantly lower than in both mineral layers.

In those 47 soils for which both CR and $\Delta_C H_{\text{SOM}}$ estimates are available, we find a strong impact of land type on the correlation between the two quantities (Fig. 4b). In the eight arable soils, the CR of unamended samples and the energy content of SOM follow a close linear relationship with a slope that is indistinguishable from one (0.94, CI [0.76, 1.13]) and a slight offset of -80 kJ mol⁻¹ C (CI [-179, 18]). In contrast, we observe an inverse relationship with a negative slope in the forest data, although this relationship is not significant ($n = 38$, $p = 0.176$). It can be primarily attributed to samples from the LF layer, and the slope is less negative if the data is restricted to the mineral layers of the forest soils ($n = 21$, $p = 0.51$).

Discussion:

Our results highlight the strengths and the limitations of the joint analysis of C and energy flows in soils via calorimetry. The trajectory of cumulative heat and CO₂ emissions provides a succinct overview of the coupled net C and energy balances during incubations (Fig. 2a), and the sensitive CR_{rate} can reveal changes in microbial metabolism and substrate use over time (Fig. 2b, Endress 2024a, Wirsching 2024). When combined, these cumulative and rate-based assessments disclose both which processes contributed most to the total C and energy flux and which processes dominated at different times. The connection between the CR and the efficiency of microbial growth in particular has long been recognized (Hansen et al., 2004) and it has been extended to metabolic pathways other than aerobic growth (Chakrawal et al., 2020). However, the direct correspondence between CR and CUE only pertains to pure growth reactions on well-characterized substrates. Therefore, it is only applicable if other sources of CO₂ and heat are negligible, and our results corroborate the idea that this is only justified during the exponential growth phase following amendment with labile substrates (Fig. 2, 3) (Hansen et al., 2004; Barros et al., 2016; Wirsching et al., 2024). Beyond this special case, the interpretation of measured CR values requires a quantitative framework with specific assumptions about dominant processes, including maintenance metabolism. Such a process-based approach faces two main challenges. First, the CR integrates the heat and CO₂ release of many chemical and physical sources into a single metric, and these individual process contributions must be disentangled to obtain a correct interpretation of the CRs numerical value (Barros et al., 2016). This quantification can be achieved via targeted measurements of variables that complement the information contained in the CR. These may include microbial biomass to obtain independent estimates of growth yield and turnover, ¹³C labeling to detect the priming of SOM (Kästner et al., 2024; Wirsching et al., 2024), or O₂ consumption and anaerobic soil volume to quantify anaerobic contributions (Endress et al., 2024b; Schlüter et al., 2024).

Second, many processes may produce a wide range of CR values depending on quantitative details such as the involved energy contents or stoichiometry, and thus cannot be associated with a fixed CR value *a priori* (Fig. 2c). To address this challenge, the detailed properties of dominant processes need to be quantified. For example, this may include the estimation of yield coefficients from the formation of products, such as biomass, storage compounds (Mason-Jones et al., 2023) or fermentation and anaerobic respiration products (Zheng et al., 2024), the composition and energy content of SOM (Kästner et al., 2024), biomass and necromass (Chakrawal et al., 2022; Camenzind et al., 2023), or the activity of specific enzymes.

In fact, the potential of the CR to suggest such targeted measurements represents much of its utility. When interpreted using a quantitative modeling framework, the CR enables the identification of plausible process combinations underlying the observations, thereby generating falsifiable hypotheses. This process relies on quantitatively accurate CR measurements due to the sensitivity of the CR that results from its definition as a quotient, and the improvement of experimental setups to achieve the required accuracy is an ongoing endeavor (Barros et al., 2011; Endress et al., 2024b; Fricke et al., 2024; Yang et al., 2024). The quantitative analysis also presents special opportunities and challenges from a modeling point of view. Biogeochemical models of soil C cycling are frequently characterized by substantial equifinality, resulting in parameters that are poorly identifiable (Marschmann et al., 2019). Heat measurements provide an additional variable for calibration and validation (Chakrawal et al., 2021), and thermodynamic considerations can help to constrain certain parameters such as yield coefficients and growth rates (Desmond-Le Quéméner and Bouchez, 2014; Trapp et al., 2018; Zheng et al., 2024). Nonetheless, the wide range of parameter values that yield similar CR values complicate the inference process (Fig. 2c). While this issue can to some extent be alleviated by the measurement of key variables as suggested above, parameter values calibrated primarily using calorimetric data are likely to be poorly constrained and must be

interpreted with caution (a more detailed exploration of equifinality is presented in the methods section).

Our theoretical examination of exogenous and endogenous maintenance illustrates how the complexity of microbial metabolism may cause deviations from predictions that are generated based on the thermodynamics of simple growth reactions (Fig. 3). Such deviations offer an opportunity to tackle some of the ambiguity of non-growth processes in soil, both experimentally and in mechanistic models. The need to assign energy flows (i.e., heat release) in addition to the various carbon flows that are typically used to describe maintenance (van Bodegom, 2007; Wang and Post, 2012) forces us to clarify the biochemical details of these processes, or at least to make specific assumptions about them. For example, our results can be used to generate testable predictions regarding the expected temporal patterns of the CR and CUE in the presence of maintenance (Fig. 2, 3), depending on the added substrate (i.e., ΔH_{exo}) and the presumed mode of endogenous maintenance (e.g., bulk biomass consumption with $\Delta H_{endo} \approx 490 \text{ kJ mol}^{-1} \text{ C}$, see Fig. 2b). While only a limited number of studies have evaluated CUE and CR dynamically and with sufficient accuracy so far, the few existing results display a wide range of temporal patterns that warrant further investigation (Barros et al., 2010; Endress et al., 2024a, 2024b; Wirsching et al., 2024; Yang et al., 2024). From a modeling perspective, more explicit representations of microbial biomass and non-growth processes may be leveraged to derive mechanistic predictions, for example based on the formation and consumption of storage compounds (Manzoni et al., 2021), variable C:N ratios (Chakrawal et al., 2022) or other distinct biomass pools as in dynamic energy budget models (e.g., Marschmann et al., 2024).

The wide range of CR values in unamended soils revealed by our literature compilation highlights the need for a broad exploration of the bioenergetics of non-growth metabolism in soil. While the compilation covers only a limited number of soils (and even fewer research groups) with a bias towards forest soils, the results span much of the range of physiologically

plausible CR values. This high variability likely reflects the vast chemical diversity of SOM and its bioavailable fractions as well as the metabolic capabilities of communities in natural (unamended) soils (Ahamed et al., 2023; Zheng et al., 2024). In such systems with negligible growth, the CR may reflect (i) the net consumption of SOM without significant decline in biomass (exogenous maintenance) or (ii) the net consumption of biomass or specific biomass components like storage compounds (endogenous maintenance). While the CR alone cannot disclose which of these is prominent (see methods for details), it nonetheless provides insights into the balance of C and energy limitation of microorganisms when little substrate is available. For example, we found a striking linear correspondence between the CR and the energy content of SOM in arable soils (Fig. 4b). This finding suggests that microbes utilize SOM with an energy content similar to that of the average SOM in these soils. Specifically, microbes appear to utilize more energy rich compounds for maintenance if available, instead of a strong preference for, e.g., more easily decomposable but energy poor SOM (Gunina and Kuzyakov, 2022; Wang and Kuzyakov, 2023). This is opposite to the pattern found in forest soils, where microbes metabolized compounds of higher energy if the average energy content of SOM was low, particularly in the LF layers. We speculate that the high availability of organic C in the LF layer may be the primary cause this pattern, allowing microbes to selectively use substrates with high energy. In contrast, microbes utilized low energy substrates in the mineral layers of forest soils despite higher average SOM energy content, indicating a preference for easily decomposable compounds and selective stabilization of energy-rich reduced substances (Keiluweit et al., 2017; Kästner et al., 2024). More studies measuring the CR of unamended soils, especially of arable and grassland soils, are required to corroborate and extend these findings. Finally, while such CR values cannot be directly used to explain those obtained during the lag or retardation phases after substrate amendments, a comparison between the two offers another promising next step to illuminate the bioenergetics of non-growth processes in soils.

366 Materials and methods:

367 Growth and non-growth reactions and their energetics

368 The derivation of the microbial growth reaction (Eqn. 1) and its energetics (Eqn. 2 and 3) has
369 been presented in detail before (Chakrawal et al., 2020; Endress et al., 2024a). In brief, we
370 consider an aerobic catabolic reaction fueled by external substrate S ,



372 expressed for the consumption of one mol C of S , with a catabolic reaction enthalpy $\Delta_{cat} H_S$
373 equal to the combustion enthalpy $\Delta_c H_S$ of the substrate. If $\Delta_c H_S$ is unknown, it may be estimated
374 using Thornton's rule (Thornton, 1917) via the relative degree of reduction γ_S of the substrate:

$$375 \quad \Delta_c H_S = \frac{\gamma_S}{4} \cdot 455 \pm 15 \text{ kJ mol}^{-1} \text{ C}$$

376 where

$$377 \quad \gamma_S = \frac{4n_C + n_H - 2n_O - 3n_N}{n_C} \text{ (Eqn. 4)}$$

378 is calculated using the number n_X of atoms of element X in the compound. This formulation
379 assumes that CO_2 , NH_3 and H_2O are the reference compounds with zero degree of reduction
380 (Chakrawal et al., 2020; Kästner et al., 2024). Note that Eqn. 4 can also be used to estimate the
381 reaction enthalpy of an aerobic endogenous maintenance reaction converting biomass to CO_2 .
382 In the case of anaerobic catabolic reactions, the reaction enthalpy has to be estimated from the
383 enthalpies of formation of the involved compounds using the law of Hess or obtained from the
384 literature (for examples, see Chakrawal et al., 2020; Endress et al., 2024a; Kästner et al., 2024).

385 For the anabolic reaction, we use the electron balance approach for the formation of one mol C
386 of biomass B (Battley, 2009):

$$\frac{Y_B}{Y_S} S \rightarrow B + \left(\frac{Y_B}{Y_S} - 1 \right) CO_2 + \Delta_r H_{ana}$$

which yields $\Delta_r H_{ana} = 0$ based on Thornton's rule. To obtain the overall growth reaction expressed per mol C of substrate consumed and with a fixed yield coefficient Y , the catabolic and anabolic reactions are multiplied by $\left(1 - Y \frac{Y_B}{Y_S} \right)$ and Y , respectively. Their sum then yields Eqn. 1, and the sum of their reaction enthalpies yields the heat production per mol of C consumed (Eqn. 2). Note that this approach can also be used to estimate the reaction enthalpy of other processes, such as the formation of necromass from biomass during turnover (see also below). In this case, biomass serves as a substrate for the formation of necromass and CO_2 , and the reaction enthalpy depends on their relative degrees of reduction as well as the (necromass) yield coefficient of the process according to Eqn. 2.

Finally, the CR value associated with any individual reaction is obtained as the ratio of its reaction enthalpy to its stoichiometric coefficient of CO_2 production (Eqn. 3). If several processes $i = 1, 2, \dots$ occur simultaneously, the overall CR is given by the ratio of the sum of all reaction enthalpies $\Delta_r H_i$ to that of all coefficients of CO_2 production $n_{CO_2,i}$, each weighted by the respective reaction rate r_i :

$$CR = \frac{\sum_i \Delta_r H_i \cdot r_i}{\sum_i n_{CO_2,i} \cdot r_i} \text{ (Eqn. 5)}$$

Dynamic modeling

A wide variety of systems of ordinary differential equations (ODEs) can be constructed based on the flows of C and energy outlined above to explore, e.g., the effects of maintenance processes, microbial dormancy or SOM utilization and their interactions (Chakrawal et al., 2020, 2021;

Endress et al., 2024b, 2024a; Wirsching et al., 2024). A simple ODE system to simulate a typical soil incubation experiment with substrate amendment is given by

$$\begin{aligned}
 \frac{dS}{dt} &= -G - M_{exo} \\
 \frac{dB}{dt} &= YG - M_{endo} \\
 \frac{dCO_2}{dt} &= (1 - Y)G + M_{exo} + M_{endo} \\
 \frac{dQ}{dt} &= \Delta_r H_G G + \Delta_{cat} H_S M_{exo} + \Delta_r H_{endo} M_{endo}
 \end{aligned}
 \tag{Eqn. 6}$$

where B and S denote the concentrations of biomass and added substrate, respectively, and CO_2 and Q denote the CO_2 and heat released by microbial metabolism, which may be measured via calorimetry. The flux G represents the microbial growth reaction and takes the form $G = v\phi B$, where v denotes the maximum specific growth rate and $\phi = \phi(S) \in [0,1]$ represents the effect of substrate saturation/availability on growth (for example, $\phi(S) = \frac{S}{K+S}$ yields typical Michaelis-Menten or Monod kinetics). Similarly, the flux M_{exo} represents exogenous maintenance utilizing the same added substrate S and can thus be written as $M_{exo} = m_{exo}\phi B$ with a specific exogenous maintenance rate m_{exo} . Finally, $M_{endo} = m_{endo}B$ represents endogenous maintenance with specific rate m_{endo} . Note that this simple formulation assumes CO_2 as the only product of maintenance fluxes. For all reactions, the reaction enthalpies are calculated as outlined above, and the corresponding rates of heat release are given by the product of these reaction enthalpies and the reaction rates (Eqn. 5).

The simulations shown in Fig. 2 and 3 were obtained using a model that also considers the activity state of the microbial population via the index of physiological state $r \in [0,1]$, which denotes the active fraction of biomass (Panikov, 1995; Blagodatsky et al., 1998; Endress et al., 2024b). The dynamics of r are described by

434
 435 $\frac{dr}{dt} = Yvr \left(\frac{S}{S+K_r} - r \right)$ (Eqn. 7)
 436 with half-saturation constant K_r , such that microbes become active in the presence of sufficient
 437 substrate S and turn inactive as substrate gets depleted. Since only the active fraction performs
 438 the growth reaction, the corresponding flux G of the extended model reads $G = v\phi B \cdot r$. In
 439 addition, the model considers a dynamic switching from exogenous to endogenous
 440 maintenance as substrate availability becomes insufficient to fuel maintenance requirements
 441 (Wang and Post, 2012). Therefore, we set $M_{endo} = (1 - \phi)m_{exo}B$ for a total maintenance rate of
 442 $m_{exo}B$ independent of substrate concentration.

443 For simplicity of notation and conceptual analysis, we assume that the specific maintenance
 444 coefficients are the same for the active and inactive biomass fractions, but differences between
 445 active and inactive maintenance requirements can easily be incorporated via additional
 446 parameters (Endress et al., 2024b) to reflect the lower energy demand of inactive cells (Dijkstra
 447 et al., 2022).

448 A summary of all model variables and parameters including values and units is provided in
 449 Table 1. Parameter values were chosen to represent typical dynamics after glucose addition as
 450 obtained via calibration, e.g., in (Chakrawal et al., 2021; Endress et al., 2024a, 2024b).
 451 Simulations were performed in Python (version 3.9.18) using numerical integration of the ODE
 452 system via the *radau* method of the *solve_ivp* function in the *scipy.optimize* package (version
 453 1.11.4, Virtanen et al., 2020).

454 Theoretical relationship between CR and CUE in the presence of maintenance

455 The theoretical relationship between the CR and CUE for simple growth reactions is given by
 456 Eqn. 3 and has been examined in detail before (Hansen et al., 2004; Chakrawal et al., 2020;
 457 Yang et al., 2024). To derive the relationship in the presence of maintenance, it is helpful to
 458 introduce an auxiliary variable θ denoting the fraction of the total consumed carbon that is

459 partitioned to the growth reaction. For the case of exclusively exogenous maintenance fueled by
 460 the same substrate as growth, this fraction

$$461 \quad \theta = \frac{G}{G + M_{exo}} = \frac{v}{v + m_{exo}}$$

462 is constant. To calculate the true CUE at each point in time, we divide the net change in
 463 biomass by the amount of total consumed C to get

$$464 \quad CUE = \frac{\frac{dB}{dt}}{\frac{dS}{dt}} = \theta Y \text{ (Eqn. 8)}$$

465 Similarly,

$$466 \quad CR = \frac{\frac{dQ}{dt}}{\frac{dCO_2}{dt}} = \frac{\Delta_r H_G G + \Delta_{cat} H_S M_{exo}}{(1-Y)G + M_{exo}} = \frac{\left(1 - Y \frac{Y_B}{Y_S}\right) \Delta_{cat} H_S v + \Delta_{cat} H_S m_{exo}}{(1-Y)v + m_{exo}} = \frac{\left(1 - \theta Y \frac{Y_B}{Y_S}\right) \Delta_{cat} H_S}{1 - \theta Y} \text{ (Eqn. 9)}$$

467 so that the relationship between CUE and CR is equivalent to that of a pure growth reaction with
 468 a reduced yield coefficient $\theta Y \leq Y$. Therefore, the presence of exogenous maintenance does
 469 not cause deviations from the blue curve in Fig. 3, but merely results in shifts along this curve.

470 In the case of simultaneous growth and endogenous maintenance, the fraction

$$471 \quad \theta = \frac{G}{G + M_{endo}} = \frac{v\phi}{v\phi + m_{endo}}$$

472 is not constant, but instead attains a maximum of $\frac{v}{v + m_{endo}}$ under substrate saturation. This
 473 maximum will approach a value of 1 if the maximum growth rate far exceeds the maintenance
 474 rate (i.e., $v \gg m_{endo}$). Under such conditions, almost all carbon flow occurs through the growth
 475 reaction. As the substrate saturation ϕ declines over the course of an incubation, θ decreases

476 towards its minimum value of 0, indicating that all carbon flow is due to endogenous
477 maintenance.

478 For CUE, we have

479
$$CUE = \frac{Yv\phi - m}{v\phi + m}$$

480 which simplifies to

481
$$CUE = (1 + Y)\theta - 1$$

482 Thus, CUE varies between the value of the yield coefficient Y if all consumed carbon is derived
483 from substrate and fuels the growth reaction (i.e., $\theta = 1$) and the value of -1 if all consumed
484 carbon is derived from biomass and fuels endogenous maintenance (i.e., $\theta = 0$).

485 For CR, we obtain

486
$$CR = \frac{v\phi\Delta_rH_G + m\Delta_rH_{endo}}{(1 - Y)v\phi + m}$$

487 which simplifies to

488
$$CR = \frac{\theta \cdot \Delta_rH_G + (1 - \theta)\Delta_rH_{endo}}{1 - \theta Y}$$

489 Therefore, the system yields a CR value equal to that of the growth reaction if endogenous
490 maintenance is negligible and a value equal to that of the endogenous maintenance reaction if
491 growth is negligible. Varying θ from 0 to 1 yields the black curve in Fig. 3. Note that in Fig. 3, we
492 chose a low value of $\Delta_rH_{endo} = 220 \text{ kJ mol}^{-1} \text{ C}$ for visualization purposes. The true value of
493 Δ_rH_{endo} will depend on the composition and thus the energy content of the biomass being
494 consumed. For example, the aerobic decomposition of bulk biomass with an average degree of

495 reduction of $\gamma_B \approx 4.284$ (Yang et al., 2024) yields $\Delta_r H_{endo} \approx 487 \text{ kJ mol}^{-1} \text{ C}$ according to
 496 Thornton's rule (Thornton, 1917).

497 **Equifinality in models with maintenance and turnover**

498 As highlighted by Eqns. 8 and 9, the incorporation of exogenous maintenance as a direct matter
 499 and energy flux from added substrate to CO_2 and heat results in no qualitative change in model
 500 CUE and CR. Given any parameterization (v, m_{exo}, Y) of the ODE system (Eqn. 6) an equivalent
 501 parameterization $(\tilde{v}, \tilde{m}_{exo}, \tilde{Y})$ yielding identical dynamics can be found for any value of \tilde{m}_{exo} :

$$502 \quad \tilde{v} = v + m_{exo} - \tilde{m}_{exo}$$

$$503 \quad \tilde{Y} = \frac{v}{\tilde{v}} Y$$

504 In particular, choosing $\tilde{m}_{exo} = 0$ yields a system with identical dynamics in all variables,
 505 including heat, but without any explicit exogenous maintenance flux. Notably, this is due to $\tilde{v} \cdot$
 506 $\tilde{Y} = v \cdot Y$, i.e., the two parameter sets yield the same maximum specific growth rate. For this
 507 reason, the dynamics remain identical if the physiological state r is also considered (Eqn. 7).

508 Similarly, equifinality and the associated parameter non-identifiability that is widespread in
 509 biogeochemical models (Sierra et al., 2015; Marschmann et al., 2019) can arise from
 510 simultaneous representations of endogenous maintenance and microbial turnover. For example,
 511 consider the system

$$512 \quad \frac{dS}{dt} = -G - M_{exo}$$

$$513 \quad \frac{dB}{dt} = YG - M_{endo} - D$$

$$514 \quad \frac{d\text{CO}_2}{dt} = (1 - Y)G + M_{exo} + (1 - Y_{endo})M_{endo} + (1 - Y_D)D$$

516

517

518

$$\frac{dQ}{dt} = \Delta_r H_G G + \Delta_{cat} H_S M_{exo} + \Delta_r H_{endo} \dot{M}_{endo} + \Delta_r H_D D$$

519

$$\frac{dP}{dt} = Y_{endo} \dot{M}_{endo}$$

520

$$\frac{dN}{dt} = Y_D D$$

521

Here, endogenous maintenance yields additional products P with yield Y_{endo} besides CO_2 , such

522

as byproducts of the maintenance reactions, EPS compounds, and the like. In addition, biomass

523

is turned over to necromass N at a rate $D = dB$ with yield Y_D , while the remaining carbon is

524

released as CO_2 . In this system, the transformation of biomass into other products is governed

525

by the 4 parameters m_{endo} , Y_{endo} , d and Y_D . However, the parameter set

526

$$\tilde{m}_{endo}, \tilde{Y}_{endo}, \tilde{d}, \tilde{Y}_D$$

527

yields equivalent dynamics for

528

$$\tilde{Y}_{endo} = \frac{m_{endo}}{\tilde{m}_{endo}} Y_{endo}$$

529

$$\tilde{d} = m_{endo} + d - \tilde{m}_{endo}$$

530

$$\tilde{Y}_D = \frac{Y_D d + Y_{endo} m_{endo} - \tilde{Y}_{endo} \tilde{m}_{endo}}{\tilde{d}}$$

531

and any plausible value of \tilde{m}_{endo} . Specifically, the energy balance ensures that they also yield

532

the same total rate of heat release, since the rate of product formation is the same. Similarly,

533

the energy contents of the compounds P and N given by their respective degrees of reduction

534

γ_P and γ_N cannot be inferred from heat release, because

535

$$\Delta_r H_{endo} \dot{M}_{endo} + \Delta_r H_D D = \left(m_{endo} \left(1 - Y_{endo} \frac{\gamma_P}{\gamma_B} \right) + d \left(1 - Y_D \frac{\gamma_N}{\gamma_B} \right) \right) \Delta_c H_B \cdot B$$

536

$$= \left(m_{endo} \left(1 - Y_{endo} \frac{\tilde{\gamma}_P}{\gamma_B} \right) + d \left(1 - Y_D \frac{\gamma_N + \frac{Y_{endo} m_{endo}}{Y_D d} (\gamma_P - \tilde{\gamma}_P)}{\gamma_B} \right) \right) \Delta_c H_B \cdot B$$

for any plausible value of \tilde{y}_P . Note that these considerations also hold if $Y_{endo} = 0$, i.e., if endogenous maintenance only yields CO_2 . Overall, these simple examples illustrate that the rate and yield coefficients as well as the energy contents of products of several biomass-consuming processes, including endogenous maintenance and turnover, cannot be inferred from typical calorimetric and biomass data alone. Instead, they require additional targeted measurements or, in the case of modeling, specific assumptions about the involved compounds and processes.

To reduce these issues of parameter identifiability in the example system above, endogenous maintenance and death can be combined into a single equivalent process C with parameters

$$c = d + m_{endo}$$

$$Y_c = \frac{Y_D d + Y_{endo} m_{endo}}{c}$$

$$\gamma_c = \frac{Y_{endo} m_{endo} \cdot \gamma_P + Y_D d \cdot \gamma_N}{Y_{endo} m_{endo} + Y_D d}$$

which yields both CO_2 and a product compound of average energy content with degree of reduction γ_c . In principle, this approach can be applied to any number of processes that transform a single substrate (e.g., biomass) into many poorly characterized products (e.g., necromass, metabolic byproducts). The explicit representation of these individual processes is only meaningful if additional data is available for model calibration (e.g., the energy content of necromass).

Unamended soil data compilation

To study the bioenergetics of soil microbial maintenance, we compiled CR values measured in unamended soils from the literature. If available, we also analyzed measurements of average

SOM energy content determined via TG-DSC in those soils to study the connection between maintenance metabolism and SOM quality. Only soils classified as arable, grassland or forest soils were included in the analysis. We used the mean values reported in the studies for each soil, i.e., each value represents the mean of several replicates (typically 2 or 3). All values were converted to a unit of $\text{kJ mol}^{-1} \text{ C CO}_2$ or $\text{kJ mol}^{-1} \text{ C SOM}$ for CR and SOM energy content, respectively. The compiled data are provided as supporting material (S1 Data).

Statistics

To assess patterns in the compiled CR and average SOM energy content data as well as the relationship between the two, we used linear mixed models with additional fixed effects of land use type (arable, grassland, forest) and soil layer (0-5 cm, 5-10 cm, LF horizon, H horizon) as well as a random effect of site to account for measurements obtained from multiple plots within the same study area (see S1 Data). The analysis was performed using the *mixedlm* function of the *statsmodels* package (version 0.14.0, Seabold and Perktold, 2010) in Python (version 3.9.18).

573 **References:**

- 574 Ahamed, F., You, Y., Burgin, A., et al., 2023. Exploring the determinants of organic matter
575 bioavailability through substrate-explicit thermodynamic modeling. *Frontiers in Water* 5,
576 1169701. doi:10.3389/frwa.2023.1169701
- 577 Barros, N., 2021. Thermodynamics of Soil Microbial Metabolism: Applications and Functions.
578 *Applied Sciences* 11, 4962. doi:10.3390/app11114962
- 579 Barros, N., Feijóo, S., Hansen, L.D., 2011. Calorimetric determination of metabolic heat, CO₂
580 rates and the calorespirometric ratio of soil basal metabolism. *Geoderma* 160, 542–547.
581 doi:10.1016/j.geoderma.2010.11.002
- 582 Barros, N., Feijóo, S., Pérez-Cruzado, C., et al., 2017. Effect of soil storage at 4 °C on the
583 calorespirometric measurements of soil microbial metabolism. *AIMS Microbiology* 3,
584 762–773. doi:10.3934/microbiol.2017.4.762
- 585 Barros, N., Fernandez, I., Byrne, K.A., et al., 2020. Thermodynamics of soil organic matter
586 decomposition in semi-natural oak (*Quercus*) woodland in southwest Ireland. *Oikos*
587 129, 1632–1644. doi:10.1111/oik.07261
- 588 Barros, N., Hansen, L.D., Piñeiro, V., et al., 2016. Factors influencing the calorespirometric
589 ratios of soil microbial metabolism. *Soil Biology and Biochemistry* 92, 221–229.
590 doi:10.1016/j.soilbio.2015.10.007
- 591 Barros, N., Salgado, J., Rodríguez-Añón, J.A., et al., 2010. Calorimetric approach to metabolic
592 carbon conversion efficiency in soils: Comparison of experimental and theoretical
593 models. *Journal of Thermal Analysis and Calorimetry* 99, 771–777. doi:10.1007/s10973-
594 010-0673-4
- 595 Batjes, N.H., 2016. Harmonized soil property values for broad-scale modelling (WISE30sec)
596 with estimates of global soil carbon stocks. *Geoderma* 269, 61–68.
597 doi:10.1016/j.geoderma.2016.01.034
- 598 Battley, E.H., 2009. Is electron equivalence between substrate and product preferable to C-mol
599 equivalence in representations of microbial anabolism applicable to "origin of life"
600 environmental conditions?. *Journal of Theoretical Biology* 260, 267–275.
601 doi:10.1016/j.jtbi.2009.05.032
- 602 Blagodatskaya, E., Blagodatsky, S., Anderson, T.-H., Kuzyakov, Y., 2014. Microbial Growth and
603 Carbon Use Efficiency in the Rhizosphere and Root-Free Soil. *PLoS ONE* 9, e93282.
604 doi:10.1371/journal.pone.0093282
- 605 Blagodatskaya, E., Kuzyakov, Y., 2013. Active microorganisms in soil: Critical review of
606 estimation criteria and approaches. *Soil Biology and Biochemistry* 67, 192–211.
607 doi:10.1016/j.soilbio.2013.08.024
- 608 Blagodatskaya, E., Kuzyakov, Y., 2008. Mechanisms of real and apparent priming effects and
609 their dependence on soil microbial biomass and community structure: critical review.
610 *Biology and Fertility of Soils* 45, 115–131. doi:10.1007/s00374-008-0334-y
- 611 Blagodatsky, S.A., Heinemeyer, O., Richter, J., 2000. Estimating the active and total soil
612 microbial biomass by kinetic respiration analysis. *Biology and Fertility of Soils* 32, 73–81.
613 doi:10.1007/s003740000219
- 614 Blagodatsky, S.A., Yevdokimov, I.V., Larionova, A.A., Richter, J., 1998. Microbial growth in soil
615 and nitrogen turnover: Model calibration with laboratory data. *Soil Biology and*
616 *Biochemistry* 30, 1757–1764. doi:10.1016/S0038-0717(98)00029-7
- 617 Bölscher, T., Vogel, C., Olagoke, F.K., et al., 2024. Beyond growth: The significance of non-
618 growth anabolism for microbial carbon-use efficiency in the light of soil carbon
619 stabilisation. *Soil Biology and Biochemistry* 193, 109400.
620 doi:10.1016/j.soilbio.2024.109400

- Calabrese, S., Chakrawal, A., Manzoni, S., Van Cappellen, P., 2021. Energetic scaling in microbial growth. *Proceedings of the National Academy of Sciences* 118, e2107668118. doi:10.1073/pnas.2107668118
- Camenzind, T., Mason-Jones, K., Mansour, I., Rillig, M.C., Lehmann, J., 2023. Formation of necromass-derived soil organic carbon determined by microbial death pathways. *Nature Geoscience*. doi:10.1038/s41561-022-01100-3
- Chakrawal, A., Calabrese, S., Herrmann, A.M., Manzoni, S., 2022. Interacting Bioenergetic and Stoichiometric Controls on Microbial Growth. *Frontiers in Microbiology* 13, 859063. doi:10.3389/fmicb.2022.859063
- Chakrawal, A., Herrmann, A.M., Manzoni, S., 2021. Leveraging energy flows to quantify microbial traits in soils. *Soil Biology and Biochemistry* 155, 108169. doi:10.1016/j.soilbio.2021.108169
- Chakrawal, A., Herrmann, A.M., Šantrůčková, H., Manzoni, S., 2020. Quantifying microbial metabolism in soils using calorespirometry — A bioenergetics perspective. *Soil Biology and Biochemistry* 148, 107945. doi:10.1016/j.soilbio.2020.107945
- Crowther, T.W., Van Den Hoogen, J., Wan, J., et al., 2019. The global soil community and its influence on biogeochemistry. *Science* 365, eaav0550. doi:10.1126/science.aav0550
- Desmond-Le Quémener, E., Bouchez, T., 2014. A thermodynamic theory of microbial growth. *The ISME Journal* 8, 1747–1751. doi:10.1038/ismej.2014.7
- Dijkstra, P., Martinez, A., Thomas, S.C., et al., 2022. On maintenance and metabolisms in soil microbial communities. *Plant and Soil* 476, 385–396. doi:10.1007/s11104-022-05382-9
- Endress, M.-G., Chen, R., Blagodatskaya, E., Blagodatsky, S., 2024a. The coupling of carbon and energy fluxes reveals anaerobiosis in an aerobic soil incubation with a *Bacillota*-dominated community. *Soil Biology and Biochemistry* 195, 109478. doi:10.1016/j.soilbio.2024.109478
- Endress, M.-G., Dehghani, F., Blagodatsky, S., et al., 2024b. Spatial substrate heterogeneity limits microbial growth as revealed by the joint experimental quantification and modeling of carbon and heat fluxes. *Soil Biology and Biochemistry* 109509. doi:10.1016/j.soilbio.2024.109509
- Frey, S.D., Lee, J., Melillo, J.M., Six, J., 2013. The temperature response of soil microbial efficiency and its feedback to climate. *Nature Climate Change* 3, 395–398. doi:10.1038/nclimate1796
- Fricke, C., Lodovico, E.D., Meyer, M., Maskow, T., Schaumann, G.E., 2024. Design, calibration and testing of a novel isothermal calorespirometer prototype. *Thermochimica Acta* 738, 179785. doi:10.1016/j.tca.2024.179785
- Geyer, K.M., Kyker-Snowman, E., Grandy, A.S., Frey, S.D., 2016. Microbial carbon use efficiency: accounting for population, community, and ecosystem-scale controls over the fate of metabolized organic matter. *Biogeochemistry* 127, 173–188. doi:10.1007/s10533-016-0191-y
- Gunina, A., Kuzyakov, Y., 2022. From energy to (soil organic) matter. *Global Change Biology* 28, 2169–2182. doi:10.1111/gcb.16071
- Hansen, L.D., Macfarlane, C., McKinnon, N., Smith, B.N., Criddle, R.S., 2004. Use of calorespirometric ratios, heat per CO₂ and heat per O₂, to quantify metabolic paths and energetics of growing cells. *Thermochimica Acta* 422, 55–61. doi:10.1016/j.tca.2004.05.033
- Heijnen, J.J., Kleerebezem, R., 2010. Bioenergetics of Microbial Growth, in: *Encyclopedia of Industrial Biotechnology*. John Wiley & Sons, Inc., Hoboken, NJ, USA, p. eib084. doi:10.1002/9780470054581.eib084
- Herrmann, A.M., Bölscher, T., 2015. Simultaneous screening of microbial energetics and CO₂ respiration in soil samples from different ecosystems. *Soil Biology and Biochemistry* 83, 88–92. doi:10.1016/j.soilbio.2015.01.020

672 Jackson, R.B., Lajtha, K., Crow, S.E., et al., 2017. The Ecology of Soil Carbon: Pools,
673 Vulnerabilities, and Biotic and Abiotic Controls. *Annual Review of Ecology, Evolution,*
674 *and Systematics* 48, 419–445. doi:10.1146/annurev-ecolsys-112414-054234
675 Jobbágy, E.G., Jackson, R.B., 2000. THE VERTICAL DISTRIBUTION OF SOIL ORGANIC
676 CARBON AND ITS RELATION TO CLIMATE AND VEGETATION. *Ecological*
677 *Applications* 10.
678 Joergensen, R.G., Wichern, F., 2018. Alive and kicking: Why dormant soil microorganisms
679 matter. *Soil Biology and Biochemistry* 116, 419–430. doi:10.1016/j.soilbio.2017.10.022
680 Kästner, M., Maskow, T., Miltner, A., Lorenz, M., Thiele-Bruhn, S., 2024. Assessing energy
681 fluxes and carbon use in soil as controlled by microbial activity - A thermodynamic
682 perspective A perspective paper. *Soil Biology and Biochemistry* 193, 109403.
683 doi:10.1016/j.soilbio.2024.109403
684 Keiluweit, M., Wanzek, T., Kleber, M., Nico, P., Fendorf, S., 2017. Anaerobic microsites have an
685 unaccounted role in soil carbon stabilization. *Nature Communications* 8, 1771.
686 doi:10.1038/s41467-017-01406-6
687 Kempes, C.P., Van Bodegom, P.M., Wolpert, D., et al., 2017. Drivers of Bacterial Maintenance
688 and Minimal Energy Requirements. *Frontiers in Microbiology* 8.
689 doi:10.3389/fmicb.2017.00031
690 Kuzyakov, Y., Blagodatskaya, E., 2015. Microbial hotspots and hot moments in soil: Concept &
691 review. *Soil Biology and Biochemistry* 83, 184–199. doi:10.1016/j.soilbio.2015.01.025
692 Lehmann, J., Kleber, M., 2015. The contentious nature of soil organic matter. *Nature* 528, 60–
693 68. doi:10.1038/nature16069
694 Lestido-Cardama, Y., Barros Pena, N., Pérez-Cruzado, C., 2024. Sensitivity of thermal analysis
695 and calorimetry to assess the impact of forest management on soils. *Journal of Thermal*
696 *Analysis and Calorimetry*. doi:10.1007/s10973-024-13702-7
697 Liang, C., Schimel, J.P., Jastrow, J.D., 2017. The importance of anabolism in microbial control
698 over soil carbon storage. *Nature Microbiology* 2, 17105.
699 doi:10.1038/nmicrobiol.2017.105
700 Manzoni, S., Čapek, P., Porada, P., et al., 2018. Reviews and syntheses: Carbon use efficiency
701 from organisms to ecosystems – definitions, theories, and empirical evidence.
702 *Biogeosciences* 15, 5929–5949. doi:10.5194/bg-15-5929-2018
703 Manzoni, S., Ding, Y., Warren, C., et al., 2021. Intracellular Storage Reduces Stoichiometric
704 Imbalances in Soil Microbial Biomass – A Theoretical Exploration. *Frontiers in Ecology*
705 *and Evolution* 9, 714134. doi:10.3389/fevo.2021.714134
706 Manzoni, S., Taylor, P., Richter, A., Porporato, A., Ågren, G.I., 2012. Environmental and
707 stoichiometric controls on microbial carbon-use efficiency in soils. *New Phytologist* 196,
708 79–91.
709 Marschmann, G.L., Pagel, H., Kügler, P., Streck, T., 2019. Equifinality, sloppiness, and
710 emergent structures of mechanistic soil biogeochemical models. *Environmental*
711 *Modelling & Software* 122, 104518. doi:10.1016/j.envsoft.2019.104518
712 Marschmann, G.L., Tang, J., Zhalnina, K., et al., 2024. Predictions of rhizosphere microbiome
713 dynamics with a genome-informed and trait-based energy budget model. *Nature*
714 *Microbiology* 9, 421–433. doi:10.1038/s41564-023-01582-w
715 Mason-Jones, K., Breidenbach, A., Dyckmans, J., Banfield, C.C., Dippold, M.A., 2023.
716 Intracellular carbon storage by microorganisms is an overlooked pathway of biomass
717 growth. *Nature Communications* 14, 2240. doi:10.1038/s41467-023-37713-4
718 Maynard, D.S., Crowther, T.W., Bradford, M.A., 2017. Fungal interactions reduce carbon use
719 efficiency. *Ecology Letters* 20, 1034–1042. doi:10.1111/ele.12801
720 Panikov, N.S., 1995. *Microbial Growth Kinetics*. Chapman and Hall, London, Glasgow.
721 Schimel, J.P., Schaeffer, S.M., 2012. Microbial control over carbon cycling in soil. *Frontiers in*
722 *Microbiology* 3. doi:10.3389/fmicb.2012.00348

- Schlüter, S., Lucas, M., Grosz, B., et al., 2024. The anaerobic soil volume as a controlling factor of denitrification: a review. *Biology and Fertility of Soils*. doi:10.1007/s00374-024-01819-8
- Seabold, S., Perktold, J., 2010. statsmodels: Econometric and statistical modeling with python. 9th Python in Science Conference.
- Sierra, C.A., Malghani, S., Müller, M., 2015. Model structure and parameter identification of soil organic matter models. *Soil Biology and Biochemistry* 90, 197–203. doi:10.1016/j.soilbio.2015.08.012
- Sinsabaugh, R.L., Manzoni, S., Moorhead, D.L., Richter, A., 2013. Carbon use efficiency of microbial communities: stoichiometry, methodology and modelling. *Ecology Letters* 16, 930–939. doi:10.1111/ele.12113
- Sinsabaugh, R.L., Turner, B.L., Talbot, J.M., et al., 2016. Stoichiometry of microbial carbon use efficiency in soils. *Ecological Monographs* 86, 172–189. doi:10.1890/15-2110.1
- Tao, F., Huang, Y., Hungate, B.A., et al., 2023. Microbial carbon use efficiency promotes global soil carbon storage. *Nature* 618, 981–985. doi:10.1038/s41586-023-06042-3
- Thornton, W.M., 1917. XV. The relation of oxygen to the heat of combustion of organic compounds. *The London, Edinburgh, and Dublin Philosophical Magazine and Journal of Science* 33, 196–203. doi:10.1080/14786440208635627
- Trapp, S., Brock, A.L., Nowak, K., Kästner, M., 2018. Prediction of the Formation of Biogenic Nonextractable Residues during Degradation of Environmental Chemicals from Biomass Yields. *Environmental Science & Technology* 52, 663–672. doi:10.1021/acs.est.7b04275
- Treseder, K.K., Balser, T.C., Bradford, M.A., et al., 2012. Integrating microbial ecology into ecosystem models: challenges and priorities. *Biogeochemistry* 109, 7–18.
- van Bodegom, P., 2007. Microbial Maintenance: A Critical Review on Its Quantification. *Microbial Ecology* 53, 513–523. doi:10.1007/s00248-006-9049-5
- Virtanen, P., Gommers, R., Oliphant, T.E., et al., 2020. SciPy 1.0: Fundamental Algorithms for Scientific Computing in Python. *Nature Methods* 17, 261–272. doi:10.1038/s41592-019-0686-2
- von Stockar, U., Liu, J.-S., 1999. Does microbial life always feed on negative entropy? Thermodynamic analysis of microbial growth. *Biochimica et Biophysica Acta (BBA) - Bioenergetics* 1412, 191–211. doi:10.1016/S0005-2728(99)00065-1
- von Stockar, U., Marison, I.W., 1993. The definition of energetic growth efficiencies for aerobic and anaerobic microbial growth and their determination by calorimetry and by other means. *Thermochimica Acta* 229, 157–172. doi:10.1016/0040-6031(93)80323-3
- von Stockar, U., Maskow, T., Liu, J., Marison, I.W., Patiño, R., 2006. Thermodynamics of microbial growth and metabolism: An analysis of the current situation. *Journal of Biotechnology* 121, 517–533. doi:10.1016/j.jbiotec.2005.08.012
- Wang, C., Kuzyakov, Y., 2023. Energy use efficiency of soil microorganisms: Driven by carbon recycling and reduction. *Global Change Biology gcb*.16925. doi:10.1111/gcb.16925
- Wang, G., Jagadamma, S., Mayes, M.A., et al., 2015. Microbial dormancy improves development and experimental validation of ecosystem model. *The ISME Journal* 9, 226–237. doi:10.1038/ismej.2014.120
- Wang, G., Post, W.M., 2012. A theoretical reassessment of microbial maintenance and implications for microbial ecology modeling. *FEMS Microbiology Ecology* 81, 610–617. doi:10.1111/j.1574-6941.2012.01389.x
- Wieder, W.R., Allison, S.D., Davidson, E.A., et al., 2015. Explicitly representing soil microbial processes in Earth system models. *Global Biogeochemical Cycles* 29, 1782–1800. doi:10.1002/2015GB005188
- Wieder, W.R., Bonan, G.B., Allison, S.D., 2013. Global soil carbon projections are improved by modelling microbial processes. *Nature Climate Change* 3, 909–912. doi:10.1038/nclimate1951

774 Wirsching, J., Endress, M.-G., Di Lodovico, E., et al., 2024. Coupling energy balance and
775 carbon flux during cellulose degradation in arable soils. *Soil Biology and Biochemistry*
776 109691. doi:10.1016/j.soilbio.2024.109691
777 Yang, S., Di Lodovico, E., Rupp, A., et al., 2024. Enhancing insights: exploring the information
778 content of calorespirometric ratio in dynamic soil microbial growth processes through
779 calorimetry. *Frontiers in Microbiology* 15, 1321059. doi:10.3389/fmicb.2024.1321059
780 Zheng, J., Scheibe, T.D., Boye, K., Song, H.-S., 2024. Thermodynamic control on the
781 decomposition of organic matter across different electron acceptors. *Soil Biology and*
782 *Biochemistry* 193, 109364. doi:10.1016/j.soilbio.2024.109364

783

784 **Data availability statement:**

785 All data analyzed in this study is provided as supplementary material. All modeling code is
786 available at [FINAL REPO LINK].

787 **Supplementary material captions:**

788 **S1 Data.** Compiled data on the CR and average SOM energy content of unamended soils.

789

Figures and figure captions:

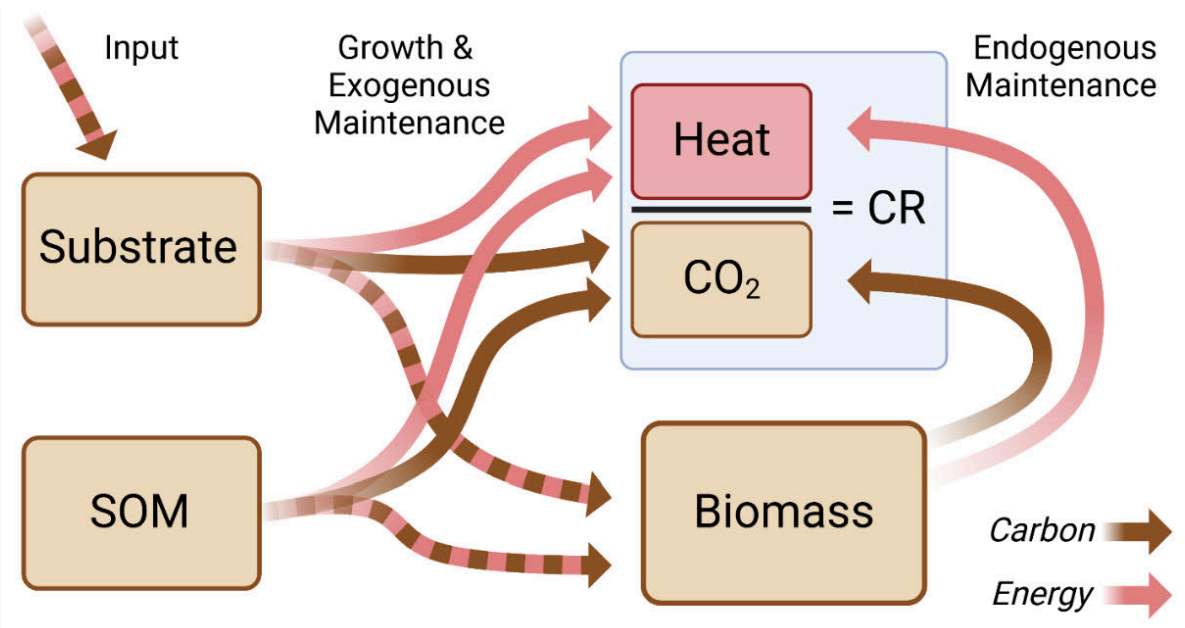


Fig. 1: Illustration of major C and energy fluxes in typical incubation experiments. Substrates added to soil as well as native SOM are utilized by microbes to fuel both their growth and maintenance requirements (here termed exogenous maintenance). Alternatively, microbes may consume their own biomass to sustain themselves if insufficient resources are available (here termed endogenous maintenance). In an aerobic setting, all these processes release heat and CO₂ at specific rates. Thus, their ratio (CR) can be leveraged to study the coupling between C and energy dynamics in the soil system over time.

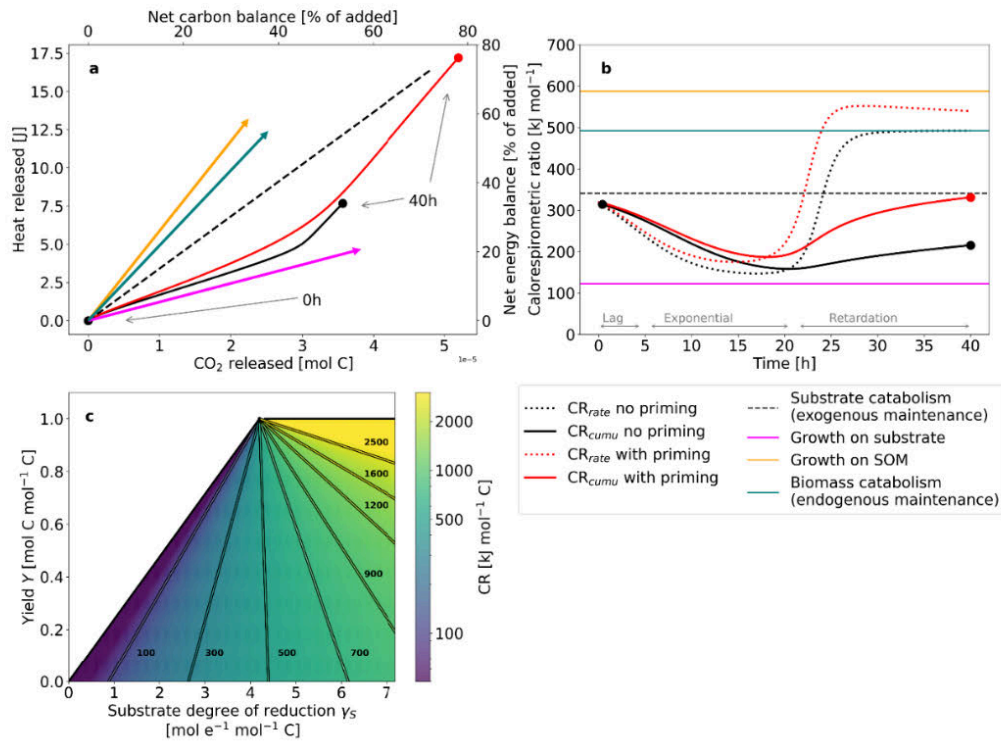
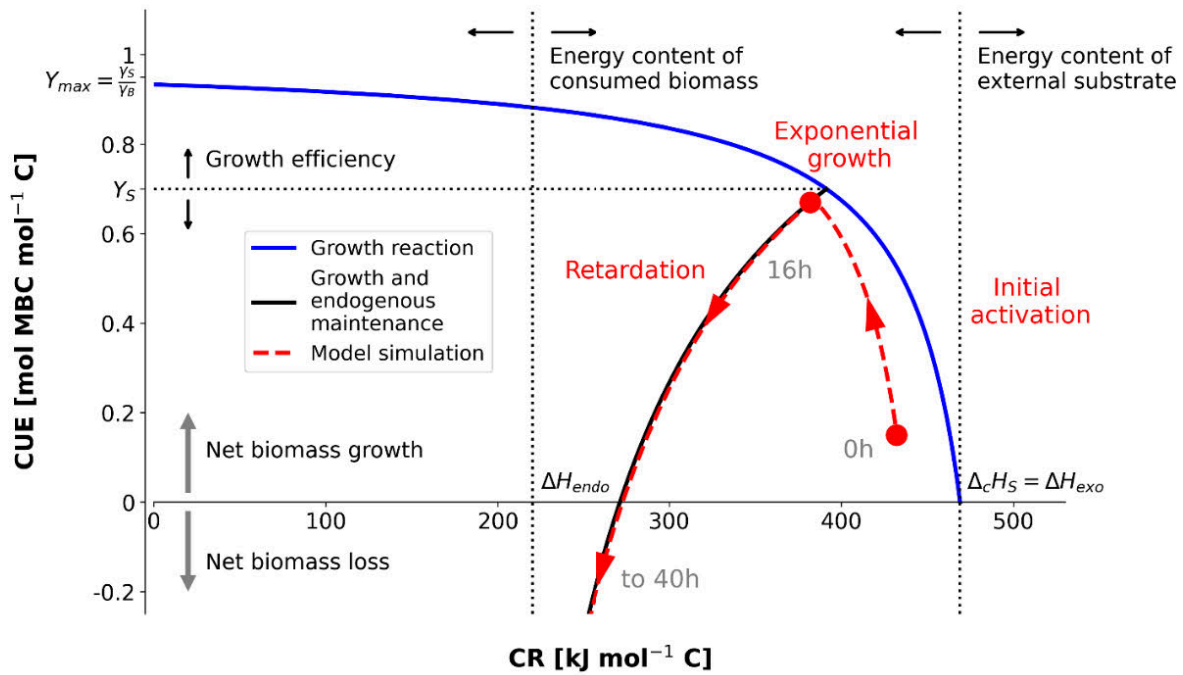


Fig. 2: Simulated patterns of heat and CO₂ release and CR after substrate addition with (black) and without (red) additional consumption of SOM (positive priming) **a** In a plot of cumulative heat release against cumulative CO₂ release, the diagonal corresponds to complete oxidation of the added substrate. Deviations reveal the presence of other processes, such as efficient aerobic growth fueled by added substrate (magenta), growth fueled by highly reduced SOM (orange), or biomass consumption for endogenous maintenance (teal). **b** The CR calculated from cumulative values (solid black and red) resembles the cumulative curves shown in panel a. In contrast, the CR calculated from the corresponding rates shows much more pronounced variations and reflects shifts in the dominant processes over time. **c** Identical CR values can result from different combinations of substrate energy content (measured as relative degree of reduction, γ_s) and growth yield (Y) in a simple growth reaction. Thus, the underlying process cannot be inferred from CR alone. The black line indicates the maximum theoretic yield based on simple thermodynamic considerations.

814 **Fig. 3**



815

816 **Fig. 3:** Theoretical and simulated relationship between CUE and CR in the presence of
817 endogenous and exogenous maintenance. The presence of endogenous maintenance modifies
818 the relation between CUE and CR predicted for the pure growth reaction on glucose (blue) in
819 the direction of lower apparent CUE (black). In a model simulation (dashed red), glucose initially
820 fuels microbial exogenous maintenance during the initial lag phase (with CR equal to $\Delta H_{exo} =$
821 $\Delta_c H_S$). During the subsequent phase of efficient exponential growth, most C is channeled
822 through the growth reaction. After substrate depletion, microbes switch to endogenous
823 maintenance (with a CR of ΔH_{endo}), resulting in an eventual decline of microbial biomass during
824 the retardation phase by the end of the incubation. Details are presented in the methods
825 section.

826

Fig. 4

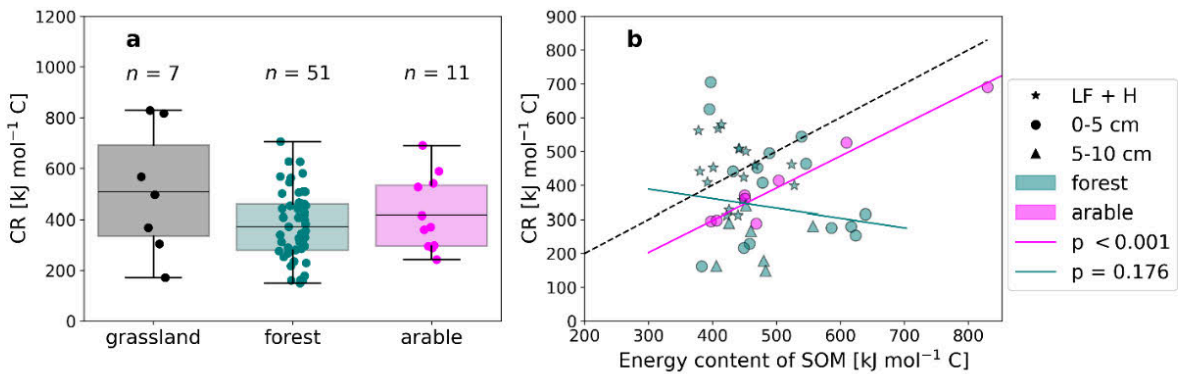


Fig. 4: Compilation of CR vales for unamended soils from the literature as well as their relation to SOM energy content. **a** Most available estimates of CR for unamended soils were obtained from forest soils. Each point represents a mean value of replicates reported by the respective study (total of 7 studies). There is no significant effect of land use on CR. **b** In those studies that also measured the average energy content of SOM via TG-DSC, both CR and energy content vary widely across soils, with no clear correlation. However, in the eight arable soils with available estimates, there is a close linear relationship between the two quantities, with CR values of $\sim 80 \text{ kJ mol}^{-1}$ lower than SOM energy content.

Discussion

The studies presented in this thesis investigated the temporal patterns of microbial C and energy use under a wide range of conditions and across several different experiments and models. In the following, I briefly summarize the results of each study and discuss the relevance, limitations and future implications of these findings relative to the objectives of this dissertation. In particular, I focus on aspects of (i) the CUE and EUE, (ii) the CR, (iii) the bioenergetics of complex processes such as selective SOM utilization and trophic interactions, and (iv) the process-based modeling of coupled C and energy fluxes.

Temporal variations in microbial carbon and energy use efficiency

The results of this thesis revealed how a diverse set of factors including O₂ and nutrient limitation, priming of SOM and maintenance metabolism can impact microbial CUE and EUE, and how these factors cause distinct temporal patterns over the course of typical soil incubation experiments after the addition of labile substrate.

Transitions from aerobic to anaerobic metabolism cause a drop in efficiency.

In Endress et al. (2024a), both experimental and model CUE estimated from observed biomass changes and cumulative CO₂ release followed a characteristic pattern of high efficiency during exponential growth and low efficiency during lag and retardation phases (Chapter 1, Fig. 5a). Using the dynamic model, we were able to identify two major underlying causes of this pattern. First, more carbon was channeled through catabolism to fuel maintenance requirements early and late during the incubation. Second, the transition from aerobic respiration to anaerobic fermentations around the time of maximum activity resulted in reduced efficiency due to the low biomass yield coefficients of fermentations (<0.3) compared to that of aerobic respiration (>0.6). In general, the thermodynamic basis of low microbial CUE under anoxic conditions is well understood, including its representation in mechanistic models (e.g., Boye et al., 2017; Bajracharya et al., 2022; Zheng et al., 2024). However, in our study, we were able to leverage this general understanding in a dynamic modeling framework to disentangle and quantify the factors governing the temporal CUE pattern over the course of a specific experiment.

Moreover, the findings demonstrated the gradual onset of anaerobiosis in a typical, initially aerobic, soil incubation characterized by a moderate moisture content. A possible interpretation involves the formation and expansion of anaerobic microsites in the soil due to the high O₂ demand of the growing microbial population. The importance of this mechanism for soil C cycling and stabilization has increasingly been recognized, even in well-drained soils (Keiluweit et al., 2016, 2017; Lacroix et al., 2022). A recent study also utilized pathway-specific gene abundance to identify increased lactic acid fermentation and glycolysis along with suppressed tricarboxylic acid cycle and pentose phosphate pathway activities as the cause of lowered CO₂ emissions in an alpine meadow (Wang et al., 2024). The combination of such an analysis with our bioenergetic approach offers a promising option to comprehensively describe microbial transitions between metabolic pathways and their consequences for C cycling. In particular, I highlight how the CR can be used to dynamically monitor shifts in dominant pathways in a subsequent section (Utility and limitations of the calorespirometric ratio).

Local nutrient limitation changes the kinetics, but not the efficiency of microbial growth.

In contrast, the results of Endress et al. (2024b) revealed no signs of anaerobic metabolism, and microbial growth was predominantly fueled by aerobic respiration of glucose. Remarkably, we also found no significant effect of nutrient limitation on the overall efficiency of the microbial population (Chapter 2, Fig. 4a). Instead, CUE and EUE attained high values in the range of 0.5 to 0.7 consistent with efficient aerobic growth in all treatments, and their relationship adhered closely to theoretical predictions. However, the kinetics of microbial growth were significantly different under nutrient limitation, with reduced and delayed rates of microbial activity (Chapter 2, Fig. 2). This is in line with similar experimental results (Shi et al., 2021; Inagaki et al., 2023) and recent theoretical advances on the interacting effects of substrate stoichiometry and bioenergetics (Chakrawal et al., 2022). In addition, modeled patterns of microbial activity were similar to those in Chapter 1 (compare Chapter 1, Fig. 5b and Supplementary Fig. S3c to Chapter 2), implying a comparable temporal pattern of CUE and EUE due to the effects of microbial maintenance. Intriguingly, the model predicted an overall smaller active fraction in spatially heterogeneous incubations, which is consistent with a reduced co-location of substrate and consumers (Pinheiro et al., 2015; Babey et al., 2017). Combined with the constant efficiency across

treatments, this implies that the growth of the soil microbes with sufficient exposure to glucose was enough to compensate for the fraction of microorganisms located outside of substrate hotspots, which remained inactive and only performed maintenance (Supplementary Fig. S3b to Chapter 2). In contrast, theory indicates that this averaging across heterogeneous conditions generally does not yield the same dynamics as observed in a homogeneous system (e.g., Chakrawal et al., 2020a), and the precise conditions under which such a comparison is or is not feasible in soil systems must be further investigated.

CUE estimates must account for the additional utilization of SOM due to priming.

The study of Wirsching et al. (2024) represents the most complex examination of temporal CUE and EUE patterns in this thesis (Chapter 3, Fig. 6). Specifically, we were able to disentangle the microbial utilization of added cellulose from that of native SOM through the use of ^{13}C -labeled substrate. This approach revealed a substantial positive priming effect of up to 30% of the added substrate in all studied soils (Chapter 3, Fig. 2, Fig. 3), consistent with reports in the literature (e.g., Blagodatskaya et al., 2014b; Perveen et al., 2019). Microbial cellulose utilization was efficient during the exponential growth phase with CUE values in the range of 0.4 to 0.5, slightly below those observed for glucose. The efficiency of microbial growth on primed SOM was even lower (<0.4 on average), as expected for these more complex compounds (Öquist et al., 2017; Manzoni et al., 2018; Ahamed et al., 2023). Overall, dynamic estimates of the C and energy balances were in close agreement and indicated a net increase of C and energy in all soils after one month, which was largely caused by a substantial amount of undecomposed residual cellulose in the soil (Chapter 3, Fig. 6). After accounting for the positive priming of SOM, this net storage of C was equivalent to roughly half the amount of added substrate, with very low mineralization rates by the end of the incubation (Chapter 3, Fig. 2). This highlights the fact that the fate of both added substrate and native SOM must be considered to obtain an accurate assessment of the net C gain or loss after substrate amendment (Dijkstra and Keitel, 2024).

Moreover, the temporal patterns of CUE of both cellulose and SOM utilization were qualitatively comparable to those observed in the first and second chapters (Supplementary Fig. S2 to Chapter 3), despite the fact that microbes grew on multiple substrates and growth occurred over a much longer time period (weeks compared to days) due to the slower microbial decomposition of cellulose. This highlights the broad applicability of our approach

and indicates that general biological constraints steer the dynamics in the soil in our study cases, as discussed below.

Changes in the active biomass fraction govern the overall dynamics of CUE.

The findings presented in Endress and Blagodatsky (*in prep.*) provide the theoretical underpinnings of the ubiquitous pattern of CUE and EUE after single-pulse substrate addition. In essence, the temporal dynamics of microbial CUE reflect those of the active fraction of microbes, because only the active fraction channels C through anabolic reactions to produce new biomass via growth. Since the dynamics of the r variable display a unimodal pattern in all model simulations, so too does CUE. This unimodal pattern is consistent with experimental measures of microbial activity such as respiration and heat production and indicates an adequate performance of the index of physiological state r . Other processes, such as anaerobic pathways or SOM utilization, contribute additional variation to this fundamental pattern. For example, the dominant active pathways determine the maximum efficiency that can be reached by the active fraction of microbial biomass. Notably, the carbon and energy flow is dominated by maintenance reactions of the inactive fraction during the initial lag phase and the retardation phase after substrate depletion. These reactions do not yield any net increase in biomass. In fact, the switch to endogenous maintenance in the absence of external substrates eventually causes a negative CUE that results in a net decrease of biomass, as observed in the results of Chapter 3 (Chapter 3, Fig. 2) and many similar experiments (for an example including the application of the index of physiological state r , see Blagodatsky et al., 1998).

Assessment of microbial CUE and EUE is limited by biomass quantification.

Given its definition as the fraction of C channeled through anabolism, a direct assessment of CUE requires accurate estimates of microbial biomass in the soil. Yet, no universal and unambiguous method to obtain such estimates exists (Blagodatskaya and Kuzyakov, 2013). Chloroform fumigation-extraction (CFE, Vance et al., 1987) represents the most widespread approach, yet its accuracy depends on the conversion factor between chloroform-extractable C and soil microbial C (Glanville et al., 2016). This factor is frequently treated as a constant (Čapek et al., 2023), which neglects its documented variability across soils (Sparling and West, 1988; Dictor et al., 1998) and propagates this uncertainty if novel approaches are calibrated via the CFE method. Therefore, the development and improvement of biomass

quantification procedures represent a major limitation to our quantitative understanding of soil microbial CUE.

In our studies, we have used CFE-derived biomass estimates (Chapter 3) as well as estimates derived from soil DNA content and substrate-induced respiration (SIR, Anderson and Domsch, 1978, Chapter 1, Chapter 2) for the calibration of model parameters and initial conditions. While DNA- and respiration-based estimates were in good agreement in Endress et al. (2024a), growth estimates based on DNA increase were lower than those based on respiration in Endress et al. (2024b), probably due to dynamic changes in the conversion factor between DNA and biomass (Čapek et al., 2023). This further highlights the need for method intercomparison and development. Finally, our results corroborate the idea that efficiency estimates based solely on the release of heat and CO₂ are generally problematic, especially in the case of complex substrates and additional SOM utilization (Chapter 3, Hagerty et al., 2018). Notably, heat-based estimates are currently the only practical method for the estimation of EUE. Independent estimates of EUE do not only require the accurate quantification of biomass but also of its energy content, making them even more challenging to obtain (see Wang and Kuzyakov, 2023, for an overview of EUE calculations).

Information content and limitations of the calorespirometric ratio

Similar to the findings on CUE and EUE, our results revealed that the temporal patterns of the CR can be leveraged to monitor dynamic changes in microbial metabolism over the course of soil incubation experiments.

The CR can be used to identify shifts in metabolic pathways.

In Endress et al. (2024a), the time course of the CR was characterized by two distinct trends, an initial increase to around 550 kJ per mol C followed by a sharp drop to around 230 kJ per mol C around the time of peak activity (Chapter 1, Fig. 3). These values fall outside the plausible range of values expected for aerobic growth on glucose and can be interpreted to indicate a shift toward anaerobic metabolic pathways (Chakrawal et al., 2020b). Specifically, a gradual onset of glucose fermentation to lactate followed by further fermentation to acetate and propionate predicts a temporal pattern consistent with observations. Critically, this interpretation is based on theoretical considerations instead of direct experimental evidence, such as the measurement of fermentation products or the activity of specific enzymes.

However, this hypothesis is supported by several indirect lines of evidence besides the CR pattern. First, members of the *Bacillota* phylum, known for their extensive fermentative capabilities (Cruz Ramos et al., 2000; Seeliger et al., 2002; Wiegel et al., 2006; Mosher et al., 2012), dramatically expanded during the incubation and eventually dominated the community (Chapter 1, Fig. 4). Second, we observed N₂O emissions indicating denitrification under anaerobic conditions, yet they were insufficient to explain CO₂ and heat emissions quantitatively (Supplementary Fig. S1 to Chapter 1). I note that the detection of additional gaseous products like N₂O and CH₄ represents a simple yet powerful way to enhance the interpretation of experimental results in the CR framework, especially if CO₂ is already analyzed by gas chromatography (as in Chapter 1). Third, 14% of the C added as glucose was unaccounted for between biomass and cumulative CO₂ at the end of the incubation, consistent with the accumulation of fermentation products in the dynamic model (Supplementary Fig. S6 to Chapter 1). Finally, a rough estimation of total O₂ availability indicated that complete aerobic oxidation of all added glucose was not feasible in the vials used for incubation. Together, these considerations suggest that the CR pattern can be used to track changes in metabolic pathways dynamically. Most importantly, identifying the possibility of fermentations would have been difficult based on C fluxes alone. Instead, this was only enabled by the joint consideration of heat and CO₂.

The CR can be used to assess the energy content of primed SOM.

The results of Wirsching et al. (2024) provide another example of the additional information that can be gleaned from the CR. In this study, we observed a substantial positive priming effect after the addition of cellulose based on ¹³C-labeling (Chapter 3, Fig. 2, Fig. 3). The amount of added substrate, as well as microbial biomass, are important determinants of the extent of SOM mineralization due to priming (Schimel, 2023), and this relationship can be explored from a carbon-centered perspective. However, such a methodology does not reveal any details about the composition of the primed SOM. By including the rate of heat release in our quantitative modeling framework, we were able to estimate the energy content of the SOM that was actually utilized by microbes in the studied soils (Supplementary Fig. 4 to Chapter 3). The analysis revealed diverse outcomes, with microbes utilizing SOM of lower, equal, or higher energy content than the average energy content of SOM in their respective soils. While we made no attempt to systematically interpret these novel findings in the study, developing and testing mechanistic explanations underlying the observations and linking

them to existing concepts of SOM bioavailability and preferential degradation represent important next steps to understanding the dynamics of soil C stocks (Gunina and Kuzyakov, 2022; Wang and Kuzyakov, 2023; Kästner et al., 2024). For example, this involves connecting SOM energy content to other properties that determine bioavailability, such as molecular weight and C/N-ratio (Ahamed et al., 2023), or explicitly accounting for the distribution of energy contents across SOM compounds as revealed by LDI-FT-ICR-MS (Simon et al., 2024).

The CR can identify plausible process combinations underlying experimental observations.

The theoretical analysis presented in Endress and Blagodatsky (*in prep.*) concludes that much of the utility of the CR lies in its ability to identify processes or process combinations that are consistent with the dynamics observed in experiments. Specifically, the CR can be used to generate falsifiable hypotheses about the dominant sources of CO₂ and heat and to suggest targeted measurements for testing these hypotheses. For example, in Endress et al. (2024a), the hypothesized transition to anaerobic pathways can be confirmed or rejected via the direct detection (or lack thereof) of fermentation products in follow-up studies or experiments. Besides its value for the interpretation of experimental results, the explicit representation of heat release also forces us to clarify our assumptions about conceptual and modeled C fluxes. For instance, the presumed composition of the external substrates or internal biomass compounds consumed to fuel maintenance requirements has a distinct effect on the CR signature of maintenance metabolism, but it is largely irrelevant if only CO₂ release is considered (Chapter 4, Fig. 3). Therefore, the CR enables and requires a nuanced understanding of the studied processes, both in the interpretation of experimental results and the design of mechanistic models.

In general, the CR should not be used to estimate microbial CUE directly.

Interest in the CR is in no small part driven by its connection to the efficiency of microbial growth and thus CUE. In particular, early studies highlighted a one-to-one correspondence between the CR and CUE in the case of simple growth reactions (Hansen et al., 2004), and the CR has subsequently been suggested as a method for CUE determination under certain conditions (Geyer et al., 2019). However, this correspondence is no longer applicable if other processes such as anaerobic reactions or SOM utilization are present (Chakrawal et al.,

2020b), and the required accuracy of CR measurements to obtain reliable CUE estimates is difficult to achieve using current setups (Yang et al., 2024). The results presented in all four chapters support these criticisms, and we conclude that the CR can only be used to estimate CUE under narrow conditions, such as during the exponential growth phase after labile substrate addition (as done in Chakrawal et al., 2021). In general, the relation between CR and CUE is nuanced, and the more complex model predictions in Endress and Blagodatsky (*in prep.*) are in good agreement with observations in the few experiments with sufficient CUE and CR estimates (e.g., compare Chapter 4, Fig. 3 to Chapter 2, Fig. 4b and Chapter 3, Fig. 7).

The CR is highly sensitive to the relative timing of heat and CO₂ observations.

In Endress et al. (2024b), we observed erratic patterns in the dynamic CR that were incompatible with simple model predictions (Chapter 2, Fig. 5, and Supplementary Fig. S4 to Chapter 2). By extending the model to account for delayed CO₂ detection relative to heat detection, we were able to reproduce many features of the measured CR curves. We speculate that this delay is caused by the transport of CO₂ from the site of production in the soil to the site of its detection (alkali solution in the headspace above the sample). Our findings add to related issues regarding the parallel measurement of heat and CO₂ from soil samples reported in the literature (Barros et al., 2010; Yang et al., 2024). They emphasize the need for improvements to existing experimental setups and the design of novel calorimeters, which represent an ongoing endeavor (Fricke et al., 2024). The study also illustrates how models can account for artificial patterns caused by experimental procedures, although a spatially explicit modeling approach to the transport of gases and heat in the system would be required to assess the observed delay and its causes quantitatively.

In addition, the results of Endress et al. (2024b) show that the CR calculated from the cumulative release of heat and CO₂, as opposed to the highly sensitive CR based on rates, is a robust tool to assess the overall balance of C and energy in the system. This finding is in line with the theoretical conclusions reached by Endress and Blagodatsky (*in prep.*, Chapter 4, Fig. 2). In particular, the combination of the CR with the ratio of CO₂ production to O₂ consumption and the ratio of heat production to O₂ consumption clearly revealed aerobic growth fueled by glucose as the dominant process in all incubations (Chapter 2, Fig. 3). This complementary nature of the three ratios was already discussed by Hansen et al. (2004) and

has recently regained some attention (Smart et al., 2024), but the information contained in a joint dynamic analysis of all three quantities - heat, CO₂ and O₂ - is yet to be leveraged.

Unraveling the complexity of microbial life in soil using bioenergetics

The findings of this thesis primarily pertain to the microbial carbon and energy use after the addition of well-defined, labile substrates to sieved and homogenized soil samples under laboratory conditions. Yet, the results and bioenergetic considerations also have the potential to elucidate other aspects of microbial life in soil, such as microbial C cycling in unamended soils or the role of complex interactions in microbial communities and across trophic levels.

Do microbes selectively utilize specific SOM compounds in amended and unamended soils?

The simultaneous screening of heat and CO₂ enabled us to estimate the energy content of SOM mineralized after cellulose addition due to the priming effect (Wirsching et al., 2024). While this analysis by itself revealed the microbial utilization of SOM of a wide range of energy contents in a diverse set of soils, it is particularly valuable when combined with estimates of the average energy content of SOM in those soils as obtained via combustion calorimetry or TG-DSC (e.g., Baraldi et al., 1998; Barros et al., 2020; Lorenz, 2024). The selective utilization of SOM by microorganisms can then be inferred from a comparison of the two estimates as discussed above (see also Supplementary Fig. S4 to Chapter 3) and offers many avenues for further investigation. In particular, the selective utilization of certain SOM compounds implies the selective stabilization of other compounds under the studied conditions, with implications for the fate of the quantity and quality of SOM stocks (Gunina and Kuzyakov, 2022; Wang and Kuzyakov, 2023; Kästner et al., 2024).

The same rationale can also be applied to unamended soils and soil samples. Given that most microbes are inactive most of the time and the conditions they experience cannot be compared to those after the addition of large amounts of labile substrate (Kuzyakov and Blagodatskaya, 2015), this scenario may be even more important for the fate of SOM at larger scales. However, almost all of the limited available data for the CR of unamended soils have been collected by a small number of researchers, in particular by Barros and colleagues (e.g., Barros et al., 2011, 2017, 2020; Barros, 2021; Lestido-Cardama et al., 2024). I note that such CR values should also be available from the unamended control samples used in

substrate addition experiments, but those data are rarely reported. Nonetheless, in the few studies that measured both the CR of unamended samples and the energy content of SOM in the soil, the relationship between the two quantities is intriguing (Chapter 4, Fig. 4). In arable soils, there is a very close positive correlation, indicating that microbes do not preferentially utilize SOM of higher or lower energy content. On the other hand, a weak inverse relationship is found in samples obtained from forest soils, perhaps driven by selective utilization of energy-rich substrates in organic horizons with high C content. An in-depth analysis of the causes underlying this pattern is currently prevented by the small number of samples, but this will be an important and attractive option as more data becomes available.

The role of microbial community composition and trophic interactions remains to be explored in a bioenergetic framework.

Soils harbor an enormous diversity of microbial life (Anthony et al., 2023), and this diversity is central to the biogeochemistry of the system (Mau et al., 2015; Crowther et al., 2019). In contrast, the microbial community is frequently dominated by the expansion of one or few taxa after a pulse of labile substrate in experiments (Eilers et al., 2010; Mau et al., 2015; Morrissey et al., 2017; Papp et al., 2020; Stone et al., 2021). While this can give important hints for understanding experimental observations, as it did in Endress et al. (2024a), such experiments do not reflect natural soil conditions. Therefore, future studies should consider combining bioenergetic investigations as presented in this thesis with an analysis of the microbial community and its successional stages under a wider range of conditions, including unamended and undisturbed soil samples with intact structure (Thomson et al., 2010; Ruamps et al., 2011), repeated substrate additions (Wu et al., 2020; Peng et al., 2024) or the addition of more complex substrate mixtures (Blagodatskii et al., 2008; Min et al., 2021).

Trophic interactions in soil food webs add another layer of complexity, yet they are critically important for many soil functions such as SOM and nutrient cycling (Schimel and Schaeffer, 2012; Grandy et al., 2016; Richter et al., 2019). Energy flux across trophic levels in the soil system has been investigated with a particular focus on nematode consumers (e.g., Ferris, 2010; Wan et al., 2022). However, such investigations typically rely on empirical estimates of energy transfer that are ultimately based on the flux of C through the system, instead of independent measures such as heat release. Recent efforts have started to unveil connections between the soil nematode community and microbial activity, CUE, and EUE, suggesting

nematode faunal analysis as a useful proxy for microbial substrate turnover and efficiency (van Bommel et al., 2024). A mechanistic, bioenergetic description based on coupled measurements of C and energy flux would help to substantiate these observed correlations.

Utility of process-based models with coupled microbial carbon and energy turnover

Throughout this thesis, the use of process-based dynamic models was central to the quantitative interpretation of experimental results and to the conceptual advancement of our understanding of microbial C cycling. Below, I briefly summarize the strengths, the limitations, and the options for future extensions of these models.

The incorporation of heat dynamics enhances the capabilities of microbial C cycling models.

The representation of heat dynamics was key to the utility of the models in all chapters of this thesis. In Endress et al. (2024a), only the quantitative pattern of the CR enabled the identification of plausible anaerobic pathways. An analysis based on the dynamics of C pools alone would be unlikely to yield similar conclusions. In Wirsching et al. (2024), the incorporation of heat flux allowed us to estimate SOM energy content from the difference between the total observed heat release and the expected heat release due to the consumption of ^{13}C -labeled cellulose. While we did not perform an in-depth analysis of the dynamic CR in Endress et al. (2024b), the heat flux nonetheless provided valuable insights for the improvement of the experimental setup to enable such investigations in the future. Furthermore, the cumulative CR confirmed aerobic growth on glucose as the main biochemical process in all incubations. Finally, the coupling between CO_2 and heat release represents the basis for all of the model predictions regarding maintenance metabolism and the CR of unamended soil samples in Endress and Blagodatsky (*in prep.*).

Experimental observations of heat release were also instrumental during model calibration. The availability of another time series for calibration greatly enhanced the quality of parameter estimates (see also Chakrawal et al., 2021). Sometimes, it even enabled the convergence of calibration routines in the first place. Specifically, relatively few or even no additional parameters had to be introduced to describe the dynamics of the heat variable, since the reaction enthalpy of the dominant processes can be derived from other parameters in

combination with independent information such as the energy contents of the involved compounds (Kästner et al., 2024). Notably, isothermal microcalorimetry provides measurements at an extremely high temporal resolution (on the order of seconds). This is in stark contrast to C pools such as biomass and CO₂, which are typically measured only a few times over the course of incubation (see for example Chapter 1, Fig. 3, and Chapter 3, Fig. 2). I note that this dramatic difference in the number of data points between variables necessitates the use of weighted residuals to avoid overfitting of the heat observations. Nonetheless, the highly resolved dynamics facilitate the quantitative judgment of properties such as the time of maximum activity or the return of activity to basal levels.

Current models can be extended to improve process representations.

To demonstrate the feasibility and the utility of simulating coupled C and energy fluxes and to allow for model calibration to small datasets, the dynamic models used in this thesis are of low complexity compared to many contemporary models of soil C cycling (Sulman et al., 2018). For example, they utilize simple formulations to simulate the anaerobic soil volume fraction (Endress et al., 2024a), the consumption of nutrients from the surrounding soil (Endress et al., 2024b), the priming of SOM, and the residual undecomposed fraction of cellulose (Wirsching et al., 2024). Similarly, they all rely on a small number of C pools characterized by constant energy contents, as well as on macrochemical (i.e., black-box) fluxes between these pools.

Fortunately, numerous options are readily available to extend these models and to improve the representations of the processes of interest as required. Ideally, these extensions should be grounded in established physical rules (Tang et al., 2024). Among many others, these options include mechanistic descriptions of O₂ supply and demand in the soil pore space, including spatially explicit formulations (Schlüter et al., 2024), the explicit representation of extracellular enzymes for the decomposition of SOM and polymeric substrates such as cellulose (as in, e.g., the MEND model, Wang et al., 2015) or the incorporation of nitrogen dynamics and microbial stoichiometry more generally (Chakrawal et al., 2022). The representation of the microbial community can be extended to account for different functional groups and life history strategies (e.g., Fierer, 2017; Piton et al., 2023), for example via trait-based approaches (Marschmann et al., 2024; Sircan et al., 2025). At the same time, the structure of microbial biomass can be more finely resolved, e.g., using structural and reserve

biomass pools as in DEB models (Marschmann et al., 2024) or via the incorporation of storage compounds (Manzoni et al., 2021; Mason-Jones et al., 2023). Soil solution chemistry and interactions of organic C with mineral phases in the soil, e.g., via sorption, represent another aspect that was not considered in this thesis. Coupling microbial-explicit C dynamics with models of soil solution chemistry such as the open-source program PHREEQC (Parkhurst and Appelo, 2013) could elucidate the role of physico-chemical interactions in future investigations, for example, to study the impacts of soil salinization (Mavi and Marschner, 2017).

In all of these cases, the central challenge with respect to bioenergetic modeling consists of assigning appropriate energy contents and heat fluxes to all of the C pools and C fluxes, respectively (or the decision to omit such fluxes if the rate of heat release is deemed negligible).

Equifinality and parameter identifiability remain important challenges.

The estimation of model parameters was significantly enhanced, and sometimes even made possible, by the incorporation of heat dynamics in the models and the availability of heat measurements for model calibration. Nonetheless, issues of calibration equifinality and poor identifiability of parameters persist in these models. The theoretical results of Endress and Blagodatsky (*in prep.*) provide particularly straightforward examples of this, with different parameter sets yielding equivalent system behavior in all modeled variables. Fundamentally, this finding is not surprising, given that the dynamics of heat release are uniquely determined by the overall energy balance in these simple models. Therefore, if all carbon pools follow equivalent trajectories under different parameterizations, so too will the heat variable.

However, parameter non-identifiability extends far beyond such narrow cases of strict equivalence (Marschmann et al., 2019). In this thesis, it manifested itself in high parameter uncertainty and poorly constrained posterior distributions of some parameters like certain yield coefficients or the half-saturation constant of the physiological state variable r (see e.g. Supplementary Fig. S4 to Chapter 1). I note that model calibration is particularly challenging if no experimental estimates of microbial biomass are available. In this case, both the growth of the biomass pool and the activation of previously dormant biomass without growth can yield highly similar dynamics of heat and CO₂ release, despite markedly different trajectories of the biomass pool. In practice, microbial biomass therefore represents the most important

variable for calibration other than the calorimetric data. A formal analysis that quantifies the additional information gained from the representation of the heat variable is, however, still missing.

Such issues present an even greater challenge as the complexity and the number of parameters of the biogeochemical models in question increase (Sierra et al., 2015). Novel calibration procedures such as constraint-based MCMC methods that flexibly incorporate *a priori* parameter and process-constraints into the calibration routine can be leveraged to address this problem by confining the space of feasible parameter combinations (Chavez Rodriguez et al., 2022). This is especially valuable if models are not calibrated to reflect the detailed dynamics of single experiments. To complement such algorithmic innovations, the number of free parameters as well as their ranges can also be reduced via independent thermodynamic and biological considerations. For example, this has been demonstrated for growth yield coefficients (Brock et al., 2017), rate coefficients (Desmond-Le Quémener and Bouchez, 2014; Delattre et al., 2019), and a range of other genome-informed microbial traits (Karaoz and Brodie, 2022; Marschmann et al., 2024).

Conclusion

In this thesis, I have demonstrated the feasibility and utility of microbial-explicit process-based modeling for the analysis of coupled carbon and energy flows in the soil system.

The models show that microbial CUE and EUE after single-pulse addition of labile substrate are tightly linked according to fundamental thermodynamic rules. Specifically, the efficiency of microbial growth exhibits complex temporal patterns that are shaped by the availability and quality of substrate and terminal electron acceptors, the additional utilization of SOM, and the activity state of the microbial community. Accurate experimental biomass quantification represents a critical challenge for the validation of CUE dynamics in these models and should be addressed via method development and intercomparison.

The results illustrate how the calorimetric ratio of heat to CO₂ release can be leveraged to monitor and quantify microbial metabolism in the soil system dynamically. In particular, the CR enables the identification of plausible processes underlying experimental observations, such as shifts in metabolic pathways or the selective utilization of SOM

compounds. Therefore, the framework allows for the formulation of specific and testable hypotheses and is most useful when combined with other sources of information, like measurements of O₂ consumption or independent estimates of the dynamics of relevant C pools such as biomass or metabolic products. When combined with estimates of SOM energy content, the CR can reveal selective utilization of SOM in both unamended soils and after substrate addition, which offers a promising option for future research.

Finally, the incorporation of heat dynamics was instrumental in the calibration of the studied models, and contributed to their ability to generate mechanistic interpretations of experimental results. The simple formulations presented in this thesis can easily be extended to increase the realism and scope of process representations. However, the estimation of model parameters continues to pose a serious challenge, which is exacerbated by increased model complexity. A combination of advanced calibration methods and independent constraints based on thermodynamic considerations and microbial traits should be leveraged to address this issue.

List of resources

The table below lists important resources used in this thesis for analysis and visualization purposes. Versions of programming languages and packages used are indicated in each article.

Name	Description	References
NIST Chemistry WebBook	Public online collection of physical and chemical properties of many compounds, e.g., enthalpies of formation and combustion	Peter Linstrom (2017)
BioRender	Online tool for figure creation used to create the schematic illustrations in all manuscripts (Chapter 1, Fig. 1 and Fig. 2; Chapter 2, Fig. 1; Chapter 3, Fig. 1; Chapter 4, Fig. 1)	BioRender.com
R and RStudio	Programming language and environment used for some statistical analyses	RStudio Team (2020); R Core Team (2023)
emmeans	Package used for ANOVA with contrasts (Chapter 2)	Lenth (2023)
Python and SciPy	Programming language and primary package used for all analyses, particularly the numerical integration of ODEs	Rossum (1995); Virtanen et al. (2020)
lmfit	Package used for model calibration	Newville et al. (2023)
emcee	Package used for MCMC analysis	Foreman-Mackey et al. (2013)

References

The references below correspond to those cited throughout this thesis, except for references cited in the results section. The references cited in each published article and prepared manuscript are listed separately in the corresponding articles/manuscripts.

- Ahamed, F., You, Y., Burgin, A., et al., 2023. Exploring the determinants of organic matter bioavailability through substrate-explicit thermodynamic modeling. *Frontiers in Water* 5, 1169701. doi:10.3389/frwa.2023.1169701
- Anderson, J.P.E., Domsch, K.H., 1978. A physiological method for the quantitative measurement of microbial biomass in soils. *Soil Biology and Biochemistry* 10, 215–221. doi:10.1016/0038-0717(78)90099-8
- Anthony, M.A., Bender, S.F., Van Der Heijden, M.G.A., 2023. Enumerating soil biodiversity. *Proceedings of the National Academy of Sciences* 120, e2304663120. doi:10.1073/pnas.2304663120
- Babey, T., Vieubl -Gonod, L., Rapaport, A., et al., 2017. Spatiotemporal simulations of 2,4-D pesticide degradation by microorganisms in 3D soil-core experiments. *Ecological Modelling* 344, 48–61. doi:10.1016/j.ecolmodel.2016.11.006
- Bajracharya, B.M., Smeaton, C.M., Markelov, I., et al., 2022. Organic Matter Degradation in Energy-Limited Subsurface Environments—A Bioenergetics-Informed Modeling Approach. *Geomicrobiology Journal* 39, 1–16. doi:10.1080/01490451.2021.1998256
- Banks, H.T., Joyner, M.L., 2017. AIC under the framework of least squares estimation. *Applied Mathematics Letters* 74, 33–45. doi:10.1016/j.aml.2017.05.005
- Baraldi, P., Beltrami, C., Cassai, C., Molinari, L., Zunarelli, R., 1998. Measurements of combustion enthalpy of solids by DSC. *Materials Chemistry and Physics* 53, 252–255. doi:10.1016/S0254-0584(98)00010-8
- Bardgett, R.D., Van Der Putten, W.H., 2014. Belowground biodiversity and ecosystem functioning. *Nature* 515, 505–511. doi:10.1038/nature13855
- Barros, N., 2021. Thermodynamics of Soil Microbial Metabolism: Applications and Functions. *Applied Sciences* 11, 4962. doi:10.3390/app11114962
- Barros, N., Feij o, S., Hansen, L.D., 2011. Calorimetric determination of metabolic heat, CO₂ rates and the calorespirometric ratio of soil basal metabolism. *Geoderma* 160, 542–547. doi:10.1016/j.geoderma.2010.11.002
- Barros, N., Feij o, S., P rez-Cruzado, C., et al., 2017. Effect of soil storage at 4  C on the calorespirometric measurements of soil microbial metabolism. *AIMS Microbiology* 3, 762–773. doi:10.3934/microbiol.2017.4.762
- Barros, N., Fernandez, I., Byrne, K.A., et al., 2020. Thermodynamics of soil organic matter decomposition in semi-natural oak (*Quercus*) woodland in southwest Ireland. *Oikos* 129, 1632–1644. doi:10.1111/oik.07261
- Barros, N., Hansen, L.D., Pi eiro, V., et al., 2016. Factors influencing the calorespirometric ratios of soil microbial metabolism. *Soil Biology and Biochemistry* 92, 221–229. doi:10.1016/j.soilbio.2015.10.007
- Barros, N., Salgado, J., Rodr guez-A  n, J.A., et al., 2010. Calorimetric approach to metabolic carbon conversion efficiency in soils: Comparison of experimental and theoretical models. *Journal of Thermal Analysis and Calorimetry* 99, 771–777. doi:10.1007/s10973-010-0673-4
- Batjes, N.H., 2016. Harmonized soil property values for broad-scale modelling (WISE30sec)

- with estimates of global soil carbon stocks. *Geoderma* 269, 61–68.
doi:10.1016/j.geoderma.2016.01.034
- Battley, E.H., 1996. On the thermodynamics of autotrophic and heterotrophic growth of *Pseudomonas saccharophila*. *Canadian Journal of Microbiology* 42, 38–45.
doi:10.1139/m96-006
- Baveye, P.C., 2023. Ecosystem-scale modelling of soil carbon dynamics: Time for a radical shift of perspective? *Soil Biology and Biochemistry* 184, 109112.
doi:10.1016/j.soilbio.2023.109112
- Bernard, L., Basile-Doelsch, I., Derrien, D., et al., 2022. Advancing the mechanistic understanding of the priming effect on soil organic matter mineralisation. *Functional Ecology* 36, 1355–1377. doi:10.1111/1365-2435.14038
- Beven, K., Freer, J., 2001. Equifinality, data assimilation, and uncertainty estimation in mechanistic modelling of complex environmental systems using the GLUE methodology. *Journal of Hydrology* 249, 11–29. doi:10.1016/S0022-1694(01)00421-8
- Blagodatskaya, E., Blagodatsky, S., Anderson, T.-H., Kuzyakov, Y., 2014a. Microbial Growth and Carbon Use Efficiency in the Rhizosphere and Root-Free Soil. *PLoS ONE* 9, e93282. doi:10.1371/journal.pone.0093282
- Blagodatskaya, E., Khomyakov, N., Myachina, O., et al., 2014b. Microbial interactions affect sources of priming induced by cellulose. *Soil Biology and Biochemistry* 74, 39–49.
doi:10.1016/j.soilbio.2014.02.017
- Blagodatskaya, E., Kuzyakov, Y., 2013. Active microorganisms in soil: Critical review of estimation criteria and approaches. *Soil Biology and Biochemistry* 67, 192–211.
doi:10.1016/j.soilbio.2013.08.024
- Blagodatskaya, E., Kuzyakov, Y., 2008. Mechanisms of real and apparent priming effects and their dependence on soil microbial biomass and community structure: critical review. *Biology and Fertility of Soils* 45, 115–131. doi:10.1007/s00374-008-0334-y
- Blagodatskii, S.A., Bogomolova, I.N., Blagodatskaya, E.V., 2008. Microbial biomass and growth kinetics of microorganisms in chernozem soils under different land use modes. *Microbiology* 77, 99–106. doi:10.1134/S0026261708010141
- Blagodatsky, S., Blagodatskaya, E., Yuyukina, T., Kuzyakov, Y., 2010. Model of apparent and real priming effects: Linking microbial activity with soil organic matter decomposition. *Soil Biology and Biochemistry* 42, 1275–1283.
doi:10.1016/j.soilbio.2010.04.005
- Blagodatsky, S.A., Heinemeyer, O., Richter, J., 2000. Estimating the active and total soil microbial biomass by kinetic respiration analysis. *Biology and Fertility of Soils* 32, 73–81. doi:10.1007/s003740000219
- Blagodatsky, S.A., Richter, O., 1998. Microbial growth in soil and nitrogen turnover: a theoretical model considering the activity state of microorganisms. *Soil Biology and Biochemistry* 30, 1743–1755. doi:10.1016/S0038-0717(98)00028-5
- Blagodatsky, S.A., Yevdokimov, I.V., Larionova, A.A., Richter, J., 1998. Microbial growth in soil and nitrogen turnover: Model calibration with laboratory data. *Soil Biology and Biochemistry* 30, 1757–1764. doi:10.1016/S0038-0717(98)00029-7
- Bölscher, T., Vogel, C., Olagoke, F.K., et al., 2024. Beyond growth: The significance of non-growth anabolism for microbial carbon-use efficiency in the light of soil carbon stabilisation. *Soil Biology and Biochemistry* 193, 109400.
doi:10.1016/j.soilbio.2024.109400
- Boye, K., Herrmann, A.M., Schaefer, M.V., Tfaily, M.M., Fendorf, S., 2018. Discerning Microbially Mediated Processes During Redox Transitions in Flooded Soils Using Carbon and Energy Balances. *Frontiers in Environmental Science* 6, 15.

- doi:10.3389/fenvs.2018.00015
- Boye, K., Noël, V., Tfaily, M.M., et al., 2017. Thermodynamically controlled preservation of organic carbon in floodplains. *Nature Geoscience* 10, 415–419. doi:10.1038/ngeo2940
- Bradford, M.A., Wieder, W.R., Bonan, G.B., et al., 2016. Managing uncertainty in soil carbon feedbacks to climate change. *Nature Climate Change* 6, 751–758. doi:10.1038/nclimate3071
- Braissant, O., Bonkat, G., Wirz, D., Bachmann, A., 2013. Microbial growth and isothermal microcalorimetry: Growth models and their application to microcalorimetric data. *Thermochimica Acta* 555, 64–71. doi:10.1016/j.tca.2012.12.005
- Braissant, O., Wirz, D., GÃ¶pfert, B., Daniels, A.U., 2010. Use of isothermal microcalorimetry to monitor microbial activities. *FEMS Microbiology Letters* 303, 1–8. doi:10.1111/j.1574-6968.2009.01819.x
- Brock, A.L., K stner, M., Trapp, S., 2017. Microbial growth yield estimates from thermodynamics and its importance for degradation of pesticides and formation of biogenic non-extractable residues. *SAR and QSAR in Environmental Research* 28, 629–650. doi:10.1080/1062936X.2017.1365762
- Brueckner, D., Solokhina, A., Kr henb hl, S., Braissant, O., 2017. A combined application of tunable diode laser absorption spectroscopy and isothermal micro-calorimetry for calorespirometric analysis. *Journal of Microbiological Methods* 139, 210–214. doi:10.1016/j.mimet.2017.06.012
- Calabrese, S., Chakrawal, A., Manzoni, S., Van Cappellen, P., 2021. Energetic scaling in microbial growth. *Proceedings of the National Academy of Sciences* 118, e2107668118. doi:10.1073/pnas.2107668118
- Camenzind, T., Mason-Jones, K., Mansour, I., Rillig, M.C., Lehmann, J., 2023. Formation of necromass-derived soil organic carbon determined by microbial death pathways. *Nature Geoscience*. doi:10.1038/s41561-022-01100-3
- Canadell, J.G., Monteiro, P.M.S., Costa, M.H., et al., 2021. Global Carbon and Other Biogeochemical Cycles and Feedbacks, in: Masson-Delmotte, V., P. Zhai, A. Pirani, S.L. Connors, C. P  an, S. Berger, N. Caud, Y. Chen, L. Goldfarb, M.I. Gomis, M. Huang, K. Leitzell, E. Lonnoy, J.B.R. Matthews, T.K. Maycock, T. Waterfield, O. Yelek i, R. Yu, and B. Zhou (Ed.), *Climate Change 2021: The Physical Science Basis. Contribution of Working Group I to the Sixth Assessment Report of the Intergovernmental Panel on Climate Change*. Cambridge University Press, Cambridge, United Kingdom and New York, NY, USA, pp. 673–816.
-   apek, P., Choma, M., Ka stovsk  , E., et al., 2023. Revisiting soil microbial biomass: Considering changes in composition with growth rate. *Soil Biology and Biochemistry* 184, 109103. doi:10.1016/j.soilbio.2023.109103
- Chakrawal, A., Calabrese, S., Herrmann, A.M., Manzoni, S., 2022. Interacting Bioenergetic and Stoichiometric Controls on Microbial Growth. *Frontiers in Microbiology* 13, 859063. doi:10.3389/fmicb.2022.859063
- Chakrawal, A., Herrmann, A.M., Koestel, J., et al., 2020a. Dynamic upscaling of decomposition kinetics for carbon cycling models. *Geoscientific Model Development* 13, 1399–1429. doi:10.5194/gmd-13-1399-2020
- Chakrawal, A., Herrmann, A.M., Manzoni, S., 2021. Leveraging energy flows to quantify microbial traits in soils. *Soil Biology and Biochemistry* 155, 108169. doi:10.1016/j.soilbio.2021.108169
- Chakrawal, A., Herrmann, A.M.,   antr  ckov  , H., Manzoni, S., 2020b. Quantifying microbial metabolism in soils using calorespirometry — A bioenergetics perspective. *Soil Biology and Biochemistry* 148, 107945. doi:10.1016/j.soilbio.2020.107945

- Chavez Rodriguez, L., González-Nicolás, A., Ingalls, B., et al., 2022. Optimal design of experiments to improve the characterisation of atrazine degradation pathways in soil. *European Journal of Soil Science* 73. doi:10.1111/ejss.13211
- Cossetto, T., Rodenfels, J., Sartori, P., 2024. Thermodynamic dissipation constrains metabolic versatility of unicellular growth. doi:10.1101/2024.03.21.585772
- Crowther, T.W., Todd-Brown, K.E.O., Rowe, C.W., et al., 2016. Quantifying global soil carbon losses in response to warming. *Nature* 540, 104–108. doi:10.1038/nature20150
- Crowther, T.W., Van Den Hoogen, J., Wan, J., et al., 2019. The global soil community and its influence on biogeochemistry. *Science* 365, eaav0550. doi:10.1126/science.aav0550
- Cruz Ramos, H., Hoffmann, T., Marino, M., et al., 2000. Fermentative Metabolism of *Bacillus subtilis* : Physiology and Regulation of Gene Expression. *Journal of Bacteriology* 182, 3072–3080. doi:10.1128/JB.182.11.3072-3080.2000
- Davidson, E.A., Janssens, I.A., 2006. Temperature sensitivity of soil carbon decomposition and feedbacks to climate change. *Nature* 440, 165–173. doi:10.1038/nature04514
- Dejean, L., Beauvoit, B., Bunoust, O., et al., 2001. The calorimetric-respirometric ratio is an on-line marker of enthalpy efficiency of yeast cells growing on a non-fermentable carbon source. *Biochimica et Biophysica Acta* 1503, 329–340.
- Delattre, H., Desmond-Le Quémener, E., Duquennoi, C., Filali, A., Bouchez, T., 2019. Consistent microbial dynamics and functional community patterns derived from first principles. *The ISME Journal* 13, 263–276. doi:10.1038/s41396-018-0272-0
- Desmond-Le Quémener, E., Bouchez, T., 2014. A thermodynamic theory of microbial growth. *The ISME Journal* 8, 1747–1751. doi:10.1038/ismej.2014.7
- Dictor, M.-C., Tessier, L., Soulas, G., 1998. Reassessment of the Kec coefficient of the fumigation–extraction method in a soil profile. *Soil Biology and Biochemistry* 30, 119–127. doi:10.1016/S0038-0717(97)00111-9
- Dijkstra, F.A., Keitel, C., 2024. Maximising carbon sequestration through mixing compost in moist soil. *Soil Biology and Biochemistry* 191, 109330. doi:10.1016/j.soilbio.2024.109330
- Dijkstra, P., Martinez, A., Thomas, S.C., et al., 2022. On maintenance and metabolisms in soil microbial communities. *Plant and Soil* 476, 385–396. doi:10.1007/s11104-022-05382-9
- Eilers, K.G., Lauber, C.L., Knight, R., Fierer, N., 2010. Shifts in bacterial community structure associated with inputs of low molecular weight carbon compounds to soil. *Soil Biology and Biochemistry* 42, 896–903. doi:10.1016/j.soilbio.2010.02.003
- Endress, M.-G., Chen, R., Blagodatskaya, E., Blagodatsky, S., 2024a. The coupling of carbon and energy fluxes reveals anaerobiosis in an aerobic soil incubation with a *Bacillota*-dominated community. *Soil Biology and Biochemistry* 195, 109478. doi:10.1016/j.soilbio.2024.109478
- Endress, M.-G., Dehghani, F., Blagodatsky, S., et al., 2024b. Spatial substrate heterogeneity limits microbial growth as revealed by the joint experimental quantification and modeling of carbon and heat fluxes. *Soil Biology and Biochemistry* 197, 109509. doi:10.1016/j.soilbio.2024.109509
- Ferris, H., 2010. Form and function: Metabolic footprints of nematodes in the soil food web. *European Journal of Soil Biology* 46, 97–104. doi:10.1016/j.ejsobi.2010.01.003
- Fierer, N., 2017. Embracing the unknown: disentangling the complexities of the soil microbiome. *Nature Reviews Microbiology* 15, 579–590. doi:10.1038/nrmicro.2017.87
- Foreman-Mackey, D., Hogg, D.W., Lang, D., Goodman, J., 2013. emcee : The MCMC Hammer. *Publications of the Astronomical Society of the Pacific* 125, 306–312.

doi:10.1086/670067

- Frey, S.D., Lee, J., Melillo, J.M., Six, J., 2013. The temperature response of soil microbial efficiency and its feedback to climate. *Nature Climate Change* 3, 395–398. doi:10.1038/nclimate1796
- Fricke, C., Lodovico, E.D., Meyer, M., Maskow, T., Schaumann, G.E., 2024. Design, calibration and testing of a novel isothermal calorimeter prototype. *Thermochimica Acta* 738, 179785. doi:10.1016/j.tca.2024.179785
- Geyer, K., Schnecker, J., Grandy, A.S., Richter, A., Frey, S., 2020. Assessing microbial residues in soil as a potential carbon sink and moderator of carbon use efficiency. *Biogeochemistry* 151, 237–249. doi:10.1007/s10533-020-00720-4
- Geyer, K.M., Dijkstra, P., Sinsabaugh, R., Frey, S.D., 2019. Clarifying the interpretation of carbon use efficiency in soil through methods comparison. *Soil Biology and Biochemistry* 128, 79–88. doi:10.1016/j.soilbio.2018.09.036
- Geyer, K.M., Kyker-Snowman, E., Grandy, A.S., Frey, S.D., 2016. Microbial carbon use efficiency: accounting for population, community, and ecosystem-scale controls over the fate of metabolized organic matter. *Biogeochemistry* 127, 173–188. doi:10.1007/s10533-016-0191-y
- Glanville, H.C., Hill, P.W., Schnepf, A., Oburger, E., Jones, D.L., 2016. Combined use of empirical data and mathematical modelling to better estimate the microbial turnover of isotopically labelled carbon substrates in soil. *Soil Biology and Biochemistry* 94, 154–168. doi:10.1016/j.soilbio.2015.11.016
- Grandy, A.S., Wieder, W.R., Wickings, K., Kyker-Snowman, E., 2016. Beyond microbes: Are fauna the next frontier in soil biogeochemical models? Special Issue: Food Web Interactions in the Root Zone: Influences on Community and Ecosystem Dynamics 102, 40–44. doi:10.1016/j.soilbio.2016.08.008
- Gunina, A., Kuzyakov, Y., 2022. From energy to (soil organic) matter. *Global Change Biology* 28, 2169–2182. doi:10.1111/gcb.16071
- Hagerty, S.B., Allison, S.D., Schimel, J.P., 2018. Evaluating soil microbial carbon use efficiency explicitly as a function of cellular processes: implications for measurements and models. *Biogeochemistry* 140, 269–283. doi:10.1007/s10533-018-0489-z
- Hansen, L.D., Macfarlane, C., McKinnon, N., Smith, B.N., Criddle, R.S., 2004. Use of calorimetric ratios, heat per CO₂ and heat per O₂, to quantify metabolic paths and energetics of growing cells. *Thermochimica Acta* 422, 55–61. doi:10.1016/j.tca.2004.05.033
- Harris, J.A., Ritz, K., Coucheney, E., et al., 2012. The thermodynamic efficiency of soil microbial communities subject to long-term stress is lower than those under conventional input regimes. *Soil Biology and Biochemistry* 47, 149–157. doi:10.1016/j.soilbio.2011.12.017
- He, X., Abs, E., Allison, S.D., et al., 2024. Emerging multiscale insights on microbial carbon use efficiency in the land carbon cycle. *Nature Communications* 15, 8010. doi:10.1038/s41467-024-52160-5
- Heijnen, J.J., Kleerebezem, R., 2010. Bioenergetics of Microbial Growth, in: *Encyclopedia of Industrial Biotechnology*. John Wiley & Sons, Inc., Hoboken, NJ, USA, p. eib084. doi:10.1002/9780470054581.eib084
- Herrmann, A.M., Bölscher, T., 2015. Simultaneous screening of microbial energetics and CO₂ respiration in soil samples from different ecosystems. *Soil Biology and Biochemistry* 83, 88–92. doi:10.1016/j.soilbio.2015.01.020
- Herrmann, A.M., Coucheney, E., Nunan, N., 2014. Isothermal Microcalorimetry Provides

- New Insight into Terrestrial Carbon Cycling. *Environmental Science & Technology* 48, 4344–4352. doi:10.1021/es403941h
- Inagaki, T.M., Possinger, A.R., Schweizer, S.A., et al., 2023. Microscale spatial distribution and soil organic matter persistence in top and subsoil. *Soil Biology and Biochemistry* 178, 108921. doi:10.1016/j.soilbio.2022.108921
- Jackson, R.B., Lajtha, K., Crow, S.E., et al., 2017. The Ecology of Soil Carbon: Pools, Vulnerabilities, and Biotic and Abiotic Controls. *Annual Review of Ecology, Evolution, and Systematics* 48, 419–445. doi:10.1146/annurev-ecolsys-112414-054234
- Jenkinson, D.S., 1990. The turnover of organic carbon and nitrogen in soil. *Philosophical Transactions of the Royal Society of London. Series B: Biological Sciences* 329, 361–368. doi:10.1098/rstb.1990.0177
- Jenkinson, D.S., 1977. The soil biomass. *N. Z. Soil News* 25, 213–218.
- Jenkinson, D.S., 1966. Studies on the decomposition of plant material in soil. *Journal of Soil Science* 17, 280–302. doi:10.1111/j.1365-2389.1966.tb01474.x
- Jenkinson, D.S., Adams, D.E., Wild, A., 1991. Model estimates of CO₂ emissions from soil in response to global warming. *Nature* 351, 304–306. doi:10.1038/351304a0
- Jin, Q., Bethke, C.M., 2007. The thermodynamics and kinetics of microbial metabolism. *American Journal of Science* 307, 643–677. doi:10.2475/04.2007.01
- Joergensen, R.G., Wichern, F., 2018. Alive and kicking: Why dormant soil microorganisms matter. *Soil Biology and Biochemistry* 116, 419–430. doi:10.1016/j.soilbio.2017.10.022
- Karaoz, U., Brodie, E.L., 2022. microTrait: A Toolset for a Trait-Based Representation of Microbial Genomes. *Frontiers in Bioinformatics* 2, 918853. doi:10.3389/fbinf.2022.918853
- Kästner, M., Maskow, T., Miltner, A., Lorenz, M., Thiele-Bruhn, S., 2024. Assessing energy fluxes and carbon use in soil as controlled by microbial activity - A thermodynamic perspective A perspective paper. *Soil Biology and Biochemistry* 193, 109403. doi:10.1016/j.soilbio.2024.109403
- Kästner, M., Miltner, A., Thiele-Bruhn, S., Liang, C., 2021. Microbial Necromass in Soils—Linking Microbes to Soil Processes and Carbon Turnover. *Frontiers in Environmental Science* 9, 756378. doi:10.3389/fenvs.2021.756378
- Keiluweit, M., Nico, P.S., Kleber, M., Fendorf, S., 2016. Are oxygen limitations under recognized regulators of organic carbon turnover in upland soils? *Biogeochemistry* 127, 157–171. doi:10.1007/s10533-015-0180-6
- Keiluweit, M., Wanzek, T., Kleber, M., Nico, P., Fendorf, S., 2017. Anaerobic microsites have an unaccounted role in soil carbon stabilization. *Nature Communications* 8, 1771. doi:10.1038/s41467-017-01406-6
- Kempes, C.P., Van Bodegom, P.M., Wolpert, D., et al., 2017. Drivers of Bacterial Maintenance and Minimal Energy Requirements. *Frontiers in Microbiology* 8. doi:10.3389/fmicb.2017.00031
- Kooijman, S.A.L.M., 1993. *Dynamic energy budgets in biological systems: theory and applications in ecotoxicology*, 1. publ. ed. Cambridge Univ. Press, Cambridge.
- Kuzyakov, Y., Blagodatskaya, E., 2015. Microbial hotspots and hot moments in soil: Concept & review. *Soil Biology and Biochemistry* 83, 184–199. doi:10.1016/j.soilbio.2015.01.025
- Kuzyakov, Y., Friedel, J.K., Stahr, K., 2000. Review of mechanisms and quantification of priming effects. *Soil Biology and Biochemistry* 32, 1485–1498. doi:10.1016/S0038-0717(00)00084-5

- Lacroix, E.M., Mendillo, J., Gomes, A., Dekas, A., Fendorf, S., 2022. Contributions of anoxic microsites to soil carbon protection across soil textures. *Geoderma* 425, 116050. doi:10.1016/j.geoderma.2022.116050
- Lehmann, J., Kleber, M., 2015. The contentious nature of soil organic matter. *Nature* 528, 60–68. doi:10.1038/nature16069
- Lenth, R.V., 2023. emmeans: Estimated Marginal Means, aka Least-Squares Means.
- Lestido-Cardama, Y., Barros Pena, N., Pérez-Cruzado, C., 2024. Sensitivity of thermal analysis and calorimetry to assess the impact of forest management on soils. *Journal of Thermal Analysis and Calorimetry*. doi:10.1007/s10973-024-13702-7
- Levenberg, K., 1944. A method for the solution of certain non-linear problems in least squares. *Quarterly of Applied Mathematics* 2, 164–168. doi:10.1090/qam/10666
- Liang, C., Schimel, J.P., Jastrow, J.D., 2017. The importance of anabolism in microbial control over soil carbon storage. *Nature Microbiology* 2, 17105. doi:10.1038/nmicrobiol.2017.105
- Liu, J.-S., Vojinović, V., Patiño, R., Maskow, Th., Von Stockar, U., 2007. A comparison of various Gibbs energy dissipation correlations for predicting microbial growth yields. *Thermochimica Acta* 458, 38–46. doi:10.1016/j.tca.2007.01.016
- Lorenz, M., Maskow, T., Thiele-Bruhn, S., 2024. Energy stored in soil organic matter is influenced by litter quality and the degree of transformation – A combustion calorimetry study. *Geoderma* 443, 116846. doi:10.1016/j.geoderma.2024.116846
- Lotka, A.J., 1922. Contribution to the Energetics of Evolution. *Proceedings of the National Academy of Sciences* 8, 147–151. doi:10.1073/pnas.8.6.147
- Luo, Y., Ahlström, A., Allison, S.D., et al., 2016. Toward more realistic projections of soil carbon dynamics by Earth system models. *Global Biogeochemical Cycles* 30, 40–56. doi:https://doi.org/10.1002/2015GB005239
- Manzoni, S., Čapek, P., Porada, P., et al., 2018. Reviews and syntheses: Carbon use efficiency from organisms to ecosystems – definitions, theories, and empirical evidence. *Biogeosciences* 15, 5929–5949. doi:10.5194/bg-15-5929-2018
- Manzoni, S., Ding, Y., Warren, C., et al., 2021. Intracellular Storage Reduces Stoichiometric Imbalances in Soil Microbial Biomass – A Theoretical Exploration. *Frontiers in Ecology and Evolution* 9, 714134. doi:10.3389/fevo.2021.714134
- Manzoni, S., Taylor, P., Richter, A., Porporato, A., Ågren, G.I., 2012. Environmental and stoichiometric controls on microbial carbon-use efficiency in soils. *New Phytologist* 196, 79–91. doi:https://doi.org/10.1111/j.1469-8137.2012.04225.x
- Marquardt, D.W., 1963. An Algorithm for Least-Squares Estimation of Nonlinear Parameters. *Journal of the Society for Industrial and Applied Mathematics* 11, 431–441. doi:10.1137/0111030
- Marschmann, G.L., Pagel, H., Kügler, P., Streck, T., 2019. Equifinality, sloppiness, and emergent structures of mechanistic soil biogeochemical models. *Environmental Modelling & Software* 122, 104518. doi:10.1016/j.envsoft.2019.104518
- Marschmann, G.L., Tang, J., Zhalnina, K., et al., 2024. Predictions of rhizosphere microbiome dynamics with a genome-informed and trait-based energy budget model. *Nature Microbiology* 9, 421–433. doi:10.1038/s41564-023-01582-w
- Martin, W., Baross, J., Kelley, D., Russell, M.J., 2008. Hydrothermal vents and the origin of life. *Nature Reviews Microbiology* 6, 805–814. doi:10.1038/nrmicro1991
- Maskow, T., Babel, W., 2003. Thermokinetic description of anaerobic growth of *Halomonas halodenitrificans* using a static microcalorimetric ampoule technique. *Journal of Biotechnology* 101, 267–274. doi:10.1016/S0168-1656(02)00341-3
- Mason-Jones, K., Breidenbach, A., Dyckmans, J., Banfield, C.C., Dippold, M.A., 2023.

- Intracellular carbon storage by microorganisms is an overlooked pathway of biomass growth. *Nature Communications* 14, 2240. doi:10.1038/s41467-023-37713-4
- Mau, R.L., Liu, C.M., Aziz, M., et al., 2015. Linking soil bacterial biodiversity and soil carbon stability. *The ISME Journal* 9, 1477–1480. doi:10.1038/ismej.2014.205
- Mavi, M.S., Marschner, P., 2017. Impact of Salinity on Respiration and Organic Matter Dynamics in Soils is More Closely Related to Osmotic Potential than to Electrical Conductivity. *Special Issue on Soil Organic Carbon in a Changing World* 27, 949–956. doi:10.1016/S1002-0160(17)60418-1
- Maynard, D.S., Crowther, T.W., Bradford, M.A., 2017. Fungal interactions reduce carbon use efficiency. *Ecology Letters* 20, 1034–1042. doi:10.1111/ele.12801
- Min, K., Slessarev, E., Kan, M., et al., 2021. Active microbial biomass decreases, but microbial growth potential remains similar across soil depth profiles under deeply-vs. shallow-rooted plants. *Soil Biology and Biochemistry* 162, 108401. doi:10.1016/j.soilbio.2021.108401
- Morrissey, E.M., Mau, R.L., Schwartz, E., et al., 2017. Bacterial carbon use plasticity, phylogenetic diversity and the priming of soil organic matter. *The ISME Journal* 11, 1890–1899. doi:10.1038/ismej.2017.43
- Mosher, J.J., Phelps, T.J., Podar, M., et al., 2012. Microbial Community Succession during Lactate Amendment and Electron Acceptor Limitation Reveals a Predominance of Metal-Reducing *Pelosiinus* spp. *Applied and Environmental Microbiology* 78, 2082–2091. doi:10.1128/AEM.07165-11
- Newville, M., Otten, R., Nelson, A., et al., 2023. lmfit/lmfit-py: 1.2.2. doi:10.5281/zenodo.8145703
- Nunan, N., 2017. The microbial habitat in soil: Scale, heterogeneity and functional consequences. *Journal of Plant Nutrition and Soil Science* 180, 425–429. doi:10.1002/jpln.201700184
- Nunan, N., Schmidt, H., Raynaud, X., 2020. The ecology of heterogeneity: soil bacterial communities and C dynamics. *Philosophical Transactions of the Royal Society B: Biological Sciences* 375, 20190249. doi:http://dx.doi.org/10.1098/rstb.2019.0249
- Öquist, M.G., Erhagen, B., Haei, M., et al., 2017. The effect of temperature and substrate quality on the carbon use efficiency of saprotrophic decomposition. *Plant and Soil* 414, 113–125. doi:10.1007/s11104-016-3104-x
- Panikov, N.S., 1995. *Microbial Growth Kinetics*. Chapman and Hall, London, Glasgow.
- Papp, K., Hungate, B.A., Schwartz, E., 2020. Glucose triggers strong taxon-specific responses in microbial growth and activity: insights from DNA and RNA qSIP. *Ecology* 101. doi:10.1002/ecy.2887
- Parkhurst, D.L., Appelo, C.A.J., 2013. Description of input and examples for PHREEQC version 3: a computer program for speciation, batch-reaction, one-dimensional transport, and inverse geochemical calculations (Report No. 6-A43), Techniques and Methods. Reston, VA. doi:10.3133/tm6A43
- Parton, W.J., Schimel, D.S., Cole, C.V., Ojima, D.S., 1987. Analysis of Factors Controlling Soil Organic Matter Levels in Great Plains Grasslands. *Soil Science Society of America Journal* 51, 1173–1179. doi:10.2136/sssaj1987.03615995005100050015x
- Peng, X., Gao, S., Ma, S., et al., 2024. Repeated labile carbon inputs trigger soil microbial necromass decomposition through increasing microbial diversity and hierarchical interactions. *Soil Biology and Biochemistry* 191, 109344. doi:10.1016/j.soilbio.2024.109344
- Perveen, N., Barot, S., Maire, V., et al., 2019. Universality of priming effect: An analysis using thirty five soils with contrasted properties sampled from five continents. *Soil*

- Biology and Biochemistry 134, 162–171. doi:10.1016/j.soilbio.2019.03.027
- Peter Linstrom, 2017. NIST Chemistry WebBook - SRD 69. National Institute of Standards and Technology.
- Pinheiro, M., Garnier, P., Beguet, J., Martin Laurent, F., Vieubl  Gonod, L., 2015. The millimetre-scale distribution of 2,4-D and its degraders drives the fate of 2,4-D at the soil core scale. *Soil Biology and Biochemistry* 88, 90–100. doi:10.1016/j.soilbio.2015.05.008
- Piton, G., Allison, S.D., Bahram, M., et al., 2023. Life history strategies of soil bacterial communities across global terrestrial biomes. *Nature Microbiology* 8, 2093–2102. doi:10.1038/s41564-023-01465-0
- Powlson, D., Xu, J., Brookes, P., 2017. Through the Eye of the Needle — The Story of the Soil Microbial Biomass, in: *Microbial Biomass. WORLD SCIENTIFIC (EUROPE)*, pp. 1–40. doi:10.1142/9781786341310_0001
- R Core Team, 2023. R: A Language and Environment for Statistical Computing. R Foundation for Statistical Computing, Vienna, Austria.
- Richter, A., Kern, T., Wolf, S., Struck, U., Ruess, L., 2019. Trophic and non-trophic interactions in binary links affect carbon flow in the soil micro-food web. *Soil Biology and Biochemistry* 135, 239–247. doi:10.1016/j.soilbio.2019.04.010
- Roels, J.A., 1980. Application of macroscopic principles to microbial metabolism. *Biotechnology and Bioengineering* 22, 2457–2514. doi:10.1002/bit.260221202
- Rossum, G. van, 1995. Python tutorial (No. CS-R9526). Centrum voor Wiskunde en Informatica (CWI), Amsterdam.
- RStudio Team, 2020. RStudio: Integrated Development Environment for R. RStudio, PBC., Boston, MA.
- Ruamps, L.S., Nunan, N., Chenu, C., 2011. Microbial biogeography at the soil pore scale. *Soil Biology and Biochemistry* 43, 280–286. doi:10.1016/j.soilbio.2010.10.010
- Schimel, J., 2023. Modeling ecosystem-scale carbon dynamics in soil: The microbial dimension. *Soil Biology and Biochemistry* 178, 108948. doi:10.1016/j.soilbio.2023.108948
- Schimel, J.P., Schaeffer, S.M., 2012. Microbial control over carbon cycling in soil. *Frontiers in Microbiology* 3. doi:10.3389/fmicb.2012.00348
- Schl ter, S., Lucas, M., Grosz, B., et al., 2024. The anaerobic soil volume as a controlling factor of denitrification: a review. *Biology and Fertility of Soils*. doi:10.1007/s00374-024-01819-8
- Schr dinger, E., 1944. *What is Life?: The Physical Aspect of the Living Cell*. Cambridge University Press.
- Seeliger, S., Janssen, P.H., Schink, B., 2002. Energetics and kinetics of lactate fermentation to acetate and propionate via methylmalonyl-CoA or acrylyl-CoA. *FEMS Microbiology Letters* 211, 65–70. doi:10.1111/j.1574-6968.2002.tb11204.x
- Shi, A., Chakrawal, A., Manzoni, S., et al., 2021. Substrate spatial heterogeneity reduces soil microbial activity. *Soil Biology and Biochemistry* 152, 108068. doi:10.1016/j.soilbio.2020.108068
- Sierra, C.A., Malghani, S., M ller, M., 2015. Model structure and parameter identification of soil organic matter models. *Soil Biology and Biochemistry* 90, 197–203. doi:10.1016/j.soilbio.2015.08.012
- Simon, C., Miltner, A., Mulder, I., et al., 2024. Long-term effects of farmyard manure addition on soil organic matter molecular composition: C transformation as a major driver of energetic potential. doi:10.21203/rs.3.rs-4542343/v1
- Sinsabaugh, R.L., Manzoni, S., Moorhead, D.L., Richter, A., 2013. Carbon use efficiency of

- microbial communities: stoichiometry, methodology and modelling. *Ecology Letters* 16, 930–939. doi:10.1111/ele.12113
- Sinsabaugh, R.L., Turner, B.L., Talbot, J.M., et al., 2016. Stoichiometry of microbial carbon use efficiency in soils. *Ecological Monographs* 86, 172–189. doi:10.1890/15-2110.1
- Sircan, A.K., Streck, T., Schnepf, A., et al., 2025. Trait-based modeling of microbial interactions and carbon turnover in the rhizosphere. *Soil Biology and Biochemistry* 202, 109698. doi:10.1016/j.soilbio.2024.109698
- Smart, K.E., Breecker, D.O., Blackwood, C.B., Gallagher, T.M., 2024. A new approach to continuous monitoring of carbon use efficiency and biosynthesis in soil microbes from measurement of CO₂ and O₂. doi:10.5194/egusphere-2024-1757
- Smercina, D.N., Bailey, V.L., Hofmockel, K.S., 2021. Micro on a macroscale: relating microbial-scale soil processes to global ecosystem function. *FEMS Microbiology Ecology* 97, fiab091. doi:10.1093/femsec/fiab091
- Song, H.-S., Stegen, J.C., Graham, E.B., et al., 2020. Representing Organic Matter Thermodynamics in Biogeochemical Reactions via Substrate-Explicit Modeling. *Frontiers in Microbiology* 11, 531756. doi:10.3389/fmicb.2020.531756
- Sparling, G.P., West, A.W., 1988. A direct extraction method to estimate soil microbial C: calibration in situ using microbial respiration and ¹⁴C labelled cells. *Soil Biology and Biochemistry* 20, 337–343. doi:10.1016/0038-0717(88)90014-4
- Stone, B.W., Li, J., Koch, B.J., et al., 2021. Nutrients cause consolidation of soil carbon flux to small proportion of bacterial community. *Nature Communications* 12, 3381. doi:10.1038/s41467-021-23676-x
- Sulman, B.N., Moore, J.A.M., Abramoff, R., et al., 2018. Multiple models and experiments underscore large uncertainty in soil carbon dynamics. *Biogeochemistry* 141, 109–123. doi:10.1007/s10533-018-0509-z
- Tang, J., Riley, W.J., Manzoni, S., Maggi, F., 2024. Feasibility of Formulating Ecosystem Biogeochemical Models From Established Physical Rules. *Journal of Geophysical Research: Biogeosciences* 129, e2023JG007674. doi:10.1029/2023JG007674
- Tao, F., Huang, Y., Hungate, B.A., et al., 2023. Microbial carbon use efficiency promotes global soil carbon storage. *Nature* 618, 981–985. doi:10.1038/s41586-023-06042-3
- Thomson, B.C., Ostle, N.J., McNamara, N.P., Whiteley, A.S., Griffiths, R.I., 2010. Effects of sieving, drying and rewetting upon soil bacterial community structure and respiration rates. *Journal of Microbiological Methods* 83, 69–73. doi:10.1016/j.mimet.2010.07.021
- Thornton, W.M., 1917. XV. The relation of oxygen to the heat of combustion of organic compounds. *The London, Edinburgh, and Dublin Philosophical Magazine and Journal of Science* 33, 196–203. doi:10.1080/14786440208635627
- Todd-Brown, K.E.O., Randerson, J.T., Post, W.M., et al., 2013. Causes of variation in soil carbon simulations from CMIP5 Earth system models and comparison with observations. *Biogeosciences* 10, 1717–1736. doi:10.5194/bg-10-1717-2013
- Ugalde-Salas, P., Desmond-Le Quémener, E., Harmand, J., Rapaport, A., Bouchez, T., 2020. Insights from Microbial Transition State Theory on Monod's Affinity Constant. *Scientific Reports* 10, 5323. doi:10.1038/s41598-020-62213-6
- Valderrama-Bahamóndez, G.I., Fröhlich, H., 2019. MCMC Techniques for Parameter Estimation of ODE Based Models in Systems Biology. *Frontiers in Applied Mathematics and Statistics* 5, 55. doi:10.3389/fams.2019.00055
- van Bodegom, P., 2007. Microbial Maintenance: A Critical Review on Its Quantification. *Microbial Ecology* 53, 513–523. doi:10.1007/s00248-006-9049-5
- Van Bommel, M., Arndt, K., Endress, M.-G., et al., 2024. Under the lens: Carbon and energy

- channels in the soil micro-food web. *Soil Biology and Biochemistry* 199, 109575. doi:10.1016/j.soilbio.2024.109575
- Vance, E.D., Brookes, P.C., Jenkinson, D.S., 1987. An extraction method for measuring soil microbial biomass C. *Soil Biology and Biochemistry* 19, 703–707. doi:10.1016/0038-0717(87)90052-6
- Virtanen, P., Gommers, R., Oliphant, T.E., et al., 2020. SciPy 1.0: Fundamental Algorithms for Scientific Computing in Python. *Nature Methods* 17, 261–272. doi:10.1038/s41592-019-0686-2
- Vogel, H.-J., Amelung, W., Baum, C., et al., 2024. How to adequately represent biological processes in modeling multifunctionality of arable soils. *Biology and Fertility of Soils* 60, 263–306. doi:10.1007/s00374-024-01802-3
- von Stockar, U., Liu, J.-S., 1999. Does microbial life always feed on negative entropy? Thermodynamic analysis of microbial growth. *Biochimica et Biophysica Acta (BBA) - Bioenergetics* 1412, 191–211. doi:10.1016/S0005-2728(99)00065-1
- von Stockar, U., Marison, I.W., 1993. The definition of energetic growth efficiencies for aerobic and anaerobic microbial growth and their determination by calorimetry and by other means. *Thermochimica Acta* 229, 157–172. doi:10.1016/0040-6031(93)80323-3
- von Stockar, U., Maskow, T., Liu, J., Marison, I.W., Patiño, R., 2006. Thermodynamics of microbial growth and metabolism: An analysis of the current situation. *Journal of Biotechnology* 121, 517–533. doi:10.1016/j.jbiotec.2005.08.012
- Wan, B., Liu, T., Gong, X., et al., 2022. Energy flux across multitrophic levels drives ecosystem multifunctionality: Evidence from nematode food webs. *Soil Biology and Biochemistry* 169, 108656. doi:10.1016/j.soilbio.2022.108656
- Wang, C., Kuzyakov, Y., 2023. Energy use efficiency of soil microorganisms: Driven by carbon recycling and reduction. *Global Change Biology gcb*.16925. doi:10.1111/gcb.16925
- Wang, G., Jagadamma, S., Mayes, M.A., et al., 2015. Microbial dormancy improves development and experimental validation of ecosystem model. *The ISME Journal* 9, 226–237. doi:10.1038/ismej.2014.120
- Wang, G., Post, W.M., 2012. A theoretical reassessment of microbial maintenance and implications for microbial ecology modeling. *FEMS Microbiology Ecology* 81, 610–617. doi:10.1111/j.1574-6941.2012.01389.x
- Wang, Jieying, Xu, X., Liu, Y., et al., 2024. Unknown bacterial species lead to soil CO₂ emission reduction by promoting lactic fermentation in alpine meadow on the Qinghai-Tibetan Plateau. *Science of The Total Environment* 906, 167610. doi:10.1016/j.scitotenv.2023.167610
- Wieder, W.R., Allison, S.D., Davidson, E.A., et al., 2015. Explicitly representing soil microbial processes in Earth system models. *Global Biogeochemical Cycles* 29, 1782–1800. doi:10.1002/2015GB005188
- Wieder, W.R., Grandy, A.S., Kallenbach, C.M., Bonan, G.B., 2014. Integrating microbial physiology and physio-chemical principles in soils with the Microbial-MIneral Carbon Stabilization (MIMICS) model. *Biogeosciences* 11, 3899–3917. doi:10.5194/bg-11-3899-2014
- Wiegel, J., Tanner, R., Rainey, F.A., 2006. An Introduction to the Family Clostridiaceae, in: Dworkin, M., Falkow, S., Rosenberg, E., Schleifer, K.-H., Stackebrandt, E. (Eds.), *The Prokaryotes: Volume 4: Bacteria: Firmicutes, Cyanobacteria*. Springer US, New York, NY, pp. 654–678. doi:10.1007/0-387-30744-3_20
- Wirsching, J., Endress, M.-G., Di Lodovico, E., et al., 2024. Coupling energy balance and carbon flux during cellulose degradation in arable soils. *Soil Biology and*

- Biochemistry 202, 109691. doi:10.1016/j.soilbio.2024.109691
- Wu, L., Xu, H., Xiao, Q., et al., 2020. Soil carbon balance by priming differs with single versus repeated addition of glucose and soil fertility level. *Soil Biology and Biochemistry* 148, 107913. doi:10.1016/j.soilbio.2020.107913
- Wutzler, T., Blagodatsky, S.A., Blagodatskaya, E., Kuzyakov, Y., 2012. Soil microbial biomass and its activity estimated by kinetic respiration analysis – Statistical guidelines. *Soil Biology and Biochemistry* 45, 102–112. doi:10.1016/j.soilbio.2011.10.004
- Xu, X., Thornton, P.E., Post, W.M., 2013. A global analysis of soil microbial biomass carbon, nitrogen and phosphorus in terrestrial ecosystems. *Global Ecology and Biogeography* 22, 737–749. doi:10.1111/geb.12029
- Yang, S., Di Lodovico, E., Rupp, A., et al., 2024. Enhancing insights: exploring the information content of calorespirometric ratio in dynamic soil microbial growth processes through calorimetry. *Frontiers in Microbiology* 15, 1321059. doi:10.3389/fmicb.2024.1321059
- Zheng, J., Scheibe, T.D., Boye, K., Song, H.-S., 2024. Thermodynamic control on the decomposition of organic matter across different electron acceptors. *Soil Biology and Biochemistry* 193, 109364. doi:10.1016/j.soilbio.2024.109364

Appendix

For high-resolution versions of all figures, please refer to the published online versions of the supplementary materials.

Supplementary material of Endress et al. (2024a)

This supplementary material consists of the following components:

- SI Data. Excel file containing all calorimetry and biomass data analyzed in this study, as well as relative abundances of the major bacterial phyla during the incubations.
- SI OTU Table. Excel file that includes the taxonomic assignments and relative abundances for all replicates.
- SI Text. PDF file containing supplementary materials and methods, Supplementary Figs. S1–S7, Supplementary Tables S1–S2, and supplementary references.

SI Text is provided below. For SI Data and SI OTU Table, please refer to the online version of the published article.

1 **Supplementary Information:**

2 **The coupling of carbon and energy fluxes reveals anaerobiosis in an aerobic soil incubation**
3 **with a *Bacillota*-dominated community**

4 Authors:

5 Martin-Georg Endress*, Ruirui Chen*, Evgenia Blagodatskaya, Sergey Blagodatsky

6 * ... These authors contributed equally to this work

7 **Corresponding Author: Martin-Georg A. Endress**

8 **Email:** m.endress@uni-koeln.de

9 This supplementary information includes:

10 Supplementary materials and methods

11 Supplementary figures S1 to S7

12 Supplementary tables S1 and S2

13 Supplementary references

14 Other supplementary materials for this manuscript include the following:

15 SI Data

16 SI OTU Table

18 Supplementary materials and methods

19 A Correction of CO₂ emissions for alkaline pH

20 The soil used in this study is characterized by a high pH of 8.45 and the presence of CaCO₃. To
21 account for carbon remaining in the soil solution as (bi-)carbonates instead of being released as
22 CO₂ to the headspace, we compute the equilibrium concentrations of all carbon species (CO₂ +
23 H₂CO₃, HCO₃⁻ and CO₃²⁻) in the solution given the measured atmospheric CO₂ levels, assuming
24 the presence of (excess) CaCO₃. To that end, we use the constants and calculations presented
25 in (1) and the references therein.

26 In brief, the equilibrium pH of the soil solution at a given atmospheric partial pressure P_{CO_2} and
27 temperature T can be calculated from the electroneutrality requirement:

$$28 \quad 2[Ca^{2+}] + [H^+] = [HCO_3^-] + 2[CO_3^{2-}] + [OH^-] = \frac{2K_{cal}}{c} + h = b + 2c + \frac{K_w}{h} \quad (\text{Eqn. S1}).$$

29 Here, K_{cal} is the solubility product of calcite at the given temperature T , K_w is the equilibrium
30 constant of the self-ionization of water (at T), h is the equilibrium concentration of protons $[H^+]$,
31 and b and c are the equilibrium concentrations of bicarbonate and carbonate ions, $[HCO_3^-]$ and
32 $[CO_3^{2-}]$, respectively. Substituting the expressions

$$33 \quad [H_2CO_3] = K_0 P_{CO_2}$$

$$34 \quad [HCO_3^-] = [H_2CO_3] K_1 / [H^+]$$

$$35 \quad [CO_3^{2-}] = [HCO_3^-] K_2 / [H^+]$$

36 and using the known solubility (K_0) and first and second dissociation constants (K_1 , K_2) of
37 carbonic acid in water at temperature T yields the equation

$$38 \quad \left(\frac{K_0 K_1}{h} + 2 \frac{K_0 K_1 K_2}{h^2}\right) P_{CO_2}^2 + \left(\frac{K_w}{h} - h\right) P_{CO_2} + 2 \frac{K_{cal} h^2}{K_0 K_1 K_2} = 0 \quad (\text{Eqn. S2})$$

39 Equation S2 was solved symbolically for h using the *sympy* package (version 1.9) in Python
40 (version 3.9.7). We corrected for the higher incubation temperature of 28°C using the
41 temperature dependencies provided in (1). We assume no significant change in pressure during
42 the incubation.

If the chemical equilibria establish faster than (a significant amount of) additional C is released by microbes, this then allows the computation of the concentrations of all carbon species at the measurement times. The measured (cumulative) atmospheric CO₂ at each timepoint is then corrected by a factor

$$f = \frac{n_{air} + n_{sol} - n_{Ca}}{n_{air}} > 1 \text{ (Eqn. S3)}$$

where n_{air} is the (measured) amount of C in atmospheric CO₂, n_{sol} is the amount of C in dissolved carbon species, and n_{Ca} is the amount of C released due to dissolution of CaCO₃ (i.e., not of microbial origin). All quantities were expressed per gram of soil.

Since the amount of dissolved CaCO₃ and the heat release of the dissolution reaction are comparatively small, we assume that this contribution to measured heat is negligible.

B Biomass estimation by SIR and analysis of exponential phase

The phase of exponential growth was analyzed by fitting

$$R_{CO_2}(t) = A + B \cdot \exp(\mu t) \text{ (Eqn. S4)}$$

to the measured respiration rate, where A is the initial rate uncoupled from growth, B is the initial rate of the growing fraction, μ is the maximal specific growth rate of soil microorganisms, and t is incubation time. The theoretical background and derivation of equation S4 has been described in detail in previous publications (2,3). The parameters of equation S4 were optimized by minimizing the least-square sum using the *curve_fit* function in the *scipy* package (version 1.11.0) in Python. The first two respiration measurements were discarded due to the initial disturbance caused by the incubation setup.

The duration of the lag period (T_{lag}) was calculated as

$$T_{lag} = \frac{\ln(A/B)}{\mu} \text{ (Eqn. S5)}$$

and the initial active fraction (r_0) was calculated as

$$r_0 = \frac{0.1 \cdot B}{A + 0.1 \cdot B} \text{ (Eqn. S6)}$$

Estimates based on the rate of heat release instead of CO₂ release yielded similar values for T_{lag} and r_0 .

Initial soil microbial biomass C (MBC) was evaluated by the initial rate of substrate-induced respiration (SIR) (Anderson and Joergensen, 1997). The initial rate of CO₂ production [$\mu\text{g C/g/h}$] was estimated as the slope of the linear regression of the first 4 hrs of cumulative CO₂ measurements using the *linregress* function in the *scipy* package in Python ($R^2 = 0.988$). CO₂ production was then converted to microbial biomass as proposed by Anderson and Domsch (4) using the conversion factor suggested in Kaiser et al. 1992 (5) for arable soils with further correction for incubation temperature (28 °C) as detailed in Beck et al. 1997 (6). Overall, considering the conversion of $\mu\text{g C}$ to $\mu\text{L CO}_2$, since the latter was used in the original regression proposed by (5), SIR-MBC was calculated as

$$MBC = 1.89 \cdot 30 \cdot 0.73 \cdot SIR . \quad (\text{Eqn. S7})$$

C Dynamic model formulation

We describe the various aspects of the dynamic model below.

C1 ODE System

The dynamics of the incubated soil are described using a system of 8 coupled ordinary differential equations (ODE) representing the different carbon pools (glucose S , biomass X , lactate L , final fermentation products P , and CO₂) as well as oxygen (O₂) and heat (Q) per gram soil, and finally the physiological state of the microbial population, indicating the active fraction of microbes ($r \in [0, 1]$) (7). All carbon pools are measured in mol C.

All state variables and parameters along with their units and calibrated values are listed in supplementary table S2.

The full ODE system reads:

$$\frac{dS}{dt} = -U_{glu} - r_{S_a} - r_{S_i} \quad (\text{Eqn. S8})$$

$$\frac{dX}{dt} = \alpha(Y_{ae,glu}U_{glu} + Y_{ae,lac}U_{lac}) + (1 - \alpha)(Y_{f,glu}U_{glu} + Y_{f,lac}U_{lac}) - r_{X_a} - r_{X_i} \quad (\text{Eqn. S9})$$

$$\frac{dL}{dt} = (1 - \alpha)(Y_L U_{glu} + r_{S_a} + r_{S_i}) - U_{lac} - r_{L_a} - r_{L_i} \quad (\text{Eqn. S10})$$

$$\frac{dP}{dt} = \frac{8}{9}(1 - \alpha) \left(\left(1 - \frac{Y_{f,lac}Y_X}{Y_L} \right) U_{lac} + r_{L_a} + r_{L_i} \right) \quad (\text{Eqn. S11})$$

$$\begin{aligned} \frac{dCO_2}{dt} = & \alpha \left((1 - Y_{ae,glu})U_{glu} + (1 - Y_{ae,lac})U_{lac} + r_{S_a} + r_{S_i} + r_{L_a} + r_{L_i} \right) \\ & + (1 - \alpha) \left((1 - Y_{f,glu} - Y_L)U_{glu} + \left(\frac{1}{9} - Y_{f,lac} + \frac{\frac{8}{9}Y_{f,lac}Y_X}{Y_L} \right)U_{lac} + \frac{1}{9}(r_{L_a} + r_{L_i}) \right) + r_{X_a} + r_{X_i} \end{aligned} \quad (\text{Eqn. S12})$$

$$\begin{aligned} \frac{dQ}{dt} = & \alpha (\Delta H_{ae,glu}U_{glu} + \Delta H_{ae,lac}U_{lac} + \Delta_{cat}H_{ae,glu}(r_{S_a} + r_{S_i}) + \Delta_{cat}H_{ae,lac}(r_{L_a} + r_{L_i})) \\ & + (1 - \alpha) (\Delta H_{f,glu}U_{glu} + \Delta H_{f,lac}U_{lac} + \Delta_{cat}H_{f,glu}(r_{S_a} + r_{S_i}) + \Delta_{cat}H_{f,lac}(r_{L_a} + r_{L_i})) \\ & + \Delta H_M(r_{X_a} + r_{X_i}) \end{aligned} \quad (\text{Eqn. S13})$$

$$\frac{dO_2}{dt} = -\alpha \left(\left(1 - \frac{Y_X}{Y_S} Y_{ae,glu} \right) U_{glu} + \left(1 - \frac{Y_X}{Y_S} Y_{ae,lac} \right) U_{lac} + M_a + M_i \right) \quad (\text{Eqn. S14})$$

$$\frac{dr}{dt} = Y_{ae,glu}v_m r \left(\frac{S+L}{S+L+K_r} - r \right) \quad (\text{Eqn. S15})$$

Here, the following process rates were used:

$$U_{glu} = v_m r X \frac{S}{S+K_S} \quad (\text{Eqn. S16}) \dots \text{Utilization of glucose for growth (Michaelis-Menten (MM) kinetics)}$$

$$U_{lac} = v_m r X \frac{L}{L+K_L} \left(1 - \frac{S}{S+K_S} \right)$$

(Eqn. S17) ... Utilization of lactate for growth (MM, preferential use of glucose)

$$M_a = m_a r X \quad (\text{Eqn. S18}) \dots \text{Maintenance flux of the active fraction (a)}$$

$$M_i = m_i (1 - r) X \quad (\text{Eqn. S19}) \dots \text{Maintenance flux of the inactive fraction (i)}$$

$$r_{S_*} = M_* \frac{S}{S+K_S} \quad (\text{Eqn. S20}) \dots \text{Part of maintenance flux fueled by glucose utilization (* = i or a)}$$

$$r_{L_*} = (M_* - r_{S_*}) \cdot \frac{L}{L+K_L} \quad (\text{Eqn. S21}) \dots \text{Part of maintenance flux fueled by lactate utilization (* = i or a)}$$

$$r_{X_*} = M_* - r_{S_*} - r_{L_*} \quad (\text{Eqn. S22}) \dots \text{Part of maintenance flux fueled by biomass utilization (* = i or a)}$$

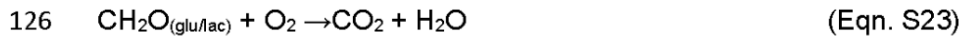
C2 Oxygen

For all of these processes, substrates (glucose, lactate or biomass) are used by microbes either aerobically or anaerobically, depending on the local availability of O₂ in the soil. Specifically, the fraction of the (growth or maintenance) flux realized via the aerobic pathway is determined by

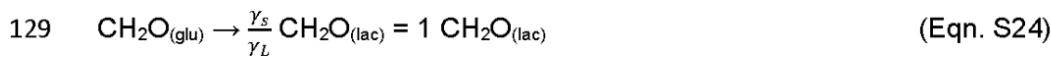
116 the aerobic fraction $\alpha = \frac{O_2}{K_{O_2} + O_2}$, while the remaining flux according to the anaerobic fraction $1 - \alpha$
 117 is realized via the anaerobic pathway. This partitioning of the metabolic reactions according to
 118 the aerobic and anaerobic fractions is inspired by the framework presented in Chakrawal et al.
 119 2020 (8), and the dynamic aerobic fraction is calculated as the (instantaneous, local) saturation
 120 of O_2 as measured by the half-saturation constant K_{O_2} , thus representing O_2 as an additional
 121 substrate. The concentration of soil O_2 changes during the simulation due to the (stoichiometric)
 122 consumption of O_2 in the aerobic reactions taking place in the closed system.

123 **C3 Metabolic pathways**

124 For both glucose and lactate, aerobic respiration to CO_2 with O_2 as electron acceptor represents
 125 the aerobic pathway, with the following catabolic reaction (expressed for 1 mol C of substrate):

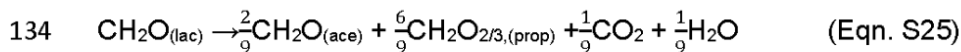


127 For glucose, we consider lactic acid fermentation as the anaerobic pathway, with the following
 128 catabolic reaction:

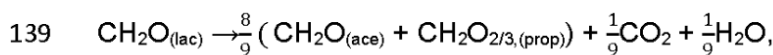


130 Here, $\gamma_S = 4$ again denotes the degree of reduction of glucose, and $\gamma_L = 4$ denotes the degree
 131 of reduction of lactic acid.

132 For lactic acid, we consider the fermentation to propionate and acetate as the anaerobic
 133 pathway, with the following catabolic reaction [Seeliger et al 2002]:



135 In our model, acetate and propionate accumulate as fermentation end products. For the
 136 purposes of the analysis, these two compounds are therefore combined into a single variable P .
 137 For the modelling purposes of simulating the flow of carbon and energy we may thus summarize
 138 Eqn. S25 as

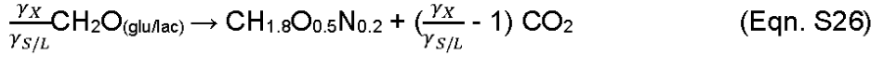


140 because we are not covering the fate of the formed acetate/propionate.

If no substrate is available, microbes start to catabolize their own biomass to fuel their maintenance requirements. In terms of carbon fluxes in our model, we represent this as a direct conversion of biomass carbon to CO₂, since we have no information regarding the specific (aerobic and anaerobic) pathways or compounds involved in this process.

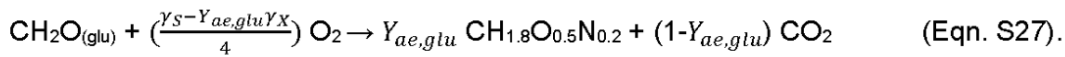
These catabolic reactions are assumed to fuel all maintenance fluxes. Thus, for a given maintenance flux specified in the model, e.g., $\alpha \cdot r_{S_a}$ (maintenance flux from aerobic utilization of glucose), the corresponding catabolic reaction (Eqn. S23) proceeds at rate $\alpha \cdot r_{S_a}$.

For the growth of microbes (U_{glu} and U_{lac}), we use the generic formula CH_{1.8}O_{0.5}N_{0.2} for microbial biomass and represent the anabolic reaction from glucose or lactic acid following the electron balance approach (9):

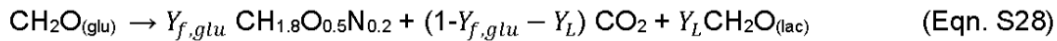


Here, $\gamma_X = 4.2$ denotes the degree of reduction of biomass, and $\gamma_{S/L} = 4$ denotes the degree of reduction of glucose or lactate. NH₃ is assumed to be the source of nitrogen in biomass. Hydrogen can be balanced by adding H₂O to either side.

The respective catabolic reactions and the anabolic reaction are then combined according to the yield coefficient (Y) of the respective pathway to form an overall growth reaction for the consumption of 1 mol C of substrate, as detailed in Chakrawal et al. 2020. For example, for the aerobic growth on glucose, the catabolic and anabolic reactions (Eqn. S23 and S26) are multiplied by $(1 - Y_{ae,glu} \frac{\gamma_X}{\gamma_S})$ and $Y_{ae,glu}$ respectively, such that their sum yields the overall growth reaction proceeding at rate $\alpha \cdot U_{glu}$:

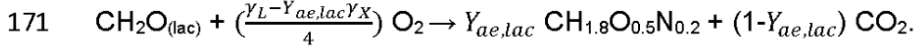


In the case of lactic acid fermentation, using multiplication factors $(1 - Y_{f,glu} \frac{\gamma_X}{\gamma_S})$ and $Y_{f,glu}$, this yields the reaction

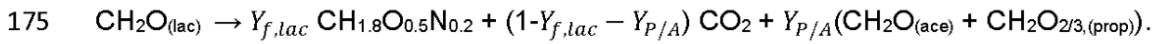


proceeding at rate $(1 - \alpha) \cdot U_{glu}$, where $Y_L = \frac{\gamma_S - Y_{f,glu} \gamma_X}{\gamma_L}$ is the stoichiometric coefficient of formed lactic acid.

167 The growth reactions for the aerobic and anaerobic growth on lactate are obtained equivalently
 168 and proceed at rates $\alpha \cdot U_{lac}$ and $(1 - \alpha) \cdot U_{lac}$, respectively. For aerobic respiration, we again
 169 sum the catabolic reaction (Eqn. S23) and anabolic reaction (Eqn. S26) using factors $(1 -$
 170 $Y_{ae,lac} \frac{Y_X}{Y_L})$ and $Y_{ae,lac}$ to get the overall growth reaction



172 For anaerobic fermentation of lactic acid to acetate and propionate, we sum the catabolic
 173 reaction (Eqn. S25) and anabolic reaction (Eqn. S26) using factors $(1 - Y_{f,lac} \frac{Y_X}{Y_L})$ and $Y_{f,lac}$ and
 174 obtain the overall growth reaction



176 Here, $Y_{P/A}$ is the yield of acetate and propionate of the growth reaction, $Y_{P/A} = \frac{8}{9} \left(1 - \frac{Y_{f,lac} Y_X}{Y_L}\right)$.

177 The ODE system (Eqn. S8-S15) is constructed using the stoichiometry and the rates of all of
 178 these reactions, following the scheme aerobic/anaerobic fraction * growth (U) * stoichiometric
 179 coefficient. We illustrate this with the rather complex expression for the CO_2 production (Eqn.
 180 S12) of the overall growth reaction for fermentation of lactic acid above. The anaerobic
 181 fermentation of lactic acid contributes to the production of CO_2 with the term

$$182 (1 - \alpha) \cdot U_{lac} \cdot (1 - Y_{f,lac} - Y_{P/A}) = (1 - \alpha) \cdot U_{lac} \cdot \left(1 - Y_{f,lac} - \frac{8}{9} \left(1 - \frac{Y_{f,lac} Y_X}{Y_L}\right)\right)$$

$$183 = (1 - \alpha) \cdot U_{lac} \cdot \left(1 - Y_{f,lac} - \frac{8}{9} + \frac{8}{9} \cdot \frac{Y_{f,lac} Y_X}{Y_L}\right) = (1 - \alpha) \cdot U_{lac} \cdot \left(\frac{1}{9} - Y_{f,lac} + \frac{8}{9} \cdot \frac{Y_{f,lac} Y_X}{Y_L}\right),$$

184 which results in this term in Eqn. S12. For maintenance rates (r), the coefficients of the catabolic
 185 reactions can be used directly.

186 **C4 Substrate utilization**

187 Both for growth and maintenance, we assume that glucose is used preferentially over lactate,
 188 and both glucose and lactate are used preferentially over biomass to fuel maintenance
 189 requirements.

Specifically, microbes first utilize the preferred substrate according to its MM-availability and make up the difference to achieve the maximum process rate (controlled by v_m and $m_{i/a}$) by using other substrates according to their availability. For maintenance, this implies a switching of endogenous and exogenous maintenance (10,11).

C5 Heat production

Combined, the processes described so far yield the differential equations for the different carbon pools as well as O_2 . To obtain the overall heat production rate, we compute the reaction enthalpies $\Delta_r H$ for each of the catabolic and growth reactions using Hess's law per mol C of substrate:

$$\Delta_r H = \sum_i a_i \Delta_f H_{product\ i} - \sum_j b_j \Delta_f H_{reactant\ j} \text{ with stoichiometric coefficients } a_i, b_j \quad (\text{Eqn. S29})$$

For the catabolic reactions, we use known values of the enthalpies of formation $\Delta_f H$ of the simple chemical compounds involved. These values are publicly available, e.g. in NIST Chemistry WebBook (12). The calculations yield the following reaction enthalpies (per mol C of substrate):

$$\Delta_{cat} H_{ae,glu} = -469 \text{ kJ} \quad (\text{Eqn. S30})$$

$$\Delta_{cat} H_{f,glu} = -18.33 \text{ kJ} \quad (\text{Eqn. S31})$$

$$\Delta_{cat} H_{ae,lac} = -458.8 \text{ kJ} \quad (\text{Eqn. S32})$$

$$\Delta_{cat} H_{f,lac} = -13.88 \text{ kJ} \quad (\text{Eqn. S33})$$

Note that these values are given for a standard reference temperature of 25°C, while experimental temperature was 28°C. In principle, the values can be corrected using the heat capacity of all of the involved compounds (Kirchhoff's law of thermochemistry), which are also publicly available, e.g. from NIST. However, the effect is negligible for our purposes. For example, we calculate a change in $\Delta_{cat} H_{ae,glu}$ of less than 0.5 kJ/mol C for the given temperature difference of 3°C. Therefore, we proceed with the analysis using the reference values. We also assume no significant change in pressure over the course of the incubation,

since we expect the consumption of O₂ to be largely balanced by the production of CO₂, which is not continuously removed in our setup (as it would be, for example, when using alkali traps).

Since the anabolic reaction is written using the electron balance approach, its reaction enthalpy is 0 regardless of substrate, i.e. $\Delta_r H_{ana} = 0$ (9). Therefore, the reaction enthalpy of the growth reaction $\Delta_{growth} H_*$ can be computed from the reaction enthalpy of the involved catabolic reaction ($\Delta_{cat} H_*$) and the yield coefficient of the pathway (Y_*):

$$\Delta_{growth} H_* = (1 - Y_* \frac{Y_x}{Y_s}) \Delta_{cat} H_* \quad (\text{Eqn. S34})$$

Moreover, we assume that the maintenance flux fueled by biomass degradation releases a similar amount of heat per CO₂ as the sum of other catabolic reactions carried out by the microbes at the time, and set the reaction enthalpy ΔH_M accordingly. Since we have no information about the biochemical pathways involved in this process, this assumption implies that the degradation of biomass compounds for maintenance predominantly happens along the same catabolic pathways that are currently used by the microbes to degrade substrate.

Specifically, at every time step in the model, maintenance from biomass decomposition contributes CO₂ at a rate $r_X = r_{Xa} + r_{Xi}$. To obtain the enthalpy ΔH_M that gives the appropriate rate of heat release, we compute the CR that would result from only the 4 catabolic reactions (aerobic and anaerobic catabolism on glucose and lactic acid) taking place. This can be calculated using Eqn. S12 and S13 by substituting the growth reaction enthalpies with their catabolic counterparts, setting all growth yields to zero, and dropping any terms with r_X . Let's call the resulting value CR_{cat} . Then, choosing $\Delta H_M = CR_{cat}$ results in the desired property, i.e., the rate of CO₂ and heat release from decomposition of biomass due to maintenance is characterized by the desired CR of

$$\frac{r_X \Delta H_M}{r_X} = \Delta H_M = CR_{cat} \text{ matching that of other catabolic reactions carried out at the time.}$$

Finally, the heat production rate of any process is calculated as the product of the process rate (mol C of substrate / h) and the reaction enthalpy (kJ / mol C of substrate).

C6 Microbial activity

The last differential equation describes the conversion of inactive biomass to active biomass and vice versa through the index of physiological state framework introduced by Panikov (7). Intuitively, microbes switch to the active state if there is sufficient substrate, and switch to an inactive state/dormancy otherwise. Since microbes utilize both glucose and lactate in our model, the effective substrate concentration used to determine changes in r is the sum of the glucose and lactate concentrations ($S+L$).

In a typical simulation, the microbes are initially largely inactive, but quickly become active due to the high concentration of added glucose. As the combined concentration of glucose and lactate depletes towards the end of the incubation, the microbial community finally turns inactive again.

D Analysis of model CR

In this section, we describe the main dynamics in the CR produced by the model. A detailed presentation of the underlying considerations can be found in Chakrawal et al 2020 (8). We follow the convention that a positive CR indicates net release of heat (negative reaction enthalpy).

First, it is straightforward to calculate the theoretical CR for each of the metabolic pathways in isolation. Since

$$CR = -\frac{\frac{dQ}{dt}}{\frac{dCO_2}{dt}} \text{ (Eqn. S35),}$$

the CR of a single catabolic reaction can be found as the ratio of its reaction enthalpy and its stoichiometric coefficient of CO_2 , both calculated for the consumption of 1 mol C of substrate.

For example, the theoretical CR of aerobic catabolism of glucose is

$$CR_{cat,ae,glu} = -\frac{\Delta_{cat}H_{ae,glu}}{a_{CO_2}} = -\frac{-469 \text{ kJ}}{1 \text{ mol } CO_2} = 469 \frac{\text{kJ}}{\text{mol C}}. \text{ (Eqn. S36)}$$

Using the stoichiometry and reaction enthalpies presented in section C, we obtain the following values for the CR of the other pure catabolic reactions:

$$CR_{cat,ae,lac} = -\frac{-458.8 \text{ kJ}}{1 \text{ mol } CO_2} = 458.8 \frac{\text{kJ}}{\text{mol C}} \quad \text{(Eqn. S37)}$$

$$CR_{cat,f,glu} = -\frac{-18.33 \text{ kJ}}{0 \text{ mol CO}_2} = \infty \frac{\text{kJ}}{\text{mol C}}. \quad (\text{Eqn. S38})$$

$$CR_{cat,f,lac} = -\frac{-13.88 \text{ kJ}}{\frac{1}{9} \text{ mol CO}_2} \approx 125 \frac{\text{kJ}}{\text{mol C}}. \quad (\text{Eqn. S39})$$

Notably, the two anaerobic reactions (fermentations) yield vastly different CR values, even though their rates of heat release per mol C of substrate are similar. Lactic acid fermentation is characterized by an arbitrarily large CR, because the reaction does not yield CO₂ as a catabolic product while still producing (a small amount of) heat. On the other hand, fermentation of lactate is characterized by a small CR due to catabolic release of CO₂, while still releasing (a similarly small) amount of heat.

Beyond pure catabolism, the theoretical CR of a growth reaction can be calculated using the heat release given by equation S34 and the stoichiometric coefficient of CO₂ in the growth reaction. For example, for aerobic growth on glucose, we have

$$CR_{ae,glu} = -\frac{(1-Y_{ae,glu} \frac{Y_X}{Y_S}) \Delta_{cat} H_{ae,glu}}{1-Y_{ae,glu}} \leq CR_{cat,ae,glu} \quad (\text{Eqn. S40}).$$

Providing an example for fermentation, e.g., for the anaerobic growth on glucose (Eqn. S28), we have

$$CR_{f,glu} = -\frac{(1-Y_{f,glu} \frac{Y_X}{Y_S}) \Delta_{cat} H_{f,glu}}{1-Y_{f,glu}-Y_L} \leq CR_{cat,f,glu}. \quad (\text{Eqn. S41})$$

In all of the considered reactions, the CR of the growth reaction is smaller than that of the corresponding catabolic reaction and decreases with increasing yield coefficient Y (13).

The total CR of the dynamic model at any given point represents the sum of all heat and CO₂ contributions of the processes currently taking place (Eqn. S35). For example, in a system with aerobic growth on glucose proceeding at rate U_{glu} and aerobic maintenance (catabolism) on glucose proceeding at rate M_{glu} , the total CR is

$$CR = -\frac{\frac{dQ}{dt}}{\frac{dCO_2}{dt}} = -\frac{U_{glu} \cdot ((1-Y_{ae,glu} \frac{Y_X}{Y_S}) \Delta_{cat} H_{ae,glu}) + M_{glu} \cdot (\Delta_{cat} H_{ae,glu})}{U_{glu} \cdot (1-Y_{ae,glu}) + M_{glu} \cdot (1)}. \quad (\text{Eqn. S42})$$

Notably, any process proceeding at a high rate or yielding large amounts of heat and CO₂ per mol C of substrate thus has a large impact on the total CR.

Temporal variations in total CR are the result of temporal variations in the contributing processes. In our model, these are a) changes in the relative rates of metabolic pathways due to changing oxygen or substrate availability and b) changes in the active fraction of microbes, since inactive microbes only contribute maintenance fluxes (catabolism), while the active fraction also contributes CO₂ and heat from the growth reactions.

For example, in a purely aerobic model (fixing $\alpha = \frac{O_2}{O_2 + K_{O_2}} = 1$), CR initially drops from the value of catabolic glucose respiration ($469 \frac{kJ}{mol\ C}$) performed by the inactive fraction to fuel their maintenance. This is due to the activation of microbes in the presence of glucose, as their growth is characterized by a lower CR (Eqn. S40). Once glucose is depleted again towards the end of the simulation, the CR returns to the level of pure catabolism, as microbes turn inactive again and only perform maintenance respiration. This pattern is illustrated in Fig. S7 and has also been described in Chakrawal et al. 2021 (14).

In the full calibrated model, the temporal CR dynamics (Fig. S7) can be summarized as follows: Initially, microbes are inactive and CR is close to the value of aerobic maintenance (catabolism) on glucose (Eqn. S23). As microbes become active, CR drops to the value of aerobic growth on glucose, as seen in the aerobic model variant (Eqn. S26). As O₂ is subsequently depleted during exponential growth, fermentation of glucose to lactate becomes a major process, elevating total CR (Eqn. S24 and associated growth reaction). Once glucose is depleted, microbes turn to the fermentation of accumulated lactate with a corresponding drop of CR (Eqn. S25 and corresponding growth reaction). Finally, this low CR is approximately maintained towards the end of the simulation, as microbes turn inactive again and only contribute CO₂ and heat via (largely anaerobic) maintenance catabolism.

E Model fitting, uncertainty analysis and evaluation

E1 Model integration and fitting

The dynamic model presented in section C was implemented in Python and integrated numerically for a time span covering 20h using the '*radau*' method of the *solve_ivp* function in the *scipy.optimize* package (version 1.11.0).

For model fitting, we used the *leastsq* method as implemented in the *minimize* function of the *lmfit* package (version 1.2.1) (which employs the Levenberg-Marquardt algorithm) to minimize

the residual sum of squares between model output and experimental measurements of (cumulative) CO₂, rate of heat release and biomass. Since heat release was measured continuously, heat data were binned to yield a single value for each measured value of CO₂ to avoid overfitting. Specifically, heat release rates were averaged across the respective periods between subsequent CO₂ measurements. To achieve a comparable fit for all three quantities, we normalized the residuals by their mean values and the length of the data series, i.e., we minimized

$$R = \sum_i \left(\sum_j^{n_i} \left(\frac{x_{i,j}^{model} - x_{i,j}^{data}}{\bar{x}_i \sqrt{n_i}} \right)^2 \right) \quad (\text{Eqn. S43})$$

where i indicates CO₂, heat or biomass, j indicates the j th measurement and n_i is the number of measurements of quantity i .

For each parameter, we provided an initial guess as well as an upper and lower bound via the *Parameters* interface of *lmfit*. For glucose, the initial concentration was fixed at the known experimental value. We also fixed initial biomass and initialized the active fraction of microbes at the estimates obtained in section B. For oxygen, we chose the initial concentration and half-saturation constant such that the initial aerobic fraction was high (>0.85), while still allowing for anaerobiosis to develop during the incubation (O₂ⁱⁿⁱ < 0.25 initial glucose).

All values are provided in supplementary table S2.

E2 Model uncertainty analysis using Markov Chain Monte Carlo simulation

While the *minimize* function of *lmfit* provides estimates of parameter uncertainty, these estimates appeared unreliable and dependent on the minimization method used. Therefore, we performed an additional uncertainty analysis via Markov Chain Monte Carlo (MCMC) simulations using the *emcee* package (15).

We used uninformative uniform priors for all parameters, defined on the interval between the lower and upper bound of each parameter. The log-likelihood of any parameter set given the data was formulated following section 3 in Banks and Joyner 2017 (16).

For sampling, we initialized 40 walkers in a small Gaussian ball around the maximum likelihood result obtained as described in section E1 and sampled for 20000 steps, discarding the first 5000 samples as 'burn-in'. After inspecting the posterior distributions (see Fig. S4) and time

series of all parameters, 300 parameter sets were selected randomly from all walkers of the chain after the burn-in period. The 5th and 95th percentiles of the various model quantities over time (e.g., CR and CUE) presented in the main figures were derived from model simulations using these parameter sets, mimicking random draws from the joint posterior distribution.

Biogeochemical models including microbial C turnover are frequently characterized by equifinality and sloppiness (17). Indeed, we find that some model parameters are poorly constrained within the provided lower and upper bounds, featuring spread-out posterior distributions (e.g., half-saturation constants K_L , K_r , and yield coefficients), a high probability near the bounds (e.g., $Y_{ae,lac}$, O_2^{ini}), while others appeared well constrained (e.g., maintenance of inactive microbes, see Fig. S4). Thus, the full model is capable of accurately reproducing the observed experimental patterns, but (some of) the individual parameters cannot be reliably inferred from the available data, and the exact numerical values of the best-fit estimates should only be interpreted with great caution. Specifically, the simplistic representation of oxygen dynamics in our model can reproduce the emergent pattern observed in the experimental data (e.g., the CR curve), but its flexibility is limited and its parameterization relies on the assumptions laid out in section E1. A more sophisticated representation would require additional data, e.g., O_2 concentrations in the headspace or fermentation product concentrations, to properly parameterize.

E3 Comparison of full model and aerobic model variant

To compare the full model with a simpler model featuring only aerobic metabolism (fixing $\alpha = \frac{O_2}{O_2 + K_{O_s}} = 1$), we calculated AIC for the weighted least squares framework following the derivation in section 3 in Banks and Joyner 2017 (16):

$$AIC = N \ln \left(\frac{\sum_i (\sum_{j=1}^{n_i} (w_{i,j}^{-2} (x_{i,j}^{model} - x_{i,j}^{data})))}{N} \right) + 2(n_p + 1) \quad (\text{Eqn. S44})$$

Here, $N = n_{CO_2} + n_{Heat} + n_{Bio}$ is the total number of measurements, i indicates the measured quantity (CO_2 , heat or biomass), n_p is the total number of free parameters, and $w_{i,j} = (\bar{x}_i \sqrt{n_i})^{-1}$ is the weight used in the least square minimization.

In the aerobic model, all parameters pertaining to anaerobic processes and lactate metabolism (i.e., yield coefficients and kinetic parameters) as well as oxygen parameters are excluded, while the model is fit to the experimental data as described in section E1.

F Contribution of denitrification

We obtain a simple upper bound on the total CO₂ contribution from denitrification in the experiment. Assuming that N₂O corresponds to no less than 10% of the nitrogenous gases (N₂, N₂O, NO) released during denitrification and using the theoretical values for the CO₂-C to N molar ratios of 1.25 (N₂), 1 (N₂O) and 0.75 (NO) during denitrification (18,19), we suggest

$$CO_{2,cumu} \leq 10 \cdot 2.5 \cdot N_2O_{cumu} \quad (\text{Eqn. S45})$$

measured in cumulative moles of N and C as a conservative estimate. In our experiment, we measured about 3 μmol N₂O / kg soil of cumulative emissions, giving a maximum CO₂ of ≤ 75 μmol CO₂ / kg soil of cumulative C emissions. On the other hand, we measured about 23 mmol CO₂ / kg soil in total, so the total contribution of denitrification was likely small (<0.5%). Consequently, we do not include carbon (and heat) fluxes associated with denitrification in the dynamic model.

G References

1. Mook, Willem G., editor. Chemistry of carbonic acid in water. In: Environmental isotopes in the hydrological cycle - Principles and applications. Paris: UNESCO; 2000. p. 143–65.
2. Blagodatsky SA, Heinemeyer O, Richter J. Estimating the active and total soil microbial biomass by kinetic respiration analysis. *Biol Fertil Soils*. 2000 Oct 5;32(1):73–81.
3. Wutzler T, Blagodatsky SA, Blagodatskaya E, Kuzyakov Y. Soil microbial biomass and its activity estimated by kinetic respiration analysis – Statistical guidelines. *Soil Biol Biochem*. 2012 Feb;45:102–12.
4. Anderson JPE, Domsch KH. A physiological method for the quantitative measurement of microbial biomass in soils. *Soil Biol Biochem*. 1978 Jan;10(3):215–21.
5. Kaiser EA, Mueller T, Joergensen RG, Insam H, Heinemeyer O. Evaluation of methods to estimate the soil microbial biomass and the relationship with soil texture and organic matter. *Soil Biol Biochem*. 1992 Jul;24(7):675–83.
6. Beck T, Joergensen RG, Kandeler E, Makeschin F, Nuss E, Oberholzer HR, et al. An inter-laboratory comparison of ten different ways of measuring soil microbial biomass C. *Soil Biol Biochem*. 1997 Jul;29(7):1023–32.
7. Panikov NS. *Microbial Growth Kinetics*. London, Glasgow: Chapman and Hall; 1995. 378 p.
8. Chakrawal A, Herrmann AM, Šantrůčková H, Manzoni S. Quantifying microbial metabolism in soils using calorimetry — A bioenergetics perspective. *Soil Biol Biochem*. 2020 Sep;148:107945.

9. Battley EH. Is electron equivalence between substrate and product preferable to C-mol equivalence in representations of microbial anabolism applicable to "origin of life" environmental conditions?. *J Theor Biol.* 2009 Sep;260(2):267–75.
10. Wang G, Post WM. A theoretical reassessment of microbial maintenance and implications for microbial ecology modeling. *FEMS Microbiol Ecol.* 2012 Sep;81(3):610–7.
11. Pagel H, Kriesche B, Uksa M, Poll C, Kandeler E, Schmidt V, et al. Spatial Control of Carbon Dynamics in Soil by Microbial Decomposer Communities. *Front Environ Sci.* 2020 Jan 30;8:2.
12. Peter Linstrom. NIST Chemistry WebBook - SRD 69 [Internet]. National Institute of Standards and Technology; 2017 [cited 2023 Oct 17]. Available from: <https://doi.org/10.18434/T4D303>
13. Hansen LD, Macfarlane C, McKinnon N, Smith BN, Criddle RS. Use of calorimetric ratios, heat per CO₂ and heat per O₂, to quantify metabolic paths and energetics of growing cells. *Thermochim Acta.* 2004 Nov;422(1–2):55–61.
14. Chakrawal A, Herrmann AM, Manzoni S. Leveraging energy flows to quantify microbial traits in soils. *Soil Biol Biochem.* 2021 Apr;155:108169.
15. Foreman-Mackey D, Hogg DW, Lang D, Goodman J. emcee : The MCMC Hammer. *Publ Astron Soc Pac.* 2013 Mar;125(925):306–12.
16. Banks HT, Joyner ML. AIC under the framework of least squares estimation. *Appl Math Lett.* 2017 Dec;74:33–45.
17. Marschmann GL, Pagel H, Kögler P, Streck T. Equifinality, sloppiness, and emergent structures of mechanistic soil biogeochemical models. *Environ Model Softw.* 2019 Dec;122:104518.
18. Swerts M, Merckx R, Vlassak K. Denitrification, N₂-fixation and fermentation during anaerobic incubation of soils amended with glucose and nitrate. *Biol Fertil Soils.* 1996;
19. Wang R, Feng Q, Liao T, Zheng X, Butterbach-Bahl K, Zhang W, et al. Effects of nitrate concentration on the denitrification potential of a calcic cambisol and its fractions of N₂, N₂O and NO. *Plant Soil.* 2013 Feb;363(1–2):175–89.
20. Sun DL, Jiang X, Wu QL, Zhou NY. Intragenomic Heterogeneity of 16S rRNA Genes Causes Overestimation of Prokaryotic Diversity. *Appl Environ Microbiol.* 2013 Oct;79(19):5962–9.

443

444 H Supplementary figures and tables

445 **Supplementary table S1.** Average gene copy numbers per cell for different bacterial phyla
 446 used for biomass calculation. Data are from (20).

Phylum	<i>Bacillota</i>	<i>Verrucomicrobiota</i>	<i>Gemmatimonadota</i>	<i>Nitrospirata</i>	<i>Cyanobacteria</i>	<i>Chloroflexota</i>
Average	6.01	1.75	1	1.67	2.35	2
Phylum	<i>Crenarchaeota</i>	<i>Planctomycetota</i>	<i>Bacteroidota</i>	<i>Actinomycetota</i>	<i>Acidobacteriota</i>	<i>Pseudomonadota</i>
Average	1	1.67	3.14	3.16	1.3	3.94
Phylum	Others					
Average	3.82					

447

448 **Supplementary table S2.** Variables (bold) and parameters of the dynamic model. Calibration
 449 results are included for all quantities that were estimated from data. For variables, the initial
 450 value indicates the value of this variable at the start of the incubation ($t = 0$), which was also
 451 estimated for the O_2 and r variables. For parameters, initial values indicate the initial guess
 452 provided to the least square minimization algorithm.

453

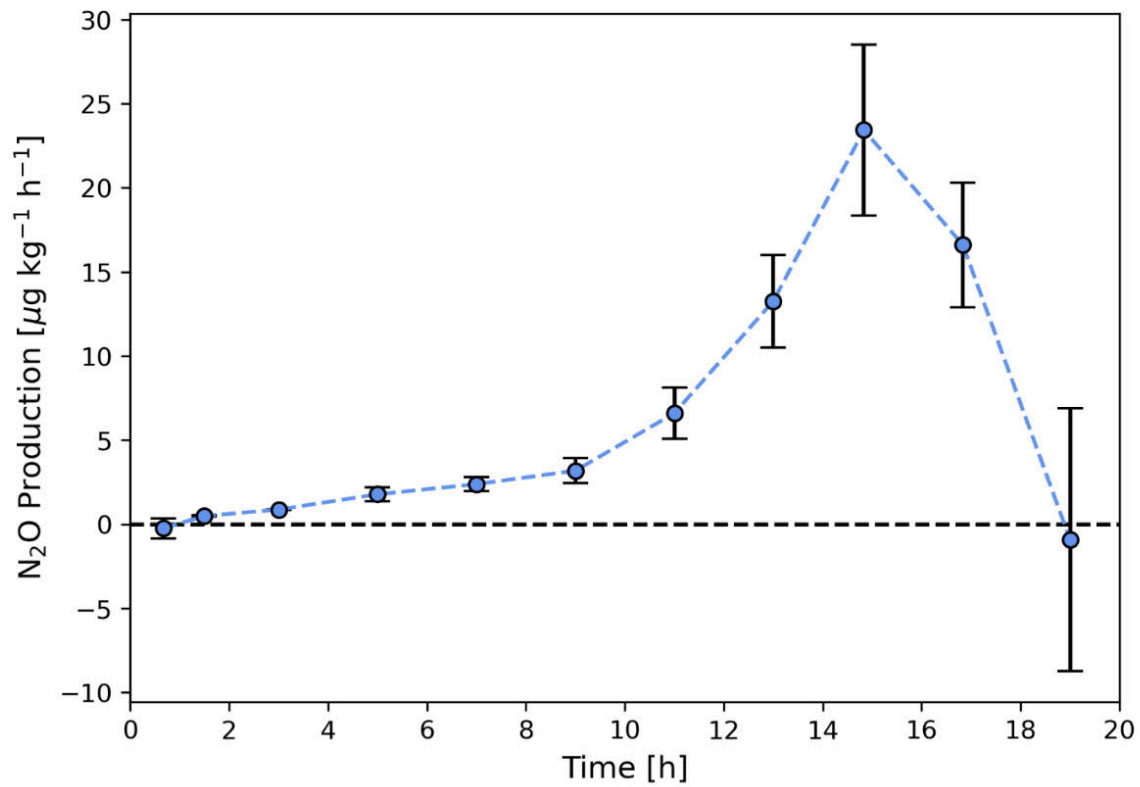
Symbol	Name	Unit	Initial value	Best-fit value	Bounds
S	Glucose concentration	mol C / g	$6.66 \cdot 10^{-5}$	-	-
X	Biomass concentration	mol C / g	$1.22 \cdot 10^{-5}$	-	-
L	Lactate concentration	mol C / g	0	-	-
P	Propionate + Acetate concentration	mol C / g	0	-	-
CO_2	Cumulative CO ₂ release	mol C / g	0	-	-
Q	Cumulative heat release	kJ / g	0	-	-
O_2	Oxygen concentration	mol O ₂ / g	$1.83 \cdot 10^{-5}$	$1.59 \cdot 10^{-5}$	$[6.66 \cdot 10^{-6}, 1.83 \cdot 10^{-5}]$
r	Index of physiological state	-	0.00385	0.0067	[0,1]
v_m	Maximum specific substrate uptake rate	1 / h	0.7	0.796	[0.001,5]
K_S	Glucose half-saturation	mol C / g	$2 \cdot 10^{-5}$	$4.66 \cdot 10^{-5}$	$[1 \cdot 10^{-6}, 1 \cdot 10^{-4}]$
K_L	Lactate half-saturation	mol C / g	$2 \cdot 10^{-5}$	$7.757 \cdot 10^{-6}$	$[1 \cdot 10^{-6}, 5 \cdot 10^{-5}]$
K_r	Activity half-saturation	mol C / g	$2 \cdot 10^{-6}$	$1 \cdot 10^{-6}$	$[1 \cdot 10^{-6}, 1 \cdot 10^{-5}]$
m_a	Specific maintenance coefficient of active fraction	1 / h	0.0126	0.027	[0, 0.1]
m_i	Specific maintenance coefficient of inactive fraction	1 / h	0.0126	0.013	[0, 0.05]
K_{O_2}	Oxygen half-saturation	mol O ₂ / g	$2.5 \cdot 10^{-6}$	-	-
$Y_{ae,glu}$	(Biomass) yield of glucose respiration	mol C biomass / mol C glucose	0.75	0.84	[0.45, 0.9]
$Y_{f,glu}$	Yield of glucose fermentation	mol C biomass / mol C glucose	0.15	0.01	[0,0.4]
$Y_{ae,lac}$	Yield of lactate respiration	mol C biomass / mol C lactate	0.20	0.11	[0.2,0.7]
$Y_{f,lac}$	Yield of lactate fermentation	mol C biomass / mol C lactate	0.075	0.28	[0,0.35]
Y_L	Lactic acid yield (as fermentation product)	mol C lactate / mol C glucose	Eqn. S28	-	-
γ_S	Degree of reduction of glucose	mol e ⁻ / mol C glucose	4	-	-
γ_X	Degree of reduction of biomass	mol e ⁻ / mol C biomass	4.2	-	-
γ_L	Degree of reduction of lactic acid	mol e ⁻ / mol C lactate	4	-	-
$\Delta_{cat}H_z$	Reaction enthalpy of catabolic reaction z	kJ / mol C substrate	Eqn. S30-33	-	-
ΔH_z	Reaction enthalpy of growth reaction z	kJ / mol C substrate	Eqn. 34	-	-
ΔH_M	Reaction enthalpy of maintenance	kJ / mol C substrate	Section C5	-	-
U_y	Uptake rate of substrate y	mol C substrate / g / h	Eqn. S16-17	-	-
M_z	Maintenance rate of fraction z	mol C substrate / g / h	Eqn. S18-19	-	-
r_{yz}	Part of maintenance rate of fraction z fueled by substrate y	mol C substrate y / g / h	Eqn. S20-22	-	-
α	Aerobic fraction, $\alpha = \frac{O_2}{O_2 + K_{O_2}}$	-	0.88	-	-

454

455

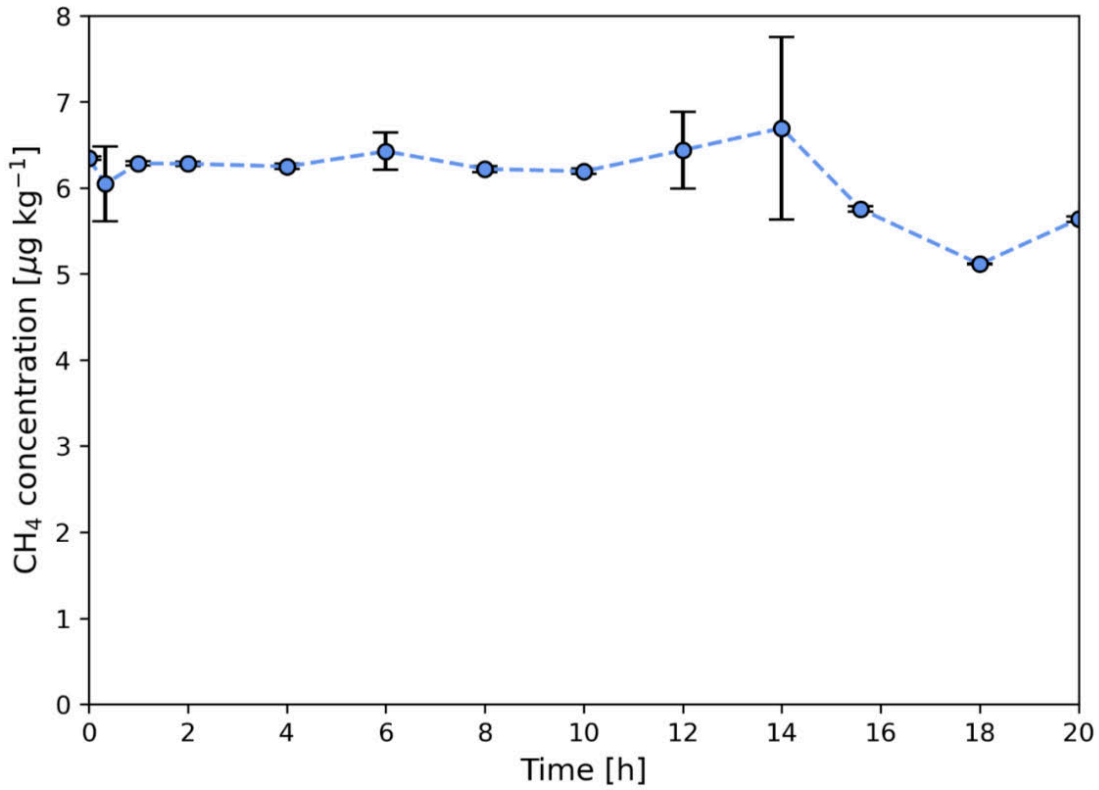
Supplementary figure S1. Rate of N₂O production during the incubation.

Shown are mean \pm SD of $n=3$ replicates per point.

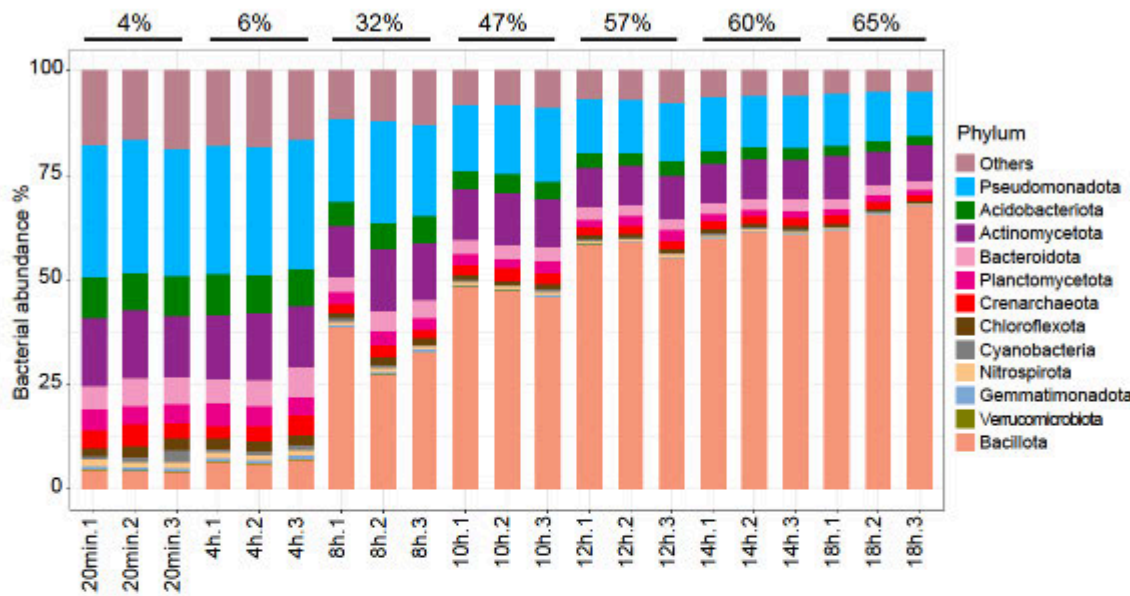


Supplementary figure S2. CH₄ concentration during the incubation.

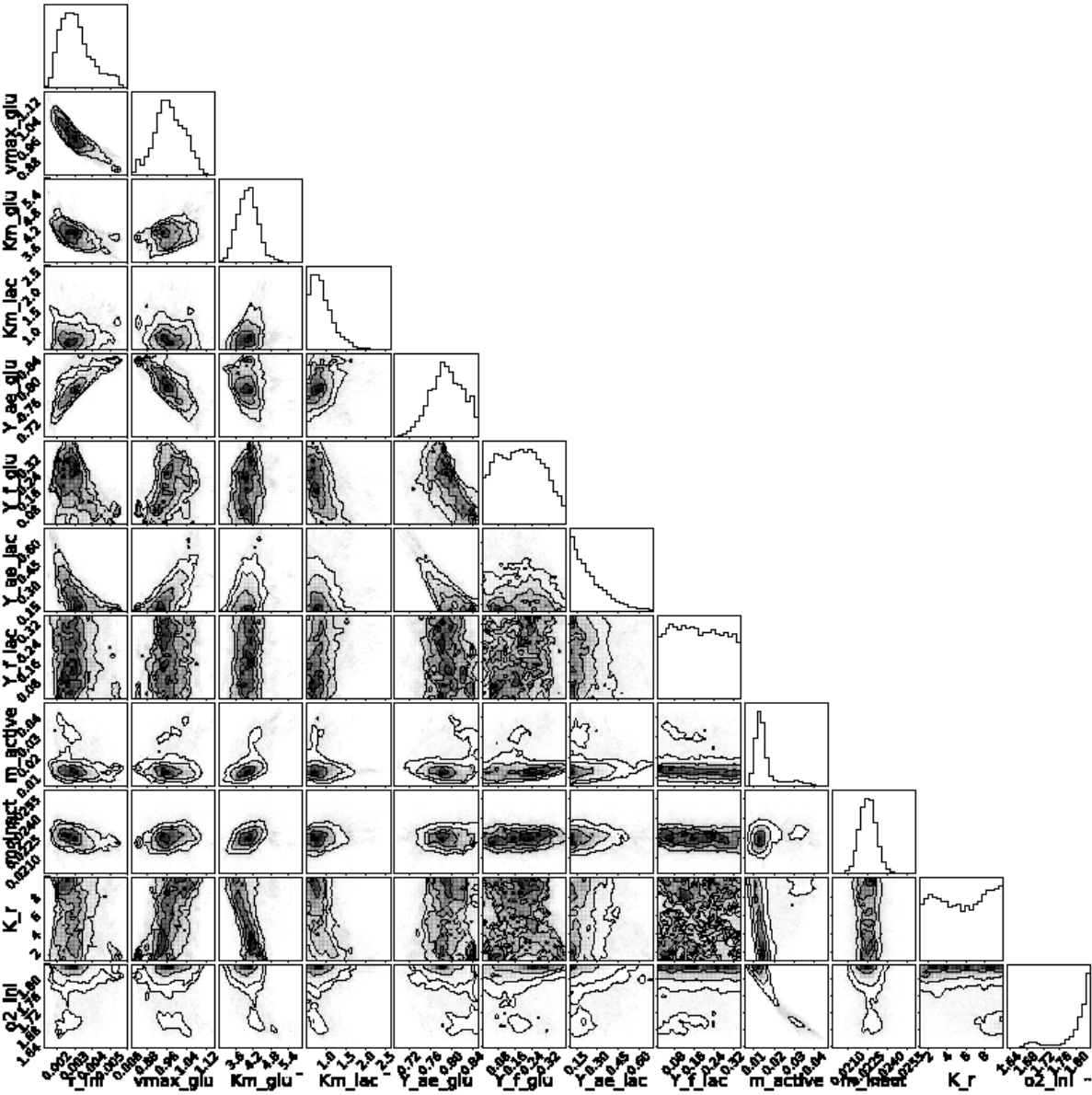
Shown are mean \pm SD of $n=3$ replicates per point.



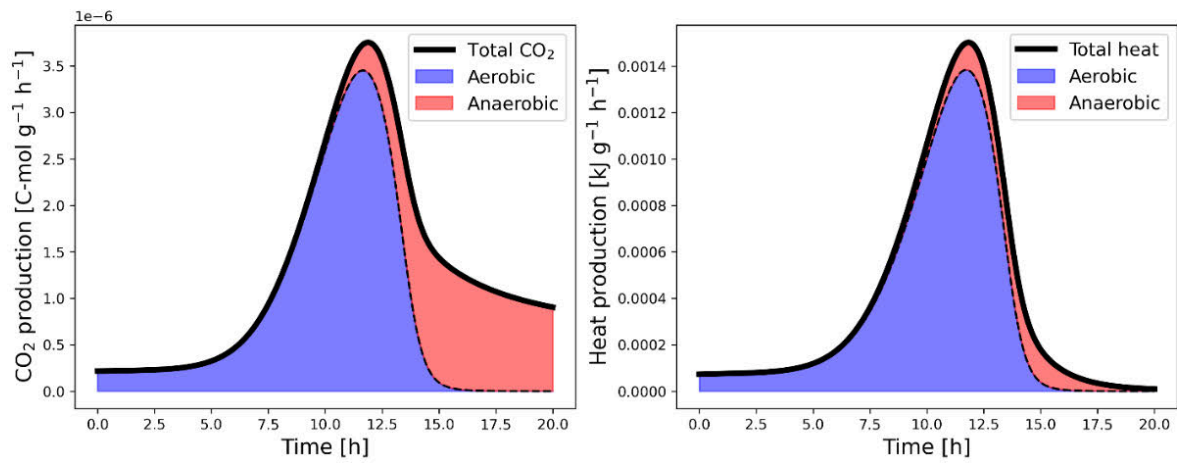
Supplementary figure S3. The relative abundance of OTUs on the level of phylum during growth on glucose for all experimental replicates. Percentages on top denote relative abundance of *Bacillota* across replicates for each time point.



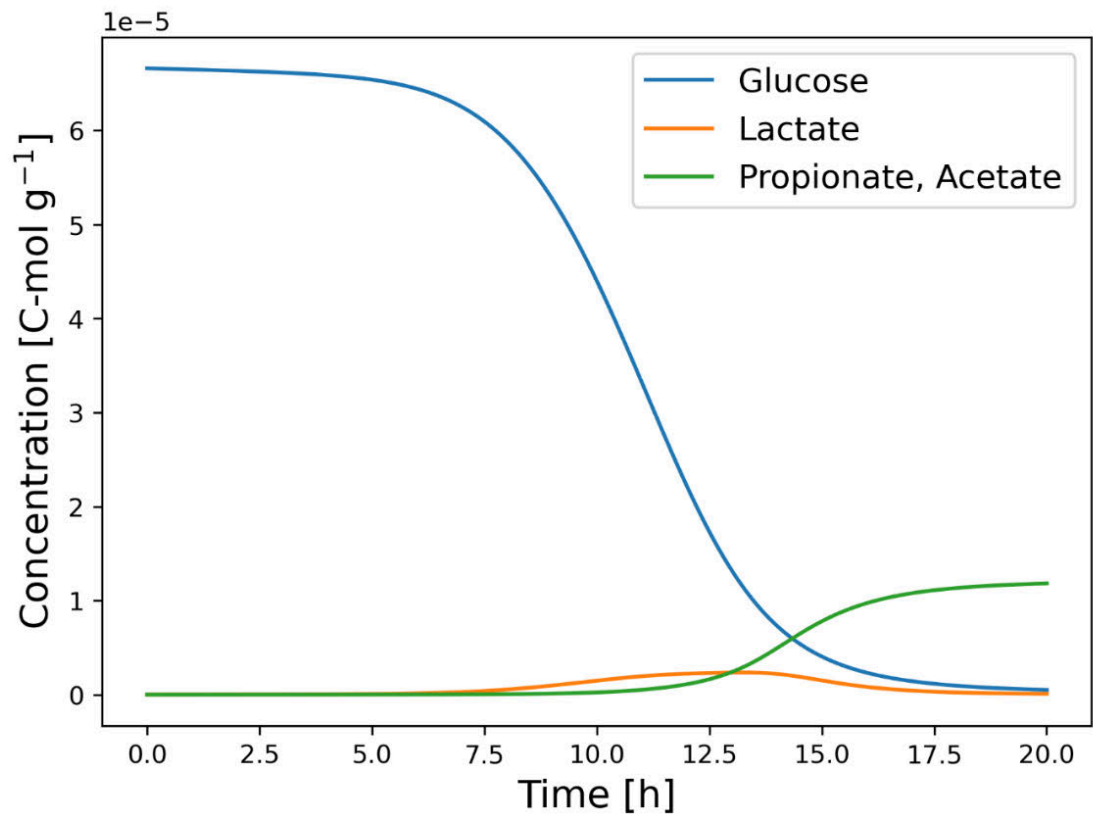
Supplementary figure S4. Posterior distributions of estimated model parameters as determined by MCMC analysis.



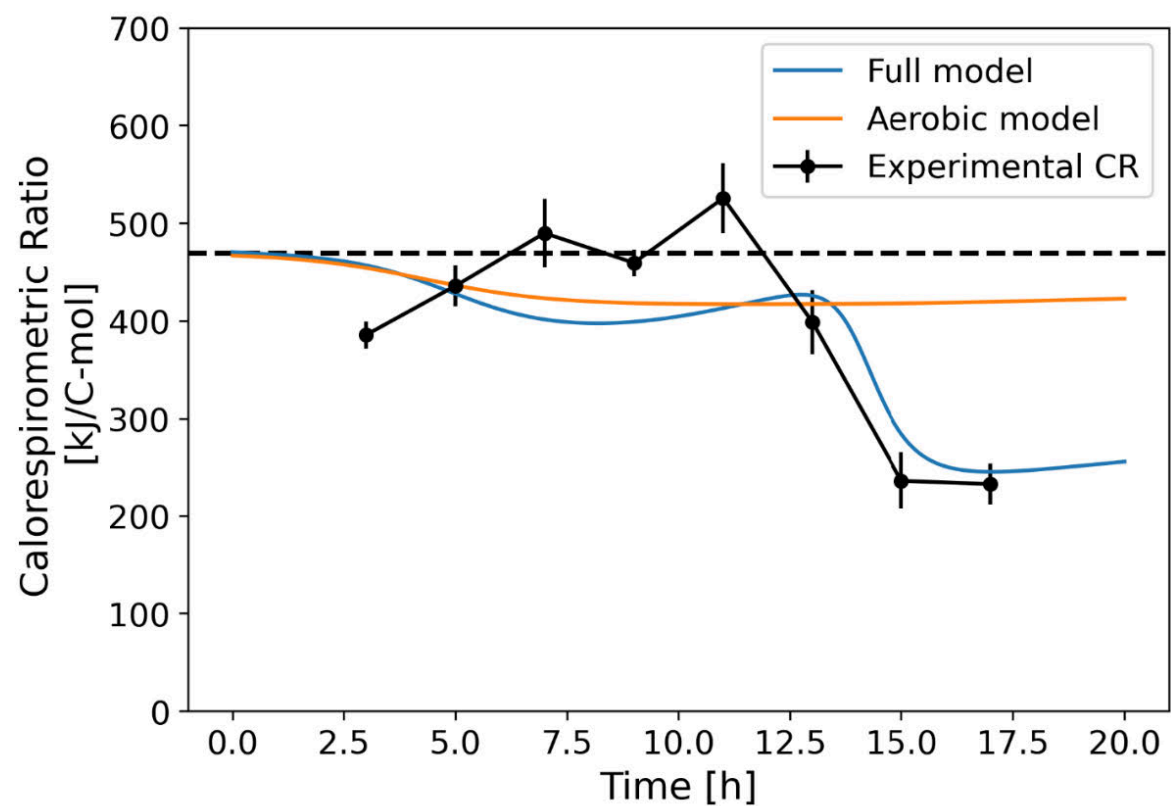
Supplementary figure S5. Contribution of aerobic and anaerobic processes to the total rates of heat and CO₂ release in the calibrated model. The contribution is determined by the time-varying anaerobic fraction.



Supplementary figure S6. Concentrations of substrate (glucose) as well as fermentation products (lactate, acetate, and propionate) in the calibrated model. Lactate is consumed by microbes as it becomes available, but acetate and propionate accumulate under the anoxic conditions.



Supplementary figure S7. Comparison of the CR pattern during the incubation as observed in data as well as the full calibrated model and a calibrated model variant featuring only aerobic respiration.



Supplementary material of Endress et al. (2024b)

This supplementary material consists of the following components:

- SI Text. PDF file containing supplementary materials and methods, Supplementary Figs. S1–S4, Supplementary Tables S1–S2, and supplementary references.
- SI Data. Excel file containing all data analyzed in this study as well as ANOVA and model calibration results.

SI Text is provided below. For SI Data, please refer to the online version of the published article.

Supplementary Information:

Spatial substrate heterogeneity limits microbial growth as revealed by the joint experimental quantification and modeling of carbon and heat fluxes

Martin-Georg Endress^{1,*}, Fatemeh Dehghani^{2,*}, Sergey Blagodatsky¹, Thomas Reitz², Steffen Schlüter³, Evgenia Blagodatskaya²

¹ Institute of Zoology, University of Cologne, 50923 Cologne, Germany

² Department of Soil Ecology, Helmholtz Centre for Environmental Research – UFZ, 06120 Halle/Saale, Germany

³ Department of Soil System Science, Helmholtz Centre for Environmental Research – UFZ, 06120 Halle/Saale, Germany

^{*} Equal contributions

Corresponding Author(s): Martin-Georg Endress

Email: m.endress@uni-koeln.de

This supplementary information includes:

Supplementary materials and methods

Supplementary figures S1 to S4

Supplementary tables S1 to S2

Supplementary references

Other supplementary materials for this manuscript include the following:

Supplementary Data S1

Supplementary materials and methods

A Statistical analysis

A1 Anovas with contrasts

To test for the effects of nutrient addition and heterogeneous substrate application on the growth kinetics as well as CUE and EUE, we performed two-way ANOVAs with a priori contrasts between treatments. Specifically, with subscripts H and X denoting homogeneous and heterogeneous substrate application, respectively, and subscripts N and W denoting treatments with and without nutrient addition, respectively, we used the following contrasts with coefficients c :

Effect of heterogeneity in treatments without nutrients: $c_{H,W} = 1, c_{X,W} = -1, c_{H,N} = 0, c_{X,N} = 0$

Effect of heterogeneity in treatments with nutrients: $c_{H,W} = 0, c_{X,W} = 0, c_{H,N} = 1, c_{X,N} = -1$

Effect of nutrients in homogeneous treatments: $c_{H,W} = 1, c_{X,W} = 0, c_{H,N} = -1, c_{X,N} = 0$

Effect of nutrients in heterogeneous treatments: $c_{H,W} = 0, c_{X,W} = 1, c_{H,N} = 0, c_{X,N} = -1$

The obtained p -values were adjusted for multiple testing using the Bonferroni method as implemented in emmeans (Lenth, 2023). All results are tabulated in S1 Data.

A2 Standard deviation of ratios

In our experimental setup, the release of CO_2 and heat as well as the consumption of O_2 were measured in triplicate in separate incubations. Therefore, it is not possible to assign any specific replicate of one quantity (e.g., heat production) to any specific replicate of another quantity (e.g., CO_2 production) to calculate their ratio (e.g., CR) for any single replicate. This is true for all the considered ratios (CR, CR_{O_2} and RQ). While the mean values of these ratios can simply be calculated using the mean values of the constituent quantities, their variability needs to be estimated separately via propagation of error. Specifically, the standard deviation σ_R of any ratio R was estimated as

$$\sigma_R = |R| \sqrt{\left(\frac{\sigma_A}{A}\right)^2 + \left(\frac{\sigma_B}{B}\right)^2 - 2 \frac{\sigma_{AB}}{AB}} \quad (\text{Eqn. S1})$$

where A, σ_A and B, σ_B denote the mean values and standard deviations of the numerator and the denominator of the ratio, respectively, and σ_{AB} is the covariance of the two estimated from the corresponding cumulative time series.

A3 Permutation tests for cumulative ratios

We tested the effect of nutrient addition and heterogeneous substrate application on the cumulative ratios using permutation tests, since we only obtain independent replicates of the numerators and denominators of those ratios but not the ratios themselves, as outlined in section A2. We describe the test procedure for the effect of nutrient addition on the CR in soils with homogeneous substrate addition below. All other pairwise tests were carried out analogously.

First, we calculate the experimentally observed difference T_{obs} between the mean values of the cumulative ratio in the treatments with and without nutrient addition,

$$T_{obs} = \overline{CR}_{H,N} - \overline{CR}_{H,W} = \frac{\overline{Heat}_{H,N}}{\overline{CO2}_{H,N}} - \frac{\overline{Heat}_{H,W}}{\overline{CO2}_{H,W}} \quad (\text{Eqn. S2}),$$

where the subscript H indicates homogeneous glucose addition, N indicates nutrient addition, and W indicates treatments without nutrient addition.

We then compute the same statistic T in 10.000 bootstrap iterations using mean values calculated after randomly permuting the N and W labels of the corresponding heat and CO_2 measurements. The p -value of the test is then obtained as the fraction of test statistics T that exceed T_{obs} . To account for the multiple tests arising from pairwise comparisons, we adjust the p -values obtained this way with the *false_discovery_control* function as implemented in *scipy.stats* (Virtanen et al., 2020) using the Benjamini-Hochberg procedure (Benjamini and Hochberg, 1995).

B Biomass quantification

Here we discuss the observed discrepancy between estimated microbial biomass carbon (MBC) growth based on either dsDNA or the carbon balance and modelling.

On the one hand, biomass growth may be estimated from the observed increase in the concentration of dsDNA. In the homogeneous treatment without nutrient addition, dsDNA increased from 9.4 $\mu\text{g DNA g}^{-1}$ at the start of the incubation to 17.3 $\mu\text{g DNA g}^{-1}$ after 47 h. This corresponds to a 1.84-fold increase in dsDNA over the course of the incubation.

To estimate the MBC increase from this increase in dsDNA, we determined the initial MBC in the soil via the chloroform-fumigation-extraction technique (Vance et al., 1987). To that end, 1.5 g of soil was fumigated with ethanol-free chloroform for 24 hours and then extracted with 6 mL of 0.025 M K_2SO_4 . The concentration difference between the fumigated sample and a non-

fumigated sample extracted simultaneously corresponds to the initial MBC. We assumed an extraction efficiency of 0.45. For the air-dried and rewetted soil, we measured a value of $155 \pm 25.04 \mu\text{g C g}^{-1}$, which was not significantly different from the value measured in the fresh soil ($178.06 \pm 25.6 \mu\text{g C g}^{-1}$, table S1). Using this initial MBC and the constant conversion factor $f_{DNA} = 16.5$ (Eqn. 1 in main text), this suggests a final MBC of $17.3 * 16.5 \approx 285 \mu\text{g C g}^{-1}$ or equivalently a $130 \mu\text{g C g}^{-1}$ net MBC increase after 47 h. Based on the rate of initial glucose addition of $400 \mu\text{g C g}^{-1}$, this corresponds to an apparent CUE of $130/400 = 32.5\%$.

On the other hand, growth may also be inferred from the carbon balance via cumulative CO_2 release. In the homogeneous treatment without nutrient addition, the average cumulative CO_2 release was $176 \mu\text{g C g}^{-1}$ after 50h. Assuming that all of the initial $400 \mu\text{g C g}^{-1}$ of glucose were consumed by that point and were either released as CO_2 or incorporated into biomass, the carbon balance thus suggests a biomass increase of $224 \mu\text{g C g}^{-1}$, in contrast to the $130 \mu\text{g C g}^{-1}$ obtained from dsDNA-based estimates. This corresponds to a 2.45-fold increase in MBC (compared to 1.84-fold based on dsDNA) and yields an estimate of $\text{CUE}_s = 224/400 = 56\%$ (compared to 32.5% based on dsDNA). Since our dynamic model is calibrated against the CO_2 measurements, this carbon balance is also reflected in model simulations.

Several aspects may contribute to this discrepancy between growth estimates based on either dsDNA or the carbon balance.

First, the discrepancy may result from temporal changes in the conversion factor f_{DNA} . For example, assuming that the net biomass growth inferred from cumulative CO_2 is correct, we would predict f_{DNA} to increase from its initial value of $\frac{155 \mu\text{g C g}^{-1}}{9.4 \mu\text{g DNA g}^{-1}} \approx 16.5$ to around $\frac{155+224 \mu\text{g C g}^{-1}}{17.3 \mu\text{g DNA g}^{-1}} \approx 21.9$ after 50h. This would indicate a smaller amount of dsDNA per MBC after exponential growth, which has also been reported in previous investigations (Čapek et al., 2023). Experimental proof of this assumption would require an application of fumigation measurements over the course of the growth dynamics during the incubation. However, the fumigation-extraction technique cannot be used with certainty in glucose-amended samples, in particular without the use of isotopically labelled substrate.

Second, these analyses are sensitive to the measured initial MBC value of $155 \mu\text{g C g}^{-1}$ in the (air-dried and rewetted) soil. Using a higher initial MBC value will tend to close the gap between the two estimates, because it elevates the total MBC increase predicted from dsDNA and lowers the relative MBC increase predicted from the carbon balance. For example, considering an

initial MBC of 178 $\mu\text{g C g}^{-1}$ as measured in the fresh soil (instead of 155 $\mu\text{g C g}^{-1}$ in the air-dried and rewetted soil, table S1), the 1.84-fold increase in dsDNA would suggest a net growth of 149.5 $\mu\text{g C g}^{-1}$ (compared to 130 $\mu\text{g C g}^{-1}$) and a CUE of 37.4% (compared to 32.5%). At the same time, the net 224 $\mu\text{g C g}^{-1}$ MBC increase suggested by cumulative CO_2 would only amount to a 2.26-fold increase from such an initial MBC of 178 $\mu\text{g C g}^{-1}$ (compared to 2.45-fold from 155 $\mu\text{g C g}^{-1}$). Thus, biases in experimental biomass estimation (e.g., (Beck et al., 1997)) also have the potential to account for some of the observed differences.

In general, biases in the experimental determination of the total dsDNA concentration could similarly skew estimates. However, since we investigated the increment of dsDNA over time in the same soil, any problems arising from varying DNA extraction efficiencies between different soils or setups were mitigated in this study.

Overall, the ODE model adequately captures the observed dynamics based on the MBC growth inferred from cumulative CO_2 , and the observed effects of substrate spatial heterogeneity and nutrient limitation do not depend on these quantitative details of the discrepancy between different MBC estimates.

C Dynamic model formulation

We describe the various aspects of the dynamic model below.

C1 ODE System

The dynamics of microbial growth in soil after glucose addition are modelled using a system of 6 coupled ordinary differential equations (ODEs) representing the 3 different carbon pools (glucose S , biomass X , and CO_2) as well as nutrient concentration (N), heat (Q), and finally the physiological state of the microbial population, indicating the active fraction of microbes ($r \in [0, 1]$, (Panikov, 1995)). All carbon pools are measured in mol C / g soil , heat is measured in kJ / g soil , and nutrient concentration is measured in $\text{mol nutrient / g soil}$.

All state variables and parameters along with their units are listed in supplementary table S2.

The rationale behind the equations will be explained in detail in the following subsections C2-C7. First, the full ODE system reads:

$$\frac{dS}{dt} = -U - M_{S_a} - M_{S_i} \quad (\text{Eqn. S3})$$

$$\frac{dX}{dt} = Y \cdot U - M_{X_a} - M_{X_i} \quad (\text{Eqn. S4})$$

$$\frac{dCO_2}{dt} = (1 - Y)U + M_{S_a} + M_{S_i} + M_{X_a} + M_{X_i} \quad (\text{Eqn. S5})$$

$$\frac{dQ}{dt} = \Delta H_G U + \Delta_{\text{cat}} H_{\text{glu}} (M_{S_a} + M_{S_i}) + \Delta H_M (M_{X_a} + M_{X_i}) \quad (\text{Eqn. S6})$$

$$\frac{dN}{dt} = I \cdot (N_0 - N) - Y \cdot U \quad (\text{Eqn. S7})$$

$$\frac{dr}{dt} = Y v_m r \left(\frac{S}{S + K_r} - r \right) \quad (\text{Eqn. S8})$$

Here, the following process rates were used:

$$U = v_m r X \frac{S}{S + K_S} \frac{N}{N + K_N} \quad (\text{Eqn. S9}) \dots \text{Utilization of glucose and nutrient for growth}$$

$$M_a = m_a r X \quad (\text{Eqn. S10}) \dots \text{Maintenance flux of the active fraction (a)}$$

$$M_i = m_i (1 - r) X \quad (\text{Eqn. S11}) \dots \text{Maintenance flux of the inactive fraction (i)}$$

$$M_{S_*} = M_* \frac{S}{S + K_S} \quad (\text{Eqn. S12}) \dots \text{Part of maintenance flux fueled by glucose utilization (* = i or a)}$$

$$M_{X_*} = M_* - M_{S_*} \quad (\text{Eqn. S13}) \dots \text{Part of maintenance flux fueled by biomass utilization (* = i or a)}$$

C2 Substrate utilization

Model simulations are initialized with a fixed amount of substrate (glucose, 400 µg C g⁻¹) which is subsequently consumed by microbes over the course of the incubation. Microorganisms utilize this substrate for growth, following Michaelis-Menten (MM) kinetics at rate U (Eqn. S9). In addition, they also take up substrate to fuel their maintenance respiration if sufficient substrate is available. Specifically, both active and inactive microbes have certain maintenance requirements (Eqn. S10 and S11) they need to meet, and they utilize glucose for this purpose according to its (MM-)availability (Eqn. S12). If the substrate concentration is insufficient to fuel these maintenance requirements, the microbes make up the difference by consuming their own biomass instead (Eqn. S13), representing a transition from exogenous to endogenous maintenance (Wang and Post, 2012; Pagel et al., 2020).

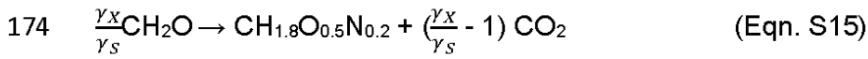
C3 Growth and maintenance reaction

The aerobic growth reaction on glucose is obtained as the sum of the corresponding catabolic and anabolic reactions, following the detailed presentation in (Chakrawal et al., 2020).

164 The catabolic reaction consists of the aerobic respiration of glucose to CO_2 with O_2 as the
 165 terminal electron acceptor, which can be expressed for the consumption of 1 mol C of the
 166 substrate:

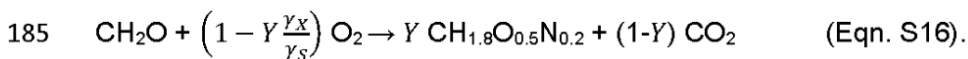


168 The formation of biomass via the anabolic reaction necessitates the assumption of a
 169 stoichiometric formula for the composition of the formed biomass. As a default, we use the
 170 generic formula $\text{CH}_{1.8}\text{O}_{0.5}\text{N}_{0.2}$ as suggested in (Chakrawal et al., 2020), but a more detailed
 171 discussion of the importance of this choice is presented in section D and can also be found in
 172 (Yang et al., 2024). We write the anabolic reaction using the electron balance approach for the
 173 formation of 1 C mol of biomass (Battley, 2009):



175 Here, $\gamma_X = 4.2$ denotes the degree of reduction of biomass assuming the stoichiometric
 176 composition introduced above, and $\gamma_S = 4$ denotes the degree of reduction of glucose. NH_3 is
 177 assumed to be the source of nitrogen in biomass. Hydrogen can be balanced by adding H_2O to
 178 either side (Chakrawal et al., 2020).

179 These catabolic and anabolic reactions are then combined to obtain the overall growth reaction,
 180 again expressed for the consumption of 1 mol C of substrate. This can be achieved by
 181 introducing the yield coefficient (Y) of microbial growth, which represents the amount biomass
 182 (in mol C) formed as a result of the consumption of 1 mol C of substrate. After multiplying Eqn.
 183 S14 and S15 by $1 - Y \frac{\gamma_X}{\gamma_S}$ and Y , respectively, their sum yields the desired overall growth
 184 reaction proceeding at rate U :



186 We assume that all maintenance reactions correspond to pure catabolism, with no net formation
 187 of biomass. For exogenous maintenance, i.e., maintenance fueled by the consumption of
 188 substrate (glucose), the catabolic reaction is given by Eqn. S14. If no substrate is available,
 189 microbes transition to endogenous maintenance and start to catabolize their own biomass to
 190 fuel their maintenance requirements. In terms of carbon fluxes in the dynamic model, we

represent this as a direct conversion of biomass carbon to CO₂ at the corresponding rates (Eqn. S13).

C4 Heat production

The reactions and processes described above in combination yield the differential equations for the three carbon pools (Eqn. S3-S5). To obtain the overall heat production rate (Eqn. S6), we compute the reaction enthalpies $\Delta_r H$ for each of the maintenance and growth reactions using Hess's law per mol C of substrate:

$$\Delta_r H = \sum_i a_i \Delta_f H_{product\ i} - \sum_j b_j \Delta_f H_{reactant\ j} \text{ with stoichiometric coefficients } a_i, b_j \quad (\text{Eqn. S17})$$

For the catabolic respiration of glucose (Eqn. S14), we use known values of the enthalpies of formation $\Delta_f H$ of the simple chemical compounds involved. These values are publicly available, e.g., in the NIST Chemistry WebBook (Peter Linstrom, 2017). The calculation yields a reaction enthalpy of $\Delta_{cat} H_{glu} \approx -469 \text{ kJ}$ (the combustion enthalpy of glucose per mol C).

Since the anabolic reaction (Eqn. S15) is written using the electron balance approach, its reaction enthalpy is 0, i.e. $\Delta_r H_{ana} = 0$ (Chakrawal et al., 2020). Therefore, the reaction enthalpy $\Delta_G H$ of the growth reaction (Eqn. S16) can be computed from the reaction enthalpy of the involved catabolic reaction ($\Delta_{cat} H_{glu}$) and the yield coefficient of the pathway (Y):

$$\Delta_G H = \left(1 - Y \frac{\gamma_X}{\gamma_S}\right) \Delta_{cat} H_{glu} \text{ (per mol C of glucose consumed)} \quad (\text{Eqn. S18})$$

Next, we compute the reaction enthalpy of maintenance respiration fueled by biomass consumption, ΔH_M . If biomass is uniformly consumed and respired to CO₂ during the process, the reaction enthalpy can be computed via the degree of reduction γ_X of the biomass using Thornton's rule (Thornton, 1917). Assuming the stoichiometric composition CH_{1.8}O_{0.5}N_{0.2}, we have $\gamma_X = 4.2$ and thus

$$\Delta H_M \approx \Delta H_T \cdot \frac{\gamma_X}{4} = -492.45 \text{ kJ (per mol C of biomass consumed)}, \quad (\text{Eqn. S19})$$

where we use $\Delta H_T \approx -469 \text{ kJ}$ (per mol of C respired) as the value of Thornton's constant for growth on glucose (Chakrawal et al., 2020).

However, we allow this parameter ΔH_M to vary during model calibration, since we have no information about the actual compounds and biochemical pathways involved in the maintenance process. Deviations from the value predicted by Eqn. S19 could for example be caused by selective consumption of biomass (e.g., of storage compounds), as well as by the utilization of some SOM for maintenance requirements. However, we do not consider SOM use in the scope of this study.

Note that all enthalpy values are given for a standard reference temperature of 25°C, while experimental temperature was 20°C. In principle, the values can be corrected using the heat capacity of all the involved compounds (Kirchhoff's law of thermochemistry), which are also publicly available, e.g. from NIST. However, the effect is negligible for our purposes. For example, we calculate a change in $\Delta_{cat}H_{glu}$ of less than 1 kJ (per mol C) for the given temperature difference of 5°C. Therefore, we proceed with the analysis using the reference values.

Finally, the heat production rate of any process in the differential equation Eqn. S6 is calculated as the product of the process rate (mol C of substrate / h) and the reaction enthalpies (kJ / mol C of substrate).

C5 Nutrient dynamics

To include a simple form of nutrient limitation in the model, we simulate a single pool of a proxy nutrient representing the availability of all essential nutrients in the soil (e.g., nitrogen, phosphorus, potassium, ..., Eqn. S7). This nutrient pool is initialized at a concentration N_0 and subsequently depleted due to consumption by the microbial growth reaction at rate YU . Its availability is controlled by a half-saturation constant K_N and has the potential to limit U if the corresponding MM-factor drops significantly below 1 (Eqn. S9). In our simulations, this is only the case in the heterogeneous treatment without nutrient addition. In the other treatments, nutrient availability was not limiting, and the inclusion of the proxy nutrient has negligible effects on the simulation results in those cases (i.e., $\frac{N}{N+K_N} \approx 1$ over the whole incubation).

Note that we assumed a one-to-one stoichiometry with carbon rates for the proxy nutrient N , but an extension to a different stoichiometry would be straightforward to include if a specific nutrient like nitrogen was considered and, e.g., also measured explicitly in the soil. In any case, the qualitative behavior of the ODE system does not depend on this stoichiometry, even though the

quantitative values of the nutrient-related parameters will be rescaled if a specific nutrient and stoichiometry is considered instead of a general proxy.

Finally, in the simulation of the heterogeneous treatment without nutrient addition, the proxy nutrient is slowly replenished via a process mimicking the diffusive supply of nutrients from the soil surrounding the microbial hotspots arising from the spatial substrate heterogeneity. In Eqn. S7, this is represented as an influx of $I \cdot (N_0 - N)$, such that N will tend to return to its initial value N_0 in the soil over time, and where the rate constant I controls the speed of this process.

C6 Microbial activity

The last differential equation (Eqn. S8) describes the transition of microorganisms between an active, growing state (fraction r) and an inactive state that only performs maintenance metabolism (fraction $1-r$). This transition is implemented using the index of physiological state framework originally introduced by Panikov (Panikov, 1995), which has been frequently utilized for kinetic analysis of substrate induced respiration in soil (e.g., (Blagodatsky et al., 2000; Chakrawal et al., 2021). In this framework, soil microbes switch to the active state if the substrate concentration is sufficient (i.e., $\frac{S}{S+K_r} > r$ with a half-saturation constant of activity K_r), and switch to an inactive state/dormancy otherwise ($\frac{S}{S+K_r} < r$). The rate of these transitions depends on the maximum growth rate of the microbial population ($v_m \cdot Y$).

In a typical simulation, the microbes are initially largely inactive ($r \approx 0$), but quickly become active due to the high concentration of added glucose. As the concentration of glucose is depleted towards the end of the incubation, the microbial community turns inactive again (Fig S3c).

C7 Model variant with CO₂ diffusion

To investigate the potential impact of a delayed CO₂ detection due to diffusion of CO₂ from the soil to the alkali solution, we used a variant of the dynamic model with an additional carbon pool C_{Alkali} representing the CO₂-C accumulating in the alkali solution as (bi-)carbonate, which is the quantity that is actually measured experimentally via a change in conductivity (Fig. 5a). While the original ODEs other than CO₂ (Eqns. S3-S4 and S6-S8) remain unchanged, the dynamics of CO₂ are now expressed as

$$\frac{dCO_{2,soil}}{dt} = (1 - Y)U + M_{S_a} + M_{S_i} + M_{X_a} + M_{X_i} - D \cdot CO_{2,soil} \quad (\text{Eqn. S20})$$

$$\frac{dC_{Alkali}}{dt} = D \cdot CO_{2,soil} \quad (\text{Eqn. S21})$$

where $CO_{2,soil}$ now denotes the CO_2 concentration at the site of production in the soil, and D represents an effective diffusion constant. The diffusion of CO_2 from the soil ($CO_{2,soil}$) to the surface of the alkali solution ($CO_{2,solution}$) is driven by its concentration gradient, which we approximate as a difference per unit difference, $D \cdot (CO_{2,soil} - CO_{2,solution})$. However, since the CO_2 is continuously removed at the surface of the alkali solution via dissolution and formation of (bi-)carbonates (i.e., C_{Alkali}), we assume $CO_{2,solution}$ to be much smaller than $CO_{2,soil}$, such that the rate of diffusion is simplified to $D \cdot CO_{2,soil}$.

In the modified model variant, all analyses involving CO_2 , in particular the calculation of CR, are then carried out using the new C_{Alkali} pool.

The rate parameter D integrates the effects of all transport processes from the soil microbes to the alkali solution like the diffusion through the liquid phase in the soil, equilibration with the gaseous phase and subsequent diffusion through the headspace, such that the interpretation of its quantitative value is difficult. During model calibration, we constrain this parameter to yield an approximate delay between CO_2 and C_{Alkali} of no more than 2.5 h.

The exact origin of the delay is uncertain. An additional experiment showed that soil height (0.9 and 1.7 cm) did not affect the delay time of the CO_2 signal, rendering liquid diffusion through the wet soil matrix an unlikely limitation. Moreover, the release of gaseous CO_2 through equilibration with dissolved CO_2 in the soil solution should be instantaneous because of the low storage capacity of the soil solution at a pH of 6.3 (Blagodatskaya and Kuzyakov, 2008). Therefore, overcoming the spatial distance of approx. 9 cm between the soil surface and the alkali solution via gaseous diffusion seems to be the most likely reason for the delay. However, process-based modeling considering all physico-chemical processes in the incubation vessel would be necessary to confirm this delay of up to 2.5 hr. Nonetheless, future studies might consider quantifying or modeling the physical (and chemical) processes involved in the transport of CO_2 from the soil to the site of detection in more detail, in particular if their aim is to combine sensitive temporal estimates like the rates of heat and CO_2 production.

D Analysis of model CR, CUE and EUE

In this section, we summarize the theoretical relationship between CUE, EUE and CR and describe the CR dynamics produced by the model. A detailed presentation of the underlying considerations can be found in Chakrawal et al. (2020). In the following, we use the convention that a positive CR indicates net release of heat (i.e., negative reaction enthalpy).

First, estimates of CUE_s and cumulative CR can be diagnosed from the dynamic model in the same way as they are obtained from experimental observations. For CUE_s , we have

$$CUE_s(t) = 1 - \frac{CO_2(t)}{S_0} \quad (\text{Eqn. S24})$$

with the initial substrate concentration $S_0 = 400 \mu\text{g C g}^{-1}$. We emphasize that Eqn. S24 is only an appropriate estimator of CUE around the time that all substrate has been consumed by microbes, and choosing $t = 50$ h yields the estimates for the end of the incubation as presented in Fig. 4, where this assumption is justified. Note that this might in turn underestimate the actual efficiency, given that glucose might have been depleted before 50 h and CUE_s is a strictly decreasing function of time due to basal respiration. The limitations of this estimator could be somewhat alleviated by the use of an isotopically labelled substrate.

For cumulative CR, we have

$$CR_{cumu}(t) = -\frac{Q(t)}{CO_2(t)}. \quad (\text{Eqn. S25})$$

and $t = 50$ h again yields the estimates presented in the main text (Fig. 3, Fig. 4). On the other hand, the model also allows the computation of the CR as the ratio of the rates of heat and CO_2 release from Eqns. S5-S6, i.e.,

$$CR = -\frac{\frac{dQ}{dt}}{\frac{dCO_2}{dt}}. \quad (\text{Eqn. S26})$$

Similarly, instantaneous estimates of CUE and EUE can be obtained, e.g., from the rates of biomass increase (or decrease) and CO_2 and heat release:

$$CUE = \frac{\frac{dX}{dt}}{\frac{dX}{dt} + \frac{dCO_2}{dt}}, \quad (\text{Eqn. S27})$$

$$EUE = \frac{\frac{dX}{dt} \frac{Y_X}{4} \Delta H_T}{\frac{dX}{dt} \frac{Y_X}{4} \Delta H_T + \frac{dQ}{dt}} \quad (\text{Eqn. S28})$$

For a single catabolic reaction, the CR can be found as the ratio of its reaction enthalpy and its stoichiometric coefficient of CO₂ (see Eqn. S17), both calculated for the consumption of 1 mol C of substrate. For example, the theoretical CR of aerobic catabolism of glucose is equal to its combustion enthalpy,

$$CR_{cat,glu} = -\frac{\Delta_{cat}H_{glu}}{a_{CO_2}} = -\frac{-469 \text{ kJ}}{1 \text{ mol } CO_2} = 469 \frac{\text{kJ}}{\text{mol C}}. \quad (\text{Eqn. S29})$$

Beyond pure catabolism, the theoretical CR of a growth reaction can be calculated using the heat release given by Eqn. S18 and the stoichiometric coefficient of CO₂ in the growth reaction (Eqn. S16). For example, for aerobic growth on glucose, we have

$$CR_G = -\frac{(1-Y\frac{Y_X}{Y_S})\Delta_{cat}H_{glu}}{1-Y} \leq CR_{cat,glu}. \quad (\text{Eqn. S30})$$

If this growth reaction is the only process taking place (i.e., no maintenance), Eqn. S27 yields

$$CUE = \frac{Y \cdot U}{Y \cdot U + (1-Y)U} = Y \quad (\text{Eqn. S31})$$

and the (instantaneous) CUE in the model is equal to the yield coefficient Y of the growth reaction. Plotting Eqn. S30 against Eqn. S29 for a range of Y yields the theoretical curves shown in Fig. 4b. Similarly,

$$EUE = \frac{Y \cdot U \frac{Y_X}{4} \Delta H_T}{Y \cdot U \frac{Y_X}{4} \Delta H_T + \Delta H_G \cdot U} = \frac{Y \frac{Y_X}{4} \Delta H_T}{Y \frac{Y_X}{4} \Delta H_T + (1-Y\frac{Y_X}{Y_S})\frac{Y_S}{4} \Delta H_T} = \frac{Y \frac{Y_X}{4}}{Y \frac{Y_X}{4} + \frac{Y_S}{4} - Y \frac{Y_X}{4}} = \frac{Y_X}{Y_S} Y = \frac{Y_X}{Y_S} CUE \quad (\text{Eqn. S32})$$

is the (instantaneous) EUE in the model for the pure growth reaction. Note that it differs from CUE by a factor of $\frac{Y_X}{Y_S}$, which determines the slope of the line in Fig. 4a. In particular, both the relationship between CUE and CR as well as that between CUE and EUE depend on the assumed biomass composition (i.e., CH_{1.8}O_{0.5}N_{0.2} with $\gamma_X = 4.2$). In Fig. 4, we also show the prediction for the formula CH_{1.8}O_{0.5}N_{0.1} with a higher C:N ratio of 10 and $\gamma_X = 4.5$ (see also Yang et al., 2024).

In contrast to the pure growth reaction, the total CR of the dynamic model at any given time is more complex. It represents the sum of the heat and CO₂ contributions of all processes that are

currently taking place in the system (e.g., growth and maintenance, Eqn. S26). For example, in a system with aerobic growth on glucose proceeding at rate U and aerobic maintenance (catabolism) on glucose proceeding at rate M , the total CR is

$$CR = -\frac{\frac{dQ}{dt}}{\frac{dCO_2}{dt}} = -\frac{U \cdot \left(\left(1 - Y \frac{Y_X}{Y_S} \right) \Delta_{cat} H_{glu} \right) + M \cdot \Delta_{cat} H_{glu}}{U \cdot (1 - Y) + M}. \quad (\text{Eqn. S33})$$

Evidently, any process proceeding at a high rate and yielding large amounts of heat and CO_2 per mol C of substrate thus has a large impact on the total CR (in the presence of substrate, this will typically be the growth reaction). Temporal variations in total CR in the model are the result of temporal variations in these contributing processes. In our simulations, these are primarily due to changes in the active fraction of microbes, since inactive microbes only contribute maintenance fluxes (catabolism), while the active fraction also contributes CO_2 and heat from the growth reaction for as long as sufficient substrate is available.

Note that the addition of maintenance respiration decreases model CUE below the value of the yield coefficient Y predicted by Eqn. S31, since it increases CO_2 release while not affecting (exogenous maintenance) or even decreasing (endogenous maintenance) biomass. Its effect on the total CR depends on the value of the parameter ΔH_M . In our simulations, we find $\Delta H_M \leq \Delta_{cat} H_{glu}$, and thus $CR \leq CR_{cat,glu}$. In general, this implies that the model will never predict (dynamic or cumulative) CR values above ~ 469 kJ / mol C, in contrast to some of the observed values. However, this discrepancy might in part be attributable to the effect of delayed CO_2 detection as highlighted in Fig. S4, as the model variant with delayed CO_2 detection predicts CR values exceeding $CR_{cat,glu}$ without any changes to chemical reactions considered.

E Model integration and fitting

The dynamic model presented in section C was implemented in Python (version 3.9.18). The system of ODEs was integrated numerically for a time of 50 h, with $t = 0$ h indicating the time of glucose addition. Integration was carried out using the *radau* method of the *solve_ivp* function in the *scipy.optimize* package (version 1.11.0, (Virtanen et al., 2020)).

For the calibration of model parameters, we used the *leastsq* method as implemented in the *minimize* function of the *lmfit* package (version 1.2.1, (Newville et al., 2023)), which employs the Levenberg-Marquardt algorithm to minimize the residual sum of squares between model output and experimentally determined rates of heat and CO_2 release. Since heat release was

380 measured at a higher temporal resolution, we normalized the residuals by the mean values and
381 lengths of the corresponding data series, i.e., we minimized

$$382 \quad R = \sum_i \sum_j^{n_i} \left(\frac{x_{i,j}^{model} - x_{i,j}^{data}}{\bar{x}_i \sqrt{n_i}} \right)^2 \quad (\text{Eqn. S34})$$

383 where i indicates CO₂ or heat, j indicates the j th measurement and n_i is the number of
384 measurements of quantity i .

385 For each parameter, we provided an initial guess as well as an upper and lower bound via the
386 *Parameters* interface of *Imfit*. For glucose, the initial concentration was fixed at the known
387 experimental value (400 µg C g⁻¹). We also fixed initial biomass at the estimated MBC value for
388 this soil (155 µg C g⁻¹, see section B).

389 Due to the initial disturbance in the experimental setup, measurements from the first 5 h of the
390 incubation were not used for model calibration.

391 All calibrated parameter values for the different treatments along with uncertainty estimates
392 obtained by *Imfit* are provided in the supplementary data file S1 Data.

393

F References

- Battley, E.H., 2009. Is electron equivalence between substrate and product preferable to C-mol equivalence in representations of microbial anabolism applicable to "origin of life" environmental conditions?. *Journal of Theoretical Biology* 260, 267–275. doi:10.1016/j.jtbi.2009.05.032
- Beck, T., Joergensen, R.G., Kandeler, E., Makeschin, F., Nuss, E., Oberholzer, H.R., Scheu, S., 1997. An inter-laboratory comparison of ten different ways of measuring soil microbial biomass C. *Soil Biology and Biochemistry* 29, 1023–1032. doi:10.1016/S0038-0717(97)00030-8
- Benjamini, Y., Hochberg, Y., 1995. Controlling the False Discovery Rate: A Practical and Powerful Approach to Multiple Testing. *Journal of the Royal Statistical Society: Series B (Methodological)* 57, 289–300. doi:10.1111/j.2517-6161.1995.tb02031.x
- Blagodatskaya, E., Kuzyakov, Y., 2008. Mechanisms of real and apparent priming effects and their dependence on soil microbial biomass and community structure: critical review. *Biology and Fertility of Soils* 45, 115–131. doi:10.1007/s00374-008-0334-y
- Blagodatsky, S.A., Heinemeyer, O., Richter, J., 2000. Estimating the active and total soil microbial biomass by kinetic respiration analysis. *Biology and Fertility of Soils* 32, 73–81. doi:10.1007/s003740000219
- Čapek, P., Choma, M., Kaštovská, E., Tahovská, K., Glanville, H.C., Šantrůčková, H., 2023. Revisiting soil microbial biomass: Considering changes in composition with growth rate. *Soil Biology and Biochemistry* 184, 109103. doi:10.1016/j.soilbio.2023.109103
- Chakrawal, A., Herrmann, A.M., Manzoni, S., 2021. Leveraging energy flows to quantify microbial traits in soils. *Soil Biology and Biochemistry* 155, 108169. doi:10.1016/j.soilbio.2021.108169
- Chakrawal, A., Herrmann, A.M., Šantrůčková, H., Manzoni, S., 2020. Quantifying microbial metabolism in soils using calorimetry — A bioenergetics perspective. *Soil Biology and Biochemistry* 148, 107945. doi:10.1016/j.soilbio.2020.107945
- Grathwohl, P., 1998. *Diffusion in Natural Porous Media: Contaminant Transport, Sorption/Desorption and Dissolution Kinetics*, Topics in Environmental Fluid Mechanics. Springer US, Boston, MA. doi:10.1007/978-1-4615-5683-1
- Lenth, R.V., 2023. emmeans: Estimated Marginal Means, aka Least-Squares Means.
- Newville, M., Otten, R., Nelson, A., Stensitzki, T., Ingargiola, A., Allan, D., Fox, A., Carter, F., Michał, Osborn, R., Pustakhod, D., Ineuhaus, Weigand, S., Aristov, A., Glenn, Deil, C., mgunyho, Mark, Hansen, A.L.R., Pasquevich, G., Foks, L., Zobrist, N., Frost, O., Stuermer, azelcer, Polloreno, A., Persaud, A., Nielsen, J.H., Pompili, M., Eendebak, P., 2023. Imfit/Imfit-py: 1.2.2. doi:10.5281/zenodo.8145703
- Pagel, H., Kriesche, B., Uksa, M., Poll, C., Kandeler, E., Schmidt, V., Streck, T., 2020. Spatial Control of Carbon Dynamics in Soil by Microbial Decomposer Communities. *Frontiers in Environmental Science* 8, 2. doi:10.3389/fenvs.2020.00002
- Panikov, N.S., 1995. *Microbial Growth Kinetics*. Chapman and Hall, London, Glasgow.
- Peter Linstrom, 2017. NIST Chemistry WebBook - SRD 69. National Institute of Standards and Technology.
- Thornton, W.M., 1917. XV. The relation of oxygen to the heat of combustion of organic compounds. *The London, Edinburgh, and Dublin Philosophical Magazine and Journal of Science* 33, 196–203. doi:10.1080/14786440208635627
- Vance, E.D., Brookes, P.C., Jenkinson, D.S., 1987. An extraction method for measuring soil microbial biomass C. *Soil Biology and Biochemistry* 19, 703–707. doi:10.1016/0038-0717(87)90052-6

- Virtanen, P., Gommers, R., Oliphant, T.E., Haberland, M., Reddy, T., Cournapeau, D., Burovski, E., Peterson, P., Weckesser, W., Bright, J., van der Walt, S.J., Brett, M., Wilson, J., Millman, K.J., Mayorov, N., Nelson, A.R.J., Jones, E., Kern, R., Larson, E., Carey, C.J., Polat, İ., Feng, Y., Moore, E.W., VanderPlas, J., Laxalde, D., Perktold, J., Cimrman, R., Henriksen, I., Quintero, E.A., Harris, C.R., Archibald, A.M., Ribeiro, A.H., Pedregosa, F., van Mulbregt, P., SciPy 1.0 Contributors, 2020. SciPy 1.0: Fundamental Algorithms for Scientific Computing in Python. *Nature Methods* 17, 261–272. doi:10.1038/s41592-019-0686-2
- Wang, G., Post, W.M., 2012. A theoretical reassessment of microbial maintenance and implications for microbial ecology modeling. *FEMS Microbiology Ecology* 81, 610–617. doi:10.1111/j.1574-6941.2012.01389.x
- Yang, S., Di Lodovico, E., Rupp, A., Harms, H., Fricke, C., Miltner, A., Kästner, M., Maskow, T., 2024. Enhancing insights: exploring the information content of calorespirometric ratio in dynamic soil microbial growth processes through calorimetry. *Frontiers in Microbiology* 15, 1321059. doi:10.3389/fmicb.2024.1321059
- Zech, A., De Winter, M., 2023. A Probabilistic Formulation of the Diffusion Coefficient in Porous Media as Function of Porosity. *Transport in Porous Media* 146, 475–492. doi:10.1007/s11242-021-01737-5
- Zhang, Y., Yang, Z., Wang, F., Zhang, X., 2021. Comparison of soil tortuosity calculated by different methods. *Geoderma* 402, 115358. doi:10.1016/j.geoderma.2021.115358

464

465 **G Supplementary figures and tables**466 **Supplementary table S1.** Basic soil properties of the soil used in this study.

Parameter	Unit	Value
Total organic carbon	%	0.74
Total nitrogen	%	0.08
N _{min}	mg / kg	25.8
pH	(in CaCl ₂)	6.3
P	mg / kg	57
K	mg / kg	161
Microbial biomass carbon (fresh soil, CFE)	µg C / g soil	178
Microbial biomass carbon (air dried and rewetted soil, CFE)	µg C / g soil	155
Clay	%	16.8
Silt	%	70.1
Sand	%	13.1

467

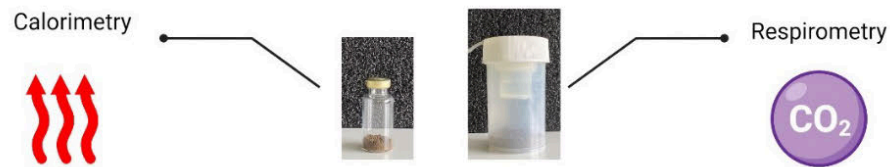
468

469 **Supplementary table S2.** Variables and parameters of the dynamic model including units. The
470 initial values, calibration results and uncertainty estimates of all quantities that were calibrated
471 with data are provided in S1 Data.

Symbol	Name	Unit
S	Glucose concentration	mol C / g
X	Biomass concentration	mol C / g
CO_2	Cumulative CO_2	mol C / g
Q	Cumulative heat	kJ / g
N	Nutrient concentration	mol nutrient / g
r	Index of physiological state	-
C_{Alkali}	Cumulative CO_2 -C in the alkali solution	mol C / g
v_m	Maximum specific substrate uptake rate	1 / h
K_S	Glucose half-saturation	mol C / g
K_r	Activity half-saturation	mol C / g
m_a	Specific maintenance coefficient of active fraction	1 / h
m_i	Specific maintenance coefficient of inactive fraction	1 / h
I	Rate coefficient for nutrient replenishment	1 / h
N_0	Initial concentration of nutrient	mol nutrient / g
K_N	Nutrient half-saturation	mol nutrient / g
D	Rate coefficient for the transport of CO_2 from the soil to the site of detection	1 / h
Y	(Biomass) yield of glucose respiration	mol C biomass / mol C glucose
γ_S	Degree of reduction of glucose	mol e ⁻ / mol C glucose
γ_X	Degree of reduction of biomass	mol e ⁻ / mol C biomass
$\Delta_{cat}H_{glu}$	Reaction enthalpy of catabolic glucose respiration	kJ / mol C glucose
ΔH_G	Reaction enthalpy of growth reaction (Eqn. S18)	kJ / mol C glucose
ΔH_M	Reaction enthalpy of maintenance	kJ / mol C biomass
U	Utilization rate of glucose for growth	mol C glucose / g / h
M_{ija}	Maintenance rate of the inactive/active fraction	mol C substrate / g / h
M_{Sija}	Part of maintenance rate of the inactive/active fraction fueled by glucose	mol C glucose / g / h
M_{Xija}	Part of maintenance rate of the inactive/active fraction fueled by biomass	mol C biomass / g / h

472

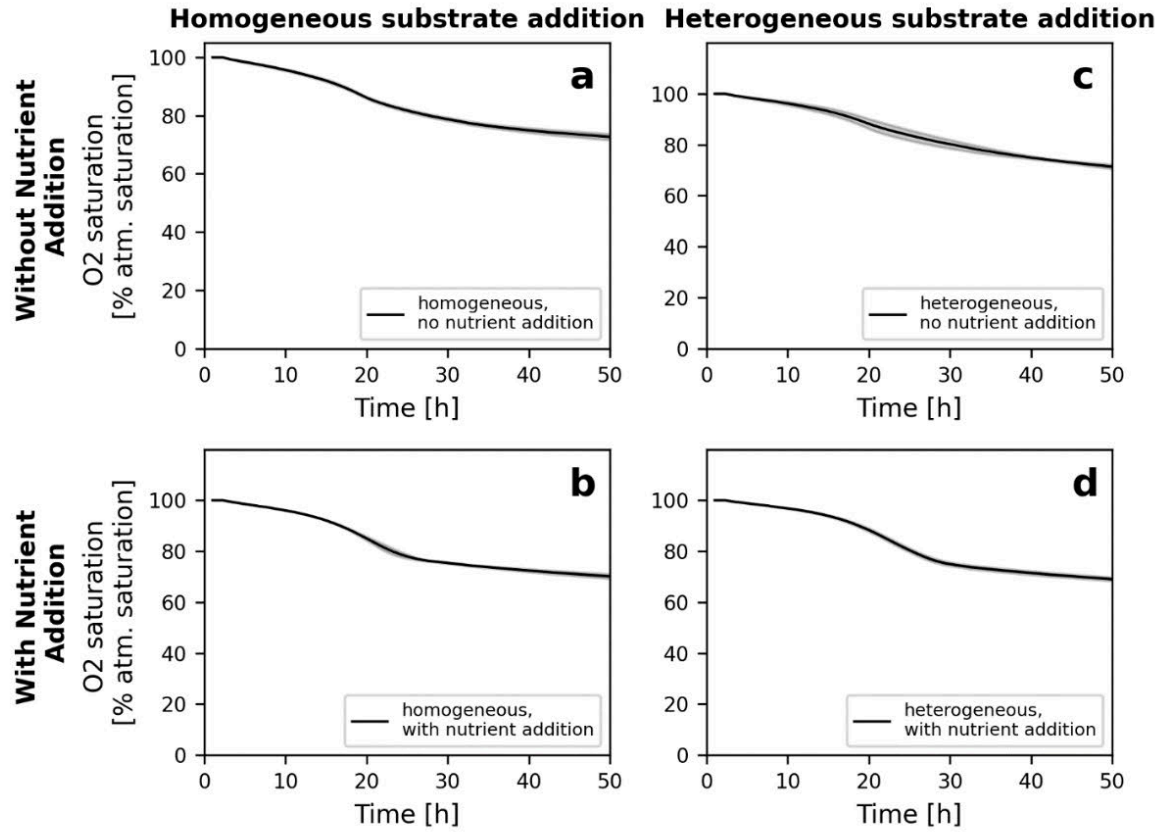
473 **Supplementary figure S1.** Incubation vessels **a** used for the determination of CO₂ release in
474 the Respicond respirometer (height 10 cm, diameter 6 cm) and **b** used for the determination of
475 heat release in the TAM air calorimeter as well as for O₂ consumption, DNA and glucose
476 measurements (height 4.3 cm + 1 cm neck, diameter 2.cm).



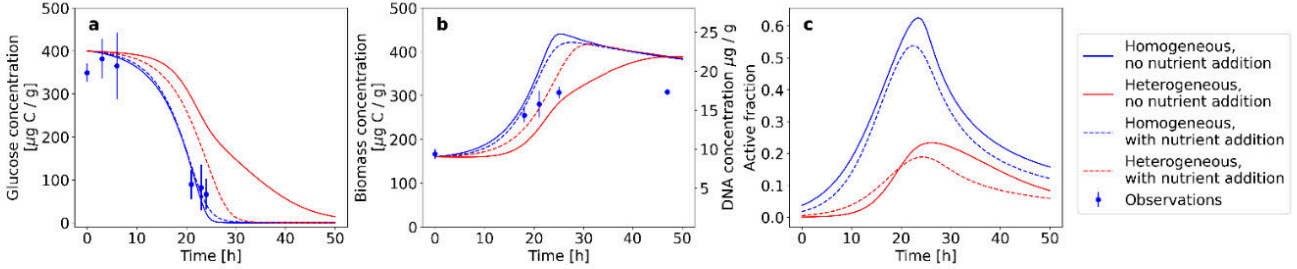
477

478

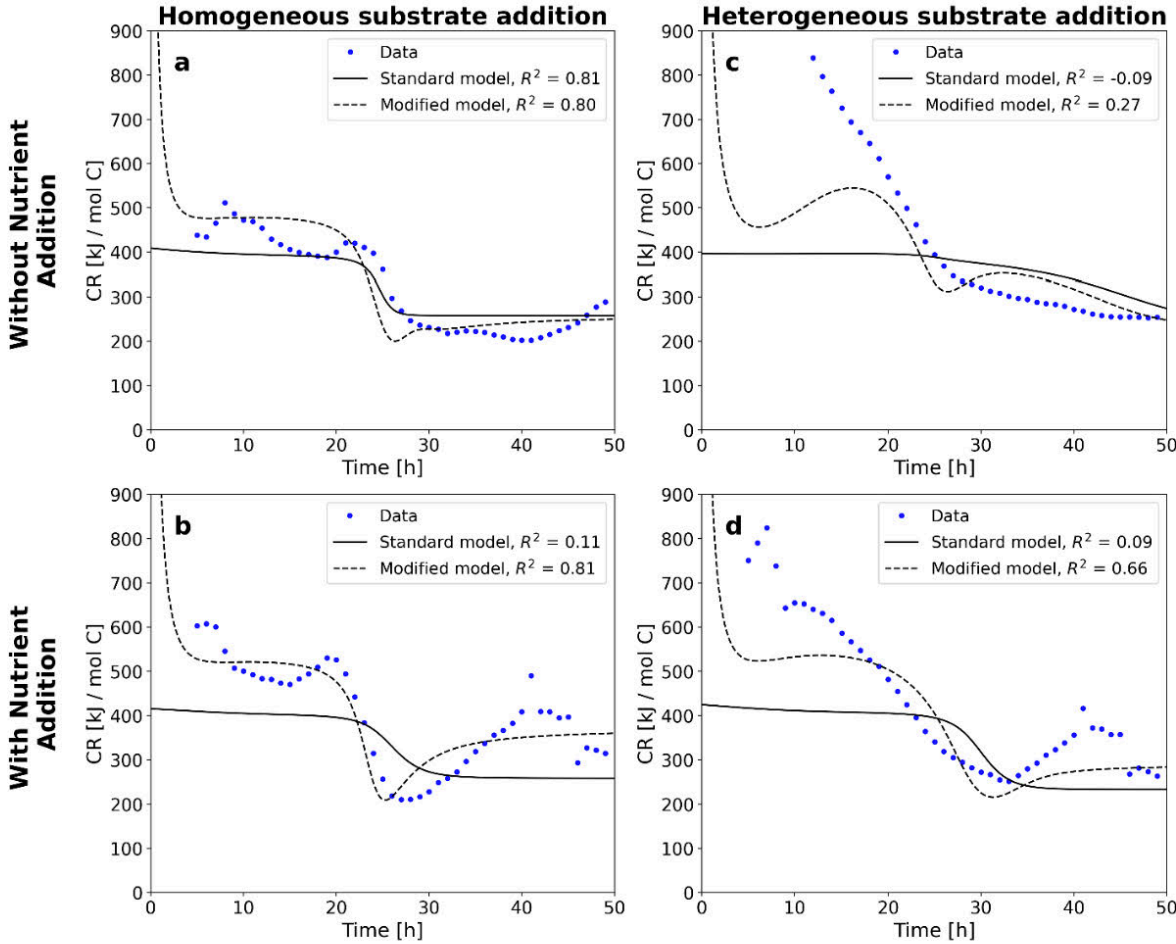
Supplementary figure S2. Headspace O₂ saturation (100% = 21.22 kPa) over the course of 50 h of incubation for all treatments. Conditions remained oxidic in all cases, with O₂ reaching ~70% atmospheric saturation after 50 h. Shown are mean ± SD of *n* = 3 replicates.



Supplementary figure S3. Dynamics of **a** residual glucose, **b** microbial biomass and **c** active fraction of microbial biomass in the ODE model. For the homogeneous treatment without nutrient addition (solid blue line), residual glucose as well as dsDNA was quantified experimentally in parallel incubations (markers, mean \pm SD, $n = 3$). Heterogeneous treatments are shown in red, homogeneous ones in blue. Solid lines indicate treatments without nutrient addition, dashed lines those with nutrient addition.



Supplementary figure S4. Observed and modeled dynamics of the calorespirometric ratio (CR) calculated from rates of heat ($n = 3$) and CO_2 ($n = 4$) release for all treatments. Solid lines show the results of simulations using the standard model formulation, which assumes instantaneous detection of CO_2 after production via microbial metabolism. Dashed lines show simulations using the modified model, in which CO_2 diffuses from the site of production (soil) to the site of detection (alkali solution), inducing a relative delay of CO_2 release compared to the rate of heat release.



Supplementary material of Wirsching et al. (2024)

This supplementary material consists of the following components:

- SI Text. PDF file containing supplementary materials and methods, Supplementary Figs. S1–S6, Supplementary Tables S1–S5, and supplementary references.

SI Text is provided below.

Supplementary material

Johannes Wirsching^{a,*}, Martin-Georg Endress^{b,*}, Eliana Di Lodovico^c, Sergey Blagodatsky^{b,d}, Christian Fricke^c, Marcel Lorenz^e, Sven Marhan^a, Ellen Kandeler^a, Christian Poll^a

^a*Institute of Soil Science and Land Evaluation, Soil Biology Department, University of Hohenheim, Germany*

^b*Institute of Zoology, Faculty of Mathematics and Natural Sciences, University of Cologne, Germany*

^c*Faculty of Natural and Environmental Sciences, University of Kaiserslautern-Landau, Germany*

^d*Campus Alpin, Institute of Meteorology and Climate Research, Department of Atmospheric Environmental Research (IMK-IFU), Karlsruhe Institute of Technology (KIT), Germany*

^e*Department of Soil Science, University of Trier; Helmholtz Centre for Environmental Research, Leipzig, Germany*

November 18, 2024

17 Pages

6 Figures

5 Table

* Authors contributed equally

Contents

1	Materials and Methods	3
1.1	Nomenclature and experimental design	3
1.2	Soil properties	4
1.3	Dynamic model formulation	7
1.4	Model integration and calibration	10
2	Results	12
2.1	Calorimetry	12
2.2	Combustion calorimetry/TG-DSC	13
2.3	Modeling	14

List of Figures

1	Flow chart of experimental setup	4
2	Uncorrected mean heat	12
3	SOM energy contents	14
4	Model CUE estimates	15
5	Model growth rate estimates	15
6	Model SOM degree of reduction estimates	16

List of Tables

1	Nomenclature of relevant terms	3
2	Soil properties	5
3	Soil properties	6
4	Model variables, rates and parameters with meaning and units.	11
5	Combustion enthalpy of SOM	13

1. Materials and Methods

1.1. Nomenclature and experimental design

Table 1: Nomenclature of relevant terms used in the article, including symbol, meaning as well as unit and equation where applicable.

Symbol	Meaning	Unit	Equation
PE	Priming effect	$\text{g C g}^{-1} \text{ soil}$	Eq. 3
$\Delta_c H_i$	Combustion enthalpy of compound i	J mol^{-1}	-
$\Delta_r H_i$	Reaction enthalpy of reaction i	J mol^{-1}	-
ΔH_{cell}	Reaction enthalpy of the growth reaction on cellulose	J mol^{-1}	Eq. 8
$P(t)$	Specific heat production rate	$\text{W g}^{-1} \text{ soil}$	Eq. 4
$Q(t)$	Specific heat	$\text{J g}^{-1} \text{ soil}$	Eq. 5
EUE_{net}	Net energy use efficiency	-	Eq. 6
CB_{net}	Net carbon balance	-	Eq. 15
CR	Calorespirometric ratio	$\text{J mol}^{-1} \text{ CO}_2\text{-C}$	Eq. 7
γ_i	Relative degree of reduction of compound i	$\text{mol e}^- \text{ mol}^{-1} \text{ C}$	Eq. 9
CUE_{L}	CUE estimate based on ^{13}C	-	Eq. 13
CUE_{RQ}	CUE estimate based on the CR	-	Eq. 14

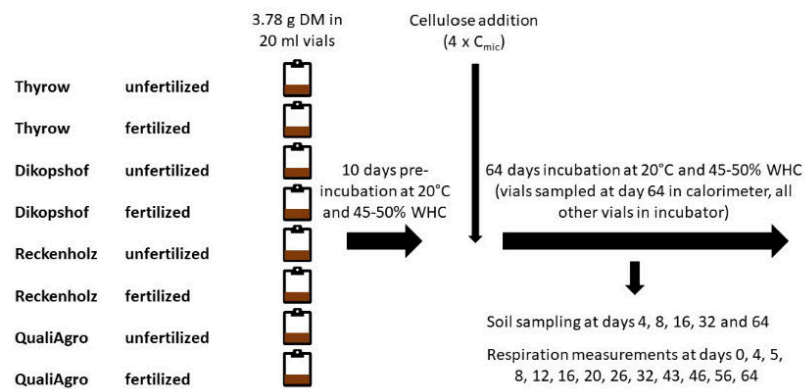


Figure 1: Flow chart illustrating the experimental design and setup used in this study. All details are provided in sections 2.1-2.7 of the main text.

1.2. Soil properties

Table 2: Soil properties

Parameter	Unit	Dikopshof						QualiAgro					
		Farmyard manure			Unfertilized			Farmyard manure			Unfertilized		
		2020	2021	2022	2020	2021	2022	2020	2021	2022	2020	2021	2022
C	[%]	0.90	1.10	1.19	0.78	0.76	0.73	1.59	1.47	1.61	1.09	1.19	1.12
N	[%]	0.10	0.14	0.12	0.10	0.09	0.09	0.17	0.17	0.17	0.14	0.15	0.12
S	[%]	0.013	0.014	0.015	0.013	0.011	0.010	0.027	0.017	0.016	0.021	0.016	0.014
H	[%]	0.28	0.27	0.28	0.26	0.23	0.26	0.33	0.30	0.33	0.27	0.27	0.25
O	[%]	2.43	2.39	2.15	2.35	1.93	1.99	2.74	2.40	2.30	2.30	2.20	2.11
C/N		9.1	7.9	9.5	7.8	8.1	8.5	9.5	8.8	9.7	7.7	7.8	9.0
C/S		69	81	82	62	73	73	60	89	101	52	77	80
H/C		0.31	0.25	0.24	0.34	0.30	0.35	0.21	0.21	0.21	0.24	0.23	0.23
O/C		2.7	2.2	1.8	3.0	2.5	2.7	1.7	1.6	1.4	2.1	1.9	1.9
pH	(CaCl ₂)	6.3	6.3	6.5	6.1	5.8	6.0	6.4	6.6	6.7	5.7	5.6	5.9
PCAL	[mg kg ⁻¹]	5.7	7.6	5.6	3.1	3.3	1.6	8.7	8.8	8.9	3.6	3.5	3.4
KCAL	[mg kg ⁻¹]	115	202	163	52	49	22	252	221	197	63	74	87

Table 3: Soil properties

Parameter	Unit	Reckenholtz						Thyrow					
		Farmyard manure			Unfertilized			Farmyard manure			Unfertilized		
		2020	2021	2022	2020	2021	2022	2020	2021	2022	2020	2021	2022
C	[%]	1.04	1.06	0.99	0.85	0.94	0.82	0.77	0.69	0.70	0.33	0.34	0.37
N	[%]	0.13	0.14	0.11	0.11	0.12	0.10	0.09	0.08	0.07	0.04	0.04	0.04
S	[%]	0.015	0.015	0.013	0.013	0.011	0.012	0.018	0.014	0.017	0.015	0.010	0.011
H	[%]	0.26	0.26	0.25	0.24	0.25	0.24	0.10	0.09	0.09	0.05	0.06	0.06
O	[%]	2.02	2.03	2.11	2.08	2.22	1.99	0.93	0.91	0.91	0.58	0.56	0.51
C/N		7.9	7.5	9.0	7.6	8.1	7.9	8.9	8.7	9.9	8.7	7.7	9.4
C/S		69	73	79	68	85	71	44	51	43	22	34	35
H/C		0.25	0.25	0.25	0.29	0.26	0.29	0.13	0.13	0.13	0.17	0.17	0.15
O/C		1.9	1.9	2.1	2.5	2.4	2.4	1.2	1.3	1.3	1.8	1.7	1.4
pH	(CaCl ₂)	5.2	5.1	5.2	4.7	4.7	4.8	5.0	5.2	5.0	4.2	4.3	4.3
PCAL	[mg kg ⁻¹]	3.0	4.8	3.8	2.4	3.6	3.1	6.6	6.1	5.5	4.3	4.5	4.8
KCAL	[mg kg ⁻¹]	44	32	38	21	26	27	101	38	59	19	3	20

1.3. Dynamic model formulation

The dynamic model used in this study builds on the formulations of Endress et al. (2024a) and Endress et al. (2024b) and the underlying rationale has been explained in detail in these publications and their respective supplementary materials.

For the purposes of our investigation, we extended these formulations to represent the dynamics of ^{13}C pools as well as SOM decomposition. Most importantly, this involves splitting each of the major carbon pools (biomass X , CO_2) into two pools representing the separate concentrations of ^{12}C and ^{13}C . In total, the dynamics of microbial growth after cellulose addition are modelled using a system of 9 coupled ordinary differential equations (ODEs) representing the concentrations of the 5 major carbon pools (^{13}C cellulose S , ^{13}C biomass ^{13}X , ^{12}C biomass ^{12}X , $^{13}\text{CO}_2$ and $^{12}\text{CO}_2$) as well as cumulative heat release (Q) and the physiological state of the microbial population ($r \in [0, 1]$), which indicates the active fraction of total biomass capable of growth (Blagodatsky and Richter, 1998). We use $X = ^{12}X + ^{13}X$ to denote total biomass. . Finally, the model also tracks the accumulation of (^{13}C and ^{12}C) necromass (N). All carbon pools are measured in mol C / g soil, cumulative heat is measured in kJ / g soil. A full list of model variables and parameters with units is provided in table 4 of this supplementary material. The full ODE system reads:

$$\frac{dS}{dt} = -U_S \quad (1)$$

$$\frac{d^{12}X}{dt} = Y_{SOM}U_{SOM} - (M_a + M_i)\frac{^{12}X}{X} - d \cdot ^{12}X \quad (2)$$

$$\frac{d^{13}X}{dt} = Y_S U_S - (M_a + M_i)\frac{^{13}X}{X} - d \cdot ^{13}X \quad (3)$$

$$\frac{d^{12}CO_2}{dt} = (1 - Y_{SOM})U_{SOM} + (M_a + M_i)\frac{^{12}X}{X} \quad (4)$$

$$\frac{d^{13}CO_2}{dt} = (1 - Y_S)U_S + (M_a + M_i)\frac{^{13}X}{X} \quad (5)$$

$$\frac{dQ}{dt} = \Delta_r H_S U_S + \Delta_r H_{SOM} U_{SOM} + \Delta_c H_X (M_a + M_i) \quad (6)$$

$$\frac{dr}{dt} = v_r v_S Y_S \cdot r \cdot \left(\frac{S - S_T}{S - S_T + K_r} - r \right) \quad (7)$$

$$\frac{d^{12}N}{dt} = d \cdot ^{12}X \quad (8)$$

$$\frac{d^{13}N}{dt} = d \cdot ^{13}X \quad (9)$$

Here, the following process rates were used:

$$U_S = v_{Sr} X \frac{S - S_T}{S - S_T + K_S} \quad \dots \text{Cellulose uptake rate} \quad (10)$$

$$U_{SOM} = v_{SOM} r X \quad \dots \text{SOM uptake rate} \quad (11)$$

$$M_a = m_a r X \quad \dots \text{Maintenance rate active fraction} \quad (12)$$

$$M_i = m_i (1 - r) X \quad \dots \text{Maintenance rate inactive fraction} \quad (13)$$

The active biomass rX utilizes both ^{13}C cellulose at rate U_S and ^{12}C SOM at rate U_{SOM} to fuel growth (Eq. 1-3). For cellulose, this utilization follows Michaelis-Menten kinetics with an additional threshold concentration S_T (Eq. 10). Effectively, S_T functions as a black box parameter to determine the concentration of cellulose at which microbes stop utilizing it as a growth substrate. This

parameter was included to reflect the substantial levels of remaining cellulose observed at the end of our incubations. In contrast, the uptake of SOM is only limited by the concentration of active biomass rX , which consumes it at a specific rate v_{SOM} (Eq. 11). In the model, the consumption of SOM eventually ceases due to the gradual inactivation of microbes as cellulose levels approach S_T (Eq. 7). CO_2 is produced by the growth reactions on cellulose and SOM according to the biomass yield coefficients of these reactions (Y_S and Y_{SOM} , respectively, Eq. 4 and 5), and additional CO_2 is released as the product of maintenance respiration (Eq. 12 and 13).

The total heat production consists of the heat release due to the two growth reactions as well as maintenance (Eq. 6). A detailed derivation of the reaction enthalpies has been presented before (Endress et al., 2024a; Chakrawal et al., 2020). In brief, we used

$$\Delta_r H_S = \left(1 - Y_S \frac{\gamma_X}{\gamma_S}\right) \Delta_c H_S \quad (14)$$

$$\Delta_r H_{SOM} = \left(1 - Y_{SOM} \frac{\gamma_X}{\gamma_{SOM}}\right) \Delta_c H_{SOM} \quad (15)$$

$$(16)$$

in combination with combustion enthalpies $\Delta_c H$ based on our measurements or the degree of reduction γ of the involved compounds:

$$\Delta_c H_S = -406 \frac{\text{kJ}}{\text{molC}} \quad (17)$$

$$\Delta_c H_X = \frac{\gamma_X}{4} \cdot -455 \frac{\text{kJ}}{\text{molC}} \quad (18)$$

$$\Delta_c H_{SOM} = \frac{\gamma_{SOM}}{4} \cdot -455 \frac{\text{kJ}}{\text{molC}}. \quad (19)$$

1.4. Model integration and calibration

We followed the procedure described in Endress et al. (2024b) for model integration and calibration:

The dynamic model presented in section 1.3 was implemented in Python (version 3.9.18). The system of ODEs was integrated numerically for a time of 64 d, with $t = 0$ d indicating the time of cellulose addition. Integration was carried out using the *radau* method of the *solve_ivp* function in the *scipy.optimize* package (version 1.11.0, Virtanen et al. (2020)). For the calibration of model parameters, we used the *leastsq* method as implemented in the *minimize* function of the *lmfit* package (version 1.2.1, Newville et al. (2023)), which employs the Levenberg-Marquardt algorithm to minimize the residual sum of squares between model output and experimental observations. For calibration, we used measured values of the 5 time series for ^{13}C and ^{12}C biomass, cumulative ^{13}C and ^{12}C CO_2 as well as the rate heat release. Since these were measured at different temporal resolutions, we normalized the residuals by the mean values and lengths of the corresponding data series, i.e., we minimized

$$R = \sum_i \sum_j^{n_i} \left(\frac{x_{i,j}^{\text{model}} - x_{i,j}^{\text{data}}}{\bar{x}_i \sqrt{n_i}} \right)^2 \quad (20)$$

where i indicates the time series, j indicates the j th measurement and n_i is the number of measurements in time series i . For each parameter, we provided an initial guess as well as an upper and lower bound via the *Parameters* interface of *lmfit*. For cellulose, the initial concentration was fixed at the known value for the added amount per gram for each soil, and we also fixed initial biomass at the estimated value for each soil. Due to the initial disturbance in the experimental

setup, measurements from the first 0.5 d of the incubation were not used for model calibration.

Table 4: Model variables, rates and parameters with meaning and units.

Symbol	Name	Unit
S	Cellulose concentration	mol C cellulose / g
^{13}X	^{13}C Biomass concentration	mol C biomass / g
^{12}X	^{12}C Biomass concentration	mol C biomass / g
$^{13}\text{CO}_2$	Cumulative ^{13}C CO_2 release	mol C CO_2 / g
$^{12}\text{CO}_2$	Cumulative ^{12}C CO_2 release	mol C CO_2 / g
Q	Cumulative heat release	kJ / g
r	Activity state of the total biomass	$0 \leq r \leq 1$
^{13}N	^{13}C Necromass concentration	mol C necromass/ g
^{12}N	^{12}C Necromass concentration	mol C necromass/ g
v_S	Maximum specific cellulose uptake rate	1 / d
v_{SOM}	Maximum specific SOM uptake rate	1 / d
v_r	Rate of biomass (in-)activation	1 / d
K_S	Half-saturation of cellulose uptake	mol C cellulose/ g
S_T	Threshold concentration for cellulose uptake	mol C cellulose/ g
K_r	Half-saturation of biomass activation	mol C cellulose/ g
m_a	Specific maintenance rate of the active fraction	1 / d
m_i	Specific maintenance rate of the inactive fraction	1 / d
Y_S	Biomass yield of cellulose utilization	mol C biomass / mol C substrate
Y_{SOM}	Biomass yield of SOM utilization	mol C biomass / mol C SOM
d	Specific biomass death/turnover rate	1 / d
γ_X	Degree of reduction of biomass	mol e^- / mol C cellulose
γ_{SOM}	Degree of reduction of SOM	mol e^- / mol C SOM
$\Delta_c H_S$	Enthalpy of combustion of cellulose	kJ / mol C cellulose
$\Delta_c H_{SOM}$	Enthalpy of combustion of SOM	kJ / mol C SOM
$\Delta_c H_X$	Enthalpy of combustion of biomass	kJ / mol C biomass
$\Delta_r H_S$	Reaction enthalpy of growth on cellulose	kJ / mol C cellulose
$\Delta_r H_{SOM}$	Reaction enthalpy of growth on SOM	kJ / mol C SOM
U_S	Cellulose uptake rate	mol C cellulose / (g d)
U_{SOM}	SOM uptake rate	mol C SOM / (g d)
M_a	Maintenance rate of active fraction	mol C biomass / (g d)
M_i	Maintenance rate of inactive fraction	mol C biomass / (g d)

2. Results

2.1. Calorimetry

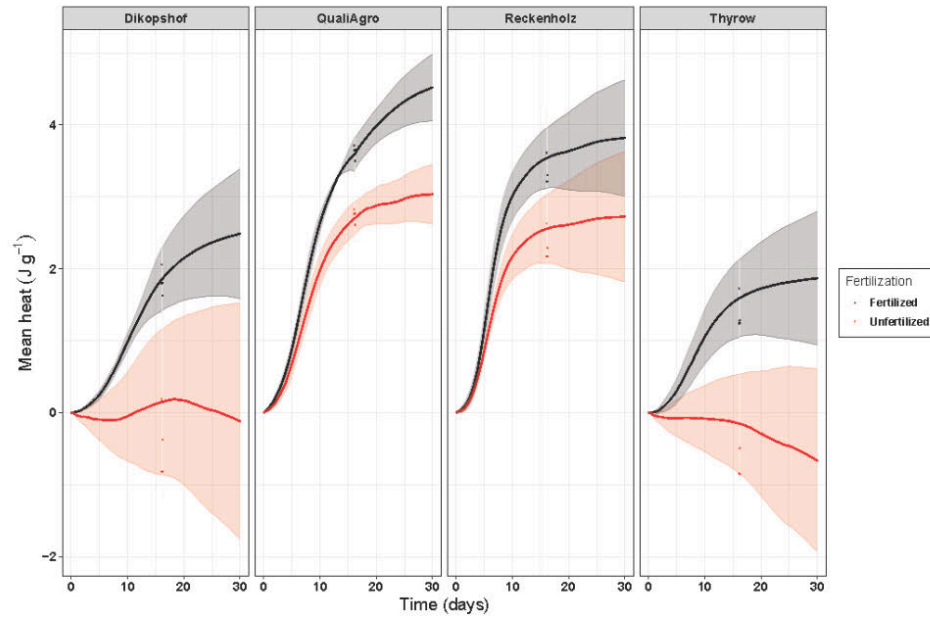


Figure 2: Uncorrected mean heat Q_t (J g⁻¹; n = 3) at all four sites and fertilized (black) and unfertilized (red) soils.

2.2. Combustion calorimetry/TG-DSC

Table 5: Combustion enthalpy of SOM
 Combustion calorimetry TG-DSC
 $-\Delta_e H_{SOM}$ [kJmol⁻¹C] $-\Delta_e H_{SOM}$ [kJmol⁻¹ C]

		mean	sd	mean	sd
Dikopshof	FYM	25.5	8.8	39.0	2.1
Thyrow	FYM	36.6	1.8	50.8	3.3
Reckenholz	FYM	35.1	3.5	37.6	1.1
QualiAgro	FYM	32.4	2.9	33.9	14.7
Dikopshof	UF	43.0	6.1	41.9	4.7
Thyrow	UF	61.0	2.5	68.3	15.1
Reckenholz	UF	42.4	4.1	37.5	0.9
QualiAgro	UF	36.3	11.9	33.1	1.0

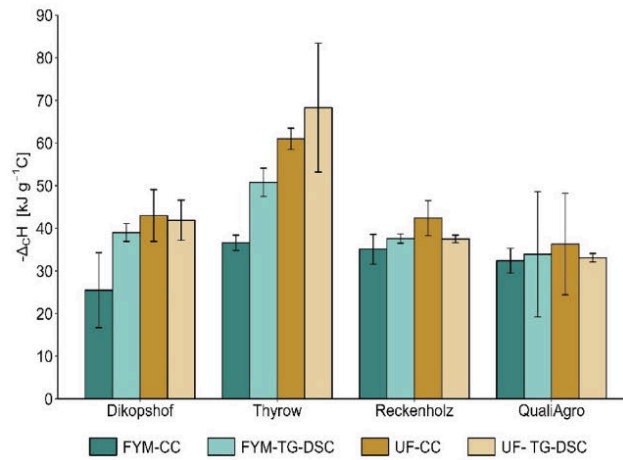


Figure 3: Quantitative values of $\Delta_c H$ obtained by combustion calorimetry and TG-DSC. TG-DSC yields higher values than combustion calorimetry in several cases (D-FYM, T-FYM). Both methods are at an early stage for determining $\Delta_c H$ of mineral soils and shortcomings of both were already identified. To date, further efforts are required to unify both in a quantitative way. However, the trends in $\Delta_c H$ with respect to the study site or treatment are similar irrespective of the used method. $\Delta_c H$ tends to be higher in the unfertilized treatment compared to the farmyard manure treatment. Highest $\Delta_c H$ values were observed in Thyrow soils. In general, more negative $\Delta_c H$ indicates more reduced and energy-rich carbon.

2.3. Modeling

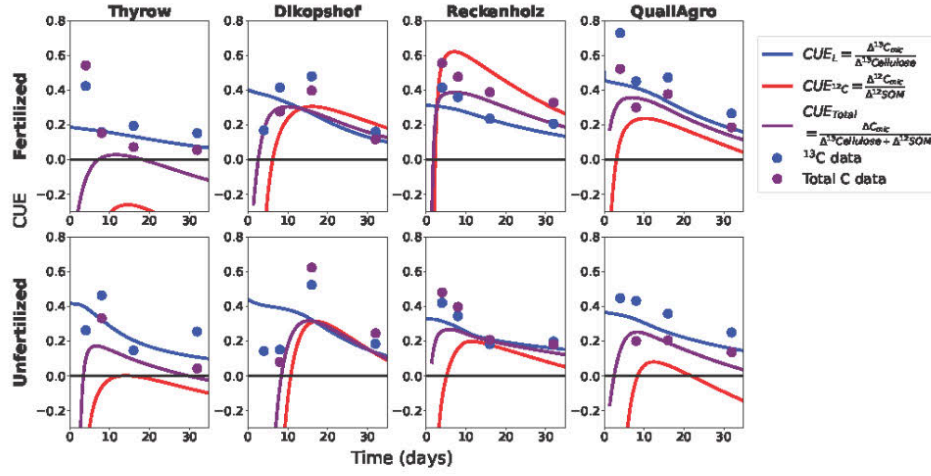


Figure 4: Modelled CUE_L for ^{12}C (red), ^{13}C (blue) and total C (purple) in all soils. The curves show the net cumulative biomass change relative to the respective substrate consumption. Therefore, positive values indicate a net gain and negative values indicate a net loss of biomass compared to the start of the incubation. Markers indicate corresponding experimental estimates.

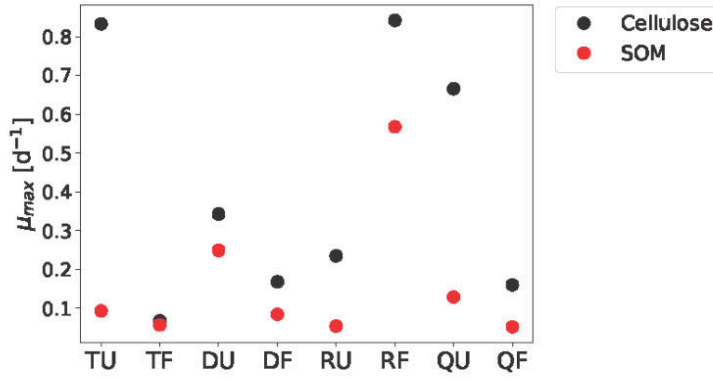


Figure 5: Model estimates of the maximum specific growth rate μ_{max} for the growth reaction using cellulose (black) and SOM (red). The quantity μ_{max} is not a model parameter, but instead derived as the product of the maximum substrate uptake rate $v_{max,X}$ and the yield coefficient Y_X of the respective substrate X .

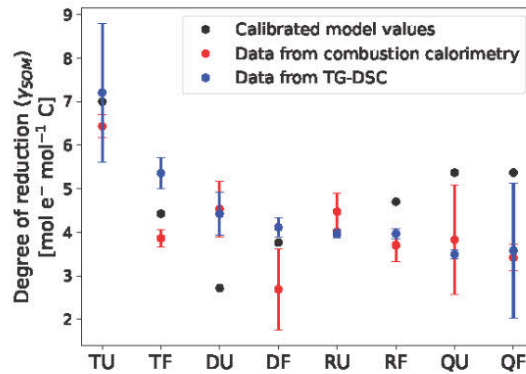


Figure 6: Model estimates of the degree of reduction γ_{SOM} of the biomass consumed by microbes (black) compared to experimental estimates for bulk SOM derived from measurements of average energy content via bomb calorimetry (red) and TG-DSC (blue).

References

- Blagodatsky, S., Richter, O., 1998. Microbial growth in soil and nitrogen turnover: a theoretical model considering the activity state of microorganisms. *Soil Biology and Biochemistry* 30, 1743–1755. URL: <https://linkinghub.elsevier.com/retrieve/pii/S0038071798000285>, doi:10.1016/S0038-0717(98)00028-5.
- Chakrawal, A., Herrmann, A.M., Šantrůčková, H., Manzoni, S., 2020. Quantifying microbial metabolism in soils using calorespirometry — A bioenergetics perspective. *Soil Biology and Biochemistry* 148, 107945. URL: <https://linkinghub.elsevier.com/retrieve/pii/S0038071720302418>, doi:10.1016/j.soilbio.2020.107945.
- Endress, M.G., Chen, R., Blagodatskaya, E., Blagodatsky, S., 2024a. The

- coupling of carbon and energy fluxes reveals anaerobiosis in an aerobic soil incubation with a Bacillota-dominated community. *Soil Biology and Biochemistry* 195, 109478. URL: <https://linkinghub.elsevier.com/retrieve/pii/S0038071724001676>, doi:10.1016/j.soilbio.2024.109478.
- Endress, M.G., Dehghani, F., Blagodatsky, S., Reitz, T., Schlüter, S., Blagodatskaya, E., 2024b. Spatial substrate heterogeneity limits microbial growth as revealed by the joint experimental quantification and modeling of carbon and heat fluxes. Under review at *Soil Biology and Biochemistry* (VSI: Soil C and energy fluxes) .
- Newville, M., Otten, R., Nelson, A., Stensitzki, T., Ingargiola, A., Allan, D., Fox, A., Carter, F., Michał, Osborn, R., Pustakhod, D., Ineuhaus, Weigand, S., Aristov, A., Glenn, Deil, C., mgunyho, Mark, Hansen, A.L.R., Pasquevich, G., Foks, L., Zobrist, N., Frost, O., Stuermer, azelcer, Polloreno, A., Persaud, A., Nielsen, J.H., Pompili, M., Eendebak, P., 2023. lmfit/lmfit-py: 1.2.2. URL: <https://doi.org/10.5281/zenodo.8145703>, doi:10.5281/zenodo.8145703.
- Virtanen, P., Gommers, R., Oliphant, T.E., Haberland, M., Reddy, T., Cournapeau, D., Burovski, E., Peterson, P., Weckesser, W., Bright, J., van der Walt, S.J., Brett, M., Wilson, J., Millman, K.J., Mayorov, N., Nelson, A.R.J., Jones, E., Kern, R., Larson, E., Carey, C.J., Polat, I., Feng, Y., Moore, E.W., VanderPlas, J., Laxalde, D., Perktold, J., Cimrman, R., Henriksen, I., Quintero, E.A., Harris, C.R., Archibald, A.M., Ribeiro, A.H., Pedregosa, F., van Mulbregt, P., SciPy 1.0 Contributors, 2020. SciPy 1.0: Fundamental Algorithms for Scientific Computing in Python. *Nature Methods* 17, 261–272. doi:10.1038/s41592-019-0686-2.

Erklärung zur Dissertation

gemäß der Promotionsordnung vom 12. März 2020

Hiermit versichere ich an Eides statt, dass ich die vorliegende Dissertation selbstständig und ohne die Benutzung anderer als der angegebenen Hilfsmittel und Literatur angefertigt habe. Alle Stellen, die wörtlich oder sinngemäß aus veröffentlichten und nicht veröffentlichten Werken dem Wortlaut oder dem Sinn nach entnommen wurden, sind als solche kenntlich gemacht. Ich versichere an Eides statt, dass diese Dissertation noch keiner anderen Fakultät oder Universität zur Prüfung vorgelegen hat; dass sie - abgesehen von unten angegebenen Teilpublikationen und eingebundenen Artikeln und Manuskripten - noch nicht veröffentlicht worden ist sowie, dass ich eine Veröffentlichung der Dissertation vor Abschluss der Promotion nicht ohne Genehmigung des Promotionsausschusses vornehmen werde. Die Bestimmungen dieser Ordnung sind mir bekannt. Darüber hinaus erkläre ich hiermit, dass ich die Ordnung zur Sicherung guter wissenschaftlicher Praxis und zum Umgang mit wissenschaftlichem Fehlverhalten der Universität zu Köln gelesen und sie bei der Durchführung der Dissertation zugrundeliegenden Arbeiten und der schriftlich verfassten Dissertation beachtet habe und verpflichte mich hiermit, die dort genannten Vorgaben bei allen wissenschaftlichen Tätigkeiten zu beachten und umzusetzen. Ich versichere, dass die eingereichte elektronische Fassung der eingereichten Druckfassung vollständig entspricht.

Teilpublikationen:

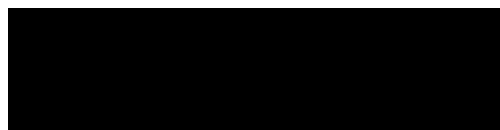
Endress, M.-G., Chen, R., Blagodatskaya, E., Blagodatsky, S., 2024a. The coupling of carbon and energy fluxes reveals anaerobiosis in an aerobic soil incubation with a Bacillota-dominated community. *Soil Biology and Biochemistry* 195, 109478. doi:[10.1016/j.soilbio.2024.109478](https://doi.org/10.1016/j.soilbio.2024.109478)

Endress, M.-G., Dehghani, F., Blagodatsky, S., et al., 2024b. Spatial substrate heterogeneity limits microbial growth as revealed by the joint experimental quantification and modeling of carbon and heat fluxes. *Soil Biology and Biochemistry* 197, 109509. doi:[10.1016/j.soilbio.2024.109509](https://doi.org/10.1016/j.soilbio.2024.109509)

Wirsching, J., **Endress, M.-G.**, Di Lodovico, E., et al., 2024. Coupling energy balance and carbon flux during cellulose degradation in arable soils. *Soil Biology and Biochemistry* 202, 109691. doi:[10.1016/j.soilbio.2024.109691](https://doi.org/10.1016/j.soilbio.2024.109691)

Endress, M.-G., and Blagodatsky, S., *in preparation*. Bioenergetics of microbial maintenance metabolism in soil.

12.01.2025, Martin-Georg Endress




Curriculum Vitae


(Pages 189-191)

Martin-Georg Alexander Endress

Curriculum Vitae



endressmg@gmail.com



Education

Since 2022 PhD student, Institute of Zoology, University of Cologne, Cologne
M. S. Quantitative Ecology and Resource Management, University of Washington, Seattle, 2021
B. S. Biology, Humboldt-Universität zu Berlin, Berlin, 2017
Abitur Andreas Gymnasium, Berlin, 2013

Employment

Since 2022 Research assistant, Institute of Zoology, University of Cologne, Cologne
2019-2021 Research assistant, School of Oceanography, University of Washington, Seattle
2016-2018 Teaching assistant, Institute for Theoretical Biology, Humboldt-Universität zu Berlin, Berlin

Scholarships & Awards

2018-2019 First year scholarship of the Quantitative Ecology and Resource Management graduate program
2014-2018 Scholarship of the German Academic Scholarship Foundation
2017 Prize for Good Teaching of the Faculty of Life Sciences,
Humboldt-Universität zu Berlin
(awarded to all members of the module 'Mathematics for Biologists')
2012 Student Award in Physics, Deutsche Physikalische Gesellschaft

Workshops und summer schools

- 2024 SoilSystems Workshop 'Data integration and model intercomparison' in Cologne, 3.-4. July, Organizer
- 2023 SoilSystems Workshop 'Scientific Writing' at the Thünen Institut in Brunswick, 23. - 25. October, Participant
- 2023 SoilSystems summer school 'Modeling in biothermodynamics and systems ecology' in Bad Urach, 5.-7. June, Instructor
- 2022 SoilSystems summer school 'Methods on microbial substrate turnover' in Leipzig, 17. - 19. October, Participant
- 2016 Summer academy of the German Academic Scholarship Foundation in Roggenburg, Focus group „Klimawandel im Spannungsfeld zwischen Natur und Kultur“, 6. - 14. August, Participant
- 2015 Summer academy of the German Academic Scholarship Foundation in Nice, Focus group „Physics of regulation and self-organization in living systems“, 20. September - 3. October, Participant

Conferences and presentations

- 09-2024, Berlin, Germany **Systems Ecology – Organic Matter, Energetics & Turnover**, Participant
- 04-2024, Vienna, Austria **EGU General Assembly 2024**, Presentation
The potential and challenges of dynamic models for investigating microbial processes
- 02-2024, Kleve, Germany **10th Rhine-Waal Soil and Plant Ecology Seminar**, Presentation
Investigating the coupling of microbial carbon and energy fluxes under nutrient limitation in soils.
- 09-2023, Halle, Germany **Annual Meeting of the DBG 2023**, Presentation
Bioenergetics as a modeling tool linking microbial dormancy, maintenance and growth in soil.
- 04-2023, Vienna, Austria **EGU General Assembly 2023**, Presentation
Using the Calorespirometric Ratio to investigate the metabolism of a growing microbialcommunity dominated by Firmicutes in glucose-amended soil.

Teaching experience

- 2016-2018 Teaching Assistant, Institute for Theoretical Biology,
Humboldt-Universität zu Berlin, Berlin
- Supervisor: Prof. Dr. Richard Kempter
- Responsibilities: Instructor (weekly seminars),
Development and grading of exercises and final examinations
- Courses taught: Mathematics for Biologists - Mathematics I (fall 2017, 2016)
Mathematics for Biologists - Mathematics II (spring 2018, 2017)
Mathematics for Biologists - Biostatistics (spring 2018, 2017)

Publications

- In prep.* **Endress M** and Blagodatsky S: Bioenergetics of microbial maintenance metabolism in soil
- 2024 Wirsching J, **Endress M**, Di Lodovico E, Blagodatsky S, Fricke C, Lorenz M, Marhan S, Kandeler E, Poll C: Coupling energy balance and carbon flux during cellulose degradation in arable soils. *Soil Biology and Biochemistry* 202. doi: <https://doi.org/10.1016/j.soilbio.2024.109691>
- 2024 van Bommel M, Arndt K, **Endress M**, Dehghani F, Wirsching J, Blagodatskaya E, Blagodatsky S, Kandeler E, Marhan S, Poll C, Ruess L: Under the lens: Carbon and energy channels in the soil micro-food web. *Soil Biology and Biochemistry* 199. doi: <https://doi.org/10.1016/j.soilbio.2024.109575>
- 2024 **Endress M**, Dehghani F, Blagodatsky S, Reitz T, Schlüter S, Blagodatskaya E: Spatial substrate heterogeneity limits microbial growth as revealed by the joint experimental quantification and modeling of carbon and heat fluxes. *Soil Biology and Biochemistry* 197. doi: <https://doi.org/10.1016/j.soilbio.2024.109509>
- 2024 **Endress M**, Ruirui C, Blagodatskaya E, Blagodatsky S: The coupling of carbon and energy fluxes reveals anaerobiosis in an aerobic soil incubation with a *Bacillota*-dominated community. *Soil Biology and Biochemistry* 195. doi: <https://doi.org/10.1016/j.soilbio.2024.109478>
- 2024 **Endress M**, Boag T, Burford B, Sperling E, Penn J, Deutsch C: Physiological causes and biogeographic consequences of thermal optima in the hypoxia tolerance of marine ectotherms. *PLoS biology*. doi: <https://doi.org/10.1371/journal.pbio.3002443>
- 2022 Deutsch C, Penn J, Verberk W, Inomura K, **Endress M**, Payne J : Impact of warming on aquatic body sizes explained by metabolic scaling from microbes to macrofauna. *Proc. Natl. Acad. Sci. USA* doi: <https://doi.org/10.1073/pnas.2201345119>